Imaging Coherent Electron Flow Through Semiconductor Nanostructures

A thesis presented

by

Brian James LeRoy

to

The Department of Physics
in partial fulfillment of the requirements
for the degree of
Doctor of Philosophy
in the subject of

Physics

Harvard University
Cambridge, Massachusetts

May, 2003

Abstract

Imaging Coherent Electron Flow Through Semiconductor Nanostructures

Advisor: Robert Westervelt   Author: Brian LeRoy

Scanning probe microscopy is used to probe coherent electron flow in semiconductor nanostructures. We have developed a technique for imaging coherent electron flow through a two-dimensional electron gas (2DEG). The images are acquired using a scanning probe microscope at low temperature. The conductance through the device as a function of tip position is measured to obtain an image of electron flow. The images of electron flow are decorated by interference fringes spaced by half the Fermi wavelength. We use the spacing of these fringes to measure the local electron density. The variation of the density with back gate voltage agrees with a parallel plate capacitor model.

We use our imaging technique to characterize the rate of energy loss for electrons traveling through the 2DEG. A source-drain voltage is applied to the electrons, which accelerates them and causes them to loss energy more quickly. By imaging the electron flow, the rate that the electrons lose their excess energy is determined. The results agree with the electron-electron scattering rate in a 2DEG for different distances and energies.

Images of electron flow through three electron-optic devices are presented. An electrostatic prism is used to control the direction of electron flow based on the density under its gate. Images are shown using a round gate as a defocusing lens for electron

waves and as a circular scatterer. The potential profile from an electrostatic gate is investigated by creating a narrow channel for electrons. By imaging the trajectories of electrons, the profile of the potential from the gate is found.

The origin of the interference fringes, which decorate all of our images of electron flow is investigated. They are due to interference between paths backscattered from the tip and ones backscattered from scattering objects at nearly the same distance. This is confirmed by the addition of a small reflecting gate, which enhances the interference fringes at the same distance from the quantum point contact. The interference fringes move as the position of the reflector is changed indicating that the fringes are due to backscattering from the reflector.

Contents

Acknowledgements

During the last five years, I have had the pleasure of working with many people here at Harvard who have made my graduate school experience very enjoyable. First of all, I want to thank my adviser, Bob Westervelt, for having an excellent lab in which to do research. He has created an environment where everyone is free to explore their own research projects yet is always willing to give suggestions and advice.

I also want to thank the other two members of my committee. Rick Heller and his group have always been available to talk to about results from our imaging experiments. They have also been very helpful in running quantum mechanical simulations of the electron flow to better understand the results. The addition of Charlie Marcus and his group has added another group of people to the second floor of McKay who are interested and knowledgeable in 2DEGs. This has provided a welcome group to discuss the experiments that I have worked on.

In our group, I have worked with several people on the imaging project. Mark Topinka and I struggled for nearly a year to get the AFM to work and take the first images of electron flow. Over the last few years, I have enjoyed teaching Ania Bleszynski and Kathy Aidala how to use the AFM and working with them to set up our group's new He-3 AFM. I look forward to seeing the results of their experiments at lower temperatures and with new materials. During my time in the group, I have had the pleasure of working with many other people. Ian Chan joined the lab the same year as I did and has helped to keep all of the computers running smoothly and is always around to answer electronics questions. Thanks to Hakho Lee for our seemingly daily cups of coffee after the lab

Chapter 1

Introduction

1.1. Motivation

For more than 15 years, the growth of high mobility two-dimensional electron gases has allowed many new experiments in the field of mesoscopic physics. These experiments have demonstrated new and unexpected phenomena including conductance quantization, the integer and fractional quantum Hall effect, and single electron tunneling [Beenakker, (1991); Sohn, (1997)]. However, most of these experiments relied on transport measurements to understand these phenomena. The use of scanning probe microscopy techniques allows the behavior of the electrons to be imaged on a much smaller length scale then is accessible with standard transport measurements.

Scanning probe microscopy provides a novel way of examining electronics devices even as they continued to be miniaturized. This is because they provide information about the local behavior of the electrons rather than an average measure over a macroscopic area. Our imaging techniques are also important for the design and implementation of new devices that rely on the coherence of the electron, for example quantum information processing devices, to perform computation. From our images we are able to determine whether the flow is coherent and to image the pattern of flow through a device. In this thesis, we examine the operation of some of these new types of devices, including their pattern of electron flow and their scattering rate.

The design of new electronic materials requires methods to investigate their

properties. We show how scanning probe microscopy can be used to investigate the local properties of these new materials. From our images of electron flow we are able to spatially profile the local electron density. The images of electron flow are also decorated by a new type of interference, which can be used in the creation of devices that rely on the coherence of the electron for their operation.

1.2. Background

The advances in mesoscopic semiconductor devices have been driven by improvements in material quality and fabrication techniques. Most notably, the mobility of GaAs/AlGaAs heterostructures continues to increase and has now reached 3×10^7 cm^2/V s [Pfeiffer, (1989)]. This increase has been caused by the development of modulation doping techniques [Dingle, (1978)] and improved sample quality. The size of devices that can be fabricated continues to decrease with improvements in electron beam lithography. It is now possible to fabricate devices containing only a few electrons [Tarucha, (1996); Ciorga, (2000); Elzerman, (2003)].

1.2.1. Two-dimensional Electron Gases

The samples that we use in all of the experiments described in this thesis contain two-dimensional electron gases in GaAs/AlGaAs heterostructures. The heterostructures are grown by molecular beam epitaxy, which ensures that the thickness of each layer can be controlled with sub-monolayer precision [Herman, (1989)]. This control of the growth properties allows arbitrary potential wells for electrons to be created. Some of the basic shapes that can be made are square wells, triangular wells, parabolic wells and

2

superlattices.

For all of the experiments in this thesis we have used samples with accumulation layers formed at the interface of GaAs and $Al_{0.3}Ga_{0.7}As$. Figure 1.1 shows the conduction band edge for a 2DEG sample. The 2DEG is formed between the GaAs and AlGaAs layers due to the offset in the conduction band for these two materials. This offset is determined by the difference in the bandgap and electron affinity for
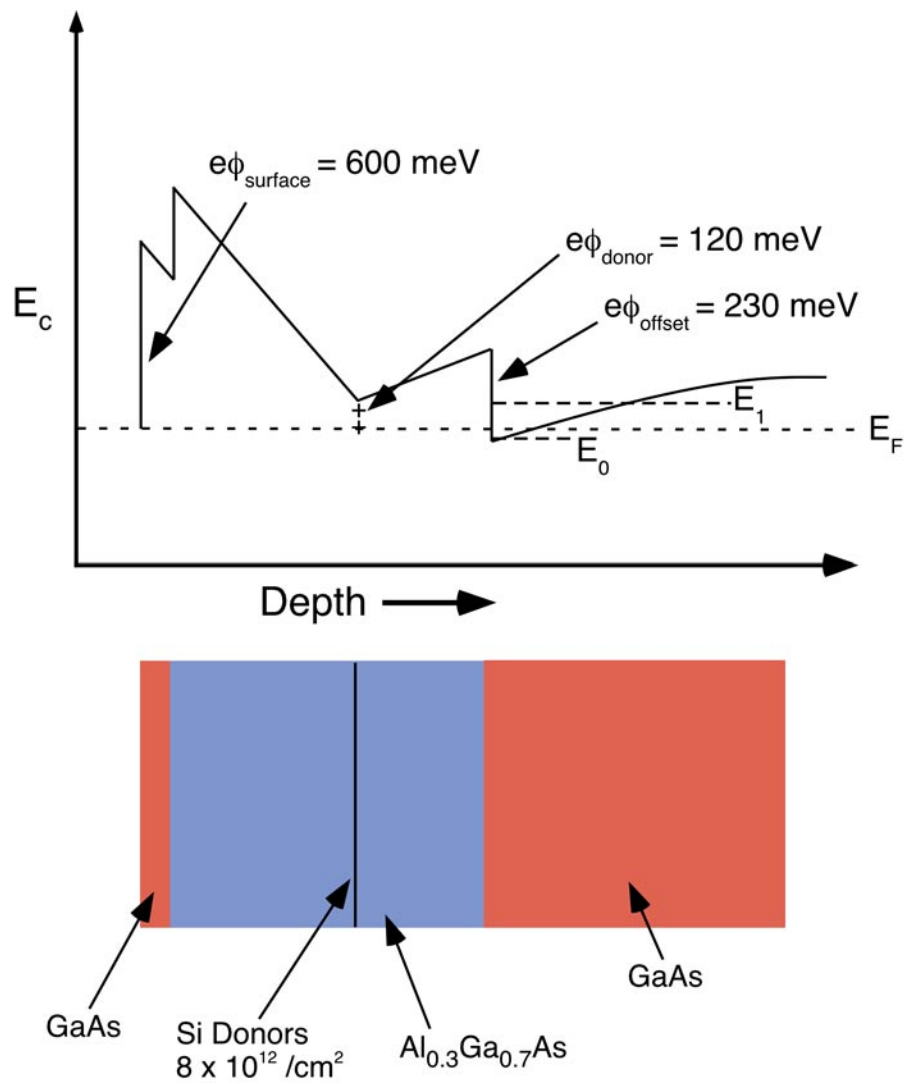
Figure 1.1 Schematic band diagram showing the conduction band edge for the samples used in this thesis. The bottom portion shows the growth layers for the heterostructure.

GaAs and $Al_{0.3}Ga_{0.7}As$. This gives an offset in the conduction band of about 230 meV [Adachi, (1985)]. The second consideration in finding the conduction band profile for the heterostructure is that the Fermi level is pinned about 600 meV below the conduction band edge due to the surface states [Davies, (1998)]. These states are compensated with the delta layer of Si donor atoms, which give up electrons to satisfy the surface states and create the 2DEG. The Si donor atoms fix the Fermi level about 120 meV below the conduction band edge at their position [Davies, (1998)]. The last step to find the conduction band profile is to calculate the slopes between these fixed points knowing the distance and electron density.

The slope of the conduction band edge is calculated using a simple parallel plate capacitor model. The distance and potential difference from the surface to the Si donor atoms is known. Using this information, the number of electrons needed to satisfy the surface states can be calculated. This leaves the rest of the Si atoms to give their electrons to the 2DEG. The electrostatic attraction between the electrons in the 2DEG and the donor atoms creates an approximately triangularly shaped potential at the interface of the GaAs and $Al_{0.3}Ga_{0.7}As$. The density of the Si donor atoms is chosen so that only the lowest subband of the potential well is occupied. The energy levels of this potential profile are well known and the wavefunction is given by an Airy function [Harris, (1989)]. The equation for the energy eigenvalues of the well is

$$E_i = \left(\frac{\hbar^2}{2m}\right)^{1/3}\left(\frac{3\pi}{2}\left(i+\frac{3}{4}\right)F\right)^{2/3}$$

where $F = 4\pi n/\varepsilon$ is the electric field due to the ionized donors, n is the electron density in the 2DEG, ε is the dielectric constant of GaAs and m is the electron effective mass, which

is 0.067 times the free electron mass. This provides the confinement in the z-direction while the electrons are free in the x and y direction creating the 2DEG.

The Fermi energy of the 2DEG can be estimated from Figure 1.1 by fixing the chemical potential throughout the sample. This gives the following equation for the Fermi Energy.

$$E_F + e\phi_{donor} + Fd - e\phi_{offset} = E_0$$

where $\phi_{donor} \approx 120$ mV, $\phi_{offset} \approx 230$ mV and d is the distance from donors to the 2DEG. The model also can give the density of Si dopants needed to satisfy the surface states:

$$\sigma = \frac{e(\phi_{surface} + \phi_{offset} - \phi_{donor})\varepsilon}{4\pi r \eta}$$

where r is the distance from the dopants to the surface, $\phi_{surface} \approx 600$ mV, and $\eta \approx 1/2$ is the fraction of dopant atoms that are thermally activated, i.e. not all Si donors are active. In the case of our heterostructure more of the electrons from the ionized donors go to the surface states than go to the 2DEG.

Since the heterostructure is grown on a GaAs [100] surface, the Fermi surface for electrons is just a circle. This gives a very simple dispersion relation between the Fermi energy, E_F, and the electron wavevector, k. This relation is given by

$$E_F = \frac{\hbar^2(k_x^2 + k_y^2)}{2m}$$

There is also a simple relationship between the wavevector, k, and the electron density, n, since the electrons are confined to two dimensions.

$$n = \frac{k^2}{2\pi}$$

The combination of these two equations shows that the Fermi energy is linear in the electron density.

1.2.2. Quantum Point Contacts

To further confine the electrons we lithographically pattern electrostatic gates on the surface of the heterostructure. The simplest pattern that can be created is a quantum point contact (QPC), which consists of two gates with a small opening between them. Figure 1.2 shows a scanning electron micrograph image of a quantum point contact. A negative voltage is put on the gates with respect to the 2DEG to push away the electrons underneath. This forces the electrons to flow through the narrow channel between the two gates and confines them to one-dimension.

The confinement of the electrons to one-dimension leads to a quantization of the conductance through the QPC [van Wees, (1988); Wharam, (1988)]. Each mode of the QPC carries the same amount of current because of the cancellation of the group velocity and the density of states, which leads to the quantization of the conductance. Figure 1.3

500 nm
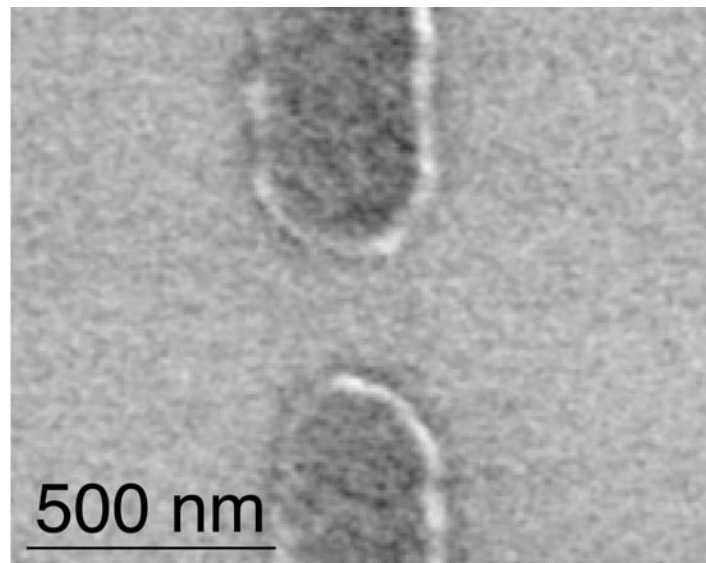
Figure 1.2 Scanning electron micrograph image of a typical quantum point contact device showing the two electrostatic gates that confine the electrons.
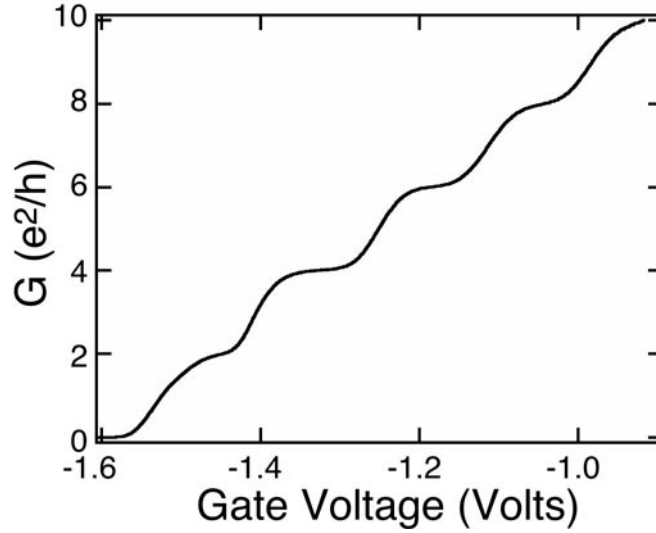
Figure 1.3 Conductance through a quantum point contact as a function of the voltage on its gate, which controls its width at a temperature of 1.7 K. The conductance shows well-defined plateaus at multiples of $2e^2/h$.

shows the measured conductance through the QPC as a function of the voltage on its gate at a temperature of 1.7 K. As the voltage is made more negative, the width of the channel is decreased and transmission through the modes of the QPC is reduced. The conductance of the QPC can be calculated using Landauer-Buttiker formalism if the transmission probabilities of each mode are known [Landauer, (1957); Landauer, (1970); Büttiker, (1986)]. The conductance, G, is given by the following equation

$$G = \frac{2e^2}{h}\sum_i T_i$$

where the summation is over all of the modes of the QPC and the T_i are the transmission probabilities of the individual modes through the QPC. If there is no scattering in the QPC, the transmission probability is either 0 or 1 for each of the modes. This shows the conductance quantized in units of $2e^2/h$ depending on the number of modes accessible in the QPC.

When the electrons are confined to one-dimensional subbands the equation for their energy versus wavevector has to be modified to account for the confinement. The new equation is

$$E = E_N + \frac{\hbar^2 k_x^2}{2m}$$

where E_N is the energy of the subband at the saddle point in the center of the QPC. It is now clear that the electrons are only free in one dimension and their energy is quantized in the other two directions. The energy of the one-dimensional subbands in the QPC can be found by measuring the conductance as a function of the gate voltage and the source-drain bias V_{sd}. As the bias is increased the electrons are able to transverse the QPC through higher subbands [Kouwenhoven, (1989)].

Figure 1.4 shows the differential conductance through the QPC as a function of its gate voltage and the source-drain voltage V_{sd} at a temperature of 1.7 K. Areas of high differential conductance are shown by the blue and yellow lines. Taking a vertical line through the data at $V_{sd} = 0$ meV, gives spikes in the differential conductance corresponding to the addition of each new mode of the QPC. Moving to finite V_{sd}, transport can take place through excited levels in the QPC giving lines of high differential conductance. These bright lines form diamonds marking the boundary of areas of constant conductance. By measuring the width of the diamonds, the spacing of the subbands in the QPC is determined.

The conductance plateaus of the QPC are not well defined when the energy spacing between the subbands of the QPC becomes smaller than the temperature. This is because conduction takes place through several subbands and the probability of transmission through each subband is no longer 0 or 1 but rather given by the electron
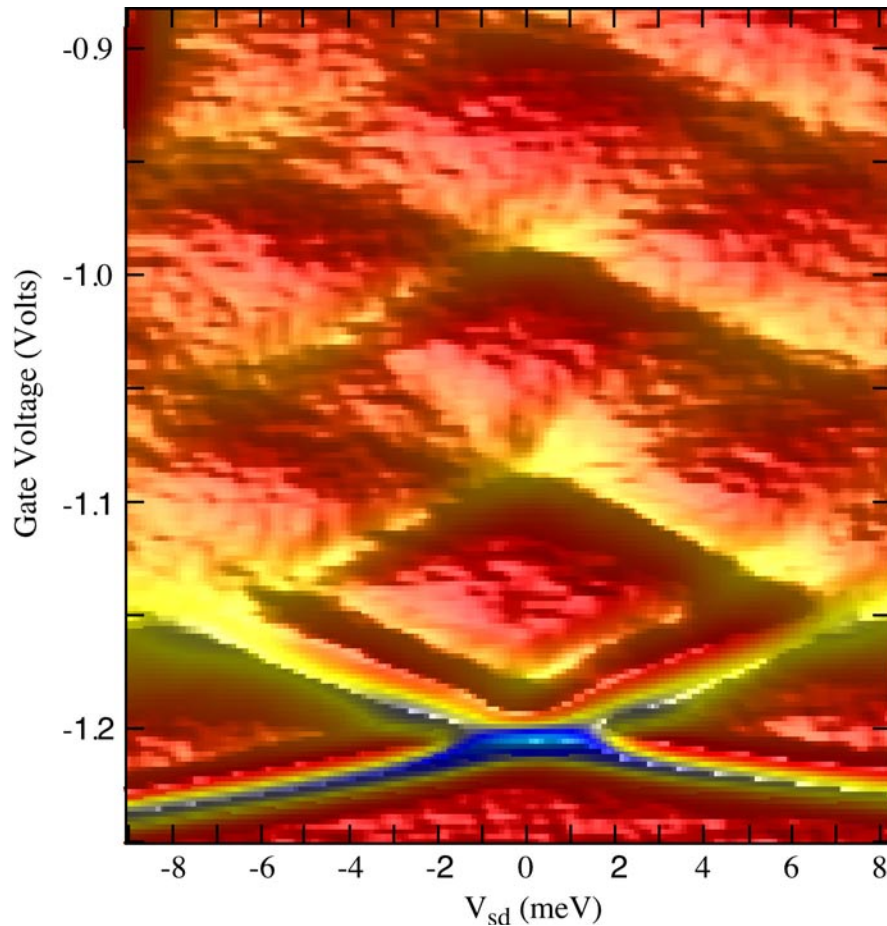
Figure 1.4 Plot of the differential conductance through a QPC as a function of the gate voltage and the source-drain bias voltage V_{sd}. Blue and yellow lines indicate areas of high differential conductance that correspond to energies in which new subbands of the QPC become accessible. The data was obtained at a temeperature of 1.7 K.

distribution at that energy. This rounds the shape of the conductance steps into the shape

of the Fermi function for the temperature of the experiment.

1.2.3. Scanning Probe Microscopy

Since the invention of the scanning tunneling microscope, there has been a rapid

increase in the use of microscopy techniques to study phenomena on a much smaller

size scale [Binnig, (1982)]. This increase was fuelled by the atomic force microscopy

technique, which can image surfaces that are not conducting [Binnig, (1986)]. In recent years, there have been many groups using low temperature scanning probe microscopes to study a wide variety of phenomena including standing waves on Cu [Crommie, (1993); Manoharan, (2000)], carbon nanotubes [Lemay, (2001); Woodside, (2002)], high temperature superconductors [Hudson, (1999); Pan, (2000)]. One very active area of research has been on semiconductor heterostructures where research has been focused in two main areas, electron flow through devices [Eriksson, (1996); Topinka, (2000); Topinka, (2001); Crook, (2000)] and the quantum hall regime [Tessmer, (1998); Yacoby, (1999); McCormick, (1999)].

Each of the methods of scanning probe microscopy uses a feedback principle to perform topographic imaging of the sample. In the case of scanning tunneling microscopy, the current from the tip to the sample is measured. This is exponentially sensitive to the distance between the tip and sample, so that it provides a sensitive measure of the surface topography and atomic resolution can be obtained. However, this technique requires that the surface is conducting, which is not the case in our semiconductors where the 2DEG is 57 nm below the surface. In the case of atomic force microscopy, the force on a small cantilever is measured. By keeping this force constant, an image of the surface is obtained. The size of the tip determines the resolution of this technique making atomic resolution difficult but non-conducting surfaces can be imaged. In order to study the behavior of electrons in a two-dimensional electron gas new techniques are needed since they are inside the heterostructure.

In the quantum Hall regime, several ways of detecting the properties of the 2DEG have been developed. These include using a single electron transistor to sense individual

charges and map out their location, which has produced images of the quantum hall states at different filling factors [Yacoby, (1999)]. There are also techniques involving the measuring of capacitance and compressibility, which leads to information about the local potential of the electrons [Tessmer, (1998); Finkelstein (2000)]. These techniques work well at high magnetic filed but are not sensitive to the electron flow without a magnetic field.

The second class of experiments using scanning probe microscopy techniques and 2DEGs involve the imaging of electron flow. These techniques all use a perturbation in the 2DEG to scatter electrons and from the response determine the pattern of electron flow. This technique has been applied to the flow through a large channel [Eriksson, (1996)], flow from a quantum point contact [Topinka, (2000); Crook, (2000a)], bending due to magnetic field [Crook, (2000b)], and electron flow in a 2DEG [Topinka, (2001)]. In the rest of this thesis, this technique and variations of it will be applied to a new set of devices to understand the electron flow through them.

1.3. Outline

This thesis presents results from experiments imaging coherent electron flow. All of the results presented were obtained using a liquid-Helium cooled scanning probe microscope [Topinka, (2002)]. The scanning probe microscope tip is used to probe the pattern of electron flow through a two-dimensional electron gas formed in a GaAs/AlGaAs heterostructure. Figure 1.5 shows images of electron flow from the (a) first, (b) second, and (c) third mode of a QPC located 700 nm past the right edge of the images. The modal pattern of the electron flow from the QPC is visible along with
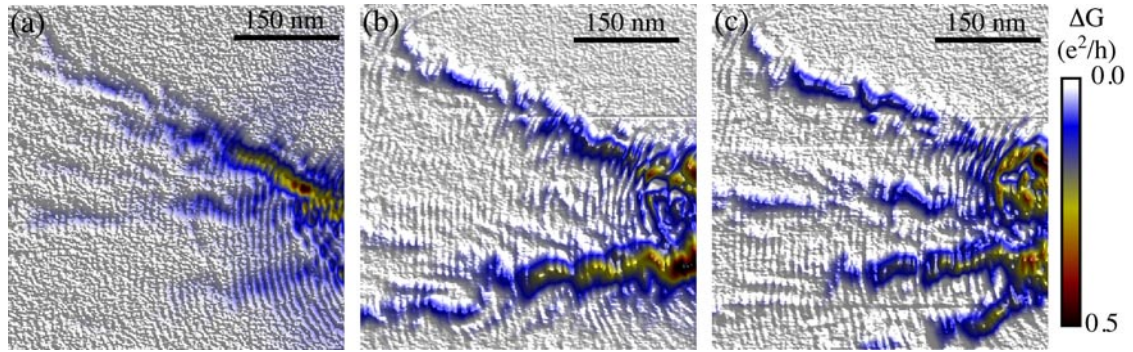
Figure 1.5 Images of the pattern of electron flow from the (a) first, (b) second, and (c) third mode of a QPC located 700 to the right of the images.

interference fringes spaced by half the Fermi wavelength.

Chapter 2 describes the procedures that we use to fabricate the devices used in these experiments. This includes the procedures for electron beam lithography, thin film deposition and chemical etching. It also details the design and operation of our two low-temperature scanning probe microscopes. This includes the design of the control electronics, the data acquisition program and the cryostats.

Chapter 3 presents the imaging techniques that we use to image coherent electron flow in a two-dimensional electron gas. The first technique uses the scanning probe microscope tip as a moveable scatterer to probe the pattern of electron flow. The second technique that we have developed oscillates the voltage on the tip to image the spatial derivative of the electron flow. The final technique that we use is sensitive to the energy of electrons hitting the tip and measures the local density of states.

Chapter 4 discusses our experiments on imaging the local density of electrons. Our images of electron flow are decorated by interference fringes spaced by half the Fermi wavelength. The spacing of these fringes gives a measure of the local electron

density. By measuring the change in wavelength as a function of back gate voltage, the results are compared with a capacitor model. We also show that images of electron flow become more diffuse as the density is reduced because the mean free path of the electrons is reduced.

Chapter 5 describes our measurements of the electron-electron scattering length in the two-dimensional electron gas. We demonstrate a technique that is sensitive to whether or not an electron has scattered. By accelerating the electrons across a quantum point contact, we decrease their scattering length. This decrease in scattering length is measured by our images of electron flow. The results for a variety of distances and Fermi energies are shown and all agree with theory for electron-electron scattering in a 2DEG.

Chapter 6 shows images from a series of experiments on electron optics devices. These are devices that control the flow of electrons using electrostatic gates in analogy to switches and lenses in optics. We show images of electron flow from a triangular electrostatic gate, which acts as a switch. We use a round gate as a defocusing lens and as a circular scatterer for electron waves. We also fabricated a narrow channel to guide the electrons and study the potential profile from the electrostatic gate.

Chapter 7 examines the origin of the interference fringes that are seen in all of our images of coherent electron flow. The fringes arise from interference of electron waves backscattered from the tip with backscattered waves from impurities that are near the same distance from the QPC as the tip. This is confirmed by using a small reflecting arc, which acts like a large number of impurities, to enhance the interference fringes at the same radius as the arc. The interference fringes move with the position of the reflector as controlled by its voltage. We have also found that enhanced backscattering from the

arc enhances the interference fringes. In the last section, we show that the interference fringes are more robust to thermal smearing near the radius of the reflector.

Chapter 8 presents some conclusions for the experiments described in this thesis. It also discusses some future experiments that can be done using our two low temperature scanning probe microscopes. These include new experiments made possible by the construction of our He-3 microscope that can reach much lower temperatures.

Chapter 2

Experimental Techniques

This chapter includes two main parts; the first half discusses the procedures needed to fabricate the samples used in our imaging experiments. The second half of the chapter covers the design and operation of our two low-temperature scanned probe microscopes (SPMs). Section 2.1 outlines the procedures used to make samples and prepare scanning probe microscope tips. The first part of section 2.1 covers the basic preparation of the samples including cleaving (section 2.1.1), cleaning (section 2.1.2), spinning PMMA (section 2.1.3), and writing patterns using the scanning electron microscope (section 2.1.4). The second part of this section includes details of chemical etching (section 2.1.5), depositing metal (section 2.1.6), annealing ohmic contacts (section 2.1.7) and wirebonding (section 2.1.8). The last part of section 2.1 in section 2.1.9 discusses the procedure used to coat the scanning probe tips with Cr. The rest of the chapter discusses the design and operation of the experimental equipment used in our experiments. The design of the He-4 system has been covered in previous theses, but the main points will be briefly highlighted in section 2.2. Much of the rest of the chapter is devoted to the design of the new He-3 system and the electronics for both SPMs. Section 2.3 has a discussion of the new SPM including the design of the cryostat, magnet and sample stick. Section 2.4 includes descriptions of all of the electronics needed to run either of the SPMs. There is a discussion of the new digital to analog control circuitry used by both SPMs in section 2.4.1. This allows faster and higher resolution scans to be

taken. After this, there is a discussion of the other electronics that are necessary for using the SPM including the surface flattening box (section 2.4.2), the feedback circuit (section 2.4.3), the high voltage amplifiers (section 2.4.4), summing amplifiers (section 2.4.5), and the computer program that is used for SPM control and data acquisition (section 2.4.6).

2.1. Sample Fabrication

This section details the procedures necessary to make the samples used in the imaging experiments in this thesis. All of our samples use two-dimensional electron gases formed in AlGaAs/GaAs heterostructures. We get the samples as unprocessed wafers from Art Gossard's group at the University of California—Santa Barbara. All of the processing is done in the two cleanrooms in Gordon McKay Lab. The procedure for defining a device consists of the following steps: cleaving a sample, creating a mesa, making ohmic contacts and lastly writing the electrostatic gates. Each of these steps requires several procedures, which will be outlined in the remainder of the chapter. The last two steps needed before imaging electron flow are wirebonding the sample and coating the SPM tip with Cr. Much of the information about sample fabrication is covered in other theses from our group. Lester Chen [Chen, (2001)] gives detailed procedures on how to use most of the pieces of equipment while Mark Topinka [Topinka, (2002)] covers some of the specific requirements of the SPM experiments.

2.1.1. Cleaving Samples

The samples generally arrive in our lab as half of a 2 inch wafer. For each of our experiments we only need a very small piece of this wafer so it is necessary to cleave the

16

wafer into small pieces. In order to cleave the wafer, the necessary tools are a diamond

scribe, Q-tip, ruler, glass slide, dust mask and ultra-high purity nitrogen. Make sure that

you are wearing the mask because GaAs dust is hazardous. If you are really concerned

about the dust you can even do this procedure in the fume hood. It is important that you

know which side of the wafer is the front. Before making any scribes ensure that you

can identify the front and if necessary make a small diagonal scratch on the back[1]. First

measure the size of the wafer that is desired and then make a scratch in the wafer with

the diamond scribe. GaAs readily breaks along its crystal axes so it is only necessary to

make a very small scratch on the edge of the wafer. Blow off the dust before breaking

the piece to keep the surface from being scratched. Put the wafer on the glass slide with

the piece to break off hanging over the edge. Then press down with a Q-tip and the piece

will cleave along this line. Blow off the dust and repeat this process until you have the

desired size and number of samples. For the SPM it is best to use pieces that are about

2 x 3 mm. If they are too big it is very difficult to attach them to the sample holder or

they may not even fit. If the samples are much smaller they are hard to work with for the

rest of the processing steps, especially the spinning of PMMA.

2.1.2. Cleaning

The samples are cleaned in three successive solvents, Trichloroethylene (TCE),

acetone and methanol. The first step is to put the samples in small Teflon beakers in

boiling TCE for 5 minutes. Make sure that the Teflon beakers have holes in them to let

---

[1] For the wafers with a back gate it is fairly easy to tell the front from the back because
the front is smooth while the back is rougher and a different color.

the TCE wash over the samples. Then transfer the samples to plastic beakers filled with

acetone and ultrasound for 5 minutes[2]. The last step is to use a new set of plastic beakers

filled with methanol. Put the samples in these beakers and then into the ultrasound for

five more minutes. After this is done the samples should be blown dry with ultra-high

purity nitrogen and they are ready for spinning. This procedure is repeated before each

spinning step but the TCE portion is usually skipped.

2.1.3. Spinning

In order to write a pattern on the samples it is necessary to spin on a resist. Since

all of our writing steps are done in the SEM we use Polymethylmethacrylate (PMMA)[3],

which is an electron beam sensitive resist. Locations that are exposed to the e-beam have

their bonds broken and can be developed away more easily. Depending on the fabrication

step either two or three layers are used. There are two reasons for using multiple layers,

the first one is to provide an undercut that facilitates the lift-off of the metal deposited.

To produce this undercut, a lighter PMMA is spun on for the bottom layers. This light

PMMA is more easily exposed which creates a larger developed area and hence an

undercut. Only the top most layer is a heavy PMMA. The other reason to use multiple

layers is that the PMMA tends to crack when drying. Each single layer has line defects,

but two layers will only have point defects where the lines intersect. By using three

layers there should be no defects unless you are very unlucky. We use 2% (by volume)

---

[2] Make sure that all the plastic beakers are labeled with their contents and that you properly dispose of them when you are finished. Otherwise, the hood is filled with beakers that contain unknown chemicals.

[3] MicroChem Corporation, 1254 Chestnut St., Newton, MA 02464

496K PMMA in Anisole for the light layer and 2% 950K PMMA in Anisole for the heavy layer. The procedure is very simple for spinning the chips. It is done in the inner cleanroom in the basement where there are two spinners and hot plates. Figure 2.1 shows the setup of one of the spinners and hot plates. Set the hotplate to 180 °C and wait for it to warm up. Set the spinner to go at 500 rpm for 5 seconds followed by 4000 rpm for 30 seconds. This should be one of the preprogrammed recipes. While the chip is spinning slowly, use a pippet to put a drop of PMMA on it. After it is finished spinning move it to the hotplate and let it bake for at least 5 minutes. Repeat the procedure until the desired number of layers are spun.
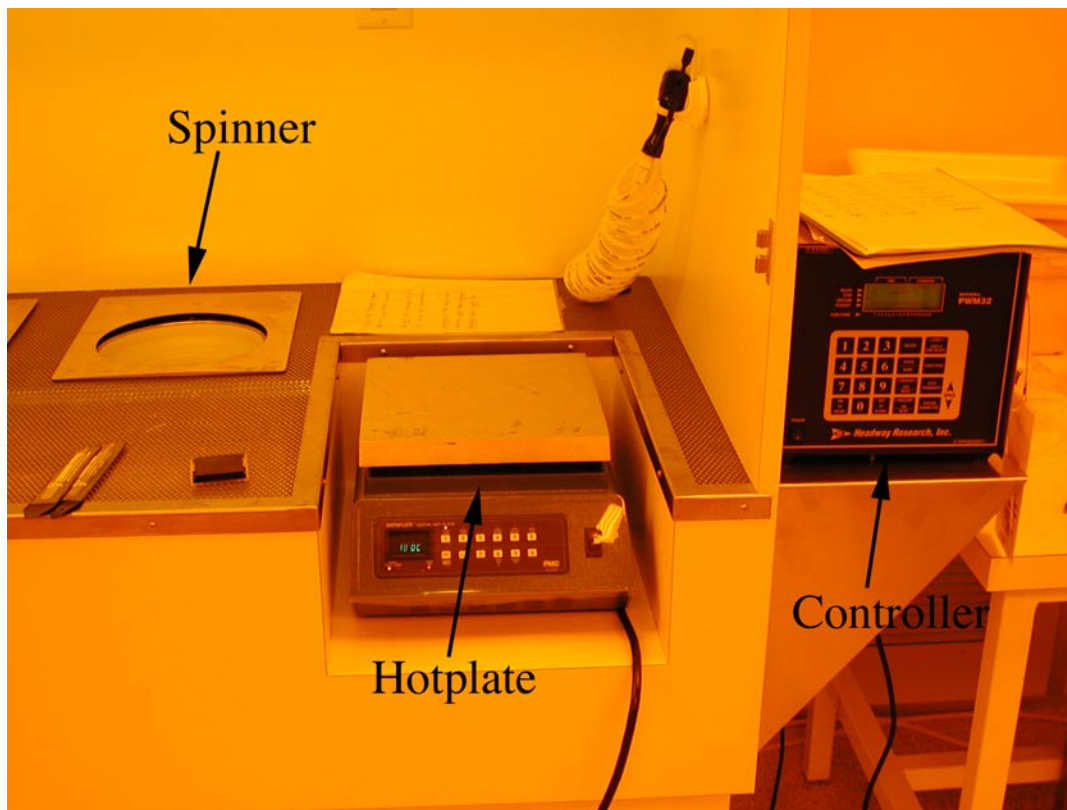
Figure 2.1 Setup of the spinner system in the basement cleanroom. The spinner is recessed in the back with a hotplate on the right. The controller is on the far right and there is a foot pedal to start and stop the spinner, which is not shown.

2.1.4. SEM

The scanning electron microscopes are the most complicated piece of equipment in the fabrication process. All of the samples discussed in this thesis were patterned on the JEOL JSM-6400. This SEM is equipped with the Nanometer Pattern Generation System (NPGS) for writing [Nabity, (1989); Nabity, (1991)]. This essentially consists of a computer that can move and blank the beam; therefore writing arbitrary patterns. Figure 2.2 shows the SEM with the viewing screens and the computer for generating patterns. This system is capable of writing 50 nm features but in this thesis all of the devices have had at least 100 nm feature sizes. The field of view of the microscope is determined by the magnification and is about 88,000 microns divided by the
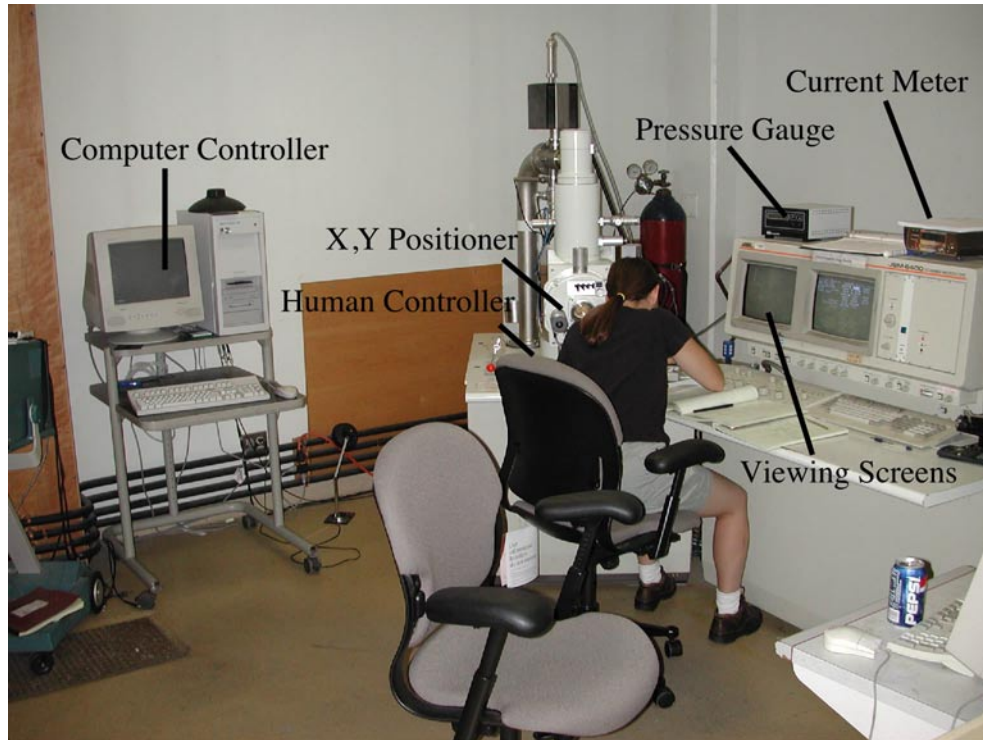
Figure 2.2 Setup of the SEM showing the viewing screens, gauges and the computer for generating patterns.

magnification. The design of patterns is done using DesignCad for the PC. Each layer

in the DesignCad file can correspond to a different magnification and current setting on

the SEM. Each magnification and current setting must be manually set by the user. The

most useful way to discuss the procedure for using the SEM is to write out the necessary

steps in a list, which is included in appendix A.

After the chip is written and the PMMA has been exposed it must be developed.

This is done by putting the sample in a mixture of isopropyl alcohol (IPA), methyl

isobutyl ketone (MIBK) and methyl-ethyl ketone (MEK). The standard recipe for the

developing solution is 375 ml IPA, 125 ml MIBK and 6.5 ml MEK. First rinse the

sample with IPA to remove any carbon paint that is on it. Then put it in the developing

solution for 1 minute before rinsing it in IPA to stop the developing. Look at the sample

in the optical microscope to see if the features have been developed. If not the sample

can be developed for a longer time. The longer the sample is in the developer the wider

the features become because the PMMA is slowly developed near the exposed areas.

2.1.5. Wet Etching

In order to define mesas for our samples we use a wet etch procedure. The mesas

allow the electrostatic gates to run off of the edge of the device without contacting the

back gate. It also allows separate ohmic contacts to be made to the device area and the

back gate. The etch mixture is a combination of Citric Acid and Hydrogen Peroxide.

The Citric acid is already mixed with water at the ratio of 1:1 by weight. This is then

combined with the Hydrogen Peroxide with ten parts citric acid for each part Hydrogen

Peroxide by volume. The procedure is described in detail in Mark Topinka's thesis

[Topinka, (2002)]. The basic steps are to put the sample in HCl followed by NH_4OH to

clean off any oxides that might be on it. Both of these should be diluted with water by a

factor of 5. The sample spends 5 seconds in each followed by a beaker of water. Then

put the sample into the etch mixture, which should be heated to 50 °C, for the desired

amount of time. The etch is quenched by putting the sample in water. The etch rates for

GaAs and AlGaAs are about 100 Å /s and 20 Å /s. In order to define the etch trenches

separating the active device area from the back gate contacts, I usually dip the sample in

the citric etch for 15 seconds. After etching, the PMMA can be removed by soaking the

sample in acetone.

2.1.6. Thermal Evaporator

There are two different thermal evaporating systems that we use. There is one

in the downstairs cleanroom for the Cr-Au gates and another one upstairs for the Ohmic

contacts[4]. Figure 2.3 shows both the inside and outside of the new evaporator in the

downstairs cleanroom. They both have fairly similar procedures to use them so I will

just give the general steps necessary to operate them. The first step is to dip the samples

in NH_4OH for 5 seconds to clean their surface, allowing the metal to stick to them better.

Then attach them with carbon paint to the Cu sample stage. Make sure that you use

the correct stage for the evaporator. Then go into the cleanroom and vent the chamber.

Load the stage and put the necessary arms, boats and metals into the evaporator. For

ohmic contacts you will need, Ni, Au and Ge. For the gates you need Cr and Au. Close

---

[4] With the continued purchase of equipment by CIMS the thermal evaporators are
constantly changing. Check the signs on the evaporators to know, which metals can be
evaporated.
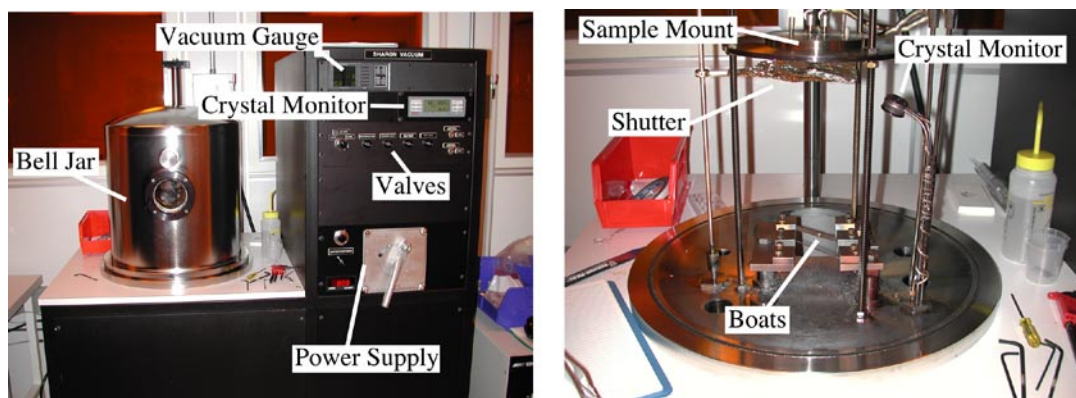
Figure 2.3 Shows the new thermal evaporator in the downstairs cleanroom used for depositing gates. The control system is shown in the left hand picture. The right hand picture shows the inside of the evaporator including the position of the boats.

the chamber and start the roughing pump. Once the pressure reaches 200 mTorr, close the roughing valve, turn off the pump and open the high vacuum valve. This starts the cryopump. Once the pressure reaches the 10^{-6} torr range, you can degas the filament for one minute. Now is also a good time to check the contacts on the boats. Slowly turn up the current and watch the boats. They should start to glow in the center first, if they glow at one end first this is a sign that there is a bad connection and you should reattach them. It is also necessary to heat up the Cr rod for about 30 seconds to let it outgas and remove the oxide from it. Once the pressure reaches a few times 10^{-7} torr you are ready to evaporate. This takes about 15 minutes in the new evaporator downstairs and about an hour in the one upstairs. Make sure that the correct parameters are set for the metal that you are depositing and then slowly turn up the current until it starts to evaporate. Once about 50 Å have been deposited, open the shutter and start the deposition on the sample. Once you have finished depositing metal, let the chamber cool for a few minutes and then close the high vacuum valve and vent it. Take out the sample stage and pump back down

the system for the next user. Remove the sample from the stage and put it in a beaker of acetone to lift-off the PMMA. You can check the progress of the lifting off in the optical microscope. However, the sample must stay in acetone or the PMMA will not lift off. If the PMMA is not lifting off, a small amount of time in ultrasound will help but be careful not to do it for too long or the metal may come off also.

For ohmic contacts the recipe that we use is the following: 50 Å of Ni, 50 Å of Au, 250 Å of Ge, 400 Å of Au, 100 Å of Ni and 400 Å of Au. This creates a eutectic mixture that allows for easy annealing of the contacts. For the gates, I usually deposit 100 Å of Cr then open the chamber and cover the device. Then I deposit a further 50 Å of Cr and 400 Å of Au on the pads for wirebonding. This makes it easier for the SPM tip to get into the device and avoids problems with the Au tending to form balls.

2.1.7. Annealing

After lifting off the excess metal and PMMA, the ohmic contacts are ready to be annealed. This is done with our thermal annealer that was built by Alex Rimberg and described in his thesis [Rimberg, (1992)]. It was originally built for annealing Indium contacts but is now almost exclusively used for NiAuGe ohmics. Figure 2.4 shows the basic setup of the annealing system. There is a cylinder of forming gas, (80% He/20% H) which flows through the box to keep the sample from oxidizing during the annealing process. The gas flow rate should be adjusted so that the bottom of the silver ball is at the 3 on the flow meter. The sample sits on a strip of Nichrome that is heated using the two transformers. The only change to the annealer is that the Nichrome was replaced and the thermometer underneath was reattached[5]. The recipe for annealing the samples
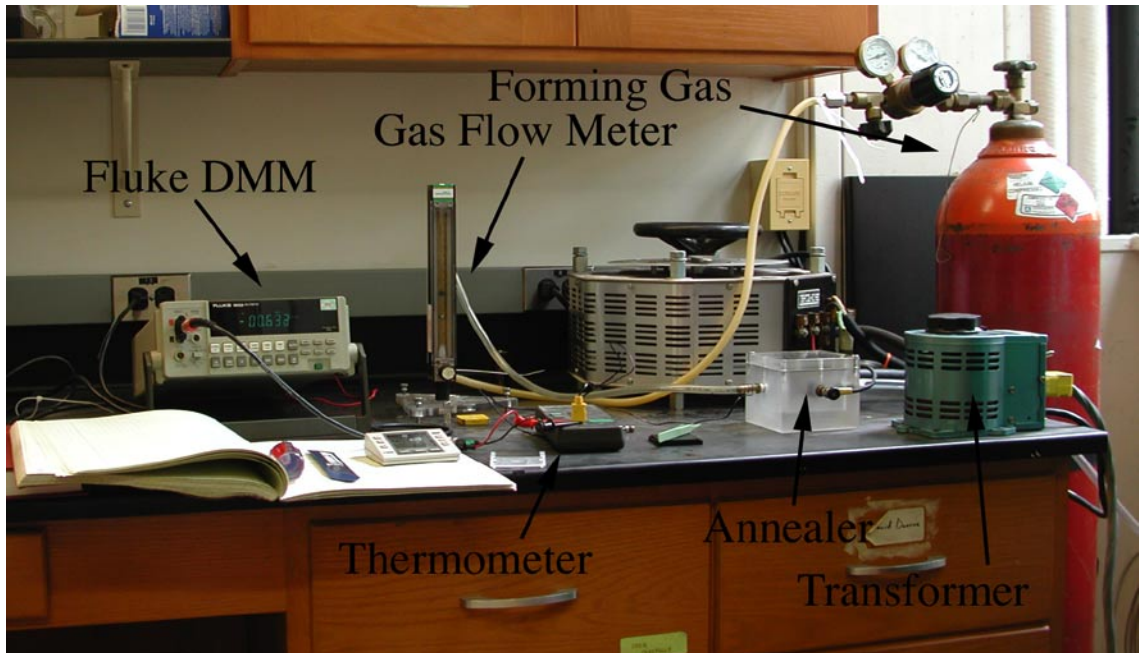
Figure 2.4 The thermal annealing setup is shown with the forming gas, thermometer and transformer.

is as follows: one minute at 110 °C to boil off any water vapor, 10 seconds at 260 °C

to warm everything up followed by 10 seconds at 380 °C. This last step is the critical

one because it is when all of the annealing takes place. For the samples with a back

gate, it is very important not to exceed 380 °C because the ohmics tend to anneal too

much and contact the back gate making the sample not usable. However, it is necessary

to get the temperature to 380 °C because this is just above the temperature where the

Au/Ge mixture melts. To get a faster reading of the temperature you can attach a Fluke

multimeter to the two pins of the thermometer and measure the voltage. It is usually a

---

[5] The Nichrome strip was bought from MWS Wire Industries, 31200 Cedar Valley Dr. Westlake Village, CA 91362. There still remain many feet of it for future use. It is a too thick for the transformers to be able to heat sufficiently so it has to be thinned before being used. The thermometer was spot welded to the back of the strip in the student shop in Lyman.

good idea to rotate the sample by 180 degrees and repeat the process to ensure that the

contacts are well annealed. Using this recipe will not produce ohmics that look like

cheese pizza as occurs for higher temperatures[6]. I have found that this recipe produces

working ohmics nearly every time and they are never shorted to the back gate. If testing

the ohmics for shorts to the back gate at room temperature it is important not to have light

on the sample. Since the GaAs is photoconductive, a false reading of the resistance will

be obtained.

2.1.8. Wire bonding

The last step in preparing the sample is to attach it to the sample holder and wire

bond to all of the pads. The arrangement of the pads and wire bonds is very important

because none of the wires can cross the device. If this occurs the tip will not be able to

reach the device. Figure 2.5 shows how the sample is mounted on the sample holder.

First a piece of lens paper is put on the sample holder using GE varnish to insulate the

sample from the holder. The sample is placed on top of this with the device near the

center. To make the arrangement of the wire bonds simpler, all of the bonding pads are

placed along the bottom of the sample. Then the gold wire can just go from the sample

holder to the pads. There are a total of 12 pads on the sample holders for both the He-3

and He-4 SPMs.

To get the wire bonder to work properly, it is necessary to thread the gold wire

correctly. For the tips that we use, the wire should go under the spool and into the second

---

[6] Other theses said that this was the look of ohmics that were well annealed and that
worked.
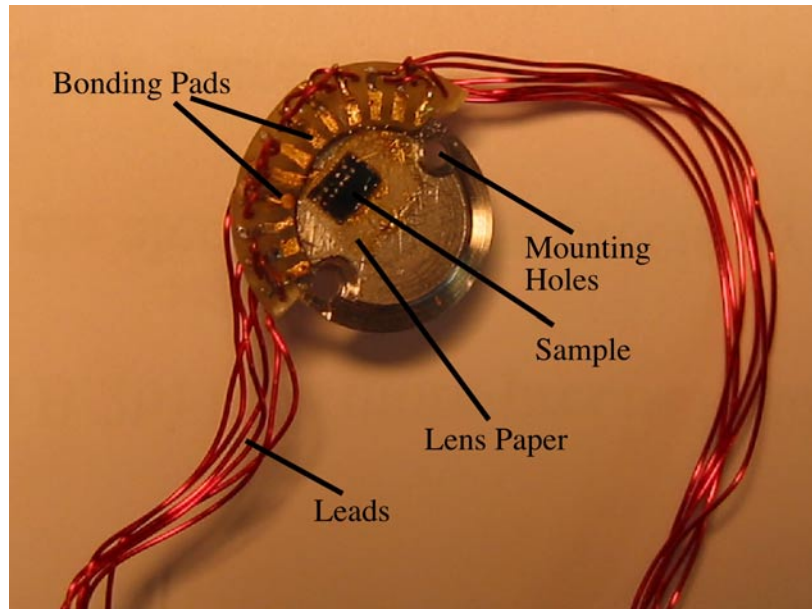
Figure 2.5 Sample holder for the new He-3 SPM showing the position of the sample and bonding pads.

hole on the arm, the one farthest from you. Then it goes down and through the clamp and into the tip. Make sure that the heater is on to heat the sample to 80 °C. It works best to use a medium setting on the force, the maximum time and 2.0 on the power. Sometimes, the power can be turned higher for the bonds on the sample holder. In order for the bonds to work, a small section of gold should be sticking out of the tip before starting to make a bond. If the wire does not feed properly between bonds, the tail adjustment can be changed to increase the amount that feeds.

2.1.9. Coating Tip

The one other time that we need to use the evaporator is when coating the tip with Cr. During the course of the deposition it is necessary to rotate the tip in order to uniformly coat it. This evaporation is done in the "clean" Sharon evaporator in the

upstairs cleanroom because it has a rotating feedthrough. Figure 2.6 shows the stage used

to rotate the tip in the evaporator. The stage attaches to the evaporator the same as the

ordinary stages but there has to be another connection made to rotate it. This is done by

a flexible braid that attaches to both the stage and the rotating feedthrough. The Cr rod

should be positioned as near to the edge of the evaporator as possible to get a good angle

to coat the tip. This ensures that the Cr comes from the side and not directly below the

tip. I coat the tip with 100 Å of Cr, rotating the stage about one revolution per 5 seconds.

The tip has to be mounted so that only the end of the cantilever is coated. If

both arms of the cantilever are coated the resistance will change. This makes the

piezoresistive cantilevers not work anymore because the Cr determines their resistance

instead of the piezoresistive Silicon. This failure shows up when the cantilever is put in
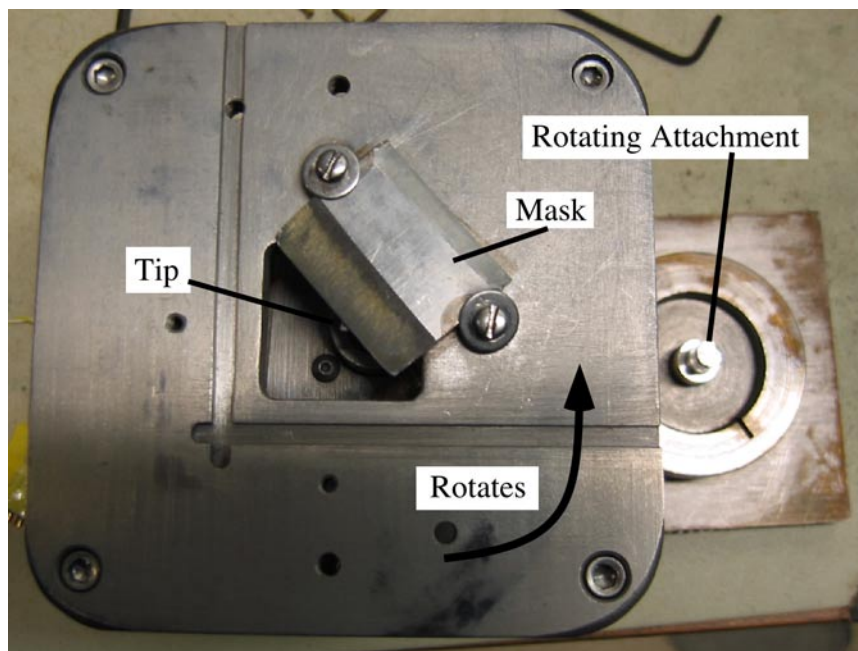
Figure 2.6 Mounting stage for coating tips with Cr. This stage attaches to the evaporator
and can be rotated using a feedthrough. The cantilever is positioned so that all but the
very end is covered by the mask..

28

the whetstone bridge and the measured signal is very noisy. To avoid this problem only a small section of the cantilever is exposed beyond the end of a piece of the metal mask. The position of the cantilever can be adjusted in all three directions by screws on the rotating stage. This is done while looking through a microscope in order to minimize the amount of the cantilever that is exposed.

2.2. He-4 System

Most of the design of this system is covered in the theses of Mark Eriksson and Mark Topinka [Eriksson, (1997); Topinka, (2002)]. Therefore this section will just highlight some of the important considerations when using this SPM. Figure 2.7 shows the He-4 SPM's cryostat. It consists of a large vacuum space for the SPM along with helium and nitrogen reservoirs. There are three electrical feedthroughs into the vacuum space along with a rotating rod that is the coarse approach mechanism. One of the connectors is a 24 pin Fischer connector for the leads going to the sample. Only twelve of these leads are wired all the way to the sample. The second connector is an 18 pin Fischer connector that goes to the cantilever bridge circuit, LED, and the two thermometers. The last connector is for the high voltage lines going to the piezotube.

Since the SPM is in vacuum, care must be taken to properly heat sink all of the leads that come into the dewar. This is accomplished through the use of high resistance wire, which has a low thermal conductivity. After a section of this wire, there are copper wires wrapped around copper spools attached to the cold plate. This thermally anchors the wires at the temperature of the cold plate. The heat sinking of the coarse approach rod is more difficult because of the requirement that it can rotate. Specially designed

29
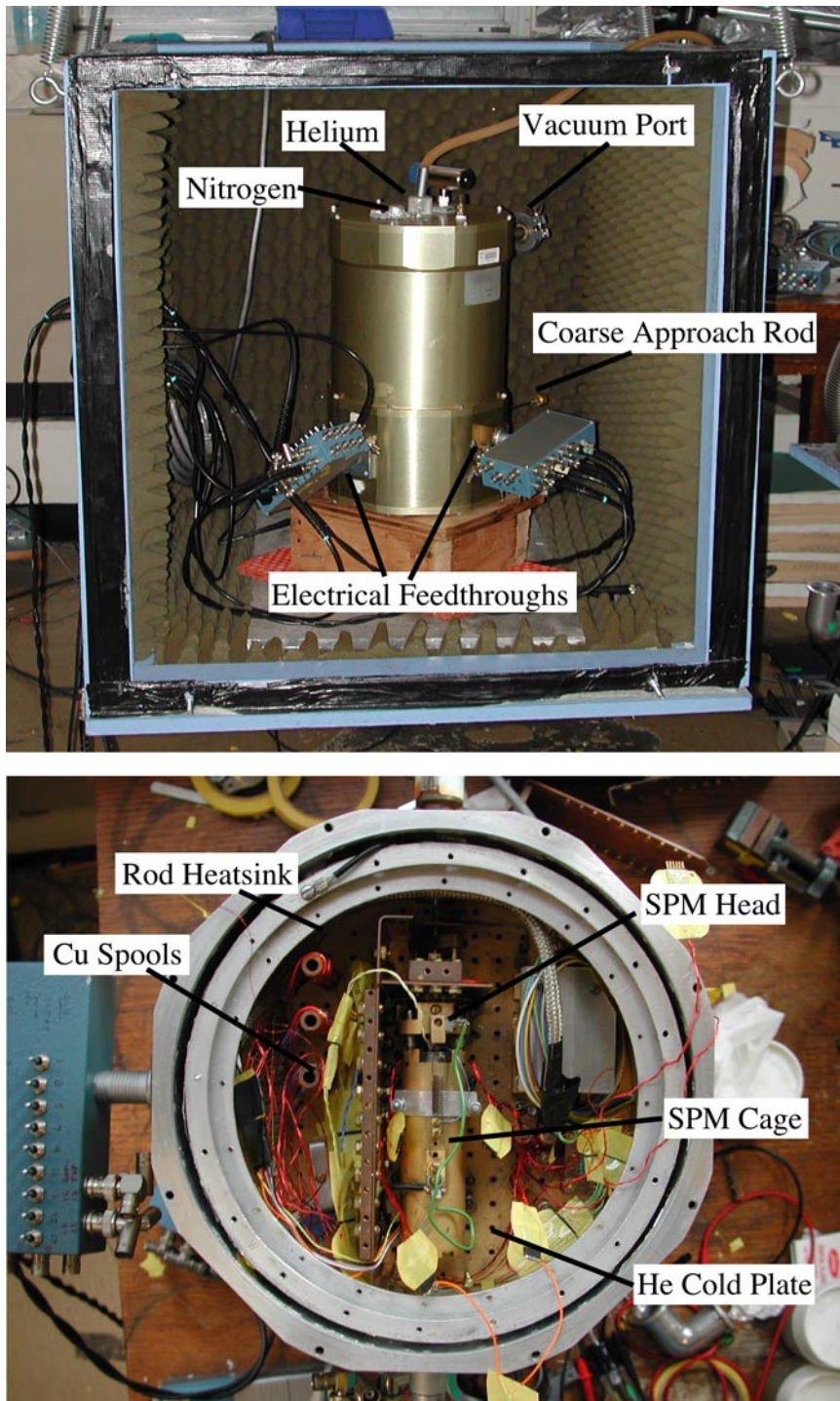
Figure 2.7 The top picture shows the outside of the He-4 cryostat with the cryogen spaces and feedthroughs indicated. The bottom picture shows the inside of the cryostat with the SPM in place.

clamps were built to heat sink the rod to both the liquid nitrogen bath and the He cold

plate. Figure 2.8 shows the design of these two clamps. The clamps are a piece of

copper with a hole drilled out for the rod to slide through. Then a slit is cut through the

piece and a screw hole drilled into it so it can be screwed down tightly to the rod. Then a

thick copper wire goes from this piece to the cold plate. This design gives a large contact

area between the rod and clamp while still allowing the rod to rotate.

The cooling procedure for this cryostat is fairly complicated compared to the

new He-3 system due to the vacuum space and nitrogen jacket. After aligning the

SPM, the radiation shields have to be put on. There are two radiation shields, one at He

temperature and another at Nitrogen. Then the top must be put on taking care to make a

good vacuum seal with the large O-ring. Then the cryostat has to be flipped over before

pumping out the vacuum space. It is a good idea to check that the position of the SPM

has not moved significantly during the process of flipping the cryostat. It takes around 90

minutes to two hours to pump out the cryostat with the turbopump cart. Then it can be
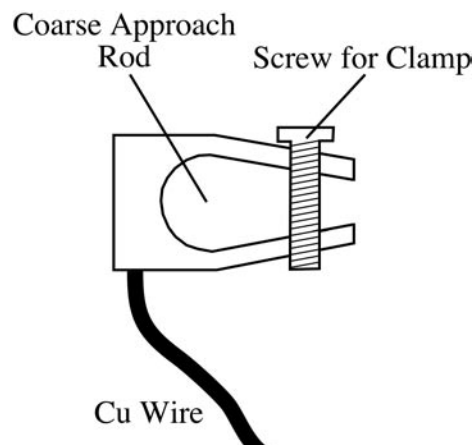
Figure 2.8 Design of clamps that go on the coarse approach rod. The clamp is slid on
the rod and then tightened using the screw. The Cu wire is attached to the cold plate to
thermally anchor the rod.

filled with liquid nitrogen in both the Nitrogen jacket and the helium space. After about two hours it will have cooled enough that helium can be put into the center space. An indication that it is cold is when there is no longer frost on the cover of the helium space. First blow out all of the Nitrogen so that solid nitrogen does not form in the Helium space causing the cryostat not to cool. Then fill it with Helium. It takes about two more hours for the SPM to reach 4.2 K. Once everything is cold, the Helium and Nitrogen last about 12 hours before needing to be refilled. The helium can be pumped on to lower the sample temerature to 1.7 K. However, when doing this, the helium only lasts about 8 hours.

2.3. He-3 System

This section describes our group's new SPM, which was built to achieve lower temperatures than accessible with our Helium-4 system. The goal was to be able to reach 400mK with this system but unfortunately we have not run it yet as a Helium-3 system. Even, as a Helium-4 system it has several advantages over the older one. This cryostat has a superconducting solenoid, which provides a perpendicular field that is rated up to 7 Tesla. In the initial test of the magnet, I was able to run it above 8 Tesla without it quenching. It also has the ability to use a magnet providing a parallel field of up to about 3 Tesla. It also has a much longer hold time, from initial tests it appears that the dewar can go for about 60 hours without refilling. This is compared to only 12 hours with the old system, which uses both Helium and Nitrogen. The last significant advantage is the turn around time, it is now possible to change a sample within just a couple of hours as compared to almost two days with the old system.

2.3.1. Cryostat Design

The design of the cryostat was modeled from the other two He-3 cryostats that our group uses. Figure 2.9 is a drawing of the dewar and the support structure for holding the magnet. The dewar has a superinsulation jacket with a 15 liter belly for holding the liquid helium. There is a small well that the magnet sits in with the SPM inside. We built the dewar fairly tall to lengthen its neck and thus lessen the heat load down the dewar due to radiation. The magnet support is built around three stainless steel tubes that attach to a support plate at the bottom. As you go down the magnet support there are a series of Cu baffles to reduce the radiation on the Helium.

The Helium-3 insert is shown in Figure 2.10. It is a very simple design, which has a small vacuum can at the bottom with a condensation neck just above. This vacuum can was pumped out before the first use and sealed by crimping and soldering the Cu tube[7]. The idea behind the insert is that He-3 gas comes down the insert and hits the condensation neck immersed in pumped He-4, which liquefies the He-3 and it falls into the bottom of the vacuum can. In the vacuum can, it is isolated from the He-4 so it can be further cooled. Once all of the He-3 is liquefied, it is pumped on to reduce its temperature down to about 400mK. The insert is made of thin walled stainless steel, 0.020", to minimize the heat load on the He-4 bath. The cryostat, magnet support and He-3 insert were built by Precision Cryogenics[8].

The magnet support piece has been wired for a superconducting solenoid. There

---

[7] We had a lot of trouble finding the proper tool for making the crimp seal. We finally borrowed one from Dave McCarthy at Varian Vacuum, 800-882-7426 ext 5768. The tool is made by CHA Industries and its part number is POD-375. I practiced making the crimp seal on another piece of copper tubing and it worked all 10 times that I tried.
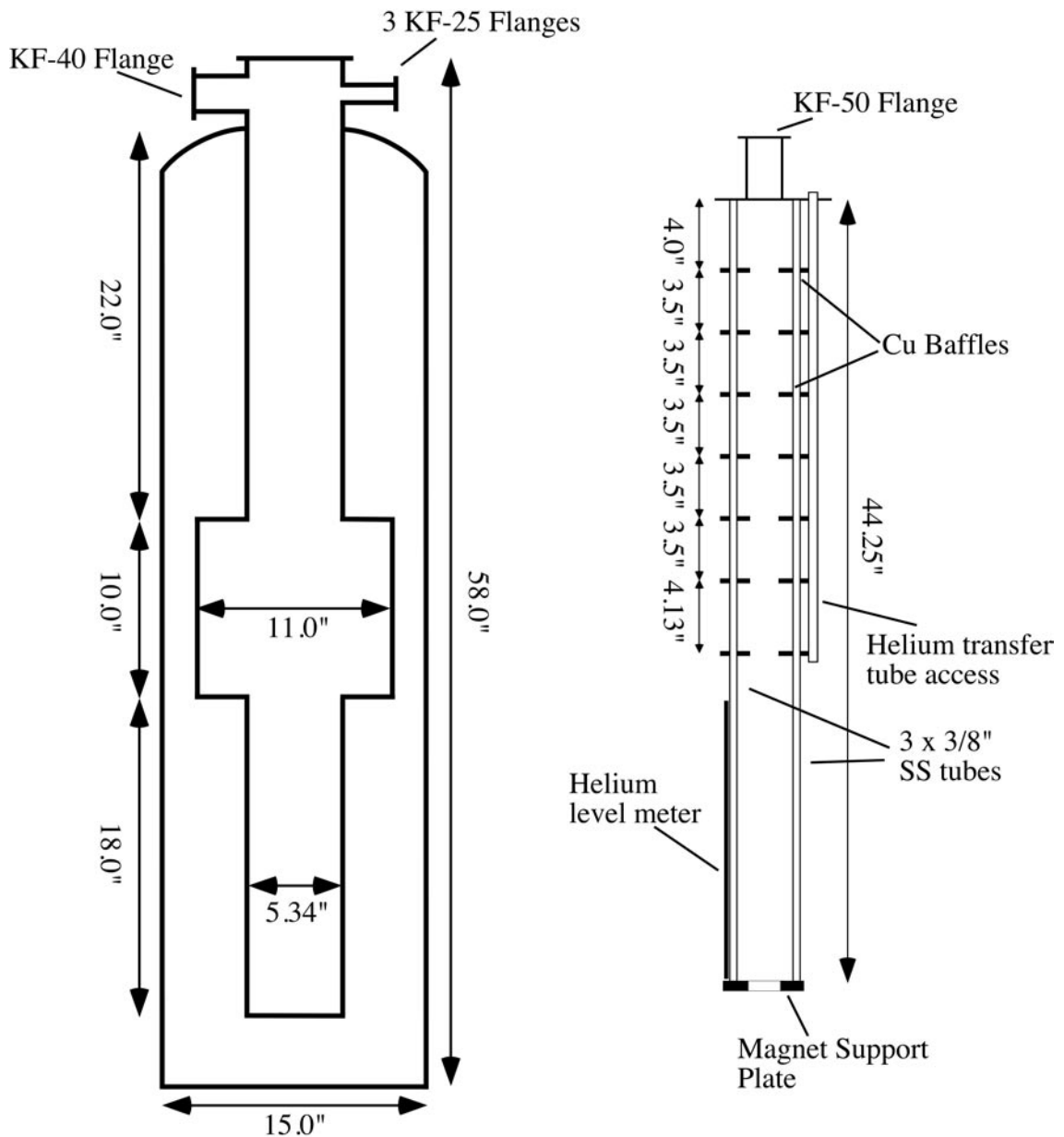
Figure 2.9 Drawing of the He-3 SPM cryostat and the magnet support. The cryostat has a superinsulation jacket with a 15 liter belly for the liquid Helium. The magnet support piece has 3 stainless steel tubes supporting the magnet with 7 Cu baffles to reduce the radiation.

---

[8] Precision Cryogenics, 7804 Rockville Rd, Indianapolis, Indiana 46214. Our group has had good luck with their work in the past but on this project they forgot to drill a hole in the bottom piece of the magnet support. So there was no way for the He-3 insert to go all the way into the cryostat.
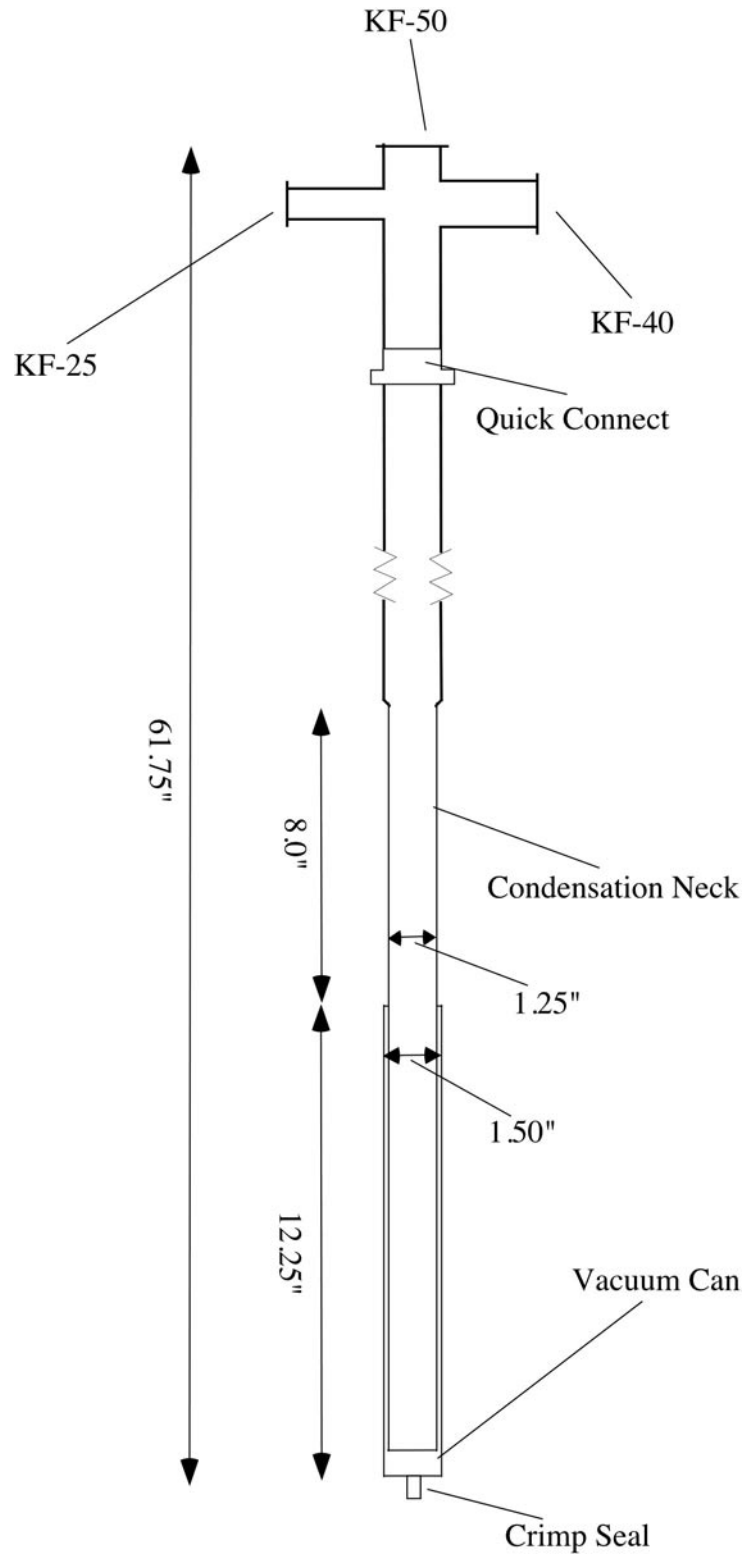
Figure 2.10 Shows the design of the He-3 insert. There is a small vacuum can at the bottom, which isolates the He-3 from the He-4 bath. The quick connect allows the height of the insert to be adjusted.

is currently a magnet that gives a field perpendicular to the sample but we are in the process of buying another magnet that gives a parallel field. The magnet leads are made from brass shim, which wraps around the outside of the support structure. Each shim goes halfway around the support structure and is covered by polyester to keep it from shorting. The magnet support also includes three 330 Ohm Allen-Bradley diagnostic resistors to use when cooling down the dewar. They are located at the top of the magnet, the bottom baffle and the top one and measure 494 Ω, 446 Ω, and 384 Ω respectively at room temperature. The last piece of equipment on the magnet support is a 17" Helium level meter from American Magnetics Inc[9]. Figure 2.11 shows the wiring diagram for the level meter and diagnostic resistors. The two ten pin connectors are color coded for the
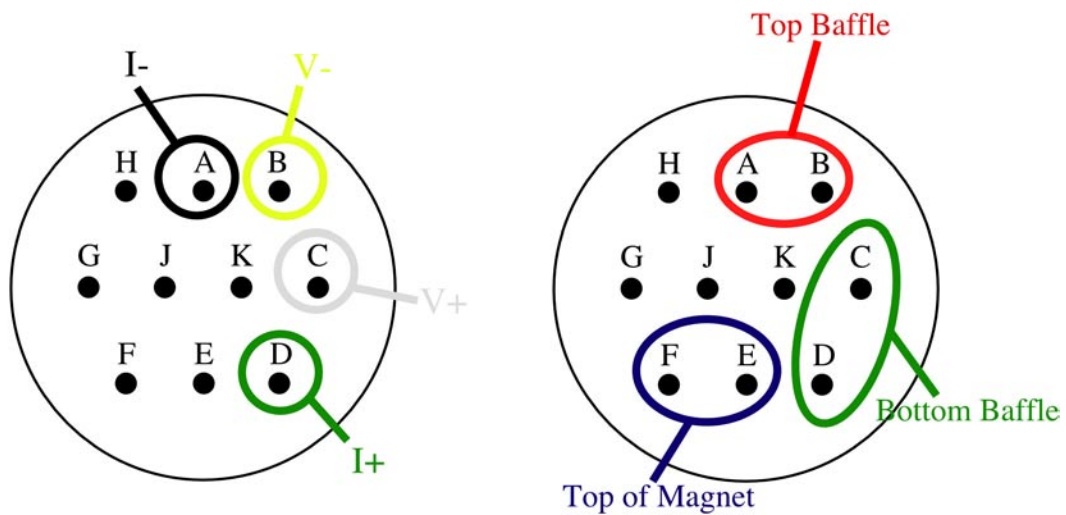
Figure 2.11 Shows the wiring layout of the two connectors on the magnet support piece of the new He-3 SPM. The left connector goes to the helium level meter and is labeled red. The right connector is labeled green and goes to the diagnostic resistors that are useful when filling the cryostat with nitrogen.

---

[9] American Magnetics Inc., P.O. Box 2509, 112 Flint Road, Oak Ridge, TN 37831-2509.

resistors, green, and the level meter, red.

2.3.2. Sample Stick

The last piece of the cryostat design is the sample stick, which goes inside the He-3 Insert. Figure 2.12 shows the sample stick with the connectors at the top, wires running along the central tube and a gearbox for the coarse approach rod. There are three connectors on the tip of the stick, which go to the sample, piezotube and miscellaneous low voltage connections. Figure 2.13 shows the layout of the three connectors at the top of the sample stick. The sample leads come from a 24 pin Fischer connector[10]. There are currently 12 leads wired all the way to the bottom of the stick but the other 12 are wrapped up near the top of the stick for future use. The sample leads are grouped into 3 sets of 36 gauge Quad Lead phosphor bronze wire from Lakeshore Cryogenics[11]. There are seven high voltage lines of which 5 are used by the piezotube. The other two lines can be used for oscillating the tip or other high frequency applications. Each of the high voltage lines is wired with ultra miniature Stainless Steel coax to accommodate both high voltage and high frequency. The last set of wires is for the cantilever bridge circuit, an LED, and other diagnostic wiring. There are a total of 10 of these 36 gauge phosphor bronze wires of which 6 are currently used. Perhaps the most difficult aspect of the sample stick was the construction of the coarse approach rod for the SPM. Since we need to be able to turn one of the screws of the SPM head when it is cold, we need a long rod to reach the bottom of the insert. We need to be able to set the height of the tip

---

[10] Fischer Connectors, Atlanta, GA 30346, www.fischer.com

[11] Lakeshore Cryotronics, 64 East Walnut St., Westerville, OH 43081 Quad Lead Wire QL-36, Coaxial Wire CC-SS and phosphor bronze wire NM-36.
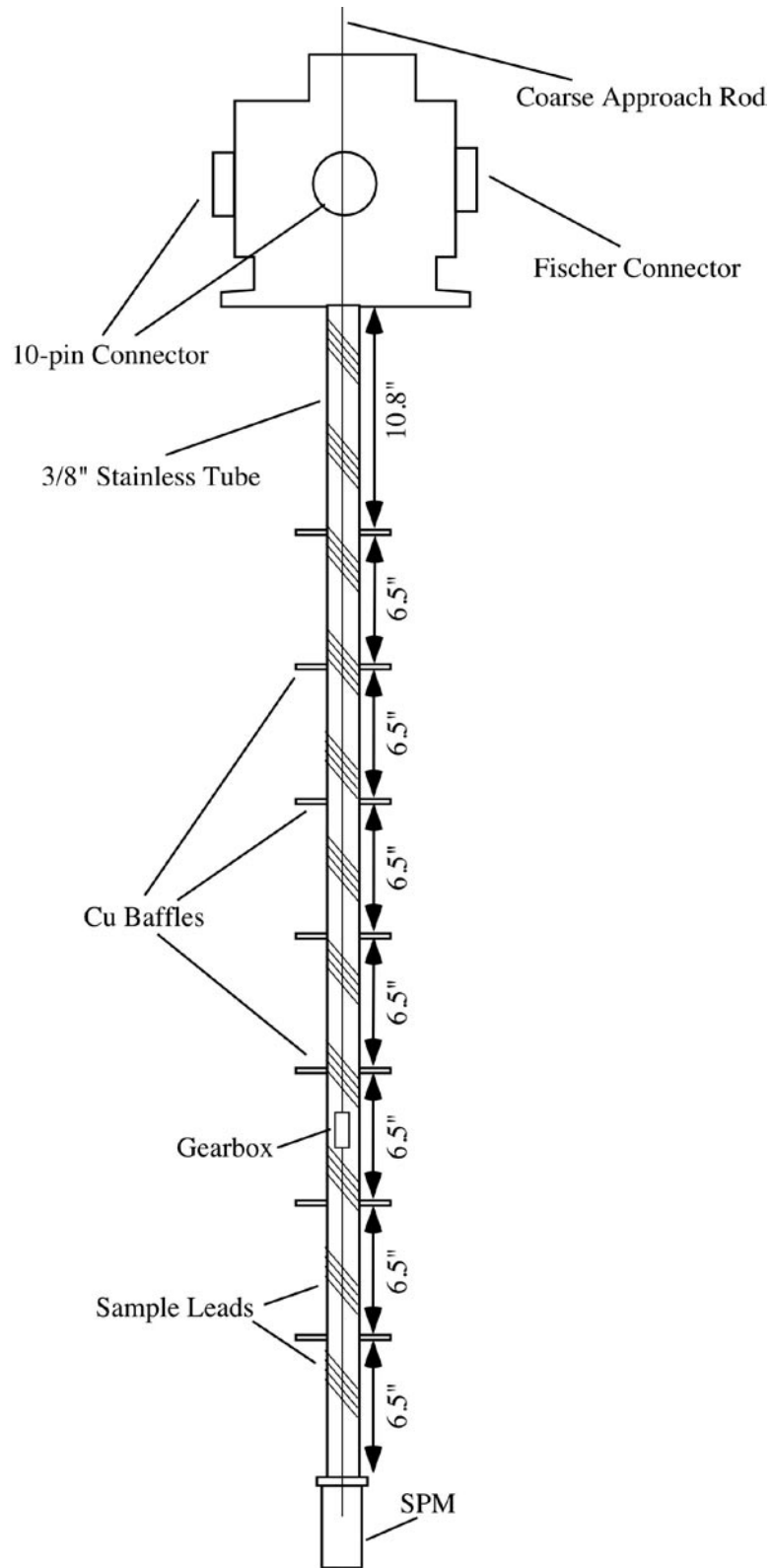
Figure 2.12 The design of the He-3 sample stick. The SPM is at the end of a 3/8"
stainless steel tube. There are seven Cu baffles along the stick. The top has three
connectors.
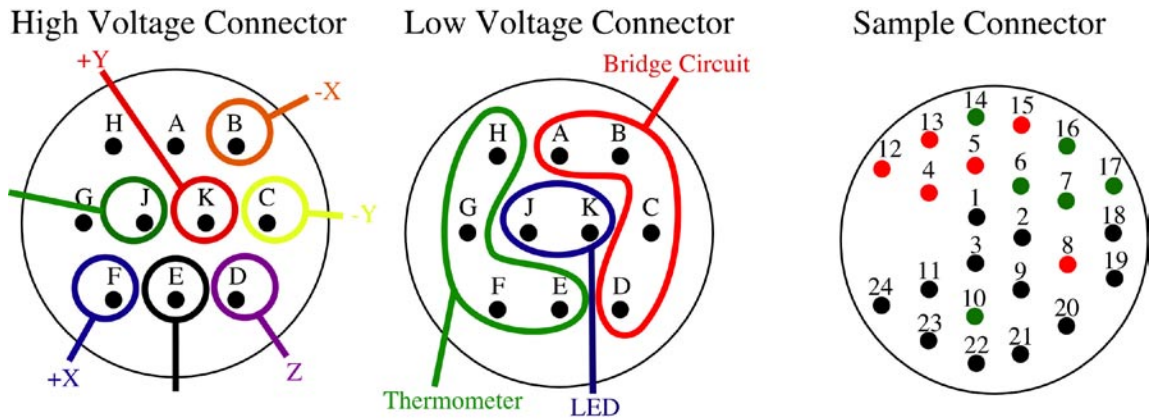
Figure 2.13 Wiring layout for the three connectors on the sample stick. The high voltage connector's lines go to the piezotube. The low voltage connector goes to the cantilever bridge circuit, an LED, and a thermometer. The sample connector has 12 of its lines wired to attach to the sample.

with micron accuracy, which requires sub one degree accuracy on the screw. The only way to be able to turn with precision the screw at the bottom using a thin-walled stainless steel tube required the use of a small gearbox. We bought a gearbox from Faulhaber[12] and broke it open. After doing this all of the parts were cleaned to remove any lubricants. Then it was reassembled and put about 3/4ths of the way down the sample stick. The gearbox does not turn as well as it did with the lubricants but more importantly it now turns at Liquid Helium temperatures. A change from the He-4 system is the number of turns necessary on the coarse approach rod, now to turn the equivalent of two turns off of the surface in the He-4 system you have to turn the rod 32 turns because of the 16:1 ratio of the gearbox. It may be a good idea to buy a motorized encoder to turn the rod instead of doing it by hand because of the number of turns required.

The last aspect of the SPM system are the two pumping systems. One of these is

---

[12] Faulhaber, 14881 Evergreen Avenue, Clearwater, FL 33762 Series 10/1 planetary gearhead with a 16:1 reduction ratio

for pumping on the He-4 bath to cool it to 1.7K. This is necessary so that the He-3 gas will liquefy as it passes the condensation neck. The second system is for pumping on the He-3 to further cool it to around 400 mK. This system must be leak tight and have the exhaust go back into the He-3 dumps so as not to lose the valuable He-3 gas. The He-4 system consists of an Alcatel 2033SD pump, which is a two-stage rotary vane pump capable of pumping 33 m³/hr[13]. This is connected to the cryostat via a KF-40 tube with a pressure gauge on this line. The pressure gauge is a Leybold DV1000 diaphragm gauge. This gauge is used since its reading is insensitive to the composition of the gas. The He-3 gas handling system is essentially a copy of the previous system that we have for the group's other He-3 cryostats [Hopkins, (1990)]. However, the pump has been changed to an Alcatel 2015H1, which is a sealed rotary vane pump. The capacity of the dumps has also been increased to 50 L to accommodate the larger volume of He-3. There is a total of 40 liters of He-3 in the system giving a reading of 775 mbar on the gauge.

2.3.3. Scanning Probe Microscope

The SPM attaches to the bottom of the sample stick by three screws. Figure 2.14 shows the brass cage of the SPM. We used the same design for the SPM as in the He-4 system except this one has a smaller diameter to fit it inside the He-3 insert. The diameter has been reduced from 1.25" to 1.125" and the sample wires must now go along the slots in the side of the cage. The piezotube is 3" long giving a scan range of between 14 and 20 microns for an applied voltage of ±200 Volts at liquid Helium temperatures. The tubes

---

[13] Alcatel Vacuum Products, 67 Sharp St., Hingham, MA 02043
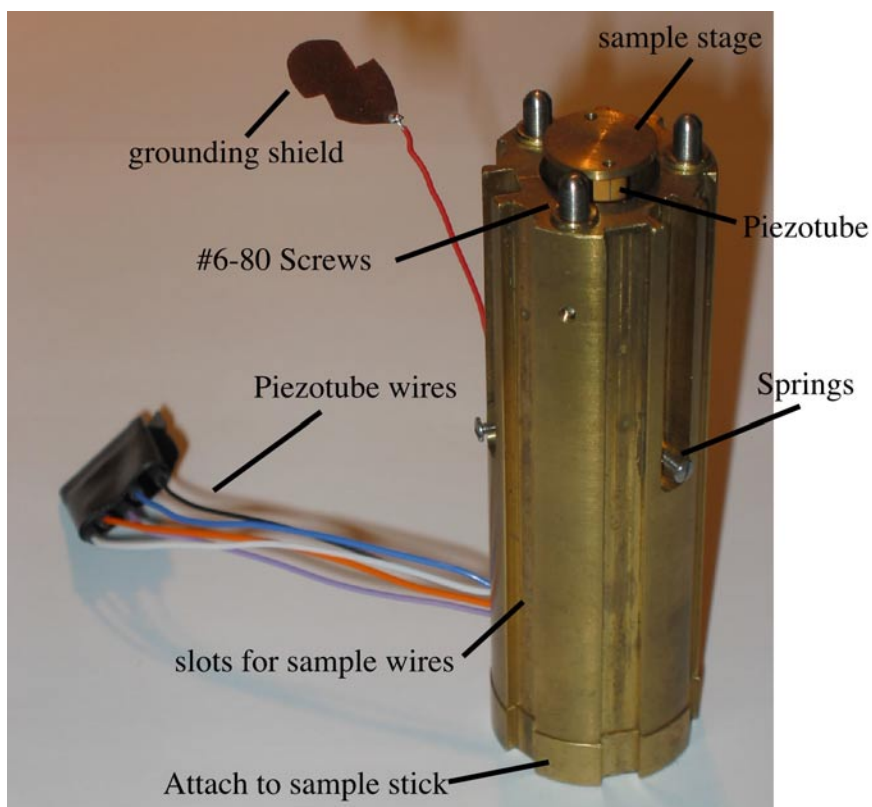
Figure 2.14 Picture of the cage of the new He-3 SPM. The 3" long piezotube is inside and attaches to the bottom. The sample sits on the end of the piezotube. There are three slots for springs along the side that attach the SPM head to the cage. The three #6-80 screws set the height and tilt of the head.

are coated with Au for attaching wires to the quadrants and are bought from Staveley

Sensors[14]. An Au coating is now used so that the tubes are non-magnetic and can be used

in high magnetic field. Extreme care should be taken when handling the tubes because

even small vibrations can cause them to crack. These cracks are not visibly apparent but

usually manifest themselves as a very large hysterisis at room temperature and/or a large

drift when cooling.

---

[14] Staveley Sensors 91 Prestige Park Circle, East Hartford, CT 06108-1918. The most recent price of the tubes was about $350 each. Sometimes when you ask for a quote the price is considerably higher but if you tell them how much you have paid in the past they will generally lower it.

Figure 2.15 shows the head of the SPM with a tip in place. The head is held in contact with the cage by three springs, which attach to the hooks. There are three #6-80 screws that set the height and tilt of the tip and rest in the grooves of the head. Alignment in the x, y direction is done at room temperature by turning the two adjustment screws on the side of the head. Only the screw for adjusting the height needs to be turned at low temperatures so this is the one that must be aligned with the coarse approach rod. The cantilevers are Piezolevers from Park Scientific Instruments[15]. We coat the ends of the cantilever with chrome to create a conducting tip to use in imaging electron flow.
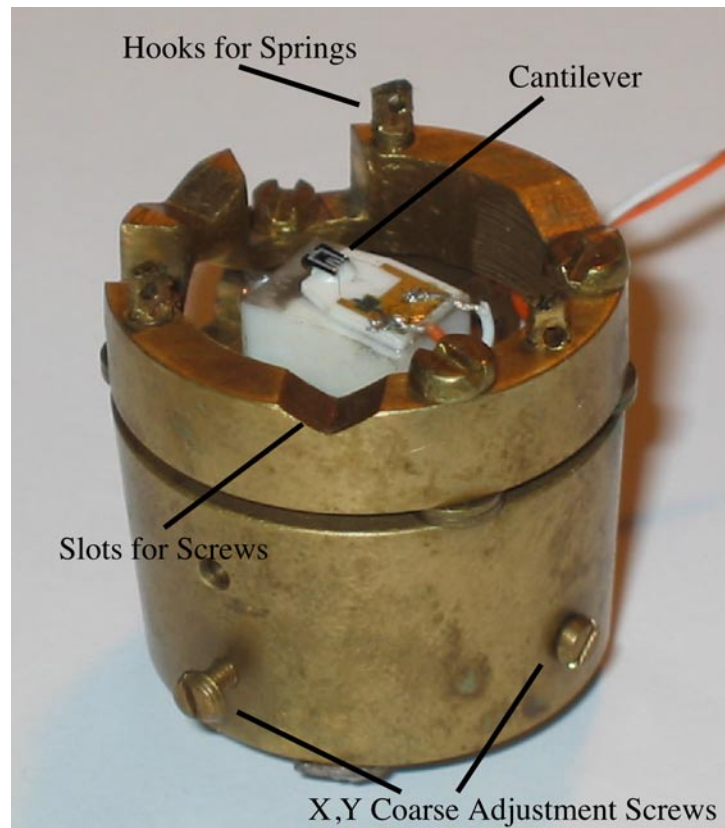
Figure 2.15 The head of the He-3 SPM. The tip sits on the end of a movable shuttle whose position is controlled by the two coarse adjustment screws. There are three hooks for springs to keep the head attach to the cage. There are also three slots for the screws to rest in that adjust the height and tilt of the cantilever.

The real test of any SPM is whether it can take good images. Figure 2.16 is a topographic image of a test pattern. This image was taken in the He-3 system. We have also taken images with a perpendicular magnetic field of 7 Tesla and saw no evidence that the magnetic field affected our ability to acquire images.

2.4. Electronics

The other main aspect of building the new SPM is the electronics to control the piezotube and sample. There has been a considerable effort to build the electronics necessary for the new SPM as well as updating the ones on the He-4 system. The
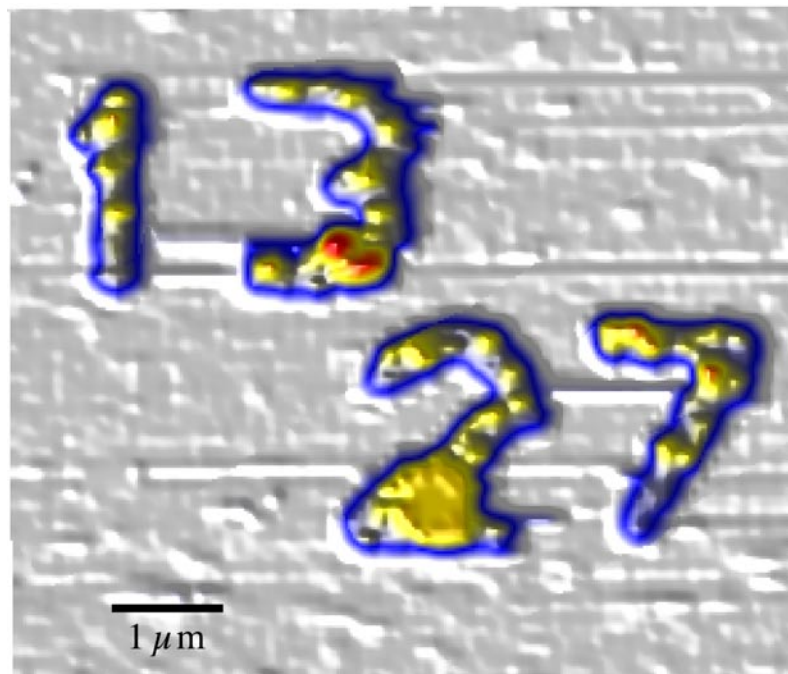
Figure 2.16 Topographic scan showing an image in the new He-3 system. The image is of one of the alignment markers.

[15] Over the course of my time in the lab, Park has been bought twice and is now part of the Digital Instruments group of companies. The website for information about the cantilevers is www.spmprobes.com

electronics for running the two SPMs are nearly duplicates of each other. This allows

for a simple interchange from one SPM to the other. Figure 2.17 shows the electronics

racks that control the He-4 microscope. The high voltage electronics on the right hand

rack control the movement of the piezotube. The left hand rack is responsible for

signals going to and from the sample, cantilever feedback and low voltage signals for the

piezotube. Each of these electronics elements will be discussed in detail in the following

subsections.
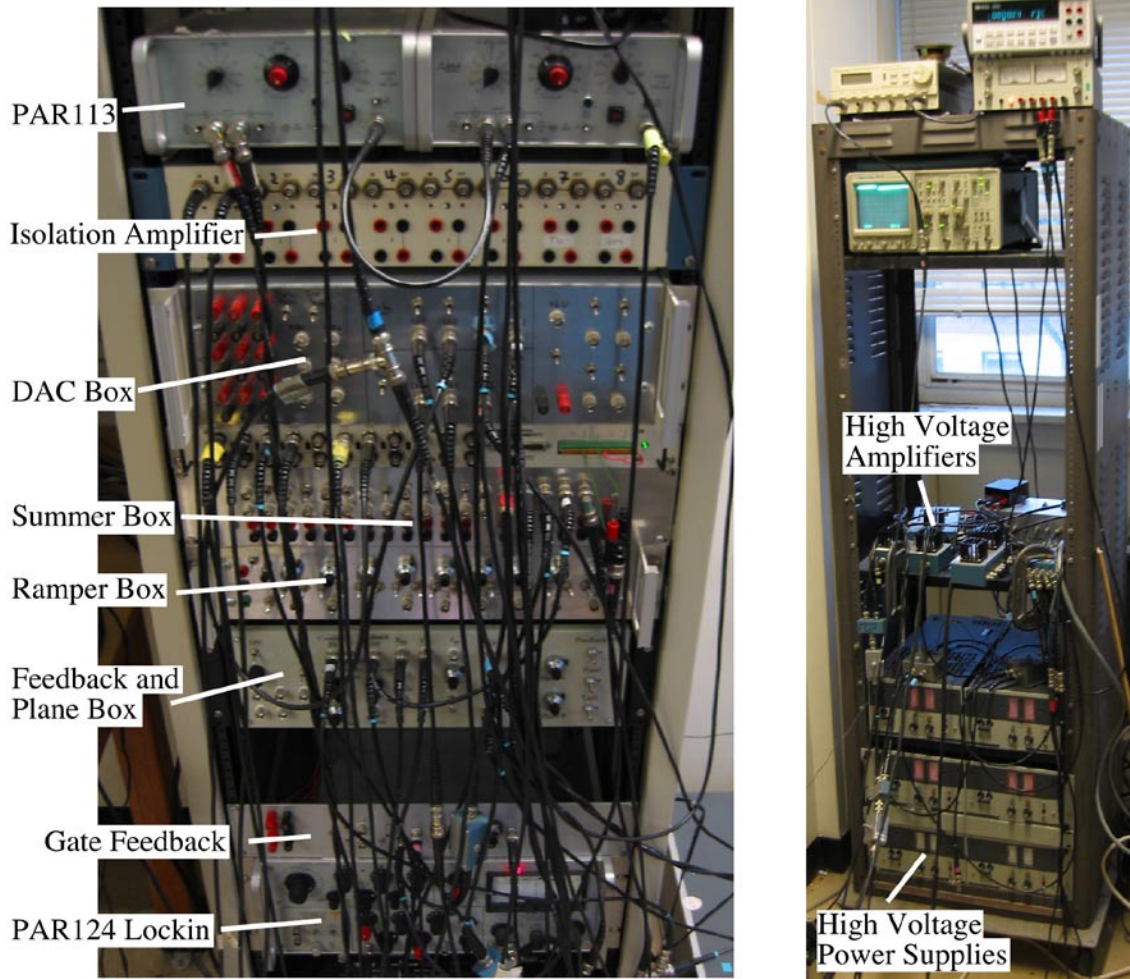
Figure 2.17 Two racks of electronics for running the SPMs. The left hand rack includes the low voltage electronics for the piezotube, tip and sample. The right hand rack has the high voltage electronics for powering the piezotube.

2.4.1. Digital to Analog Convertor Box

This is the main box for controlling the experiment via the computer. It is responsible for the x,y and z movement of the tip and the voltages on the gates and tip. It is programmed by a PCI digital output board made by National Instruments[16]. This board is capable of outputting 32 digital signals of which we use 22 for the control of the experiment. The lab now has two versions of this converter box. The old one is capable of outputting eight analog channels, is run off of batteries and is layed out on a homemade circuit board. The new box is capable of outputting 16 channels, runs off of two DC power supplies and was built on a professional printed circuit board.

Figure 2.18 sketches the main circuit diagram showing the isolation and conversion circuits. The digital signals go from the computer to the DAC box and then inside the box each of the lines goes through a digital isolator chip, (Burr-Brown ISO150[17]) which isolates the ground of the computer from the ground of the box. These chips capacitively couple the input to the output. This means that they are sensitive to changes on the input level making them rather tricky to work with. It is necessary to filter the input lines to remove any ringing on them due to the cable and to make sure that the voltage does not swing outside of 0 to 5 volts. This filtering is accomplished by the 1000 Ohm resistors at the input of each chip, which act as low pass filters with the input capacitance of the ISO150s. The 220 Ohm and 330 Ohm resistors ensure that the voltage stays within the range 0 to 5 Volts. From the isolators the 16 data signals travel to the AD669 analog to digital converter made by Analog Devices. These are 16bit converters

---

[16] National Instruments, www.ni.com PCI-DIO-32HS

[17] Burr-Brown (Texas Instruments) ISO-150

45
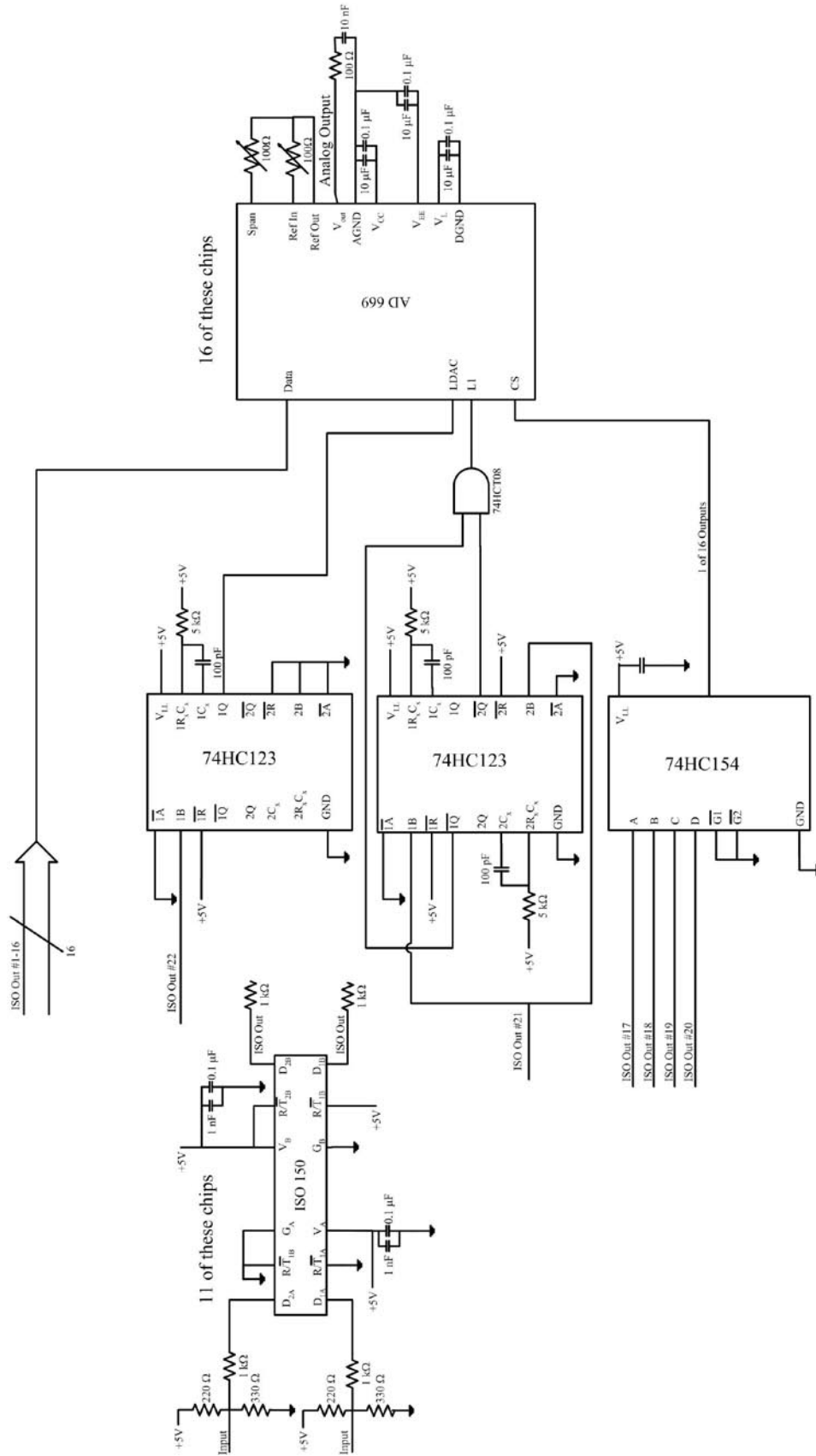
Figure 2.18 Schematic diagram of the DAC box circuit. Each input line goes through the ISO 150 as shown. Then the lines go to the converters, address decoder and control logic.

46

with a settling time of 8µs. They are double buffered with separate run (LDAC) and load

lines (L1 and CS) allowing the simultaneous updating of all the channels. This means

that we are able to update all the channels at 100kHz.

In order to achieve this fast update rate it is necessary to be able to selectively

load data into each chip. This is accomplished using four of the input lines as a binary

address, which is decoded by the 74HC154 chip. From this chip each of the decoded

lines runs to one of the load pins of the AD669. The last two input lines are used for

loading and running the AD669. The LDAC line goes through a one-shot, (74HC123)

which converts a transition from low to high to a pulse. The length of the pulse is

controlled by the resistor and capacitor on the one-shot. The last input is the L1 line,

which should load new data each time it transitions. To accomplish this it goes to two

one-shots, one creating a pulse on low to high transitions and the other on high to low.

These two pulse are passed through an and gate (74HC08) to get the resulting pulse each

time the input line transitions.

To better illustrate the timing of a load sequence Figure 2.19 shows three of

the lines. The blue trace is one of the data bits transitioning from low to high. A short

time later (caused by the time to decode) the red address line goes low. The green line

also goes to the AD669 chip and controls the transparency of the latch. When both the

red and green lines are low, the latch is transparent. When one of them goes high, the

data present at that time is latched. The length of time that the green line stays low is

controlled by the one-shot (74HC123). So the data present when the green line goes

high is loaded into the converter. Figure 2.20 shows the entire sequence of loading

three values of data followed by a conversion. The chip that we are looking at has data
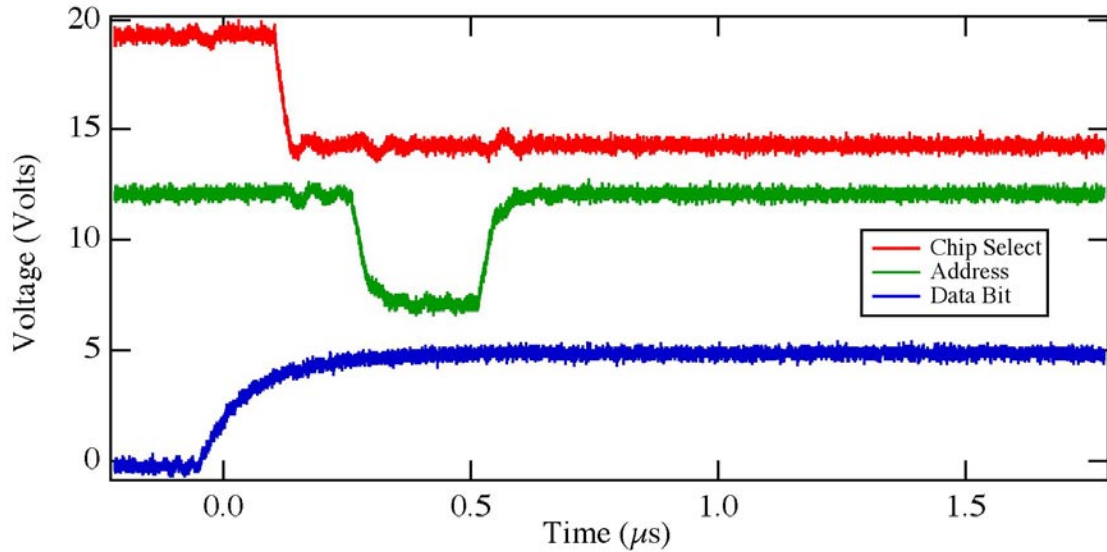
Figure 2.19 The timing of the loading of data into the AD669 chip. Data is latched in the buffer of the AD669 when either the address (red) or load buffer (green) line goes high. At that time the data bit (blue) is latched in the buffer and a new chip can be loaded. The length of time that the load buffer line stays low is set by a one-shot chip to be much shorter than the time between outputs from the computer.

loaded when the red line is low. The other two times the green line goes low, data is

being loaded into two other converters. The black line going high is the signal to start a
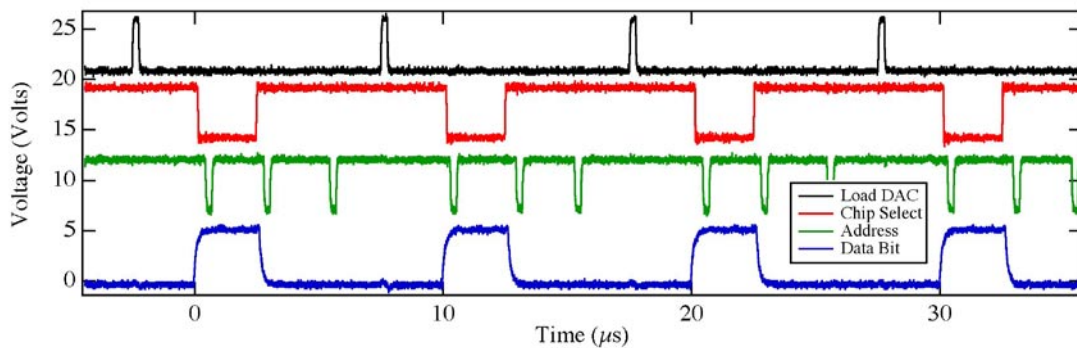
Figure 2.20 Shows the timing for a sequence of conversions by the DAC box. Each time the load buffer (green) goes low data is loaded into one of the chips based on which of the address lines (red) is also low. The data bit (blue) line shows a representative line of data. After loading all of the desired chips, the Load DAC (black) line goes high signaling the start of a conversion for all of the chips. The analog data is ready at the output 8μs later.

48

conversion on all of the DACs in the box, and their data is ready at the output 8μs later.

The analog output of the AD669 chips goes through a low pass filter to remove any of the digital noise that may be on it. Then the signal goes to the front panel where it can go to the gates, tip, piezotube and other electronics. The 16-bit outputs give a minimum step size of 0.3 mV. When this is divided down further like on the gates an even higher resolution can be obtained. On the piezotube this gives a step size of around 0.25 nm depending on the total scan range of the tube.

2.4.2. Surface Flattening Box

The second electronics box processes the x, y voltages from the DAC box to create the movements of the tip. This box receives as inputs the x and y values from the DAC box. It turns these two inputs into both a positive and negative output, which will go to the piezotube after being further amplified. This is necessary since opposite quadrants of the tube receive opposite voltages to increase the scan area. It also uses these two inputs to output a plane, which can correct for any tilt in the sample. The slope of the plane is controlled by the two potentiometers on the right hand side of the box. Figure 2.21 shows the schematic of the circuit. The input first goes through a differential amplifier followed by an optional low pass filter. At this point the positive output goes to the front panel and the negative output goes through an inverting amplifier. To produce the slope of the plane, a potentiometer is used to create a variable gain negative signal that is summed with the positive output. The potentiometer allows the signal to go from –3 to 0 times the positive signal giving slopes in the range of –1.5 to +1.5. This is done
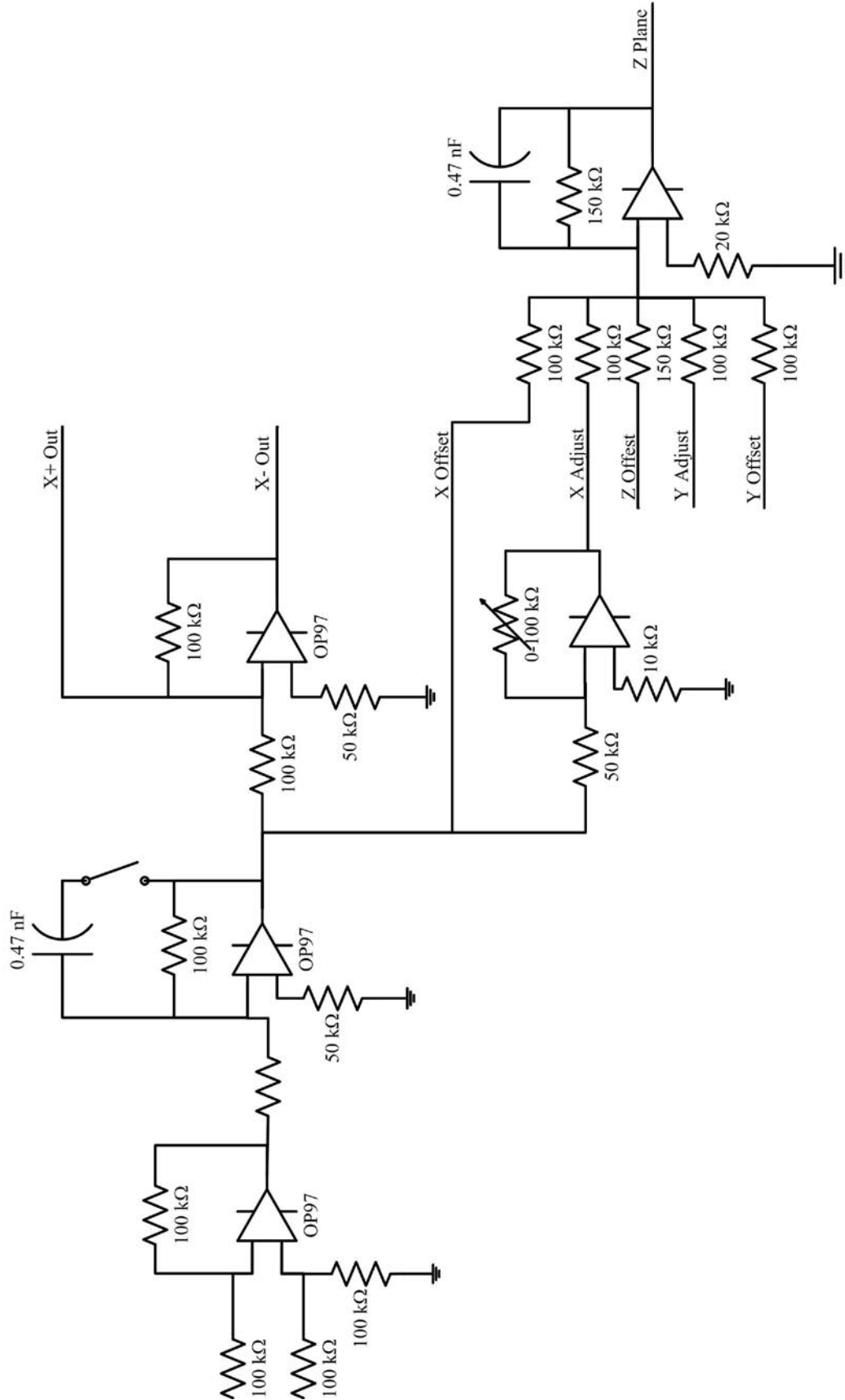
Figure 2.21 Schematic of the circuit used to fit a plane to the surface. The X and Y voltage from the computer are input. The user can adjust the slope in both directions by using the potentiometers. A Z offset may also be added.

independently for both the x and y direction. The x and y values are then added with a z offset that can also be set on the front panel. Figure 2.22 shows the recent version of this box that was built for the new Helium-3 SPM. The five outputs for the piezotube are on the right hand side of the box next to the potentiometers that control the slope. The box is a basically a copy of the previous version but done on a two-layer printed circuit board with the feedback circuit on the same board. Both of these circuits are now in one box making the connections a little bit simpler.

2.4.3. Feedback Box

Perhaps the most important box for topographic scans with an AFM is the feedback box. Since we use piezoresistive cantilevers, we attempt to keep the resistance of the cantilever constant during the scan. This ensures that the cantilever maintains the same deflection throughout the scan. Figure 2.23 shows the layout of the Microtech connectors at the bottom of the He-3 sample stick. It also shows the circuit diagram for the cantilever bridge circuit. The cantilever is one arm of a whetstone bridge circuit, allowing for a very accurate measurement of its resistance. All of the resistors in the bridge are located in the cryostat to keep the bridge well balanced as a function of

Figure 2.22 Picture of the new box containing the plane fitting electronics and the cantilever feedback circuit. The inputs and outputs are labeled with their function.

51
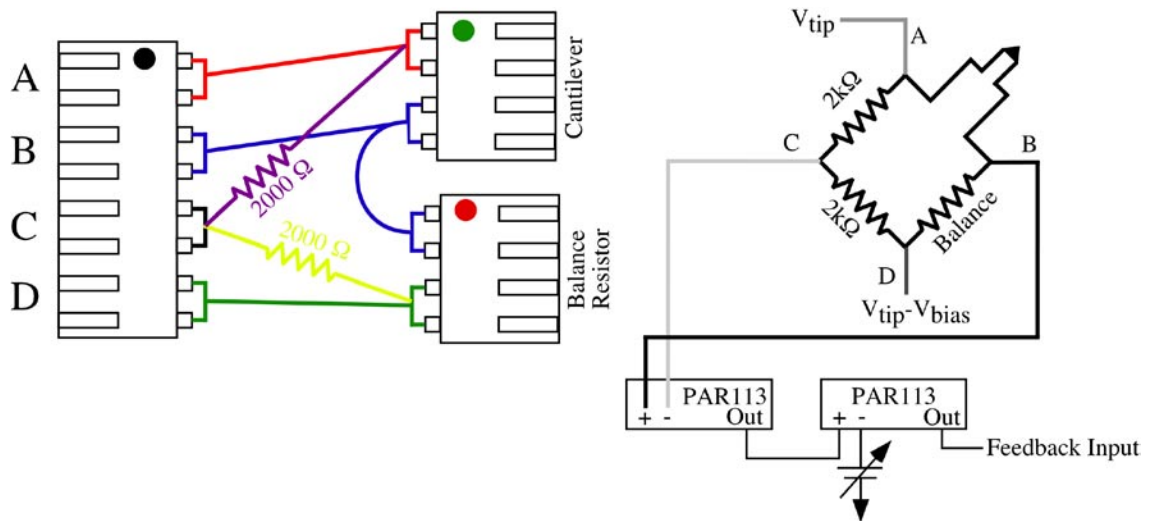
Figure 2.23 Shows the connections for the cantilever bridge circuit. The layout of the bridge circuit is shown on the right with the connections to the PAR 113 and voltage bias circuit labeled.

temperature. The balance resistor can be changed along with the cantilever to ensure that the resistors in the circuit are always well matched to each other. The cantilevers have a nominal resistance of 2000 Ohms but this is accomplished with a surface mount resistor in parallel with the cantilever. This resistor has a very different temperature dependence from the cantilever and other resistors, so it must be removed before cooling down. A balance resistor should be chosen with the same resistance as the cantilever, which is generally around 2600 Ω.

A bias voltage is applied across two points on the bridge (A to D) and the resulting voltage difference between the other two points (B and C) is measured with a pair of PAR 113s in series. A ramper box is used as one of the inputs to the second PAR 113 to null the signal coming for the first one. This allows a gain of 100,000 to be reached without the resulting output going over a couple of volts. This resulting output is sent to the input of the feedback box, which tries to keep its value at 0 by adjusting the

voltage on the z quadrant of the piezotube. If the signal from the cantilever goes up, this means that it is bending down so the piezotube needs to extend. However, if the signal goes down, it is pushing into the surface and the piezotube should retract.

Figure 2.24 shows the details of the feedback circuit. The circuit basically integrates the difference between the input and the reference and tries to keep this as close to zero as possible by adjusting the output. The switch on the capacitors controls the time constant for the integration and hence the speed of the feedback. The rotary switch on the resistors changes the scale of the gain setting on the input stage while the potentiometer adjusts the fine gain. Both of these adjustments change how much current goes into the capacitors, changing the speed of the circuit. The last amplifier is an optional inverter depending on whether increases in the input should result in increases or decreases in the output. For the cantilever feedback circuit as normally used this switch should be in the non-invert position, meaning increases in the input correspond to increases in the output. There is also an optional limit, which is set by an external voltage. This keeps the output of the feedback circuit from going above this voltage.

This box is also used as a feedback circuit for the gate. In this case the input is the output of the lockin, which measures the conductance through the QPC. The reference is supplied by the computer that sets the desired conductance. The output of the feedback circuit goes to the QPC gates, which controls the conductance through the QPC. When using the feedback circuit on the gates it is very important to limit the range of its output[18]. Generally, a diode is used to limit the amount of positive voltage that can go to

_____

[18] I have learned this from experience when the divider was not large enough and the voltage on the gate went to –4 Volts causing the device to stop working until being thermally cycled.

Figure 2.24 Schematic of the feedback circuit. The input is the signal to feedback on while the output is the signal that is adjusted. The reference sets the value that the input should equal. The limit may be used to prevent the feedback from going positive.

54

the gate. This is followed by a divider, which limits the range of the negative voltage and further reduces the positive voltages. This ensures very little positive voltage can reach the gate and only small negative voltages.

2.4.4. High Voltage Amplifiers

The last major box necessary for the operation of the SPM is the high voltage amplifier box. Figure 2.25 shows the schematic of the new amplifiers used in the He-3 system. The previous design used a PA85 op-amp from Apex Microtechnology
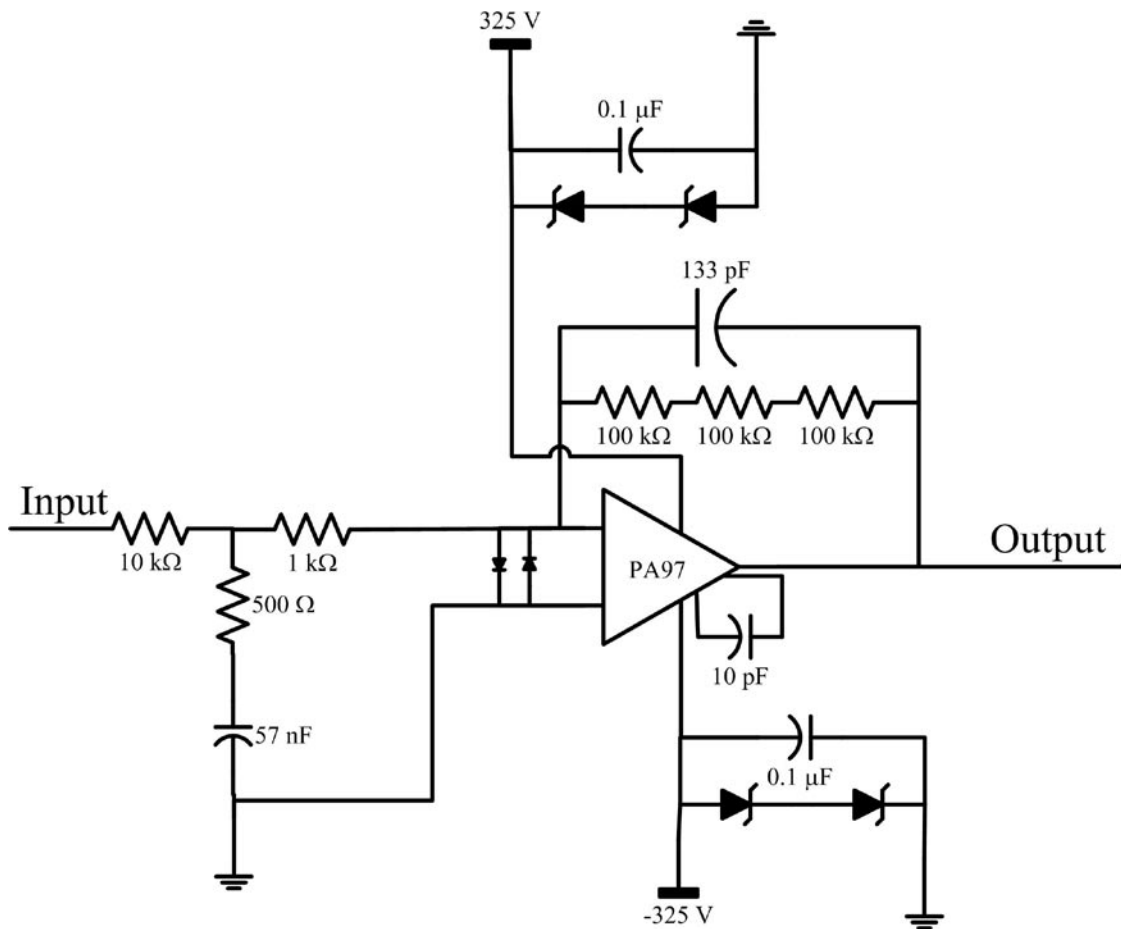
Figure 2.25 Circuit diagram for the high voltage amplifiers that power the piezotube. They are inverting amplifiers with a gain of 30 powered by +/-325 volt power supplies.

and is described in Mark Eriksson and Mark Topinka's theses [Eriksson, (1997); Topinka, (2002)]. We have decided to use a different op-amp in our design to achieve a higher scan range. We have used the PA97, which is capable of outputting more voltage but less current. Since we are just driving the piezotube, which is a capacitive load this is not a problem in our application. The box contains five identical circuits for the +X, -X, +Y, -Y and Z quadrants of the piezotube. The op-amp is in an inverting amplifier configuration with a gain of 30 giving an output range of +/- 300 Volts when driven by the DAC box, which outputs +/- 10 Volts. The diodes on the power lines are to protect the op-amp from spikes in the power, which may damage them. The diodes on the inputs keep them close together so that the output will not be too large. There is a 10 pF capacitor on two pins of the op-amp that is necessary for stability when the gain is greater than 10.

2.4.5. Other Electronics

During the course of my research, I have built a couple of other boxes that we routinely use with the SPM. I will briefly describe them here but their circuits are rather straight forward so I will not go into much detail. The first box is what around lab is known as a "Ramper Box." This box was designed by Jordan Katine and has been in use in our lab for many years [Katine, (1996)]. It consists of one output that ramps as a function of time and eight outputs that are constant. The speed of the ramp is selected using a switch on the front along with a potentiometer. The voltage for the fixed outputs is determined in the same way. The complete circuit diagrams are in Jordan's thesis.

The second box is a differential summer box. It sums the inputs from up to four

channels and puts them on the output. We mostly use this box to add voltages from different sources together before going to the gates, ohmics or tip. Figure 2.26 shows the circuit schematic. Each input goes through a differential amplifier and then into the summing amplifier. After they are all summed together, the output goes to the front panel of the box. The entire circuit is run off of two 1.2 Amp Hour 12V lead-acid batteries[19] that are enclosed in the box. The box with the summer circuit has two copies of it run off of separate sets of batteries allowing the summation of two different voltages. The use of the OP97 op-amps in the circuit gives excellent noise performance with very little power use. I have to recharge the batteries less than once a week even with daily use of the circuits.
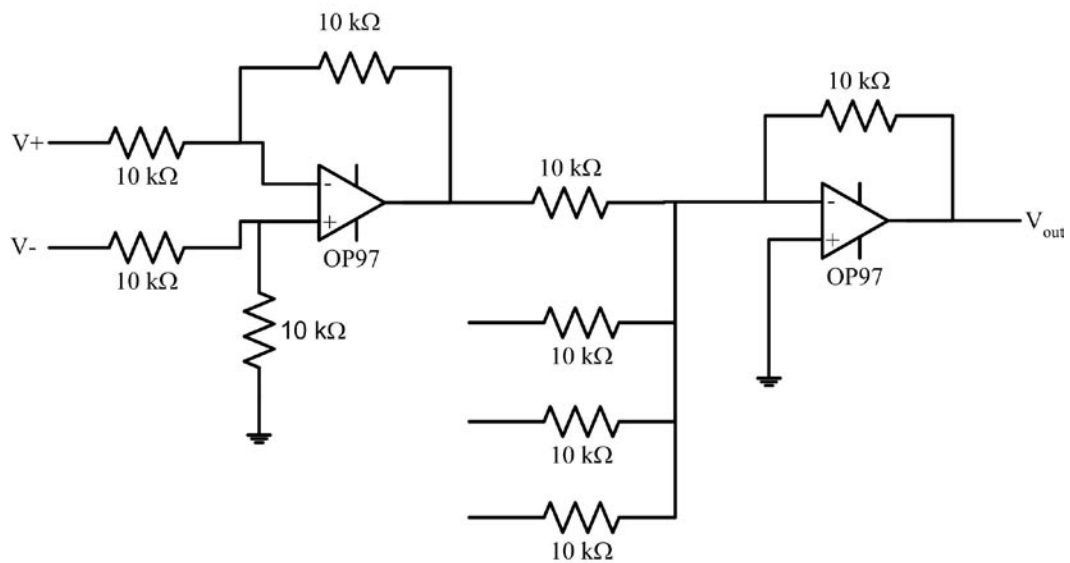
Figure 2.26 Schematic diagram of the summing circuit used in the summer box. There are four differential inputs of which one is shown which then all are summed together at the second op-amp. The output comes out at Vout.

---

[19] PowerSonic model PS-1212

2.4.6. Computer

All of the control and data acquisition is controlled by a Macintosh computer
through two National Instruments PCI cards. As mentioned previously, a digital output
card controls the signals going to the SPM. The input back to the computer is through a
PCI-MIO-16XE-10 board, which has 8 channels of 16-bit differential input. The board is
capable of sampling the input at 100kHz. The interface with the boards is handled by the
data acquisition program, AFM Program, originally written by Mark Topinka that I have
modified to handle the updated boards that we are now using[20].

Figure 2.27 shows a screen shot of the data acquisition program. The program
consists of four windows: dashboard, sweep, script, and console. The console window
provides basic feedback to the user about problems that have occurred and other
diagnostic information. The script is the main window for user input. The user enters
commands into the script window to control everything from the movement of the tip,
to the gate voltages and data analysis functions. Appendix B details all of the script
commands available in the program, which now totals over 400. The sweep window is
for acquiring and displaying one-dimensional data sets. The sweep window is mainly
used for initial testing of a new device. For example, we use it to take traces of the
conductance versus gate voltage for the QPCs. It is also used for doing data analysis
when taking 1-D slices of images. The last and most complicated window of the program

---

[20] National Instruments no longer seems to support accessing the PCI Macintosh
boards through C function calls. They only support Labview but I was able to find an
engineer who was willing to give me the drivers for the boards. The commands are the
same as used by the PC boards if you ever need help in using them just look up the PC
documentation.
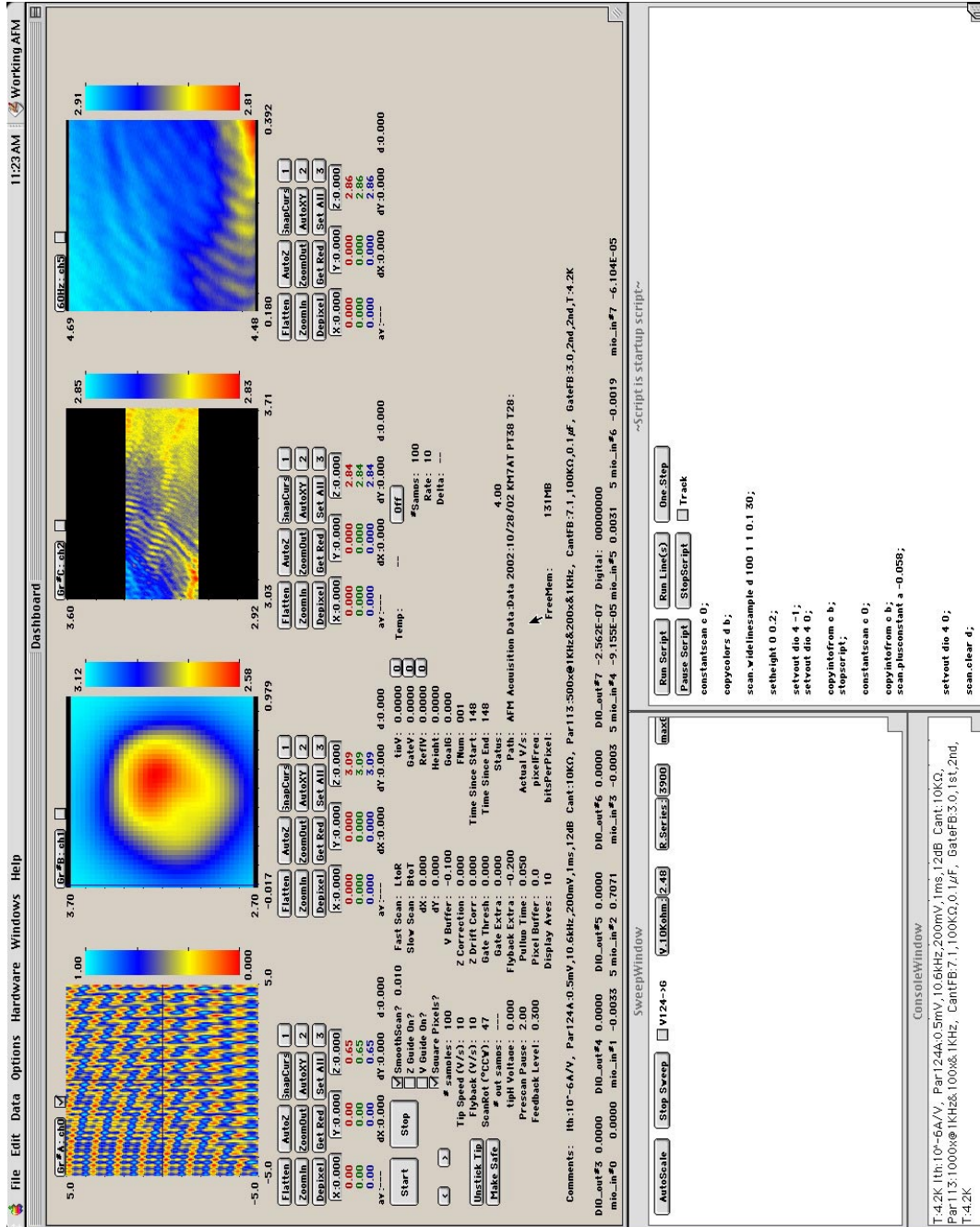
Figure 2.27 Screenshot of the AFM program showing the four windows: dashboard, sweep, script and console.

is the dashboard. It has up to four graphs showing different scans. It also has readouts of all the variables associated with the operation of the SPM. These range from the distance off the surface, the voltages on the gates, the working directory, etc. At the bottom of the window, all of the input and output values are displayed. The blue cursor in the graphs shows the current position of the tip and can be moved with the mouse. The red and green cursors define the corners of the current scan area.

One of the recent major changes to the program was to go from 12-bit analog outputs to 16-bit ones. This reduced the minimum step size for the tip from about 4 nm down to 0.25 nm. It also reduced the voltage steps on the gates from about 5 mV to 0.3mV. This was accomplished by using the new DAC box, which has 16-bit converters in it instead of an old National Instruments card. In order to do this the format of the output data had to be changed. The sequence of data to output an analog signal is now as follows. Send the data to the DAC box for each channel that is going to be changed. Then send the convert signal to all of the DACs. Repeat this process for each output. There is a minimum of three sets of data that must be sent for each conversion. This is due to the timing function of the board, so if fewer channels than this are being updated just repeat the data for one of them. All of the information is sent to the DAC box as 16-bit integers from an array, two elements of which are sent at each output to create the 32-bit word. The first 16-bits are the data. The second 16-bits are more complicated and are formatted as follows: lowest 4 bits are not used, next 4 bits are the address, next bit is unused, next is the chip select and last is the start conversion.

There are two other versions of the program, one is the data analysis version, which has all of the communication with the PCI boards removed and has larger graphs

60

for a better display of the data. We use this version to look at and analyze all of the data after acquiring it. The third version of the program is used by the people in our group working on quantum dots. It interfaces with a 20-bit digital to analog converter through the serial port. This gives a much finer control of the gate voltages but greatly limits the speed of data acquisition making it impractical for the SPM.

Chapter 3

Imaging Techniques

This chapter covers the different imaging techniques that we use to look at coherent electron flow. To find the location of our device we use standard contact topographic imaging while we use scanning gate microscopy techniques for acquiring images of electron flow. Section 3.1 describes the procedures that we use at room temperature to align the tip so that it is over the device at liquid helium temperature.

Section 3.2 discusses the procedures that are done before an image of electron flow can be obtained, these include finding the device and making sure the surface is flat. The remaining three sections of the chapter discuss techniques that we have developed to image electron flow. These techniques allow the study of different properties of the electron flow in the two-dimensional electron gas.

The first and simplest one is discussed in section 3.3 where we put a fixed voltage on the tip and scatter the electrons. By measuring the change in conductance as a function of tip position, an image of the electron flow is obtained. This technique is used to image the electron flow through the two-dimensional electron gas and to spatially profile the local electron density.

Section 3.4 outlines the second method, which is an extension of this method where we oscillate the voltage on the tip and lockin to the signal that varies at this frequency. This gives an image of the derivative of electron flow with respect to the tip position. This is very useful when studying the interference fringes oriented

perpendicular to the electron flow.

In section 3.5 we discuss our third method that involves ramping the voltage on the tip to look at the local density of states under it. This is similar to STM spectroscopy measurements of differential conductance versus tip voltage, which measure the local density of states as a function of energy.

3.1. SPM Operation – Room Temperature Alignment

The section describes the procedure used to align the scanning probe microscope (SPM) at room temperature so that the tip will be able to reach the device at liquid helium temperature. When the SPM cools, the position of the tip drifts relative to the sample. This drift is caused by several factors including the differential contraction of the piezotube and brass cage, the tilt of the SPM head and small cracks in the piezotube. The drift is fairly repeatable as long as nothing is changed with the SPM. When the SPM is cold the scan range of the piezotube shrinks by about a factor of 4 giving a total scan range of around 15x15 μm at 4.2 K. The limited scan range and drift means that the starting position of the tip has to be carefully chosen at room temperature to ensure it is within reach of the device at 4.2 K. To facilitate the positioning of the tip, each sample has an alignment grid written on it at the same time as the gates.

Figure 3.1 shows a topographic image of two –1's in the alignment grid, which are patterned by electron-beam lithography and thin-film deposition. The grid consists of two numbers at each point, which represent the x and y coordinate in units of 10 μm. The top left number is the y-coordinate and the bottom right one is the x-coordinate. The device is located at (0,0), so that the two numbers give the distance away from the

63
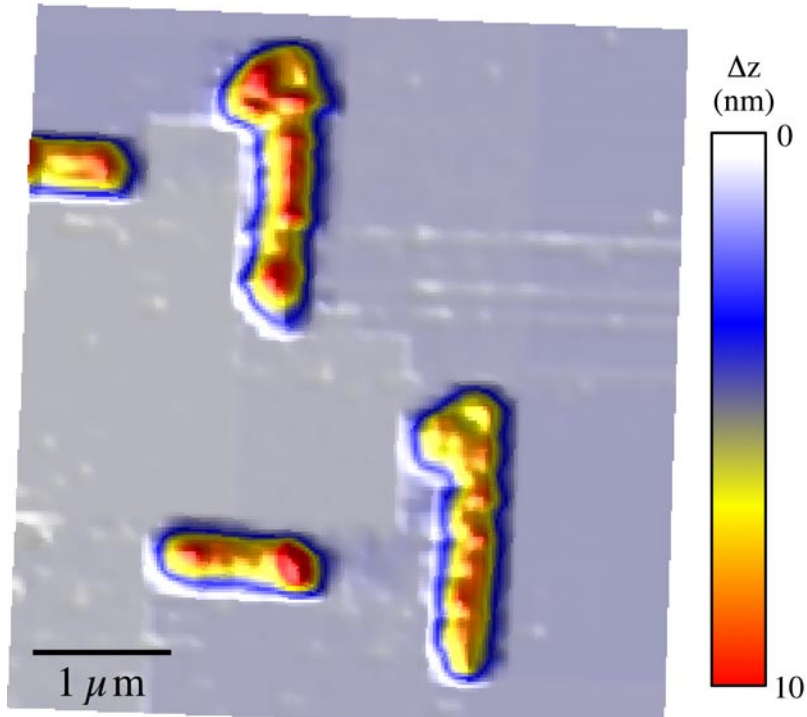
Figure 3.1 Topographic image of the x and y coordinates in the alignment grid. These are used to locate the position of the SPM tip.

device. The position of the tip is easily found by taking a topographic scan and reading the numbers. Each number is two µm tall to make it possible to quickly identify the current position. It is important not to scan directly over the device when positioning the tip because this can sometimes destroy it. On the first cooldown of a device, the tip is put somewhere near the center of the alignment grid so that when it cools down it will drift to another point on the grid. Most of the time the drift is around 50 µm. If the drift is significantly more it is a sign of a problem.

The two main problems that cause a large drift are the tube being broken or improper alignment of the sample and coarse approach screws. If the drift is mostly in the y direction, it is likely to be the second problem. The sample should sit in the same plane as the pivot point of the three coarse approach screws. This makes the tip move

straight away from the sample when the screw is turned as opposed to moving in the y direction. When the SPM is cooled, there is a differential contraction between the brass cage and the piezotube. This requires that the tip be pulled off the surface by about 0.6 mm (2 turns of the coarse approach screw) so that it does not hit the surface upon cooling. If the height of the sample with respect to the coarse approach screw is incorrect this leads to a large movement in the y direction. The second problem is a broken tube, which can usually be identified by a large hysteresis at room temperature. The first few lines in a topographic image will have a different slope than the rest of the scan.

When the SPM has cooled to liquid helium temperature, it is necessary to find the location of the tip. If it is not within reach of the device, the drift is calculated and this is used as the starting position for a second cooldown. After warming up, the position of the tip is adjusted by turning the x and y coarse position screws. The location of the tip must be adjusted so that it is correct when the cryostat is upside down since this is the orientation when it is cold. This can be done by flipping the cryostat over after each movement of the tip and finding the new location. Another method is to note the change in position when you flip the cryostat and use this to adjust the desired location. The location should not move more than around 5 μm when the cryostat is flipped over. After the tip is positioned, the SPM is cooled back down and the location of the device is checked to see if it is within reach. I have always had the device be within reach on the second cooldown as the drift is fairly repeatable. The biggest factor in the drift seems to be the piezotube because the drift is fairly constant from sample to sample and tip to tip unless the piezotube is changed.

3.2. SPM Operation – Liquid Helium Temperature

This section describes the steps necessary to acquire images of electron flow once the dewar and SPM have been cooled to 4.2 K. The first step is to approach the surface using the coarse approach rod. With the cantilever feedback on, the coarse approach screw is turned until the voltage on the Z quadrant of the piezotube needed to reach the surface is about 100 V. This allows a decent scan range and the flexibility to adjust the height based on the location of the device. Topographic scans are taken to determine the location of the device. Taking topographic scans can change the ionization of the donor atoms underneath the tip by straining the sample or inducing charge on the atoms. Therefore it is not a good idea to take topographic scans to close to the device because of the risk of changing its electrical properties. If the tip cannot reach the device, extra voltage can be added to some of the quadrants of the piezotube to extend the scan range. An extra 200 V can be safely added, which doubles the scan range. If the device can be reached, initial checks of the device properties are performed. If it is a QPC the following checks are performed, that the ohmics work, the gates work and that conductance plateaus are visible.

Assuming that everything is working so far, the flattening of the surface is adjusted. The surface flattening box discussed in Section 2.4.2 adjusts the height of the tip as a function of position so that the feedback does not have to work as hard to keep the tip on the surface. It also allows scans with the feedback off and the tip a fixed height above the surface. The plane is adjusted in a small area away from any gates or objects on the surface. Repeated topographic scans are taken and the potentiometers on the plane

66

box are adjusted until the plane that the computer fits to the surface is flat to within 0.1 %

in both directions. This gives a surface that changes less than 1 nm in a 1 μm². It works

best to adjust the plane with the scan rotation set to a multiple of 90 degrees. This makes

the potentiometers adjust the x and y slopes independently.

Now that the plane is fairly accurate, the location of the QPC is found. This

is best done by taking an electrical scan with the gates energized, which measures the

conductance across the QPC as a function of tip position. The tip is pulled off of the

surface about 100 nm to be safe and a negative voltage is put on the tip. A scan is taken

and the location of the maximal change in conductance is found. Figure 3.2 shows an

example of one such scan with the location of the QPC indicated by the arrow. In this

scan, the tip is acting as a second gate that constricts the QPC when it is near it. The

largest change occurs at the QPC because this is the location that is most sensitive to
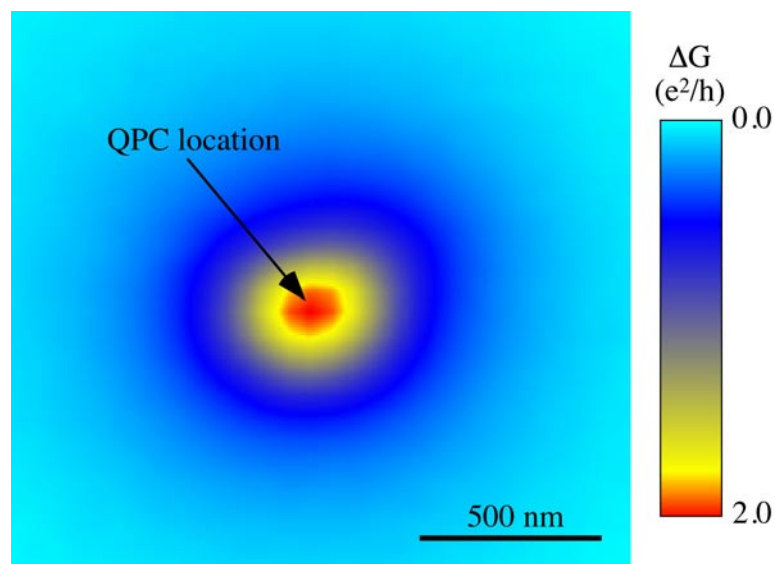
Figure 3.2 Shows a typical image of the change in conductance as a function of tip position. This is used to determine the position of the QPC, which is indicated by the arrow.

charge. This process is repeated after zooming in on this area to pinpoint the location of the QPC.

Depending on how complicated the device is, an image of the gates may be obtained. This should be done without touching the surface because that can disturb the donor atoms. The feedback circuit has been modified to allow this type of scan. There is an input marked limit, which limits the positive range of the output. When a voltage is attached here, the output is clamped by a diode so that it cannot go more than 0.3 V above this value. One of the outputs of the ramper box is attached to the limit and the voltage is set so that the feedback cannot output a positive value. This keeps the tip from pushing out but allows it to pull off the surface if it hits something. Scans are taken over the gate area, reading the Z voltage and cantilever deflection. The tip is moved progressively closer to the surface until an image of the gates appears. Figure 3.3 shows an example of the resulting scan, which measures the cantilever deflection. There is no change in the
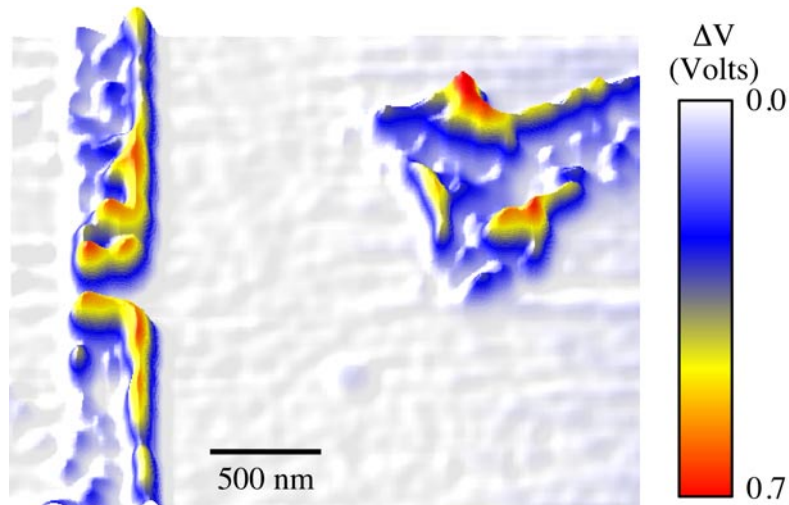
Figure 3.3 Image of the change on the cantilever voltage showing the location of the gates. This image was taken with the feedback limit enabled to keep the tip from hitting the surface of the GaAs.

deflection unless an object is sticking up from the surface and then the piezotube retracts.

Now that the location of the gates is known, a better fit to the surface is found. This is accomplished with the script command "autoflatten". The command takes a series of points, finds the surface at each one and then fits a plane to the resulting values. It finds the surface at each point by pushing into the surface many times with progressively less force. It takes the average of all of the readings of the surface height and this is the value for the height at that location. The autoflatten command has the option of excluding some of the worst points from the fit. It is generally a good idea to use this feature in case the routine does not get a good reading for some of the points on the surface. The resulting plane is put in graph A, the left hand graph in the computer program discussed in section 2.4.6. When the Z-guide is on, the values in the graph are output to the Z quadrant of the piezotube as a function of position to keep the tip a fixed distance from the surface. With the Z-guide on the accuracy of some of the points can be checked by moving the tip and slowly approaching the surface. If they appear to be good, the flattening is repeated with the Z-guide on to obtain a very accurate surface. Generally, none of the points in the fit of the plane have an error greater than 1 nm over a range of 25 μm^2. Once this is finished, everything is ready to start taking images of electron flow.

3.3. Scanned Gate Microscopy

This method of imaging electron flow uses the SPM tip as a moveable gate that scatters electron waves. The tip backscatters some of the electron waves back through the QPC reducing its conductance. When the tip is over an area of high electron flow,

there is a large amount backscattered and hence a large decrease in conductance. However, when the tip is over an area of little flow, there is a correspondingly small change in conductance. By measuring the change in conductance as a function of tip position, an image of electron flow is obtained.

Figure 3.4 is a schematic of the setup we use to image electron flow. The conductance of the device is measured between two ohmic contacts far away, which are not shown. The conductance is measured using lockin detection methods with an ac frequency of about 10 kHz across the QPC. The QPC gate is energized negatively with respect to the 2DEG creating a narrow channel through which the electrons must flow. A
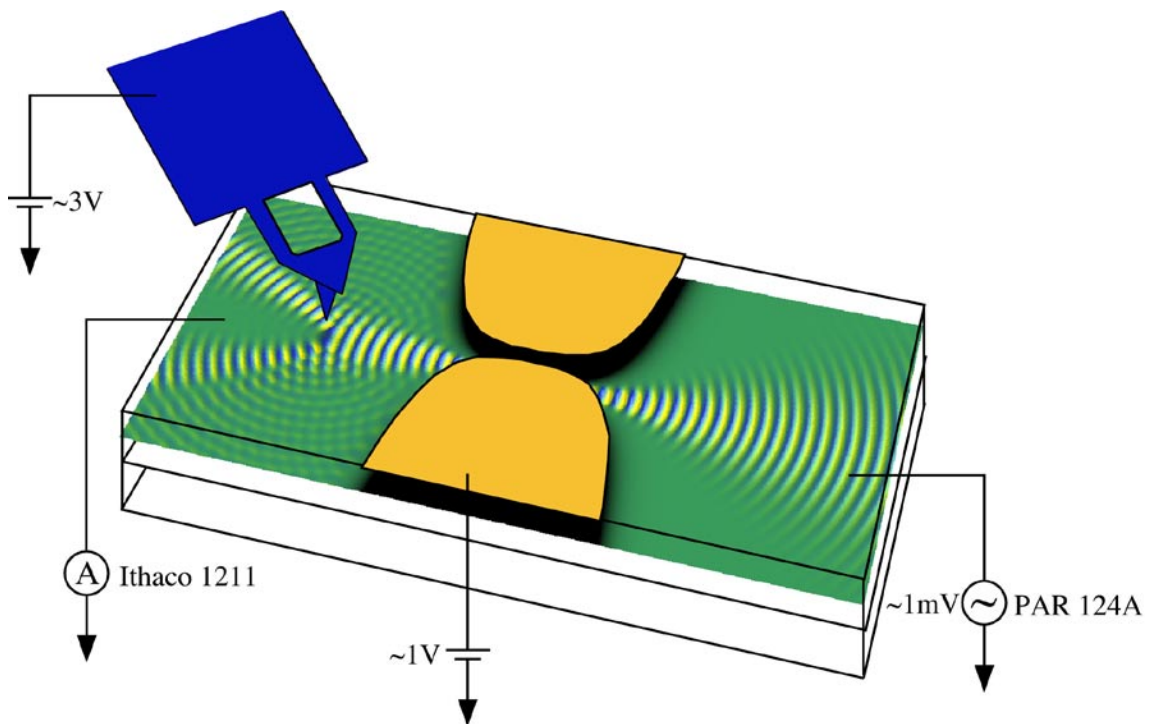
Figure 3.4 Schematic diagram showing the measurement setup used to image electron flow. A small ac voltage is put across the sample from the PAR124A lockin. The output of the Ithaco 1211 current amplifier is sent to the lockin. A fixed negative voltage is put on the tip and gate. The green wave is a simulation of an electron wave hitting the potential caused by the tip.

70

negative voltage is put on the tip, which depletes the electrons below. Figure 3.5 shows

an example of an image of electron flow obtained with this technique at a temperature

of 1.7 K. The image shows the electron flow coming from a QPC off the right side of

the scan. The blue areas are areas of high electron flow while the black are areas of no

electron flow. The image is decorated by interference fringes throughout the scan area

showing that the flow is coherent.

The most important requirement for obtaining an image with this method is that

the voltage on the tip is sufficient to deplete the electron gas below. Figure 3.6 shows the

effect of making the voltage on the SPM tip more negative. In each successive image the

voltage on the tip changes by 0.5 V going from –1.5 V up to –4.0 V. There is no change

in conductance until the tip first depletes the electron gas and then the signal quickly

increases. There is no image of electron flow in Figure 3.6 (a and b) since the voltage

on the tip is too small. Once the tip is making a depletion region the image of electron

flow is obtained. In Figure 3.6 (d-f), there is little change in the image as a function of

tip voltage. In these images, the tip's depletion region is growing but does not seem
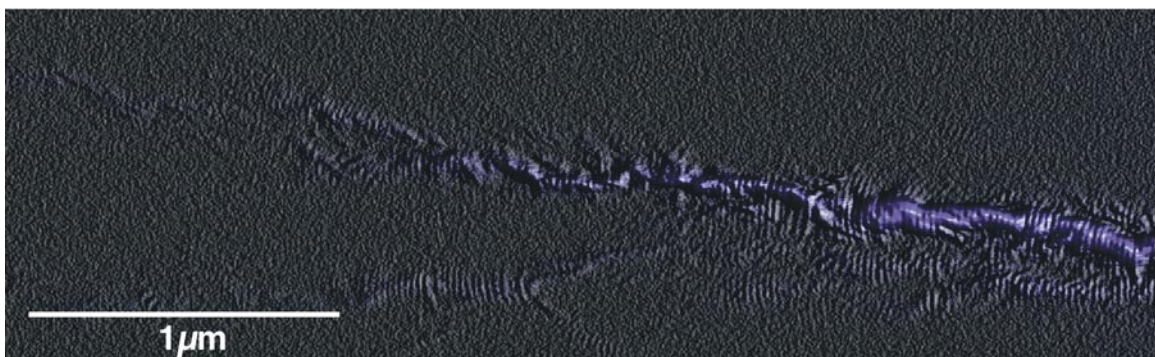
Figure 3.5 Image of electron flow from a QPC located to the right of the scan at a
temperature of 1.7 K. The flow is decorated by interference fringes throughout the entire
scan area.
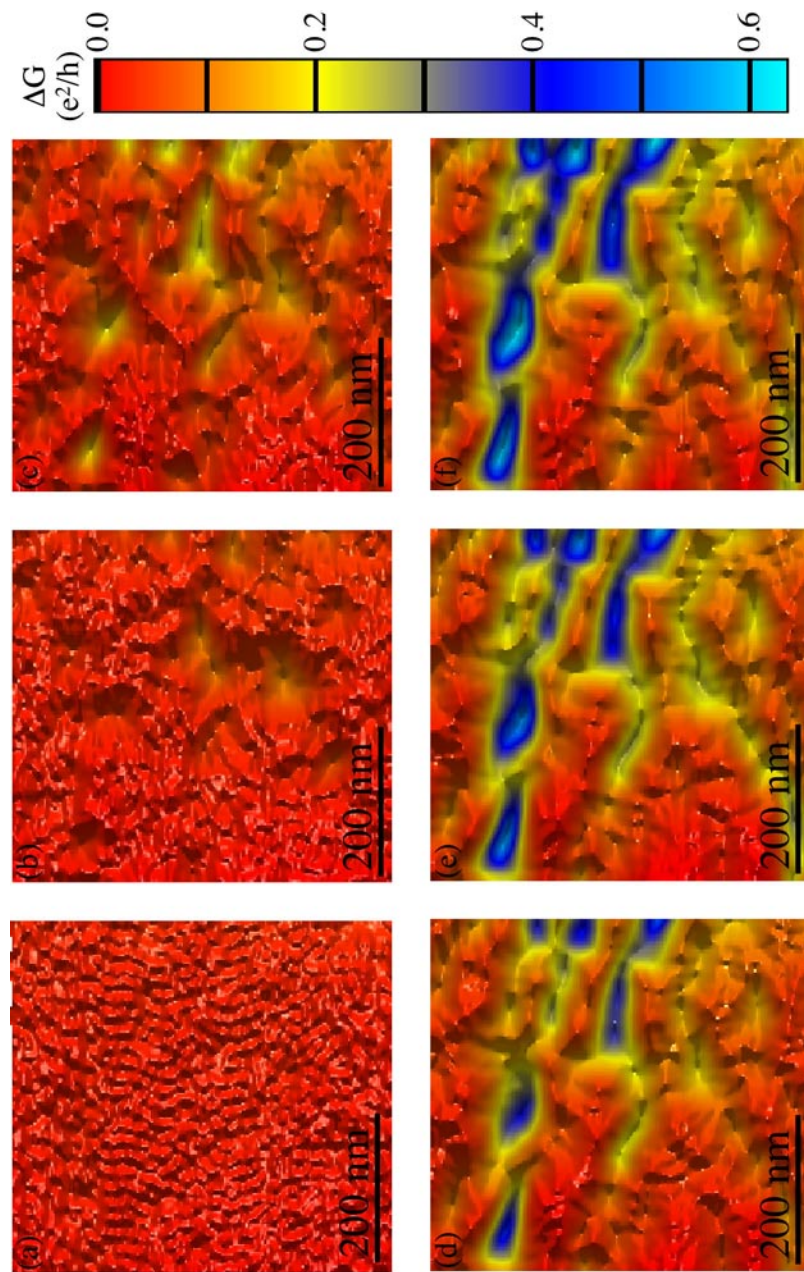
Figure 3.6 Images of electron flow taken with different voltages on the tip (a) –1.5 V, (b) –2.0 V, (c) –2.5 V, (d) –3.0 V, (e) -3.5 V and (f) –4.0 V. The image of electron flow appears when the tip depletes the electron gas around –2.5 V.

to change the pattern of electron flow. This shows that the size of the depletion region does not appear to affect the image of electron flow. This provides evidence that we are imaging the flow that was present without the tip.

To further study the importance of the depletion region we have taken a series of images for varying heights of the tip above the surface. Figure 3.7 shows the effect of increasing the height of the tip. All of the images are taken with a fixed voltage on the tip but the height increases in steps of five nm from 10 nm to 35 nm. In the first three
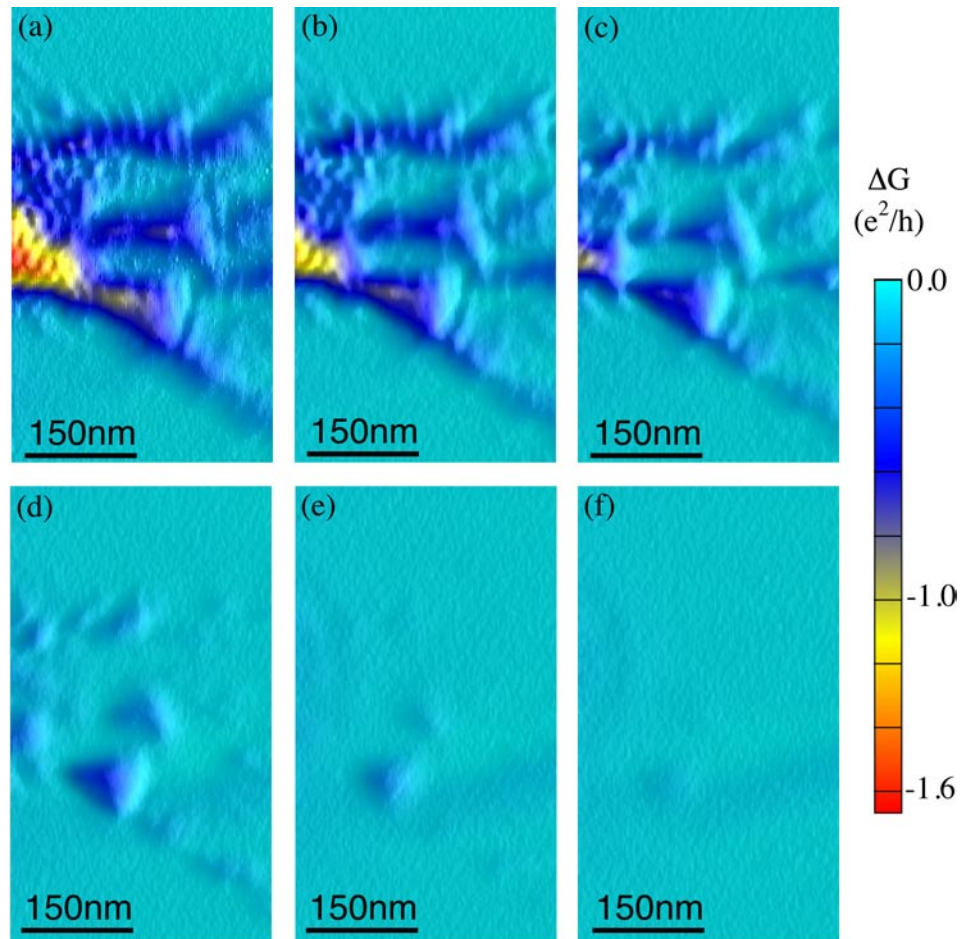
Figure 3.7 Images of electron flow for increasing heights of the tip above the surface of the device: (a) 10 nm, (b) 15 nm, (c) 20 nm, (d) 25 nm, (e) 30 nm and (f) 35 nm. The image of electron flow disappears above 20 nm when the tip no longer makes a depletion region.

images, there is an image of electron flow. This is because the tip is close enough to the surface to deplete the electron gas and backscatter electrons through the QPC. For the last three images, there is almost no signal as a function of tip position. This is because the voltage on the tip is not sufficient to deplete the 2DEG, leaving nothing to backscatter the electrons.

We have modeled the effect of the tip on the 2DEG using a 3D Poisson simulator. The details of the simulator can be found in the thesis of Mark Topinka [Topinka, (2002)]. For the simulation we modeled the tip as a sphere at the end of a cone. The angle of the cone was taken to be 12 degrees as given in the specifications for our cantilevers. The radius of the sphere used was 24 nm, which is a typical radius of the tips judging by topographic images. In the simulation, we found the size of the depleted region under the tip as a function of the distance of the tip from the surface. This shows that the tip first depletes the electron gas when it is around 25 nm from the surface. Our images of electron flow also start to appear when the tip is within 25 nm of the surface. This provides another piece of evidence that the important factor in obtaining an image of electron flow is creating a depletion region. A further confirmation of the necessity of the depletion region comes from a quantum mechanical simulation that shows that the signal increases rapidly when the tip first depletes the 2DEG [Shaw, (2002)].

Figure 3.8 illustrates why it is necessary to have a depletion region in order to acquire images of electron flow. If the tip just creates a bump in the potential felt by the electrons, it will not backscatter electrons as shown in Figure 3.8 (a). This is because the electrons still have enough energy to go over the bump and therefore will not be reflected but merely bent. However, if the voltage is increased so that the bump reaches
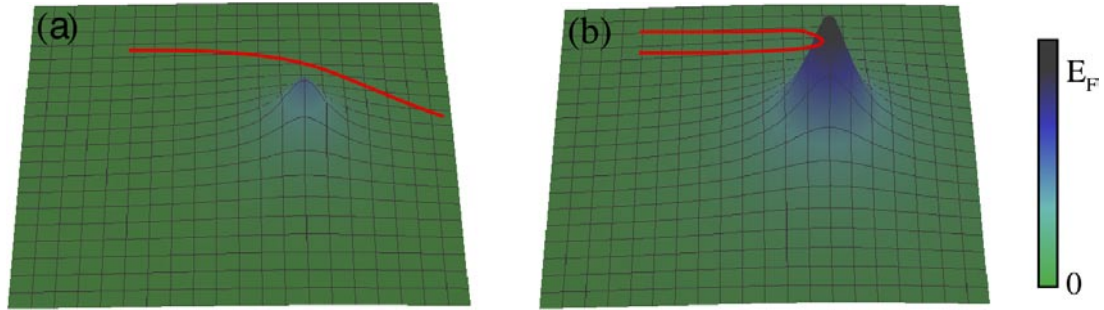
Figure 3.8 Diagram showing the importance of creating a depletion region under the tip. In (a) there is only a small bump and the electron is merely bent by the perturbation. In (b) the electron gas is depleted causing the electron to be backscattered by the potential.

the height of the Fermi energy as in Figure 3.8 (b), there is a region of depleted electrons. This area is classically forbidden for the electrons and electron waves impingent on it will be backscattered. This will scatter some of the electrons back through the QPC, which reduces its conductance. Since the measurement is only sensitive to changes in conductance this produces an image of electron flow, while the first case does not give any signal.

The depletion region is also important for the high resolution of our technique. Since the 2DEG is located 57 nm below the surface and the tip is at least a few nm above the surface, the distance from the tip to the 2DEG is at least 60 nm. This distance sets the half width of the perturbation from the tip in the 2DEG. However, we are easily able to resolve features that are much smaller than this size. Figure 3.9 illustrates how this high spatial resolution is achieved from the large depletion region below the tip. The tip acts as a hard wall scatterer meaning that the angle of incidence of a wave is the same as the angle of reflection. Therefore only an electron wave that hits normal to the tip will be directly backscattered. All the other angles will be scattered but eventually make it to the

75
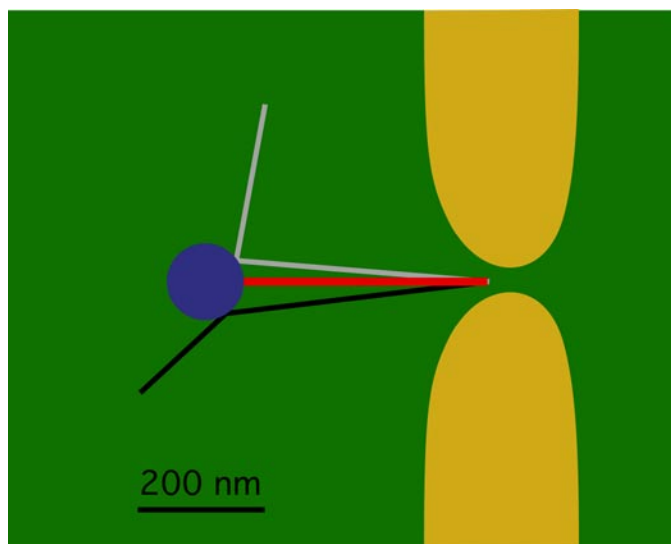
Figure 3.9 Diagram showing how the high spatial resolution is obtained. There are many paths of electrons hitting the tip but only the red path is backscattered through the QPC reducing its conductance. This is the path that hits the tip directly.

ohmic. The red path that is directly backscattered can return back through the QPC and reduce its conductance. This small part of the depletion region that backscatters electrons is also important in producing the interference fringes perpendicular to the electron flow that decorate the images. This will be discussed in more detail in Chapter 7. The small spot on the tip that backscatters electrons to the QPC determines the resolution as opposed to the entire width of the perturbation. This gives a much higher resolution than would be initially expected.

3.4.   Differential Imaging

The first method of imaging provides detail about the overall electron flow pattern but it does not give information about changes in the flow. Because the signal comes from one spot, we can use this to obtain a spatial derivative of electron flow by changing the location of this spot. We have developed a second technique that provides an image

of the change in electron flow as a function of tip position. This is the spatial derivative of the scanning gate microscopy images. This spatial derivative is useful when looking for changes in the electron flow and especially for studying the interference fringes that decorate the images. This technique picks out the signal due to the interference fringes without being sensitive to the background electron flow.

The method for obtaining these images is to oscillate the voltage on the tip to look at the spatial derivative of electron flow. The measurement setup is shown in Figure 3.10. It requires the use of two lockins, one locks in to the frequency across the QPC for measuring the conductance and the second one locks in to the frequency of the tip oscillation. The first lockin is set to a frequency around 10 kHz and the time constant for its integration is set to the minimum value. The output from this lockin goes to one of the ohmics to do a traditional conductance measurement. The measured conductance signal is sent to the input of the second lockin that is set to a frequency around 1 kHz. This second lockin is driving the oscillation of the tip voltage. The input to the second lockin is the conductance across the QPC with a modulation due to the oscillating tip voltage. Therefore, any signal that changes with tip voltage will produce a signal in this second lockin. This second lockin measures the second derivative of the current with respect to the source-drain voltage and the tip voltage, $d^2I/dV_{ds}dV_{tip}$. This is the same as measuring dG/dV_{tip}.

Figure 3.11 shows how wiggling the tip voltage produces an image of the derivative of electron flow. Changing the voltage on the tip, changes the size of the depletion region. As this depletion region moves, the location of the backscattering of electron waves also moves. If there is no change in the backscattered signal as a function

77
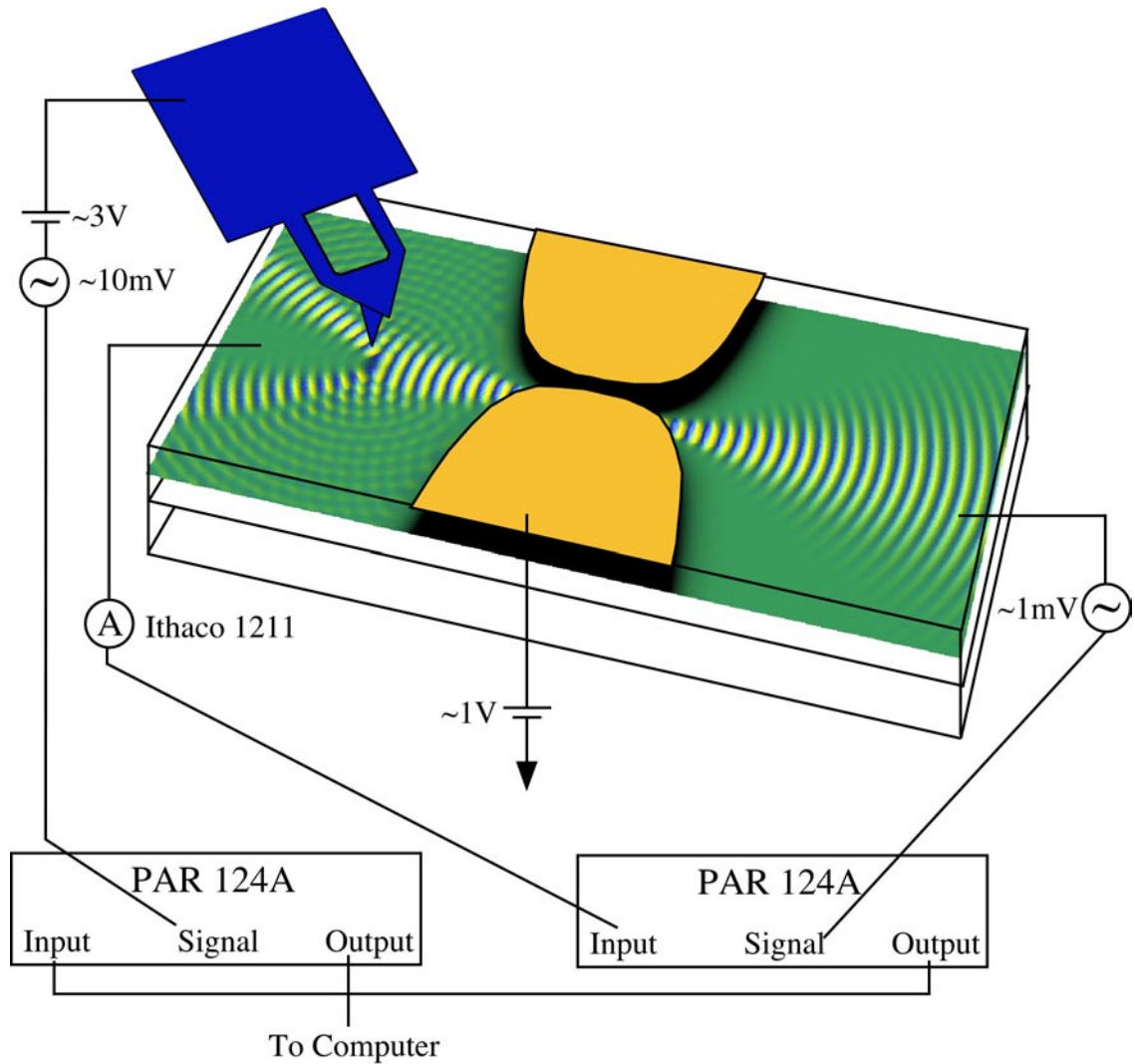
Figure 3.10 Diagram showing the connections necessary for imaging the derivative of electron flow. There are two ac voltages, one across the QPC the other on the tip. The current through the QPC is input into the first PAR124A to get the conductance across the device. This is then sent to the second lockin, which measures the differential conductance with respect to the tip voltage.

of position, the size of the depletion region will not effect the measurement. In this case, there is no signal on the second lockin because the derivative is zero. However, if the signal changes as a function of position this will show up as a modulation in the signal and the lockin will detect it giving rise to a signal. So the measurement of dG/dV_{tip} at a fixed tip voltage gives an image of the derivative of electron flow.
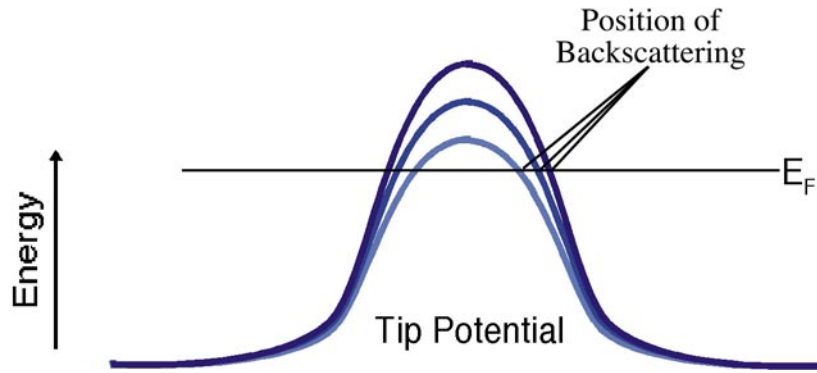
Figure 3.11 Schematic showing how the differential imaging technique works. As the voltage on the tip oscillates, the position of backscattering changes. By locking into this oscillation, only a signal that changes as a function of position is imaged.

An example of an image acquired with this technique is shown in Figure 3.12. Figure 3.12 (a) is an image of the change in conductance using the scanning gate microscopy technique. Figure 3.12 (b) shows an image of the derivative of electron flow acquired at the same time by oscillating the tip voltage and measuring dG/dV_{tip}. Notice that the interference fringes are much more pronounced in the derivative image, since the slow varying background is removed. The fringes are now clearly visible at the top of the image where they were hardly visible in the first image. This method of imaging
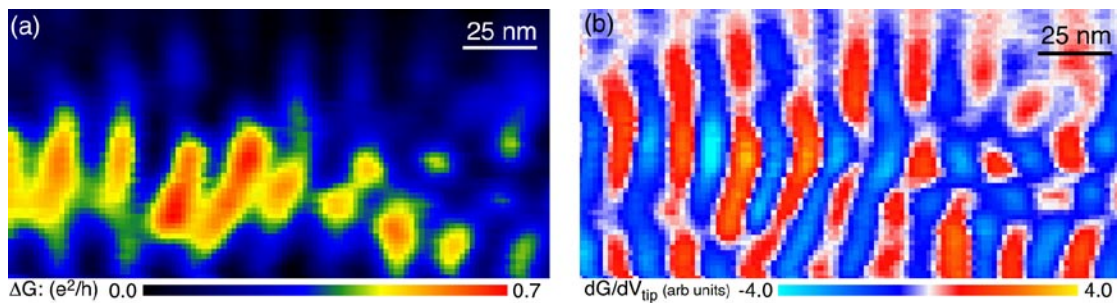
Figure 3.12 Two images of electron flow from the same area. (a) Image acquired with a fixed voltage on the tip. (b) Image acquired by locking into an ac voltage on the tip, giving the derivative in the direction of electron flow of the image in (a).

is very useful for studying the interference fringes or other phenomena that change as a function of position. The drawback to this type of imaging is the speed at which images can be acquired. Since, the second lockin needs to be 10 times slower than the first one it reduces the speed of the scan by a factor of 10.

3.5. Density of States

The first two techniques both provide information about the flow of electrons through the 2DEG. However, neither provides spectroscopic information about the energy dependence of the flow. In order to obtain this spectroscopic information a different technique is needed. This is analogous to scanning tunneling microscopy where standard images only provide information about the topography. However, spectroscopy can provide much greater detail about the underlying wavefunctions. Our third technique provides this extra level of detail by giving an energy sensitive measure of the electron flow.

The third technique is really an extension of the differential imaging technique. However, instead of scanning the tip to acquire an image of electron flow, the voltage on the tip is changed at a fixed position. This gives information about the energy dependence of the flow because the tip voltage sets the energy scale of the electrons that are backscattered. As the voltage on the tip increases, there is no backscattering and hence no change in the signal until the tip first depletes the electron gas below. Figure 3.13 illustrates the technique of imaging the local density of states. There is a spread in energy of the electrons passing below the tip due to the finite temperature of the experiment. It takes less voltage on the tip to scatter the low energy electrons so

80
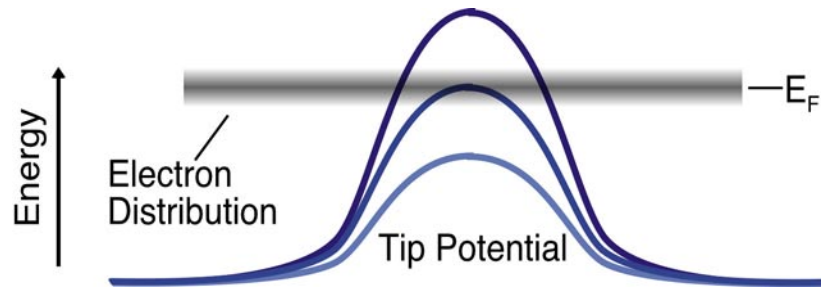
Figure 3.13 Schematic diagram showing how the density of states imaging technique works. As the voltage on the tip increases the backscattering of only certain energy electrons changes giving rise to a signal proportional to the local density of states.

they give a signal at the lowest voltage. As the voltage on the tip increases more of the electron distribution is scattered until the 2DEG is fully depleted under the tip. When the voltage on the tip is well above or below the Fermi energy there is little change in the number of electrons backscattered as a function of tip voltage. However, when the tip voltage is at the Fermi energy there is the largest change in the number of electrons backscattered with tip voltage. This measurement gives a signal that is proportional to the derivative of the electron energy distribution with respect to energy.

Figure 3.14 plots the differential conductance with respect to tip voltage, dG/dVtip versus the tip voltage. There is very little signal until the tip first depletes the electron gas around 2.5 V, then the signal rapidly rises and falls. This peak is in the shape of the electron energy distribution as shown by the red line, which is the expected Fermi distribution. There are two free parameters in this fit, the first one is the height of the signal and the second one is the location of the maximum. The height of the peak is an indication of the strength of the flow at the given point. The location of the peak gives the local Fermi energy. The wiggles in the signal for larger tip voltages are due to the size of the depletion region growing. The position of the front edge of the depletion

81
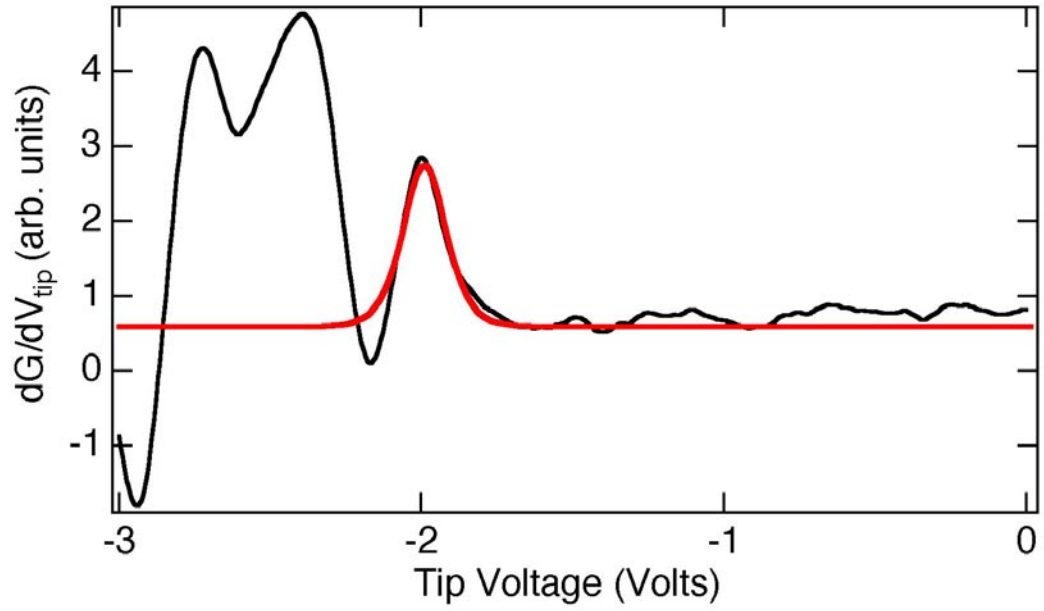
Figure 3.14 Plot of differential conductance with respect to tip voltage as a function of tip voltage. This gives the local density of states under the tip. The red line is the expected Fermi distribution of electrons.

region is moving towards the QPC and goes through the fringes seen in Figure 3.12 (b),

which gives rise to the oscillations seen in the plot.

Chapter 4

Imaging Local Electron Density

This chapter describes the results of our experiments to image local electron density. Section 4.1 describes the sample structure and basic device properties including the effect of the back gate on the electron density. Section 4.2 discusses the imaging technique and presents images of coherent electron flow for different back gate voltages. Section 4.3 details the data analysis procedures used to extract the density from an image of electron flow. The results for the local electron density are compared with the expected density using a parallel plate capacitor model and Shubnikov-de Haas measurements. The last section, 4.4, describes our results of mapping the electron density in the two-dimensional electron gas.

We measure the local electron density in the two-dimensional electron gas (2DEG) by imaging the coherent electron flow from a quantum point contact (QPC). The images show the pattern of electron flow, and they are decorated by interference fringes spaced by half the Fermi wavelength. The spacing of these fringes is our measure of the local electron density. The fringes arise from interference between backscattered paths from the tip to the QPC. As the position of the tip is changed the path length changes and the interference goes from constructive to destructive and back to constructive. If the tip is moved a distance d from one constructive interference peak to the next one, the phase accumulated along this path is 2π and must equal $2dk_F$ where k_F is magnitude of the local Fermi wavevector. In this way, the spacing of the interference fringes measures the local

value of the Fermi wavevector.

The technique discussed in this chapter can be used to profile the electron density distribution in new 2DEG devices. We are able to resolve small changes in the local density because of the high resolution of the images. The spatial resolution of the technique can profile changes in the local electron density on a length scale of about 100 nm. This scale is set by the requirement that we take the Fourier transform over several wavelengths in order to obtain precise density information.

4.1.   Sample Design and Characterization

In this experiment we have fabricated quantum point contact (QPC) devices in GaAs/AlGaAs heterostructures. The heterostructure is grown by molecular beam epitaxy on a n-type GaAs substrate. The layers in growth order are a smoothing superlattice, 1 μm GaAs, 22 nm $Al_{0.3}Ga_{0.7}As$, δ-layer of Si donor atoms, 20 nm $Al_{0.3}Ga_{0.7}As$, and a 5 nm GaAs cap layer. The two-dimensional electron gas (2DEG) is located 57 nm beneath the surface at the interface of the GaAs and $Al_{0.3}Ga_{0.7}As$ layers. Figure 4.1 shows a scanning electron micrograph of one of the devices. A negative voltage is put on the QPC gates with respect to the 2DEG to create a variable width channel through which the electrons must flow. We use the n-type conducting substrate as a back gate for our devices. The back gate is located about 2 μm below the 2DEG, allowing the density to be modified using a fairly small voltage.

Figure 4.2 shows the measured conductance through the QPC as a function of the voltage on its gate for a series of back gate voltages. This shows conductance steps at multiples of $2e^2/h$ as found previously [van Wees, (1988); Wharam, (1988)]. This is due
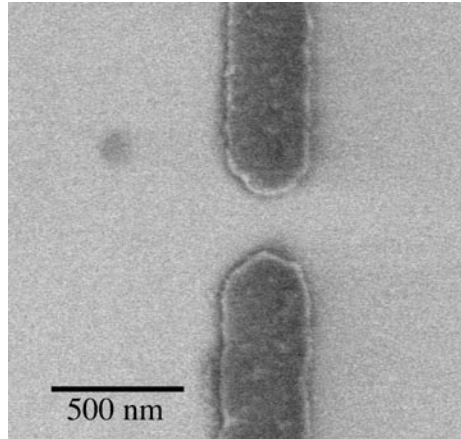
Figure 4.1 Scanning electron micrograph of a typical quantum point contact device used in the experiments.
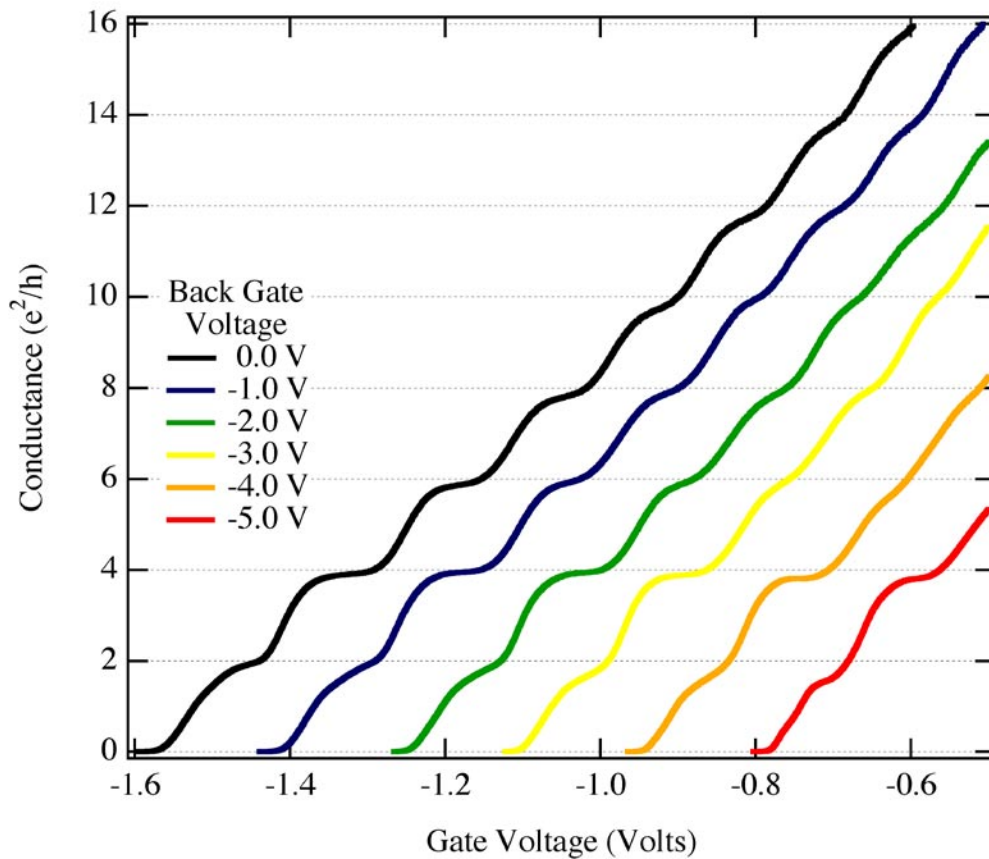
Figure 4.2 Conductance through the QPC as a function of the voltage on its gate. This shows clear conductance plateaus at multiples of $2e^2/h$. A variety of back gate voltages are plotted showing the decreasing density of the 2DEG.

to each new quantum mode of the QPC becoming accessible as its width is opened. As the back gate voltage is made more negative, the gate voltage required to pinch off the QPC is less. This is because the density is being reduced requiring less gate voltage to deplete the electron gas. The second reason is the width of the constriction must be larger for the electrons to get through since their wavelength is increasing. As the density is reduced, the plateaus no longer lie exactly on multiples of $2e^2/h$. This is due to increased backscattering near the QPC, which reduces its conductance. The plateaus are also not as well defined as the density decreases because the energy spacing between subbands of the QPC decreases. The finite temperature of the measurement means that the electrons have a spread in energy, which allows them to travel through multiple subbands causing the plateaus to blur. Each step in the conductance is the Fermi function for the occupation of the given mode of the QPC.

Before measuring the local electron density with our imaging technique, we have characterized the effect of the back gate on the average density of the 2DEG. To study the effect of the back gate voltage on the density, we have measured the density of the 2DEG using Shubnikov-de Haas oscillations. With a large perpendicular magnetic field applied to the sample, the constant two-dimensional density of states becomes a series of sharp peaks centered at the Landau levels. The positions of the Landau levels are given by $E_n = (n + 1/2)\hbar\omega_c$, where ω_c is the cyclotron frequency, $\omega_c = eB/m$. The Shubnikov-de Haas oscillations occur as each successive Landau level is emptied by increasing the magnetic field. There is a dip in the longitudinal resistance when the Fermi energy equals the energy of the Landau level giving oscillations that are periodic in the inverse magnetic field. Figure 4.3 plots the measured change in longitudinal resistance as a
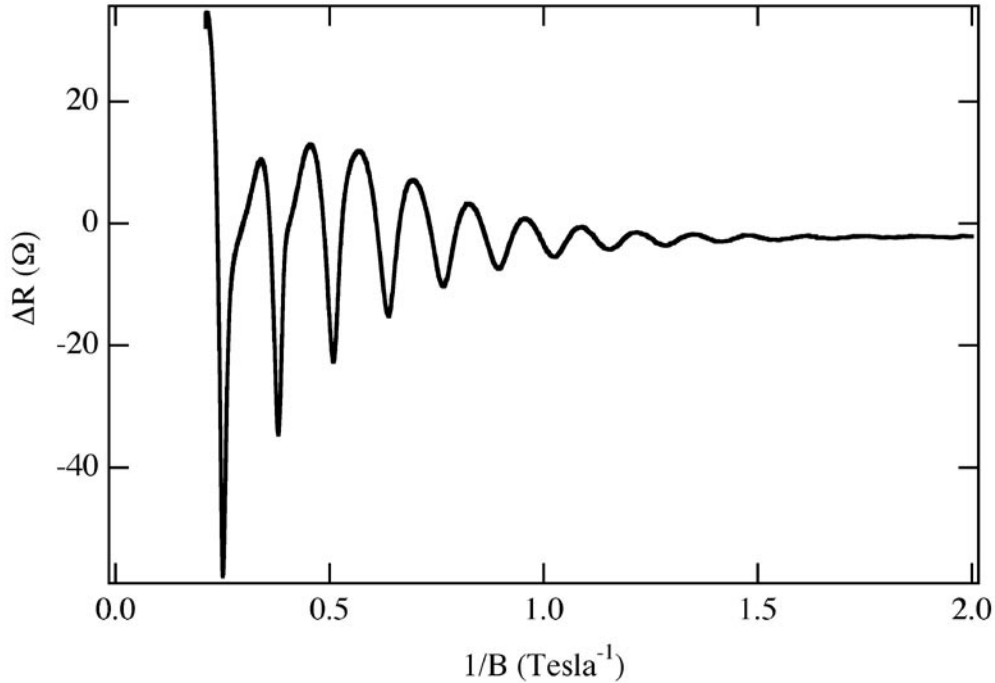
Figure 4.3 Measured longitudinal resistance as a function of inverse magnetic field showing the Shubnikov-de Haas oscillations. These oscillations are periodic in the inverse magnetic field. Their period gives the electron density in the 2DEG.

function of inverse magnetic field. This shows the Shubnikov-de Haas oscillations that are periodic in inverse magnetic field. Their period gives the density of the 2DEG using the formula $n_s = 2e/(h\ \Delta(1/B))$ where e is the electron charge, h is Planck's constant and $\Delta(1/B)$ is the period of the oscillations. This measurement was repeated for a series of back gate voltages, which reduce the density. Figure 4.4 shows the effect of the back gate voltage on the average density. Each of the Shubnikov-de Haas measurements gives one of the data points in the plot of density versus back gate voltage. This data was taken from a different piece of the same wafer as used in the imaging experiment. A four terminal resistance measurement was also done to determine the resistivity of the 2DEG. From the resistivity and the Shubnikov-de Haas measurement, the mobility as a function
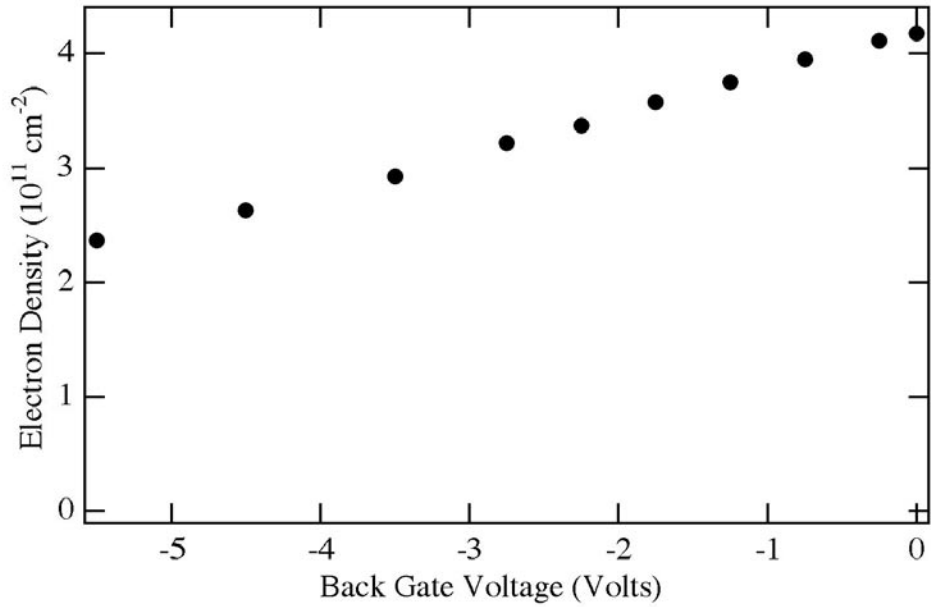
Figure 4.4 Measured density as a function of back gate voltage, showing a linear decrease in density. This measurement was done using the Shubnikov-de Haas oscillations.

of the density can be determined. This is plotted in Figure 4.5 showing a decrease in

mobility with decreasing electron density. This is due to the disordered background
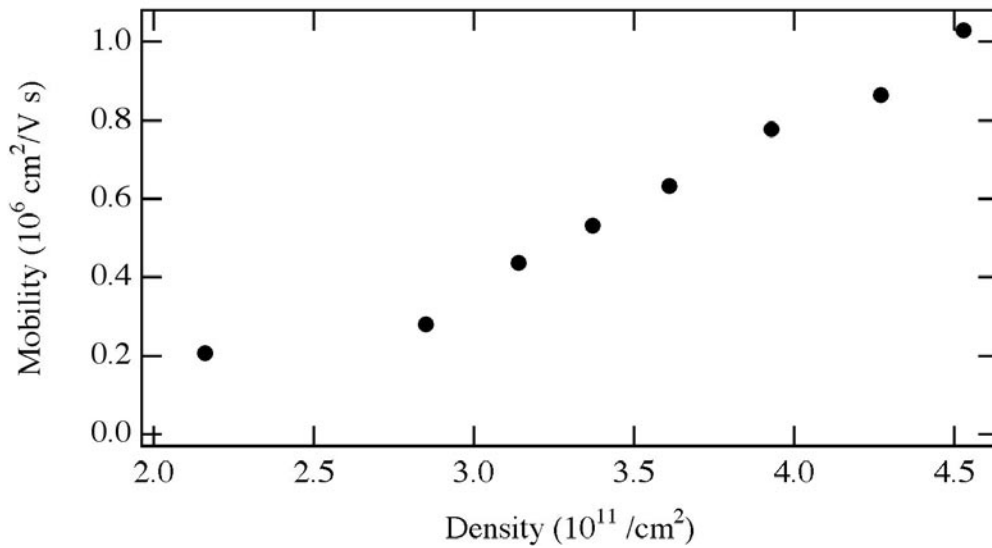
Figure 4.5 Measured mobility of the 2DEG as a function of the density. This shows the mobility decreasing due to the increasing scattering as the density is reduced.

potential becoming a larger part of the Fermi energy as the density is reduced. The bumps and dips in this potential lead to scattering, which limits the mobility. To further investigate the reduction in density and mobility, we have imaged the electron flow as a function of back gate voltage.

4.2. Imaging Electron Flow

Scanning probe microscopes can provide information about mesoscopic devices on a length scale not accessible with standard transport measurements. In this section, the local density of electrons is probed using a scanning probe microscope. This gives the density on a 100 nm length scale. Compare this with a standard Shubnikov-de Haas measurement of density that yields the average density over the entire sample but does not give any local information. The ability to image the density on these short length scales is important for the design of new mesoscopic devices. This technique can also be used to probe the density in new semiconductor heterostructures.

The experimental setup that we use to measure the local electron density is shown in Figure 4.6. This is the same setup that is used to acquire images of electron flow that was discussed in the previous chapter. The one important aspect to note is that the samples used in this experiment have a back gate that allows the density to be changed. This provides an experimental degree of freedom that allows us to check our measurements. The conductance through the QPC between two ohmic contacts is measured as a function of tip position. A negative voltage is put on the tip with respect to the 2DEG to create a small depleted region below it. This depleted region backscatters electron waves and reduces the conductance through the QPC. By scanning the tip over
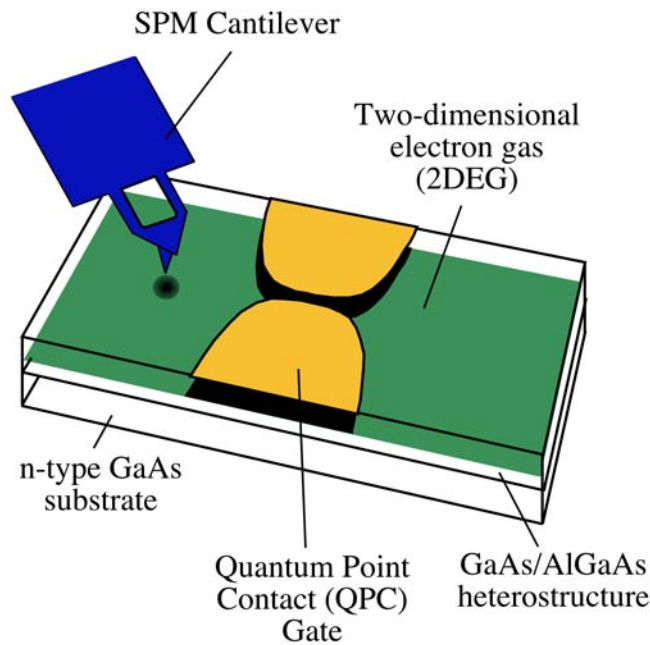
Figure 4.6 Measurement setup for imaging local electron density. The SPM tip is scanned above the surface of a GaAs/AlGaAs heterostructure with a negative voltage on it with respect to the 2DEG. The conductance as a function of tip position is recorded to obtain an image of coherent electron flow.

the sample and measuring the conductance as a function of tip position, an image of

electron flow is obtained. The images are decorated by interference fringes spaced by

half the Fermi wavelength, whose spacing is used to measure the local electron density.

Images of electron flow were obtained by raster scanning the tip over the sample

and measuring the conductance as a function of tip position. The voltage on the tip was

set at -3 V with respect to the 2DEG, which created a small depleted region in the 2DEG.

This depleted region backscatters electron waves causing the conductance to be reduced.

When the tip is over areas of high electron flow there is a large reduction in conductance

whereas when the tip is over areas of little or no flow there is a correspondingly small

change. Figure 4.7 is four images of electron flow from the QPC for four different back

gate voltages. The back gate voltage in the four images is (a) 0 V, (b) -1 V, (c) -3 V, and
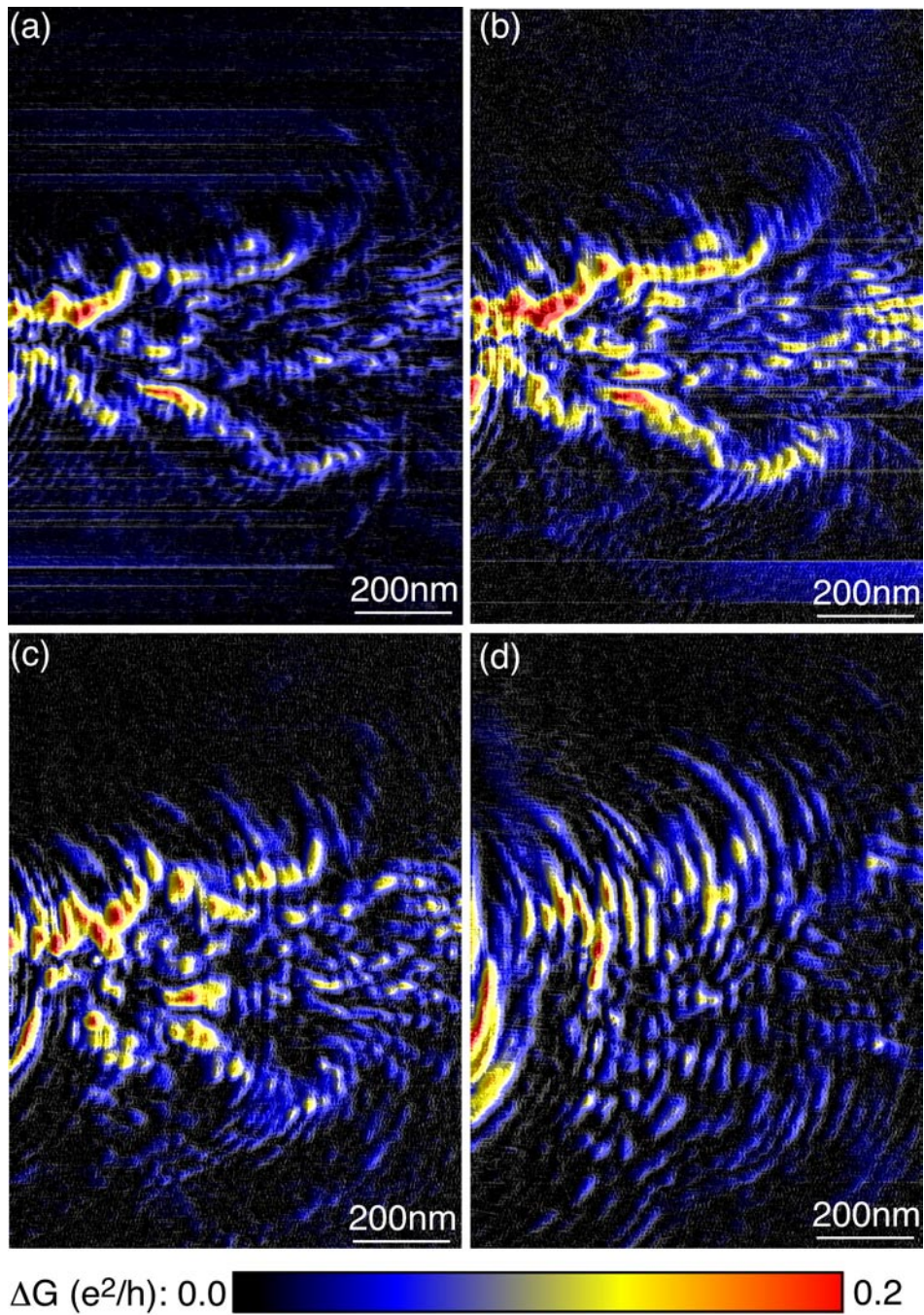
Figure 4.7 Four images of electron flow from the QPC for different back gate voltages: (a) -0.0 V, (b) -1.0 V, (c) -3.0 V and (d) -5.0 V. These show the spacing of the interference fringes increasing and the flow becoming more diffuse.

(d) –5 V. These images show how the electron flow changes with back gate voltage.

The spacing of the interference fringes that decorate the images increases as the back

gate voltage decreases. This occurs because the fringes are spaced by half the Fermi

wavelength, which is being increased by the decreasing density. The second feature is

the strength of the branches of flow becomes less pronounced with decreasing back gate

voltage. This is due to the flow becoming more diffuse since the mobility and hence the

mean free path is being reduced. Each branch of current is scattered and split into new

branches more quickly since the mean free path is shorter. This leads to an image that no

longer shows the narrow branches of current and instead becomes more uniform.

4.3. Measuring Local Density

In order to measure the local electron density, we must extract the spacing of the

interference fringes while removing the background electron flow. Since the fringes are

spaced by half the Fermi wavelength, there is a simple relation between their spacing, d,

and the electron density, n. This relation is given by $n = \pi/(2d^2)$. A measurement of the

density turns into a measurement of the spacing of the interference fringes. To isolate

the interference fringes from the background flow, we used a spatial high pass filter.

The high pass filtering was done by smoothing the data to remove the fringes and then

subtracting this smoothed version from the original. The smoothing was done along the

direction perpendicular to the fringes in order to reduce the fringe amplitude without

changing the amplitude of the branches of electron flow. This filtering left only the high

frequency components in the original scan. This analysis was done for a small section

of each scan to isolate the interference fringes. Figure 4.8 shows the high pass filtered

images of electron flow from a small section of each image in Figure 4.7. The back gate voltage for each images is as follows: (a) 0 V, (b) –1 V, (c) –3 V and (d) –5 V. As the back gate voltage becomes more negative, the spacing of the fringes clearly increases indicating that the density is being reduced. These images no longer show any evidence of the background branches of electron flow. To improve this measurement, images of the spatial derivative of electron flow could be obtained using the oscillating tip voltage technique discussed in Chapter 3. This would eliminate the need for the spatial filtering of the images since the imaging technique does the filtering automatically.

To extract the spacing of the fringes from these images, a two-dimensional fast Fourier transform (FFT) was done on each image. This gives the both the wavelength
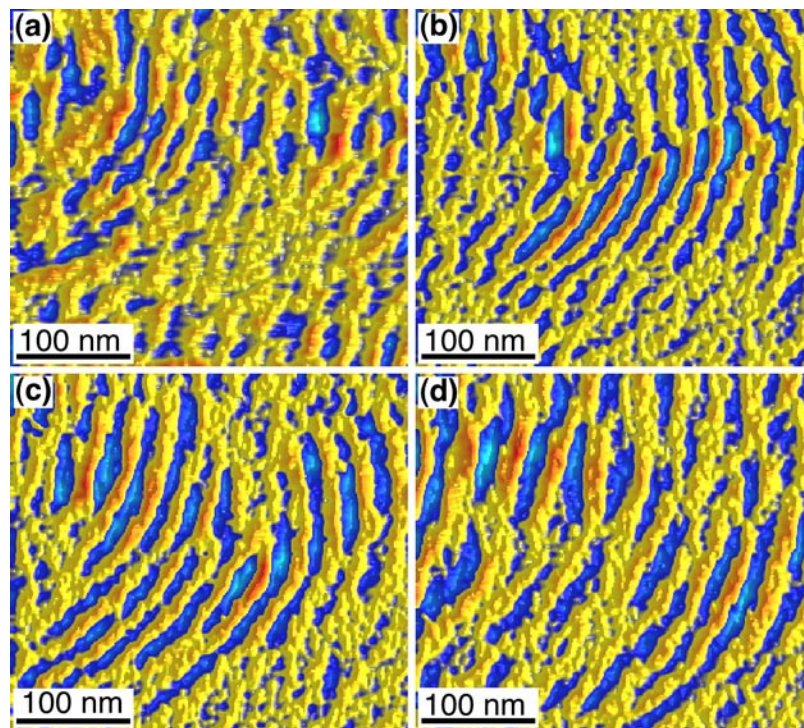
Figure 4.8 Images of the interference fringes for four different back gate voltages: (a) -0.0 V, (b) -1.0 V, (c) -3.0 V and (d) -5.0 V. These images are from a small section of the images in Figure 4.7 and have been spatially high pass filtered.

and direction of the fringes. The fringes are oriented perpendicular to the direction of electron flow, so their direction gives information about the direction of electron flow. After performing the FFT, the location of the peak was found giving the spacing of the interference fringes. An example of the FFT obtained for the -1 V on the back gate scan is shown in Figure 4.9. The red circle shows the dominant frequency in the image, which
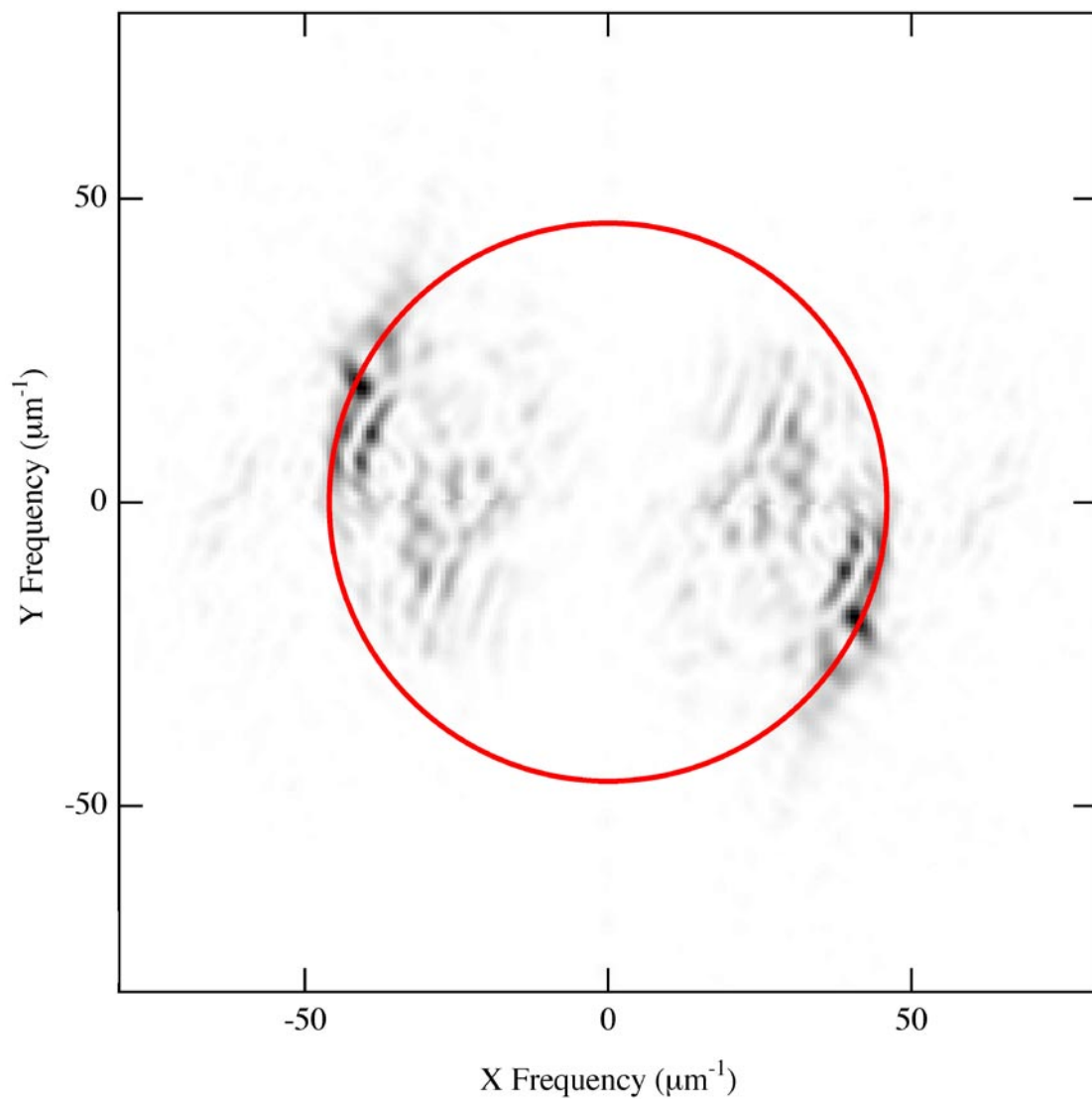
Figure 4.9 FFT of the image with -1.0 V on the back gate, Figure 4.8 (b). The red line gives the magnitude of the dominant frequency in the image.

is at a constant distance from the center of the image. The radius of the circle was chosen

so that it passed through the peak in the FFT. We are only interested in the magnitude of

this frequency in order to obtain the wavelength of the fringes. To convert this frequency

into a wavelength of the electrons, we take the inverse of the magnitude. This gives the

spacing of the fringes, which is half of the wavelength.

This process was repeated for each of the scans to obtain the wavelength as a

function of back gate voltage. The scans were taken in steps of -1 V on the back gate

starting at 0 V. To convert the wavelength to density, we use the formula $n = \pi/2d^2$, where

d is the fringe spacing. The density in each of the scans is plotted in Figure 4.10. This

shows that the density decreases linearly with back gate voltage starting slightly below

4.0×10^{11} cm^{-2}.
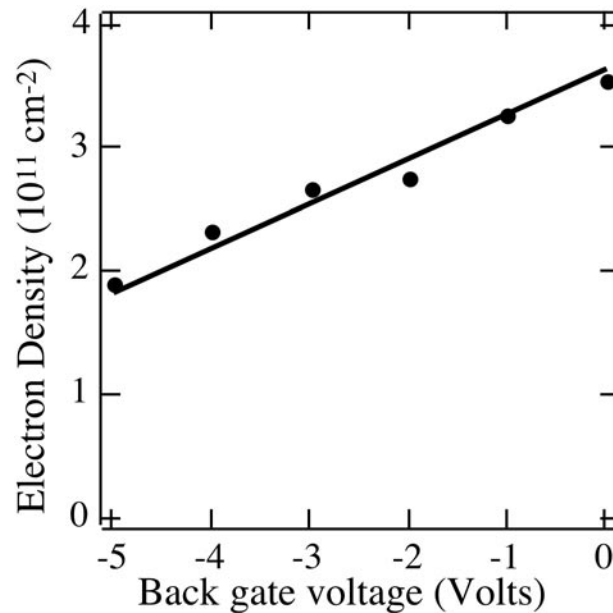
Figure 4.10 Imaged density as a function of the back gate voltage. The circles were found using the FFT technique discussed in the text. The solid line is the expected change in density from a capacitor model.

In order to compare our results with the expected change in density as a function of back gate voltage, we have used a simple parallel plate capacitor model. The conducting GaAs substrate, the back gate, is separated from the 2DEG by layers of GaAs and AlGaAs. Figure 4.11 shows the layers that we use in our capacitor model. This gives an expected change in density of 0.36 x 10^{11} cm^{-2}/V on the back gate. This is shown by the line in the plot of density versus back gate voltage in Figure 4.10. The value of the density at 0 V is the one free parameter. This was chosen to produce the best match with the measured density using our imaging technique. This value is slightly lower than the value measured by Shubnikov-de Haas oscillations on another sample from the same wafer. There are several possible reasons for this slight difference, which are outlined below. In this sample there are gates for the QPC nearby, which may lower the electron density. There is also the charged cantilever that the tip is on. According to the specifications of the piezolevers, the tip is at least 2 μm long meaning the cantilever is more than two μm away. Assuming it is 2 μm long, gives a change in
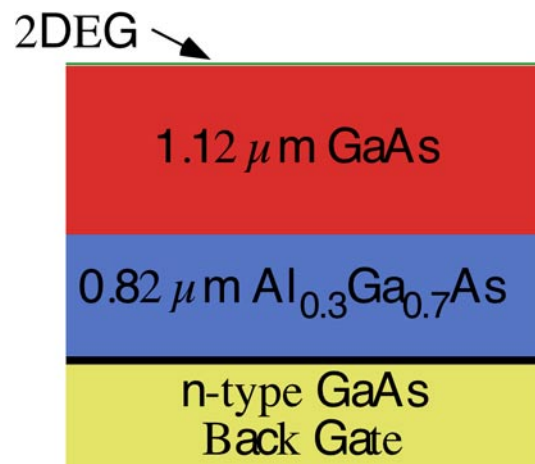
Figure 4.11 Schematic diagram of the layers used in the capacitor model for the expected change in density with back gate voltage.

density of 0.083×10^{11} cm^{-2}, which accounts for some of the discrepancy between the two measurements. The third possibility is that the density varies between the two samples, which is possible considering we see a variation of density of up to 20 percent even within a single sample.

4.4. Mapping Electron Density

To further investigate changes in density within a sample, we have imaged the local electron density at several locations to create a map of the local density. Figure 4.12 is an image of the electron flow in the sample showing the interference fringes. We divided this scan into 16 parts and found the density in each of these regions. Each of the regions that we used for creating the map was a circle with a radius of 100 nm. The regions were spaced by 200 nm. The density was found using the same procedure as
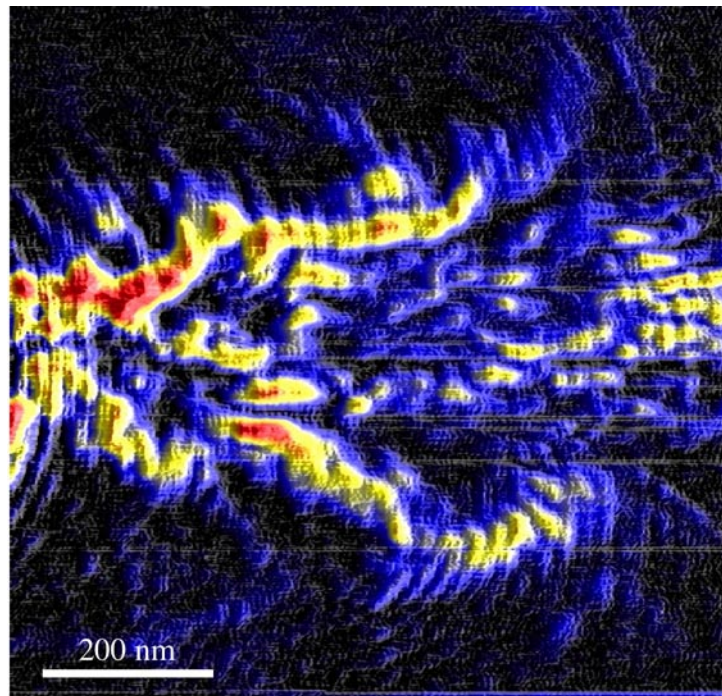
Figure 4.12 Image of electron flow used to generate the map of electron density.

in the previous section for the different back gate voltages. An example of two of the regions used in generating the density map and their FFTs is shown in Figure 4.13. In each FFT, there is a circle that gives the maximum signal, which is shown in red. The radius of this circle was taken as the spacing of the interference fringes for this region when calculating the local density of the image. For the two FFTs, the peak value along this red circle occurs at different values of f_x and f_y indicating that the electron flow is pointed in different directions in the two images. The value of the x and y coordinates of the peak were used to determine the direction of electron flow in the region. Figure 4.14 plots the measured density at each of the 16 locations. A linear interpolation was done between each of the points to produce the map of electron density. The arrows in the image represent the direction of electron flow at that location based on the direction of the fringes. From this map of electron density, we found an average density of 2.95×10^{11} cm^{-2}. This average density is in fairly good agreement with our previous imaging and Shubnikov-de Hass measurements. The measured density had a standard deviation of about 15 percent. This is fairly consistent with the simulations done by Scot Shaw [Shaw, (2002)] of the expected variation in density due to the random placement and ionization of donor atoms.

In summary, we have developed a technique for imaging the local electron density in a 2DEG. The technique relies on measuring the interference fringes in images of electron flow to obtain the local Fermi wavelength and hence the density. We are able to image spatial variations in the density on a scale of about 100 nm. The results for the change in density as a function of back gate voltage are in excellent agreement with a parallel plate capacitor model. We have also mapped the variation in the density due to
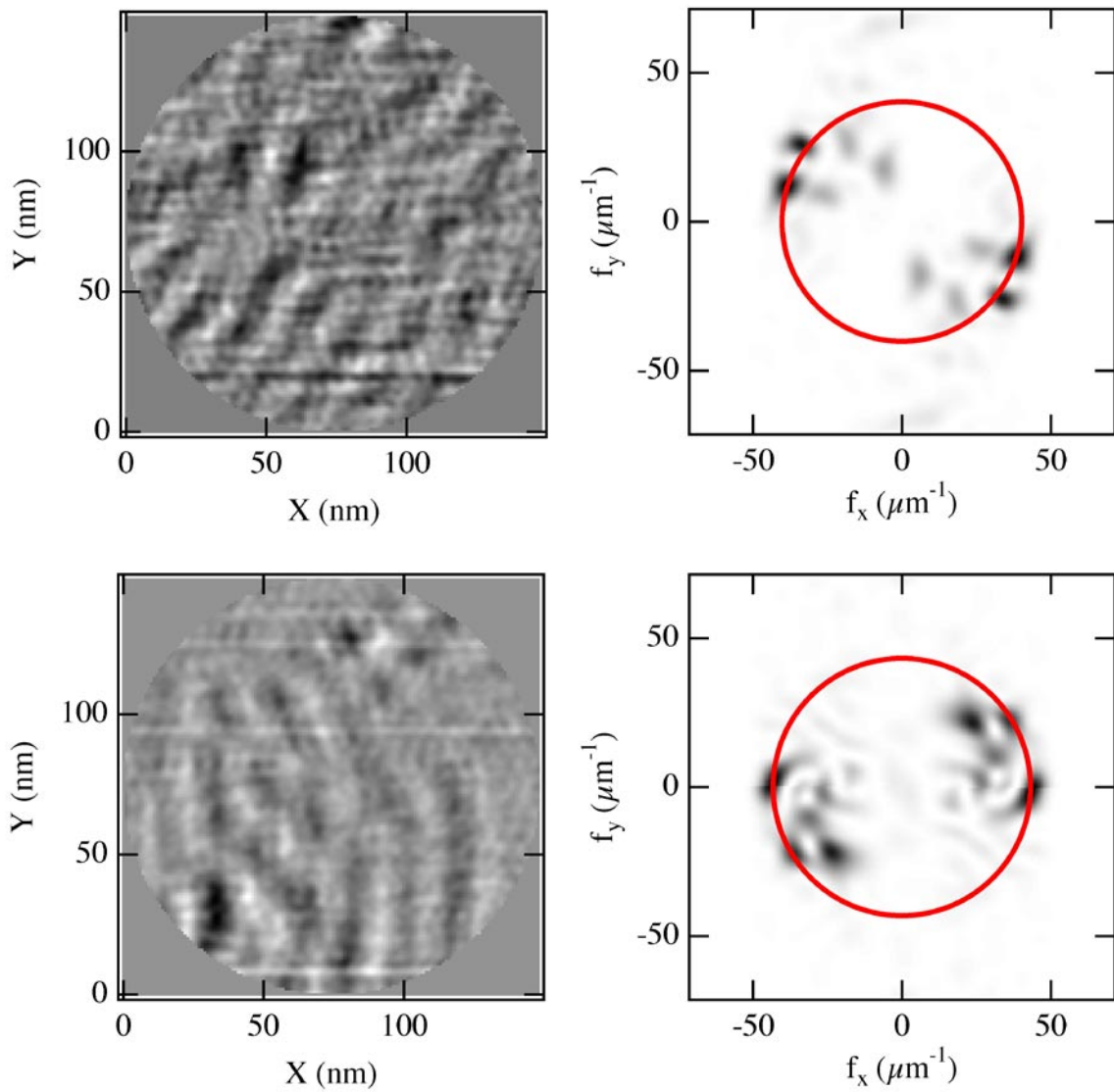
Figure 4.13 Two images of electron flow and their corresponding Fourier transforms from two locations in the image used for mapping the local electron density. The red line on the Fourier transforms shows the magnitude of the frequency corresponding to the local density.
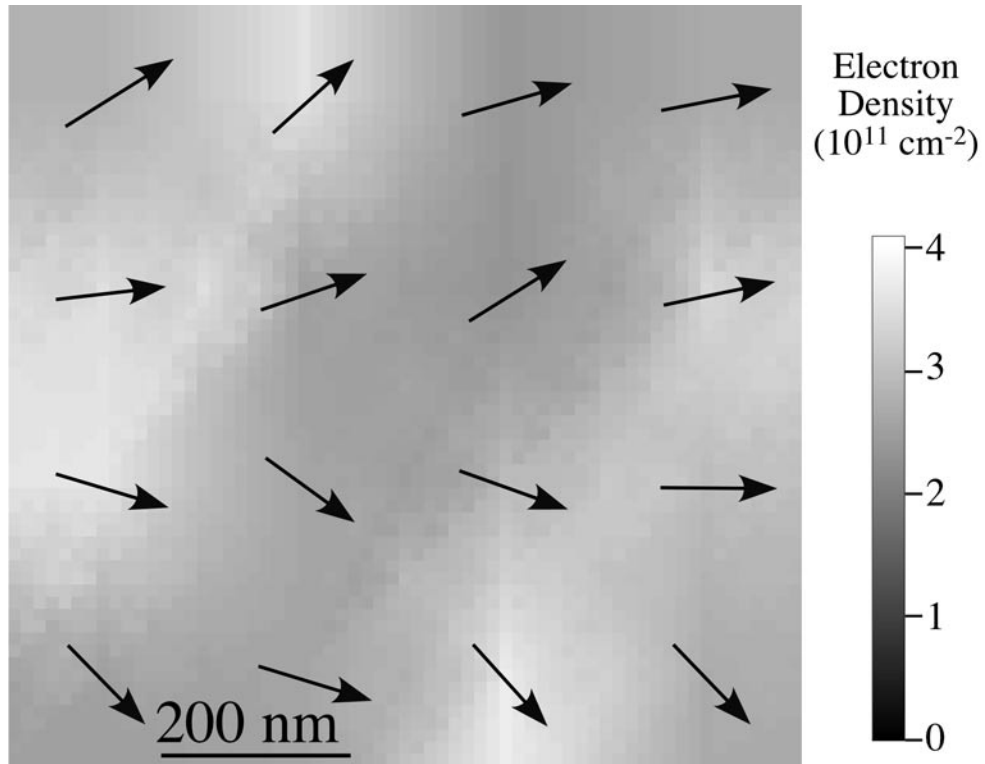
Figure 4.14 Map of the local electron density found using the FFT method described in the text. The arrows indicate the direction of electron flow at that location.

the random ionization of donor atoms. The technique is useful for probing the complex

density patterns that can be achieved with semiconductor growth and fabrication.

Chapter 5

Imaging Electron Energy Loss

In this chapter, we demonstrate a technique for measuring the electron-electron scattering rate in a two-dimensional electron gas using our imaging technique. Section 5.1 describes the technique, which involves measuring the decay of the backscattered signal as a function of the applied source-drain voltage. Section 5.2 presents images of electron flow for different applied source-drain voltages. The images of electron flow show the signal decreasing for increasing source-drain voltage indicating an increased scattering rate. Images are acquired as a function of distance and Fermi energy, showing increasing scattering with distance and decreasing Fermi energy. A comparison of all of the results with the theory for electron-electron scattering in a 2DEG is done in section 5.3. The results are in good agreement with the theory as a function of distance and energy.

The ability to image electron energy loss is important for the design and understanding of new devices that rely on the coherence of the electron. There has been much experimental interest in studying the energy loss of electrons in 2DEGs through electron-electron scattering [Yacoby, (1991); Muller, (1995), Schäpers, (1995); Predel, (2000)], electron-phonon scattering [Sivan, (1989)] and other mechanisms. However, in all of these experiments it has been very difficult to obtain spatial information about the scattering mechanisms. Most of the experiments have a fixed geometry, which does not allow for the study of the spatial dependence of the scattering

without making multiple samples [Yacoby, (1991)]. The ability to spatially image the energy loss may provide insight into the scattering mechanisms, like the ability to image electron flow provided evidence of branch formation in the 2DEG [Topinka, (2001)].

At the temperatures and experimental parameters of our measurement, the electron-electron scattering length is quite long, on the order of 20 μm.   Since we are not able to image the flow over these large distances we have to shorten the electron-electron scattering length in our measurements. This is done by applying a dc voltage between the source and drain, which accelerates the electrons. They lose this extra energy through collisions with other electrons. Our results indicate that the dominant mechanism for energy loss at the temperatures and energies of the experiment is electron-electron scattering.

5.1.   Measurement Technique

In the previous chapter we have used a technique were the tip creates a depleted region of electrons that backscatters electron waves. This produces a signal that is proportional to the electron flow at that location. In order to measure the energy relaxation, a new technique is needed that is sensitive to the energy of the electrons. Figure 5.1 illustrates the technique that we use to image the energy loss. A dc voltage V_0 is applied between the source and drain electrodes. This voltage accelerates the electrons as they go through the QPC. A fixed voltage is put on the tip with respect to the drain voltage, which scatters electrons hitting the depleted region under the tip. The voltage on the QPC gates is adjusted so that the highest energy electrons can just barely make it through the QPC, while ones that have less energy can only tunnel. A small ac signal is
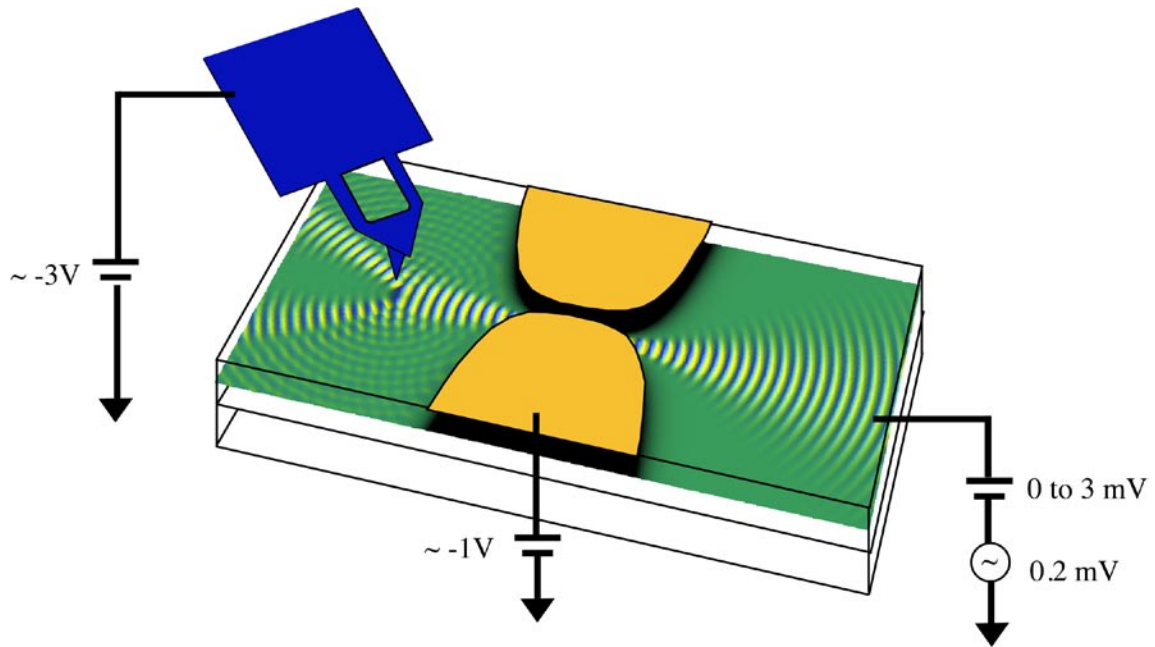
Figure 5.1 Illustrates the technique used for imaging electron flow with an applied dc bias. The voltage on the tip and gates are held fixed with enough voltage on the tip to deplete the electron gas. A dc bias is applied to one side of the QPC with a small ac voltage to achieve energy selectivity.

added to the dc voltage across the QPC to use for lockin detection. This lockin detection mechanism ensures that the measurement is only sensitive to electrons in a narrow energy band. An image of the conductance as a function of tip position is recorded. In order to understand the images of electron flow, we have to consider two cases: the electron goes from the QPC to the tip and back without losing any energy and it loses some energy on this roundtrip. The two cases are shown in Figure 5.2. In the first case, Figure 5.2 (a), the electron has not lost any energy and will be able to go back through the QPC. This backscattering will cause a reduction in the conductance when the tip is present. In the second case, Figure 5.2 (b), the electron loses energy during the roundtrip and can no longer go back through the QPC. Therefore, there will be no signal from this electron and no image of electron flow. By measuring the strength of the electron flow as a
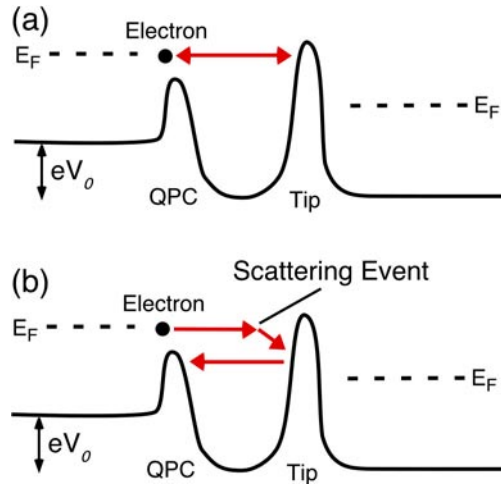
Figure 5.2 Illustrates the mechanism used for dc bias imaging. In (a) the electron does not scatter in the roundtriup from the tip to the QPC and therefore the tip reduces the conductance. In (b) the electron loses energy due to a scattering event and can not go back through the QPC. This eliminates the backscattered signal from the tip.

function of distance, the rate of electron energy loss is determined. The measurement of the electron flow is done by recording the differential conductance, $g = \partial I/\partial V_{ds}$ as a function of tip position. We are interested in how much the flow changes when the tip is present so the relevant quantity is the change in differential conductance Δg. This is found by subtracting the signal when the tip is present from the signal without the tip. As the distance from the tip to QPC increases, there is more time for the electron to lose energy and the signal should become weaker. The signal should also become weaker as the dc bias V_0 is increased because the electron has more available states to scatter into, which increases its scattering rate.

5.2. Images of Electron Flow

Figure 5.3 shows two images of electron flow from the same area. Figure 5.3 (a) has no dc voltage V_0 applied across the QPC and Figure 5.3 (b) has $V_0 = 2.4$ mV applied
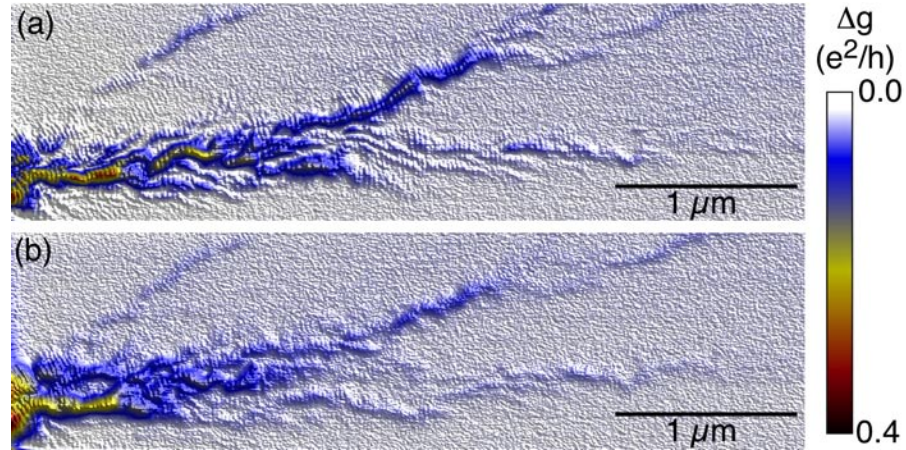
Figure 5.3 Shows two images of electron flow. (a) has no dc voltage applied, in (b) there is 2.4 mV applied across the QPC to accelerate the electrons. Near the QPC, the two images have very similar strength but as the distance increases the signal decays faster in (b) due to the increased scattering.

across the QPC, which accelerates the electrons. In each image there is a small ac voltage of 0.2 mV used for the lockin detection. Near the QPC, the images have very similar contrast, the strength of the flow is similar is each image. However, at the farthest distances the 2.4 mV bias image is much weaker. This value of V_0 increases the rate at which electrons lose energy causing the image to be fainter at large distances. By measuring the decay of the signal as a function of distance, a determination of the electron scattering time is determined. For a V_0 of 2.4 mV, the theoretical electron-electron scattering length is about 2.0 μm. This should give a decay of our signal by 63% at a distance of 1.0 μm because it is the roundtrip from the QPC to tip that is needed to produce the signal. It is also important to note that the interference fringes are present in both images showing that the measured flow is coherent. Because the fringes arise from an interference effect between different paths, a loss of coherence would destroy the interference effect. These interference fringes can give a measure of the electron energy

105

because they are spaced by half the Fermi wavelength as discussed in Chapter 4.

As the dc bias V_0 is increased, the electrons have extra energy and hence a shorter wavelength. Figure 5.4 plots the electron wavelength as a function of V_0. This is done for two different distances from the QPC. The red circles are one μm away and the blue triangles are two μm away. The value of the wavelengths was determined using a Fourier transform method. A one-dimensional line sample was taken perpendicular to the fringes. The FFT of this one-dimensional sample was found to give the spacing of the interference fringes. The solid line is a fit to the expected change in wavelength as a function of
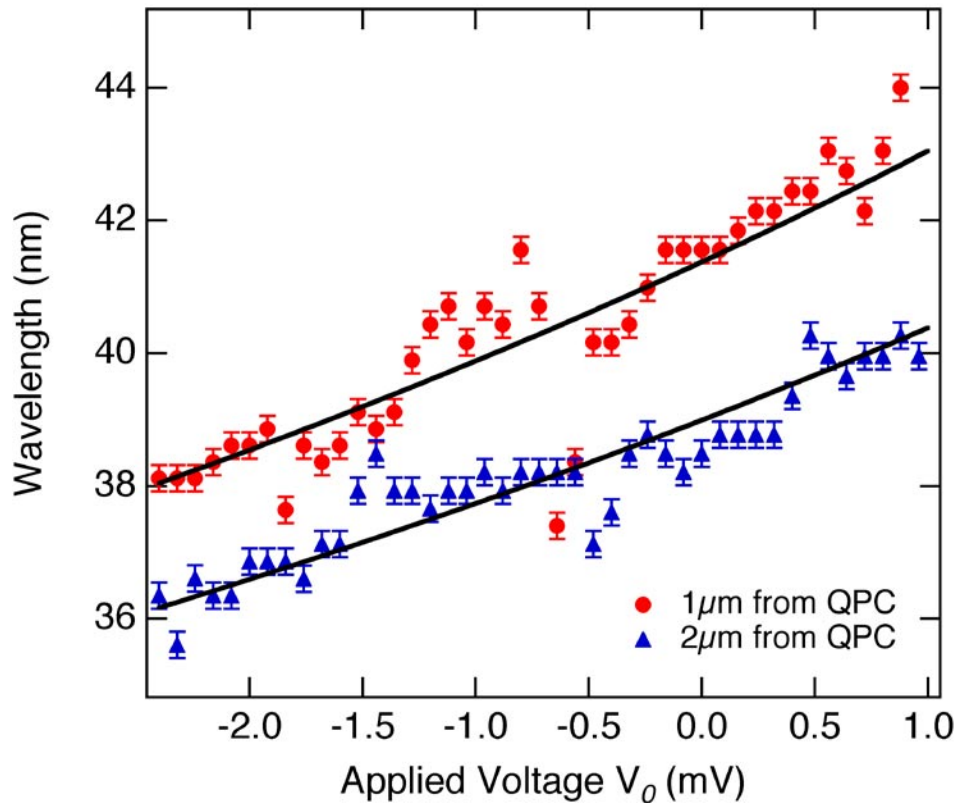
Figure 5.4 Plot of the measured wavelength of the electrons versus the applied dc voltage for two distances from the QPC. The black line is the expected wavelength based on the Fermi energy and applied voltage. This graph shows that the wavelength of the electron increases with the applied voltage as expected.

excess applied voltage. The wavelength shifts because the applied voltage V_0 is added to the energy of the electron. This gives the following equation for the wavelength versus applied voltage.

$$\lambda^{-1} = \sqrt{\frac{2m}{h^2}\left(E_F - eV_0\right)}$$

The expected fringes spacing is in very good agreement with the measured wavelength as a function of applied bias voltage. There is one free parameter in this fit, which is the Fermi energy of the 2DEG. At each of the two distances, the value needed for the best fit is within 2% of the measured Fermi energy for the scan without any excess applied voltage. There is a difference in the wavelength for the two distances, which may arise from the fall off in the potential from the QPC gate. The potential of the gate falls off fairly slowly leaving some portion even at one micron. Another possible explanation is a variation in the local electron density as discussed in section 4.4. This result shows that the electrons are being accelerated by the excess energy applied across the QPC.

To further investigate the distance dependence of the electron energy loss, we have looked at three small regions of the electron flow. These are located at three different distances from the QPC. The closest one is at 0.6 µm, followed by 1.0 µm and the farthest is at 1.4 µm. Figure 5.5 shows the electron flow at these three locations for four different dc bias voltages V_0 at a temperature of 1.7 K. The color scale is the change in differential conductance, Δg for the given tip position. The distance from the QPC to the images is as follows (a-d) 0.6 µm, (e-h) 1.0 µm, and (i-l) 1.4 µm. Moving from left to right, V_0 goes from 0 mV up to 3 mV in steps of 1 mV. As the bias is increased the strength of the signal decreases for all three distances. However, it decreases much
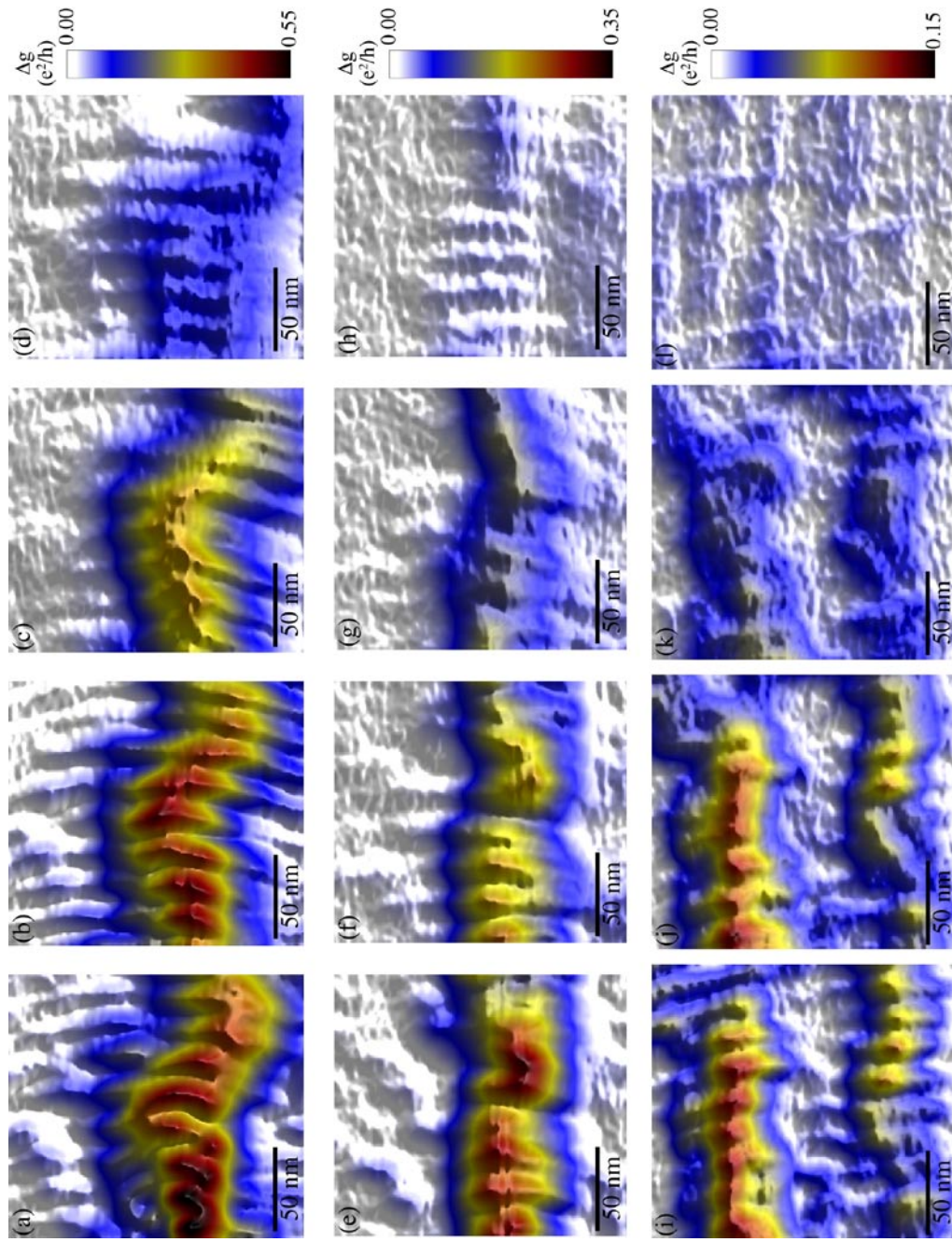
Figure 5.5 Images of electron flow for three distances and four dc bias voltages at a temperature of 1.7 K. The rows are at distances of 0.6 μm, 1.0 μm and 1.4 μm. The columns have the following applied dc voltages V_0, 0 mV, 1 mV, 2 mV and 3mV. The signal decays for increasing dc voltage and increasing distance

more quickly at the longest distance compared to the shortest one. At 1.4 µm and 3 mV, Figure 5.5 (l), we see almost no signal; it is primarily noise. This is in contrast to 0.6 µm and 3 mV, Figure 5.5 (d), where the signal is still quite strong. This shows that the electrons are losing their excess energy as they make the 2.8 µm roundtrip from the tip to the QPC in this image. However, in the shorter distance, the electron is less likely to undergo a scattering event and therefore the signal is not decaying as fast. To fully characterize the electron-electron scattering analysis of the signal as a function of the excess applied energy is necessary.

A detailed study of the energy dependence of the signal was done by looking at the electron flow image as a function of the applied dc bias V_0. This was done at the same three locations as discussed earlier. To investigate the energy dependence, the average change in conductance was measured as a function of V_0. This average change $\overline{\Delta g}$ was found by averaging the measured signal over the entire scan area. This generates one data point of $\overline{\Delta g}$ for each value of V_0. Figure 5.6 plots this measured $\overline{\Delta g}$ versus bias voltage V_0. There are three sets of data for the three different distances. Each of the values in the plot has been normalized to the value without any dc bias. This means that each curve starts at 1 in the center. The three curves have been offset from each other for clarity. In all three cases, the measured signal decreases with increasing energy. However, as the distance increases the signal decreases more quickly indicating that more scattering has occurred. This is in agreement with expectations because the electron has a longer time to scatter for the longer distances.

After studying the distance dependence of the electron-electron scattering, we looked at the effect of changing the Fermi energy of the electrons. For a fixed excess
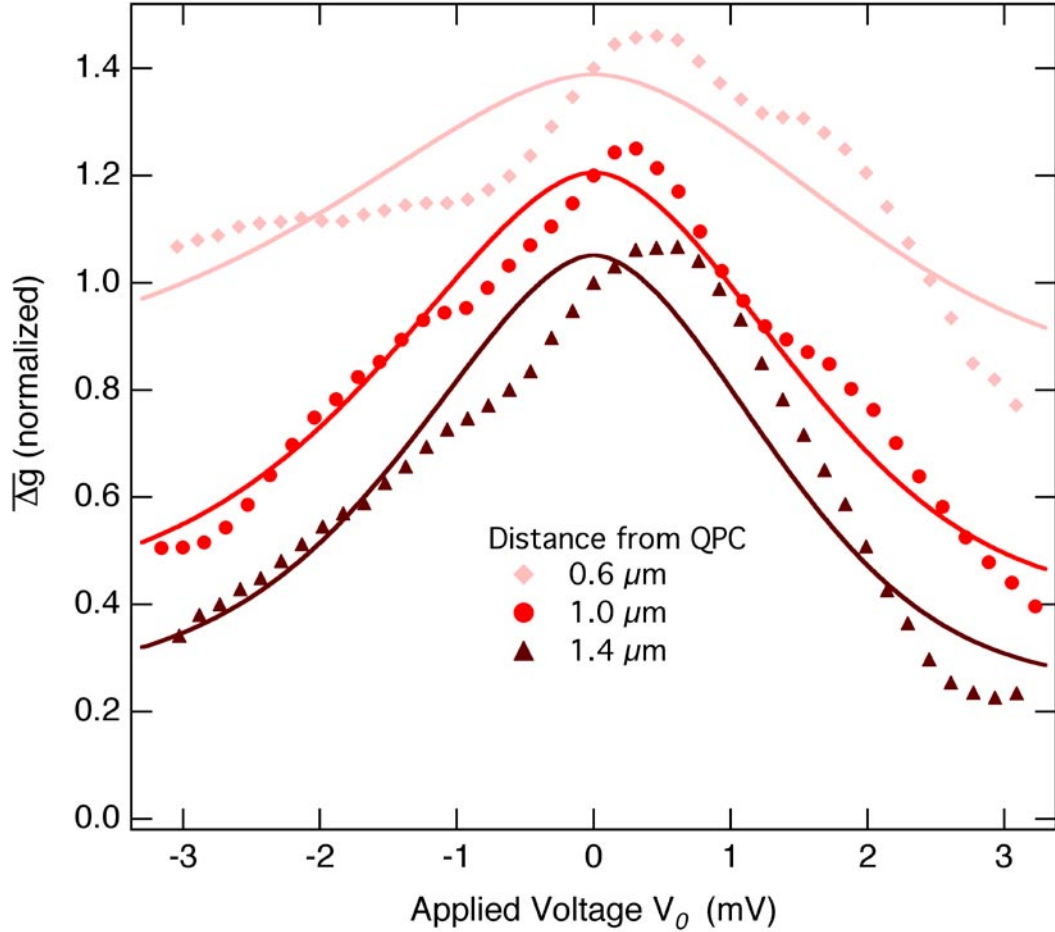
Figure 5.6 Plot of the average measured signal as a function of applied dc voltage V_0 for three different distances from the QPC. The solid lines are the expected decrease in the signal due to electron-electron scattering at the given distance and value of V_0 given a Fermi energy of 15 meV . All of the curves have been normalized to their value at $V_0 = 0$ meV and offset by 0.2 for clarity.

energy, reducing the Fermi energy increases the scattering rate because the excess energy

becomes a larger fraction of the total energy. This means more of the filled states may

participate in the scattering, which increases the scattering rate. We have repeated these

measurements at the middle distance 1.0 μm for a series of Fermi energies. In this case,

we have used a back gate voltage, which reduces the density of the 2DEG and lowers the

Fermi energy. As the back gate voltage increases, the Fermi energy is reduced and the

electron tends to scatter more quickly. Figure 5.7 shows a set of images all at the same area for a series of back gate voltages and applied dc voltages V_0. All of these images were taken at a temperature of 1.7 K. Each row is a different back gate voltage from top to bottom 0 V, -1 V and –2 V. Each column in the figure is a different value of V_0 from left to right, 0 mV, 1mV, 2mV and 3mV. In the first column, all of the images have a very similar strength but as V_0 increases, the signal fades most quickly in the bottom row. This shows the scattering rate increasing as the back gate voltage increases. This is in agreement with the expectation that decreasing the Fermi energy increases the scattering rate.

To quantitatively analyze the data we have plotted in Figure 5.8 the measured average signal $\overline{\Delta g}$ as a function of dc bias voltage V_0 for the three different back gate voltages. The points in the graph were obtained in the same manner as the ones in Figure 5.6. Once again the curves have been offset and normalized to their value at $V_0 = 0$ mV. All three curves decrease with increasing dc bias voltage as expected from the increased scattering. The more important feature in this measurement is the back gate voltage dependence of the measured signal at a fixed V_0. The measured $\overline{\Delta g}$ is lower at a given V_0 for higher back gate voltages because V_0 is a larger fraction of the Fermi energy. This shows that the decreasing Fermi energy is increasing the scattering rate.

5.3. Theoretical Scattering Rate

In this section, we compare our results with a theoretical prediction for electron-electron scattering rate in a 2DEG. To understand the energy dependence for each of these three distances, we have looked at the expected electron-electron scattering rates in

111
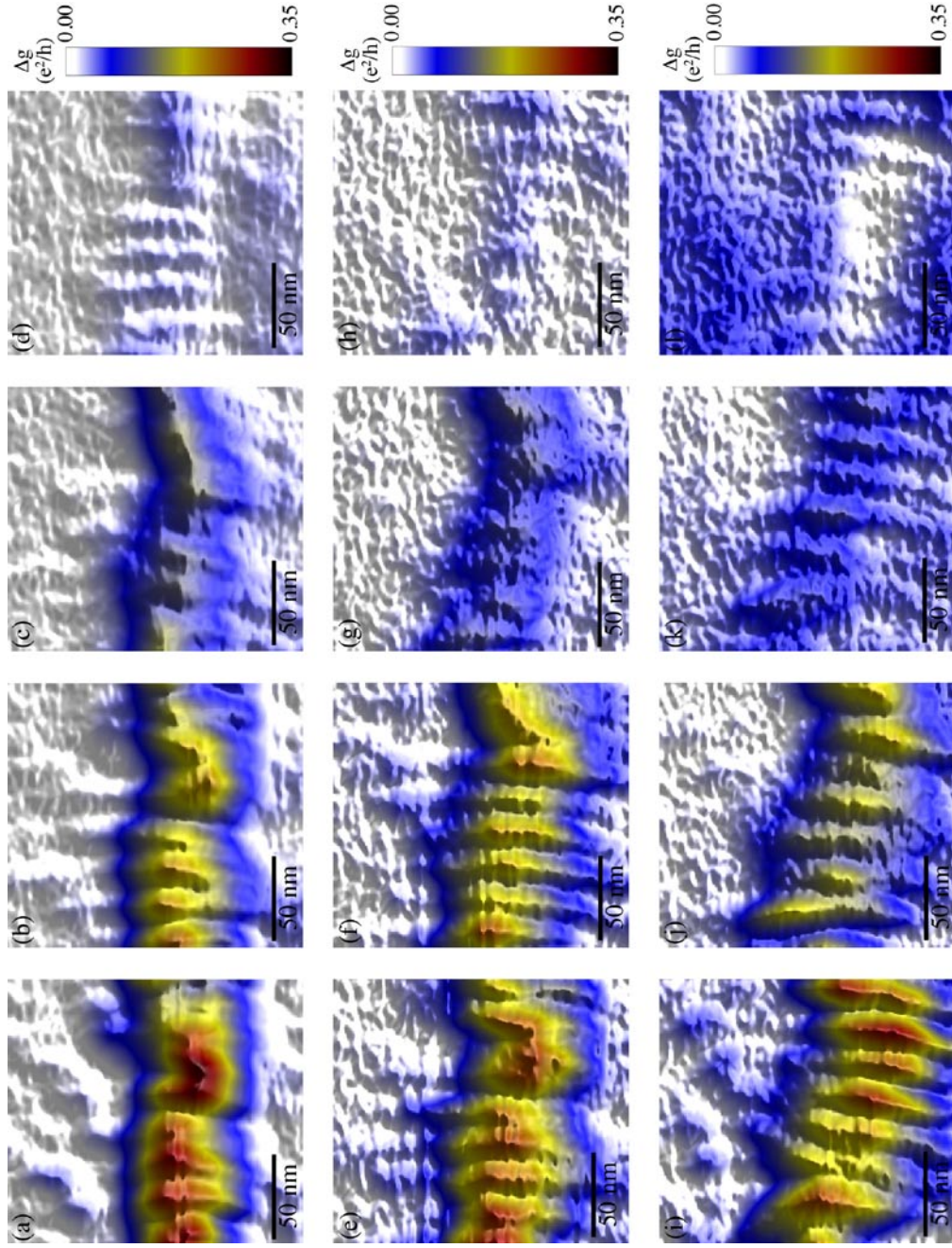
Figure 5.7 Images of electron flow for three back gate voltage and four dc bias voltages V_0. The rows are at back gate voltages of 0 Volts, -1 Volts and -2 Volts. The columns have the following values of V_0, 0 mV, 1 mV, 2 mV and 3mV. As the back gate voltage is increased, the signal decays more quickly. All of the images were taken at a temperature of 1.7 K.

112
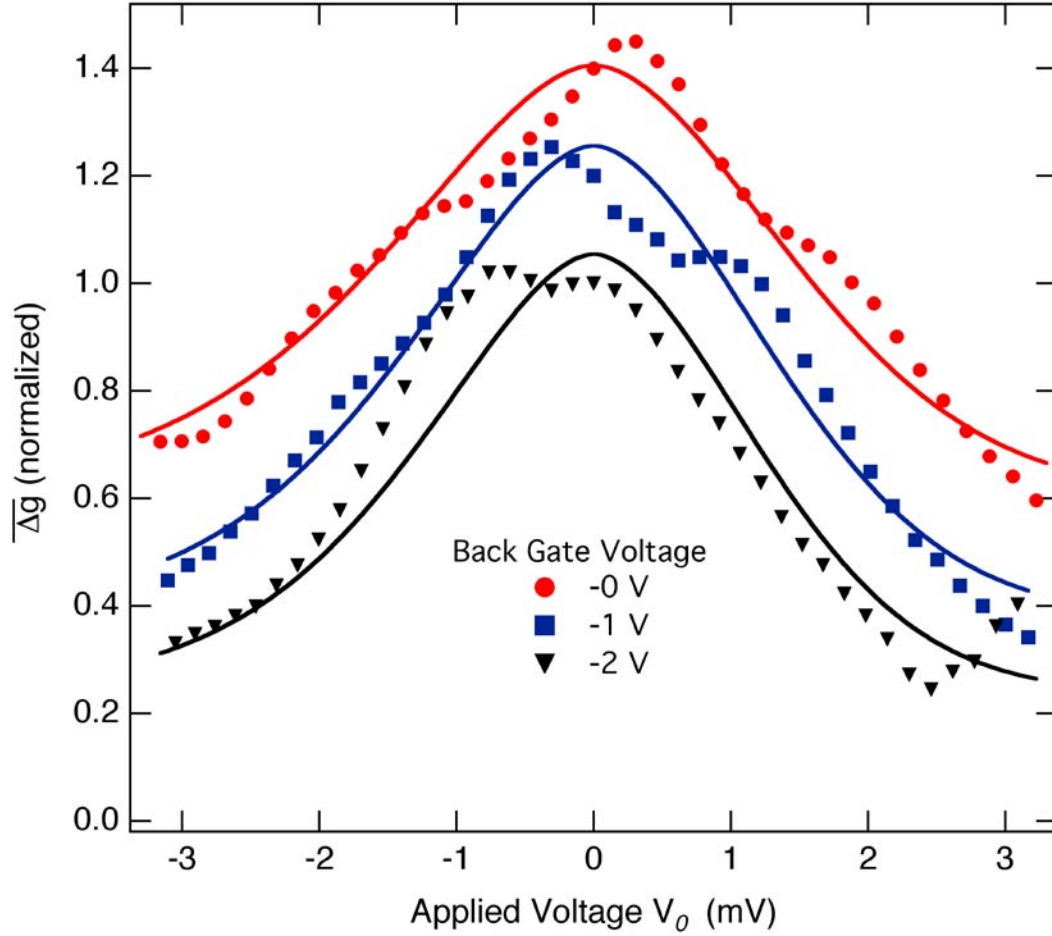
Figure 5.8 Plot of the average measured signal as a function of applied dc voltage V_0 for three different back gate voltages, which reduce the Fermi energy. The solid lines are the expected decrease in the signal due to electron-electron scattering at 1.0 μm for the given V_0 and back gate voltage. All of the curves have been normalized to their value at $V_0 = 0$ meV and offset by 0.2 for clarity.

a 2DEG. This is the dominant scattering mechanism at these temperatures and energies in the 2DEG. Giuliani and Quinn have calculated the scattering time as a function of the excess applied voltage V_0 at T = 0 K [Giuliani, (1982)]. They found the following equation for the scattering time, τ_{ee}

$$\frac{1}{\tau_{ee}} = \frac{E_F}{4\pi\hbar}\left(\frac{eV_0}{E_F}\right)^2\left[\ln\left(\frac{E_F}{eV_0}\right)+\ln\left(\frac{2q_{TF}}{p_F}\right)+\frac{1}{2}\right]$$

113

In this equation, E_F is the Fermi energy, p_F is the momentum and q_{TF} is the Thomas-Fermi screening vector in two dimensions. This equation gives a good approximation of the electron-electron scattering rate as long as the excess energy is much larger than the temperature. This is true for our large bias voltages since $kT = 0.141$ meV. Since the measured signal $\overline{\Delta g}$ requires that the electron has not undergone a scattering event, we want the probability that an electron can travel a distance L without scattering. Because the chance of an electron scattering is random and they remain ballistic over the range of our measurement, the probability that an electron will not have scattered is given by the exponential decay.

$$P \propto \exp\left(\frac{-L}{v\tau_{ee}}\right)$$

where v is the velocity after the electrons pass through the QPC and τ_{ee} is the scattering rate. This gives an approximately Gaussian distribution in the applied voltage V_0, since τ_{ee} goes as V_0^{-2}. The probability distribution is plotted in Figure 5.6 for the three different distances from the QPC. There are no free parameters in the plotting of the probability distribution because L is given by the area of the image, the applied voltage V_0 is known, and $E_F = 15$ meV is measured. There is qualitative agreement between the data and the expected distributions; the measured signal decays more quickly at longer distances. For the shortest distance, there is a larger discrepancy between the experiment and theory. This may be caused because the electrons have not been fully accelerated at such a short distance from the QPC. There is also an asymmetry in the bias direction, which may be caused by the shape of the QPC constriction.

We have also plotted the expected decrease in the signal as a function of V_0 for

114

the three different back gate voltages. This is shown by the solid lines in Figure 5.7. As in the previous figure there are no free parameters in the fit of the expected versus measured distributions. The measured values for L = 1.0 µm, the applied voltage V_0, and Fermi energy E_F are used. Once again, there is good qualitative agreement between the experimental points and the theoretical curve showing that electron-electron scattering is the dominant energy loss mechanism. The scattering rate increases as the Fermi energy decreases.

These measurements demonstrate our technique's ability to image electron energy loss in a two-dimensional electron gas. We have shown that in our experiment the dominant energy loss mechanism is electron-electron scattering. The results show good agreement between experiment and theory for the electron-electron scattering rate at a variety of distances and energies. This technique can be extended to measure electron energy loss mechanisms at higher excess energies where electron-phonon scattering becomes important. The technique can also be used in different geometries like quantum wires and dots to provide insight into the energy loss mechanisms in these confined geometries.

Chapter 6

Electron Optics

In this chapter, we examine the electron flow through electron-optic devices. These are devices that are made with electrostatic gates on the surface to control the flow of electrons through them. We have looked at several different devices to understand how electron waves flow through them. We have studied a prism, a circular scatterer and a channel. In section 6.1, we examine the electrostatic prism device. A small voltage on the prism gate changes the density underneath and changes the direction of electrons passing under it. Section 6.2 shows the results from a circular scatterer. The device is created by a circular electrostatic gate on the surface, which acts as a defocusing lens or a circular scatterer sending electron waves off in all directions depending on the voltage on the gate. We have looked at this device to understand the scattering from the tip, which also looks like a circular scatterer in the 2DEG. In section 6.3, we have studied a narrow channel created in the two-dimensional electron gas (2DEG). This is created by two electrostatic gates that confine the electrons. We are able to study the potential profile from these gates by looking at the pattern of electron flow.

Electron-optic devices have been studied for many years in 2DEGs [Spector, (1992)]. These devices rely on the ballistic transport of the electron from an injector to a collector. As the mobility of 2DEGs improves and hence their mean free path increases, the size of the devices can increase. Some of the devices that have been studied are an absorber [Spector, (1990a)], a switch [Spector, (1990b)],

a lens [Sivan, (1990)], a beam crosser [Spector, (1991)] and an elliptical reflector [Heremans, (1999)]. None of these devices work as well as expected for ideal ballistic flow of electrons due to the small background potential of the donor atoms, which leads to small angle scattering. The potential profile of the electrostatic gates also can degrade the performance of the devices. By studying these devices with an imaging technique the pattern of electron flow is obtained and the effect of the donors atoms and electrostatic gates can be understood.

We have fabricated and measured several different devices all of which use a quantum point contact (QPC) as an injector. The electron flow through the devices is studied using a low temperature scanning probe microscope (SPM) as described in Chapter 3. A negative voltage is put on the SPM tip with respect to the 2DEG to create a small depleted region. This depleted region backscatters electrons to the QPC, which reduces the conductance when the tip is over areas of high electron flow. By measuring the change in conductance as a function of tip position, an image of electron flow is obtained. We have imaged the electron flow through each device to illustrate their operation and understand the effect of the gates and donor atoms on their performance.

6.1. Electrostatic Prism

In this experiment, we have used an electrostatic prism to control the direction of electron flow in the 2DEG. Figure 6.1 is a colorized scanning electron micrograph of the device used in the experiment. It consists of a quantum point contact (QPC) on the right and a wedge shaped electrostatic gate that acts as a prism. The front edge of the prism gate is located 1 μm to the left of the QPC. The voltage on this prism gate controls
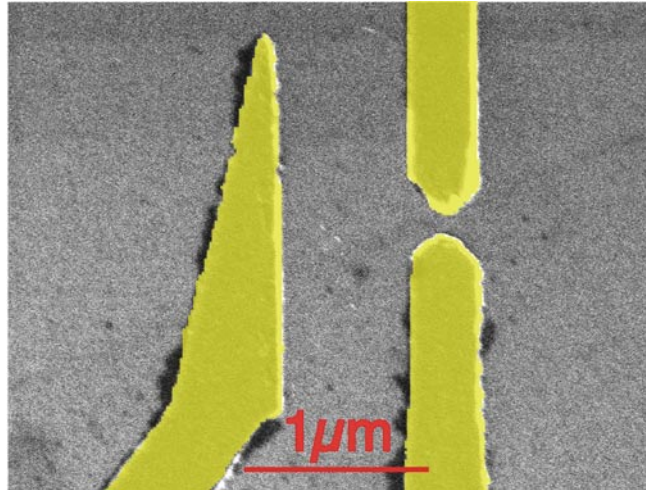
Figure 6.1 Scanning electron microscope image of the electrostatic prism device. It consists of a quantum point contact on the right and a triangular shaped prism gate located 1 μm to the left.

the direction of electrons as they leave the area under the gate. Figure 6.2 illustrates the

idea behind using an electrostatic gate to change the direction of electron flow. There
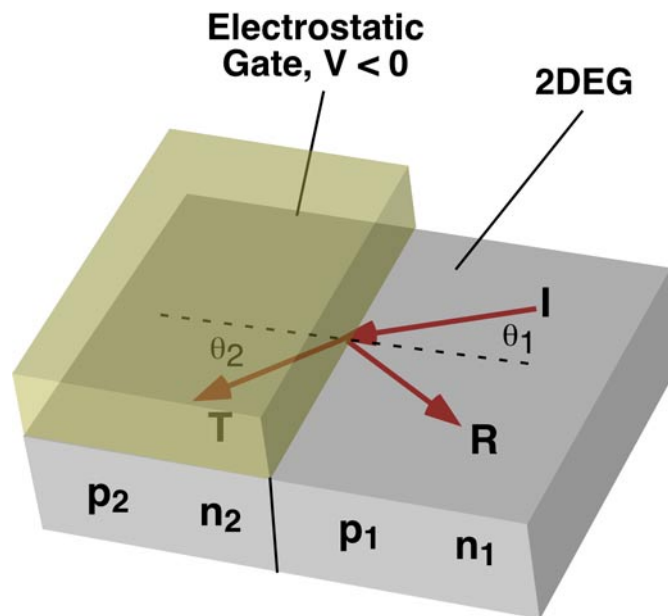
Figure 6.2 Schematic diagram showing what happens to an incoming electron wave when it hits the region of reduced density under the prism gate. The electron trajectory is bent away from the normal.

118

are two different regions of the 2DEG, one that has a gate on it and another that does not. A voltage is put on the gate, which changes the density of the 2DEG underneath and also the momentum of the electrons. As electrons travel through the ungated 2DEG and impinge on this area of changed density, they must conserve their momentum along the interface between the two regions. This means that all of the change in momentum occurs along the axis normal to the interface and the direction of the electron is changed. The equation for the conservation of momentum gives the following simple relation between the incoming and outgoing angle of the electron

$$p_1 \sin(\theta_1) = p_2 \sin(\theta_2)$$

where p_1 and p_2 are the incoming and outgoing momentums and θ_1 and θ_2 are the two angles. Using the fact that the square of the momentum in the 2DEG is proportional to the density, this equation can be rewritten as

$$\sqrt{n_1} \sin(\theta_1) = \sqrt{n_2} \sin(\theta_2)$$

where n_1 and n_2 are the densities in the two different regions. In this form, it is clear that this is just an electron analog of Snell's law in optics, where the density of the 2DEG is analogous to the index of refraction. When an electron goes from an area of low density to one of higher density it will be bent towards the normal.

We have imaged the electron flow after it travels under the prism gate for a series of different voltages on the gate. As the voltage on the gate is made more negative, the density is reduced causing the flow to bend towards the normal. This is the opposite of light entering vacuum from glass where the light bends away from the normal. This type of device can be used as a switch to control the flow of electrons [Spector, (1990b)]. A change in the voltage on the prism changes where the electrons go. If there are two

collectors then the electron flow can be shifted from one of them to the other causing the current to switch. We are able to change the density under the prism from slightly above the density of the 2DEG all the way down to 0. When the density is reduced the electrons can no longer pass under the gate and all of the flow is reflected at the front edge of the prism.

Figure 6.3 shows three images of electron flow from the prism device for (a) +0.1 V, (b) 0.0 V, and (c) –0.1 V on the prism. These images were taken on the second plateau of the QPC giving three main lobes of current. The images show the flow bending upwards as the voltage is made more negative on the gate. The lines on the images are the expected bending of the electrons for the three different prism voltages shown. The dark line on each image is the expected bending for that voltage, while the white lines are the bending for the other two voltages. This shows fairly good agreement between the measured bending of the electron flow and the expected bending.

To further emphasize the change in flow with prism voltage, Figure 6.4 shows two images of coherent flow at different prism voltages subtracted from each other. This highlights the difference between the two images. We have subtracted the image of electron flow with –0.1 V on the prism image, Figure 6.3 (c), from one with +0.1 V, Figure 6.3 (a). The areas in red are stronger in the –0.1 V image while the blue areas are stronger in the +0.1 V image. The white areas were the same in both images showing that there is no change in the current. This shows that the flow bends upwards when the voltage is made more negative.

We have demonstrated the operation of an electrostatic prism in a 2DEG by imaging the coherent electron flow that passes under the prism gate. These images show
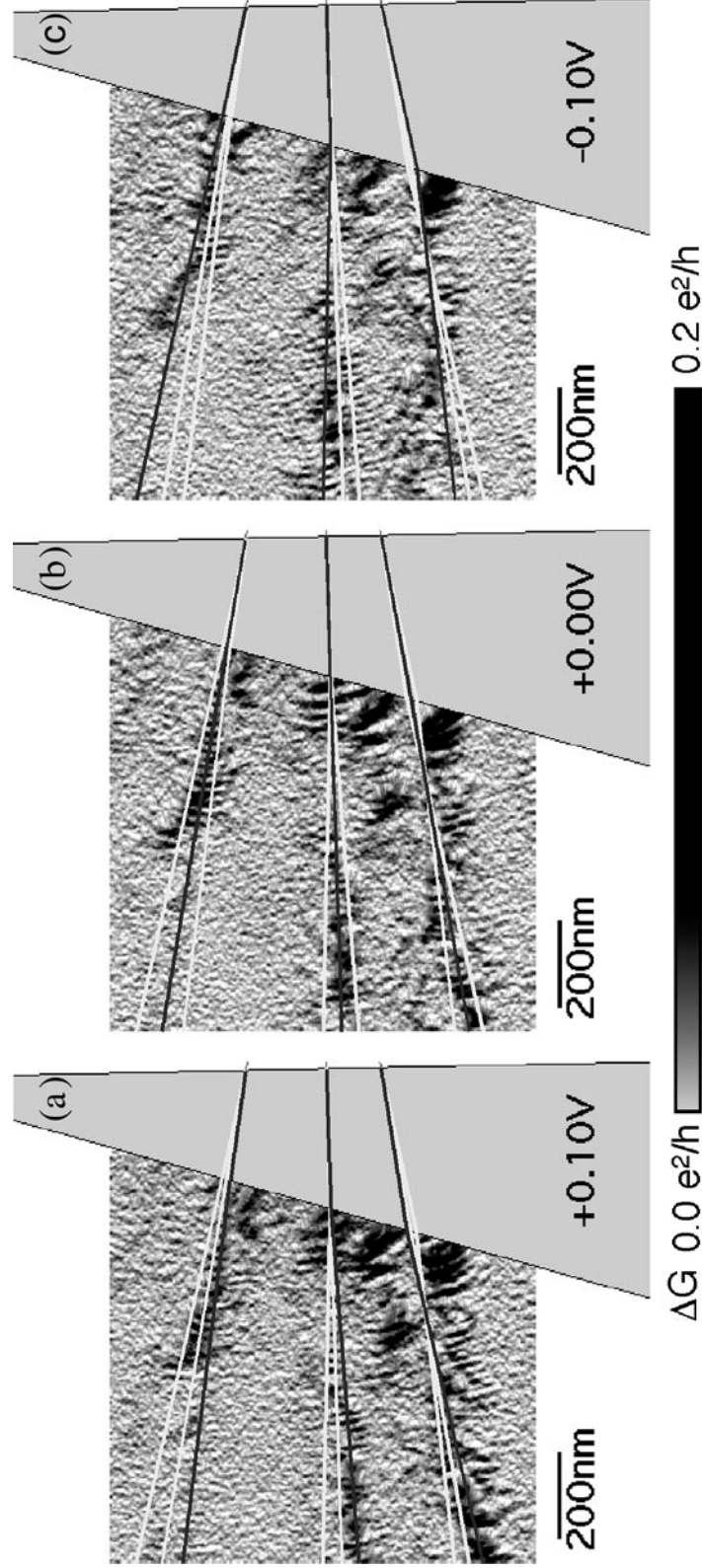
Figure 6.3 Three images of electron flow for different voltages on the electrostatic prism gate, (a) +0.1 V, (b) 0.0 V and (c) -0.1 V. The lines on the images represent the expected direction of electron flow for the three different gate voltages. The black line is the direction for the given image. As the voltage on the prism is made more negative the electron flow is directed more upwards.

121
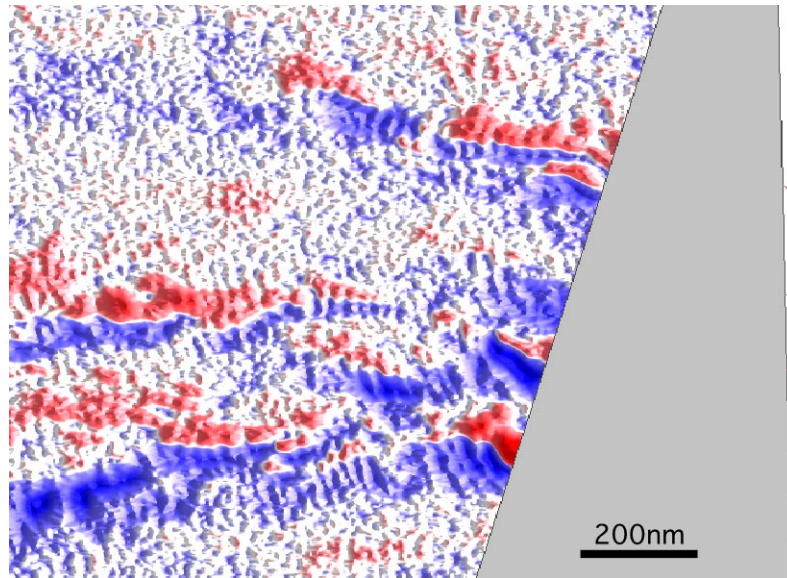
Figure 6.4 Image showing the effect of changing the prism gate voltage. The red areas are stronger when the gate voltage is -0.1 V and the blue areas are stronger when it is +0.1 V.

how the prism can be used as a coherent switch for electrons by adjusting the voltage on its gate. It can also be used as an energy selective scatterer for a fixed voltage on the gate because the amount of bending depends on the electron energy.

6.2. Circular Scatterer

The second device that we have studied is a circular scatterer, which is created by a round electrostatic gate on the surface. Figure 6.5 is a scanning electron microscope image of the device used in this experiment. There is a QPC on the right hand side of the image and a circular ball on the left hand side that acts as the scatterer. The ball has a lithographic diameter of 1 μm and it is located 2 μm from the QPC. There are two modes of operation for this device depending on the voltage on the ball. If the voltage is less than the voltage needed to deplete the 2DEG under the ball, then the device acts
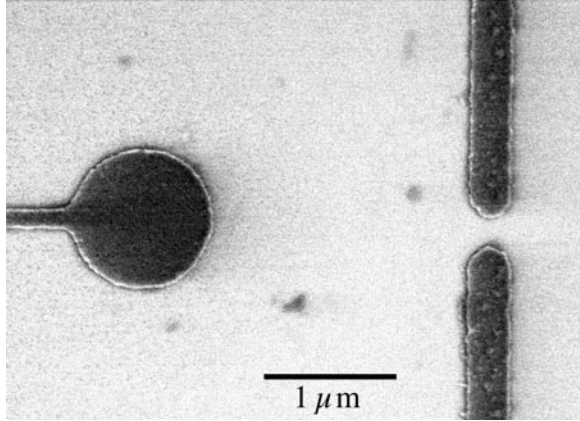
Figure 6.5 Scanning electron microscope image of the device used in the circular scatterer experiment. The quantum point contact is located on the right hand side with a 1 μm diameter circle located two μm in front of it.

as a defocusing lens for electrons passing underneath. Once the voltage is increased so that the 2DEG is depleted under the device, then the ball acts as a large circular scatterer for electrons. The addition of the second scattering object in addition to the SPM tip makes a triangular path returning to the QPC. This new path creates elliptically shaped interference fringes and is important for studying transport phenomena that rely on an enclosed area.

Figure 6.6 is a schematic diagram of the expected bending of the electron flow as it passes under the ball for different voltages. The electron trajectories are bent as they enter and exit the region of reduced density under the ball. This is the same mechanism as in the previous section where the electrostatic prism bends the electron paths passing underneath. If there is no voltage on the ball, then there is no bending and the electron follows the black path. If there is a slight negative voltage on the ball, the electron density will be less under the ball than in the rest of the 2DEG. This causes the electron to bend away from the normal as it enters the area under the ball and bend towards the

123
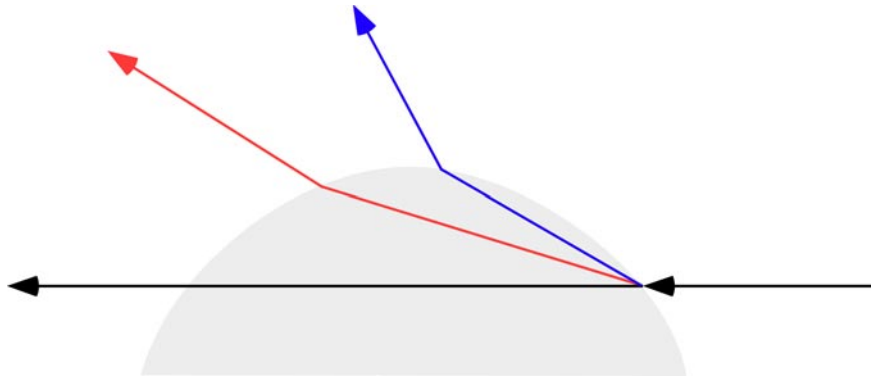
Figure 6.6 Schematic diagram showing the trajectories of electrons passing under the ball for different voltages on it. The black line is for 0 V, the red one is for slightly negative and the blue is for more negative. This shows that the electron bends upwards as the voltage is decreased.

normal as it exits this area. This path is shown by the red line passing under the ball.

If the voltage becomes more negative, the bending will be more pronounced and the electron will follow the blue path.

Figure 6.7 shows the electron flow through the device when it is acting as a defocusing lens for electrons. To create Figure 6.7 two images of the electron flow are taken with different voltages on the ball. The two voltages used to create the image are
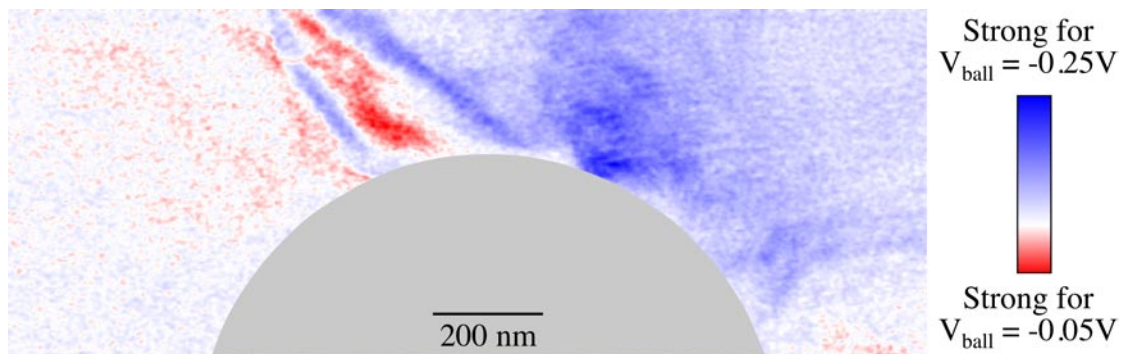
Figure 6.7 Image showing the effect of changing the voltage on the ball. As the voltage is made more negative on the ball, the electron flow is bent upwards indicated by the blue areas being above the red ones. The gray indicates the location of the ball and the QPC is located 2 μm to the right of the ball.

124

–0.05 V and –0.25 V. The gray area is the outline of the ball, which was not scanned because the tip is not able to deplete the 2DEG under the metal gate. Then these two images are subtracted from each other to find the effect of changing the voltage on the ball. In this image, the areas that are red are stronger for the –0.05 V on the ball while the blue areas are stronger for –0.25 V on the ball. This shows that making the voltage on the ball more negative bends the electron trajectories more upwards. This is expected as seen by the schematic diagram in Figure 6.6.

Figure 6.8 shows the mechanism that creates elliptical shaped interference fringes when the ball is scattering electron waves. The fringes are created by a two bounce scattering process where the two bounces are off of the tip and off of the ball. As the tip is moved the path length for this two bounce path changes. When the phase accumulated along the path changes by π the interference goes from constructive to destructive. The location of the ball and QPC are fixed. This means that the line of constant phase is an ellipse with the ball and QPC as the foci. If the tip moves along this line, the fringe
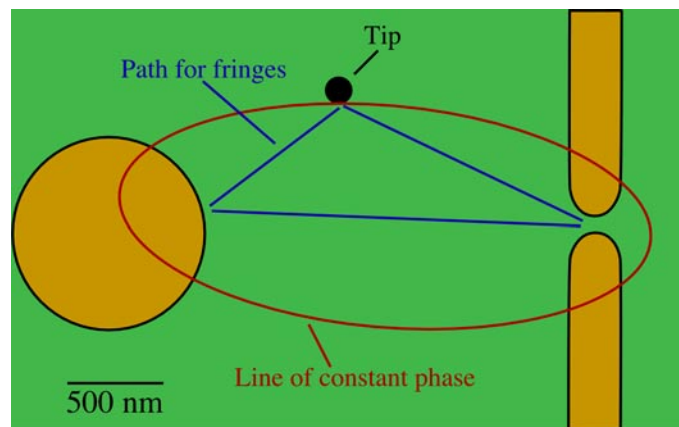
Figure 6.8 Schematic diagram showing how the elliptical fringes are formed. They are due to a path that goes from the QPC to the ball and then the tip as indicated by the blue lines. The red line shows the line of constant phase for this scattering path.

125

will remain constructive or destructive. However, if the tip is moved off of this line the accumulated phase will change and the fringe strength will change. This is what produces the elliptically shaped interference fringes once the ball is fully energized. The presence of elliptical fringes demonstrates that the interference is caused by a two-bounce mechanism.

Figure 6.9 is a diagram showing the locations of the images of electron flow used in this experiment. The red area in front of the ball was imaged to look for the effect of the ball on the pattern of electron flow. The yellow area above the ball was imaged to look for the presence of elliptical interference fringes. This area was chosen because it is away from the electron flow when the ball is not energized but some of the flow is scatterered into the region when the ball is energized. Elliptical interference fringes in this area are due to a two-bounce mechanism involving the tip and the ball.

Figure 6.10 shows the electron flow for two voltages on the ball from the red area in Figure 6.9. In Figure 6.10 (a) the ball is not energized and we are looking at
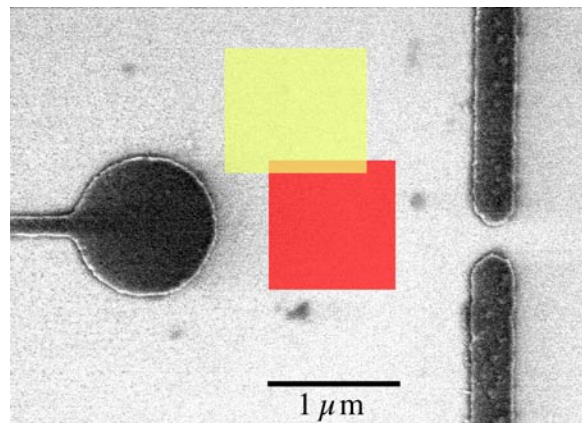
Figure 6.9 Diagram showing the areas of the images of electron flow. The red box is the area of the images in Figure 6.10. The yellow box is the area for the images in Figure 6.11.

126
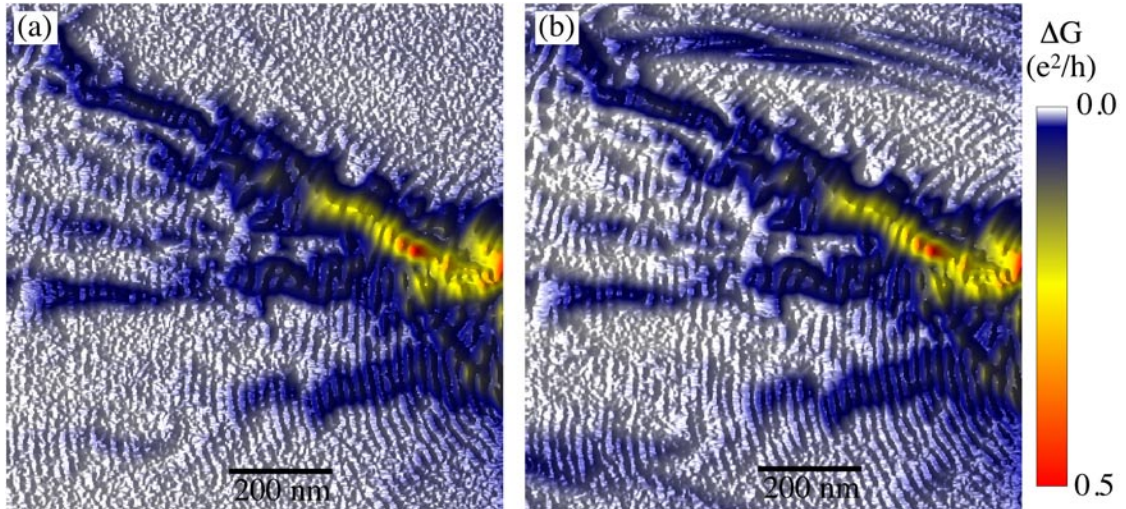
Figure 6.10 Two images of electron flow in front of the ball from the red area in Figure 6.9. (a) Ball is not energized and (b) the ball is energized creating elliptically shaped interference fringes near the top of the image.

the electron flow from the QPC in the area in front of the ball. In Figure 6.10 (b) the voltage on the ball is –0.5 V, which is sufficient to deplete the 2DEG underneath and electrons cannot pass under the ball. This causes the ball to act as a scatterer for electron waves, which is seen by the presence of electron flow in new areas of the image. The electron flow before hitting the ball does not noticeably change. However, There are new interference fringes that appear near the top of the image. These are due to interference of paths that bounce off of the ball and the tip. They are no longer pointed along the direction of electron flow, as the interference fringes are when the ball is not energized. They are elliptically shaped and appear in areas where there was no electron flow without the ball energized.

We have examined the elliptical fringes more closely by imaging the electron flow in a different region. This new region is up and to the left of the area imaged in Figure 6.10 and is shown by the yellow area in Figure 6.9. Figure 6.11 shows the
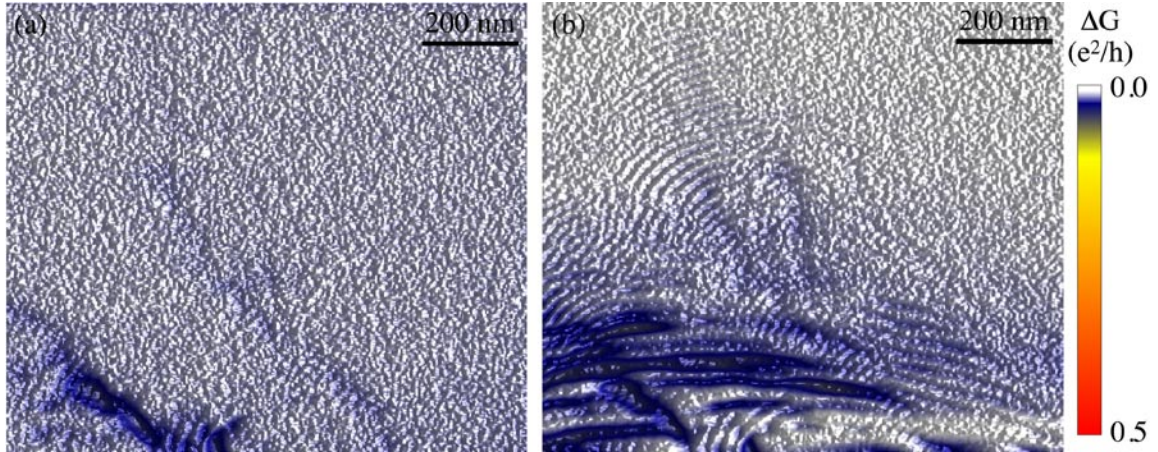
Figure 6.11 (a) Image of electron flow without the ball energized from the yellow area in Figure 6.9. (b) Image of electron flow with the ball energized showing the formation of elliptically shaped fringes.

electron flow for the cases of the ball not energized and energized. We picked a region where there was little flow without the ball energized since we are only interested in the elliptical fringes. The presence of electron flow in new areas when the ball is energized shows that the ball is scattering the flow into these areas. Figure 6.11 (b) shows clear fringes that are elliptically shaped. The two foci of the ellipses are the QPC and the ball. This is because the ellipses are created due to a triangular path involving the ball, tip and QPC. The elliptical fringes demonstrate a new type of interference fringe in our images caused by a two-bounce scattering mechanism.

In this section, we have presented images of electron flow through a device with a QPC and a circular gate. We have shown two different uses of the circular electrostatic gate on the surface. For small voltages on the gate, it acts as a lens for electrons passing underneath. Once the 2DEG is depleted under the gate, it acts as a scatterer for electron waves. This causes new interference fringes to form in the images of electron flow. These new fringes are elliptically shaped since they involve a two-bounce mechanism

from the tip and gate.

6.3. Narrow Channel

We have investigated the electron flow through a narrow channel formed by two electrostatic gates in a two-dimensional electron gas. We have looked at the effects of the two walls on the pattern of electron flow. Figure 6.12 is an atomic force microscope topographic image of the device taken in our SPM. It consists of a quantum point contact on the right with a channel towards the left. The walls of the channel are defined by two electrostatic gates that are 2 μm apart. The width of the channel can be adjusted by changing the voltage on the two walls. Images of electron flow were taken from the gray area shown on the device. When the two gates defining the walls of the device are
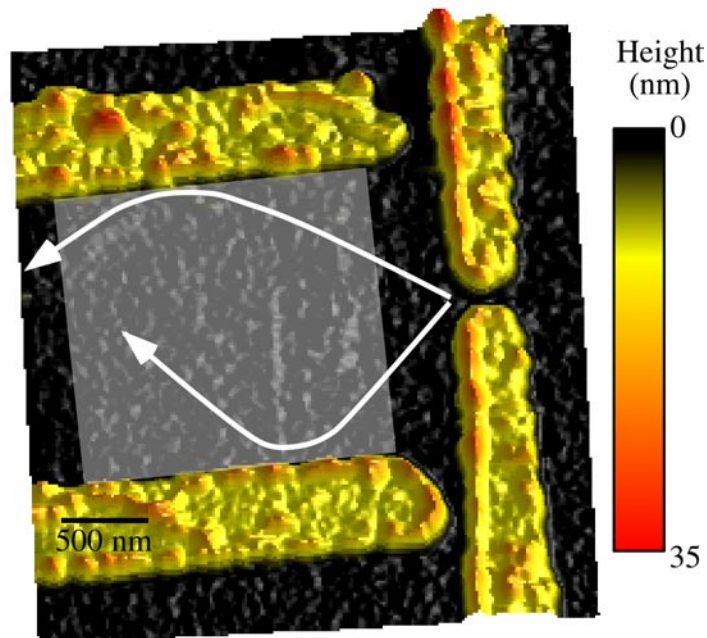
Figure 6.12 AFM image of the device with the two electrostatic gates that act as walls to form a channel for the electrons. The gray area is the imaged area for the images of electron flow in Figure 6.13. The white lines represent possible electron trajectories when the two wall are energized.

129

energized the electrons will be confined in the narrow channel causing the electron flow to follow the paths indicated by the white lines.

Figure 6.13 shows the effect of energizing the two walls that form the channel for electrons. In Figure 6.13 (a), the walls are not energized and the flow just spreads out as at moves away from the QPC located on the right. In Figure 6.13 (b), the walls have been energized and the flow is deflected by the presence of the wall. The walls confine the area of electron flow to be within the channel increasing the signal on the left hand side of the images, which is 2 μm from the QPC. This can be seen by the faint background signal that is now visible on the left hand side of the image. The other feature to notice in Figure 6.13 (b) is how the electron paths are bent by the electrostatic gates at the top and bottom of the image. They do not bounce directly off but rather the electron moves along the wall for a short distance before moving away from the wall.

There have been several calculations done on the effect of electrostatic gates on the potential in the 2DEG [Davies, (1995); Larkin, (1995)]. They found that the potential falloff is approximately inversely proportional to the distance from the gate. This means that electrons travel near the edge of electrostatic gates due to the smooth potential from the gate. If the potential from the gate were a hard flat wall, then the electron would immediately bounce off at the angle of incidence. However, our images show the electron taking a much more curved path as it nears the wall. This would occur if the electron slowed down as it neared the wall. This would be the case if the potential varied slowly nearing the wall.

To demonstrate the effect of different potential profiles, we have calculated the trajectory for an electron nearing a wall for four different potential shapes. Because the
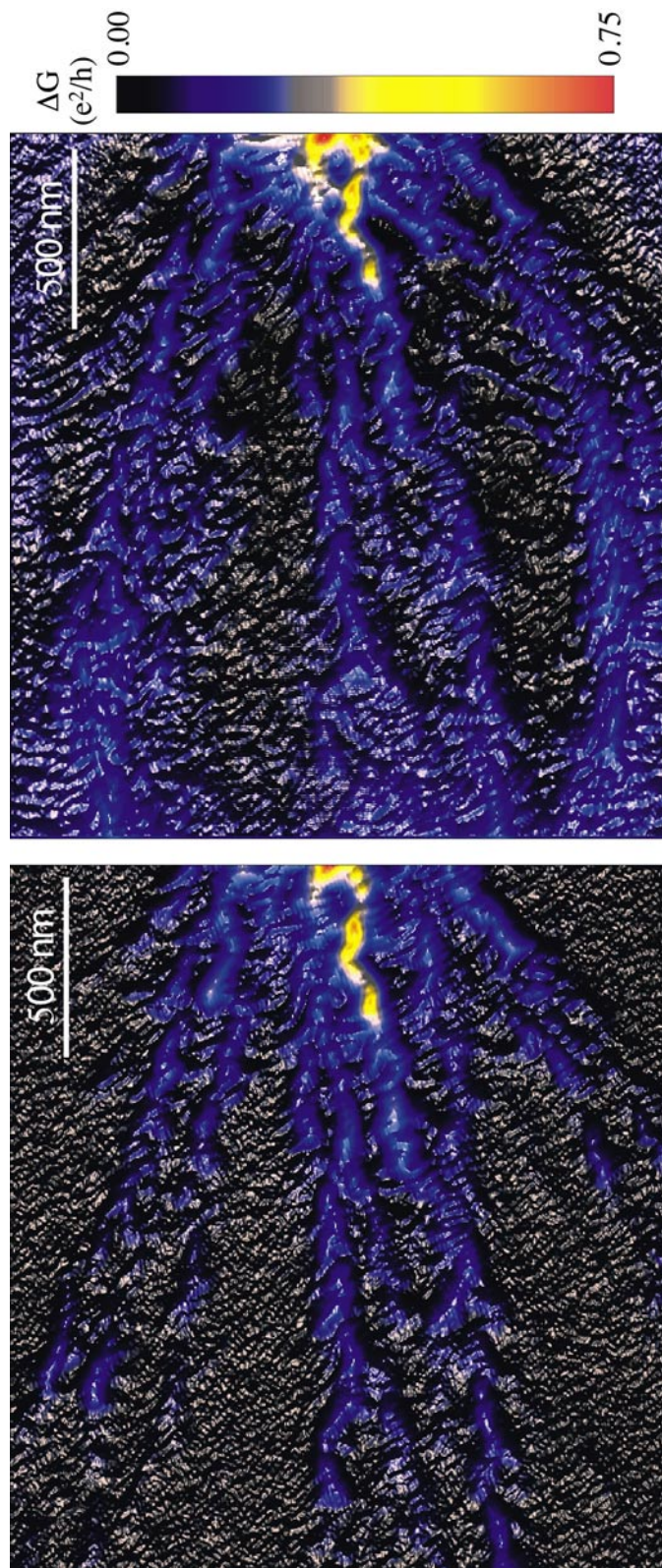
Figure 6.13 Two images of electron flow through the channel device from the area indicated by the gray box in Figure 6.12. (a) The walls of the channel are not energized and the flow just spreads out after leaving the QPC. (b) The walls of the device are energized, which confines the electrons to the narrow channel. The electron flow can be seen bending near the bottom due to the potential profile of the wall.

131

wall is several μm long, we assume for simplicity that the potential is uniform along the wall. This reduces the calculation to one-dimension were the only axis is the distance from the wall. The electron will always have the same momentum in the x-direction along the wall. To solve for the y-direction, we have treated the electron as a classical object and solved the equation of motion for the trajectory. To solve for the position of the electron we just use the equation

$$m\frac{d^2y}{dt^2} = -\frac{dV}{dy}$$

where m is the electron effective mass and V is the potential from the gate. Figure 6.14 shows the trajectories for an electron coming near the wall for several different potential profiles of the wall. The electrons start 700 nm from the wall with an initial velocity equal to the Fermi velocity, which is 2 x 10^5 m/s in our samples. The incoming angle
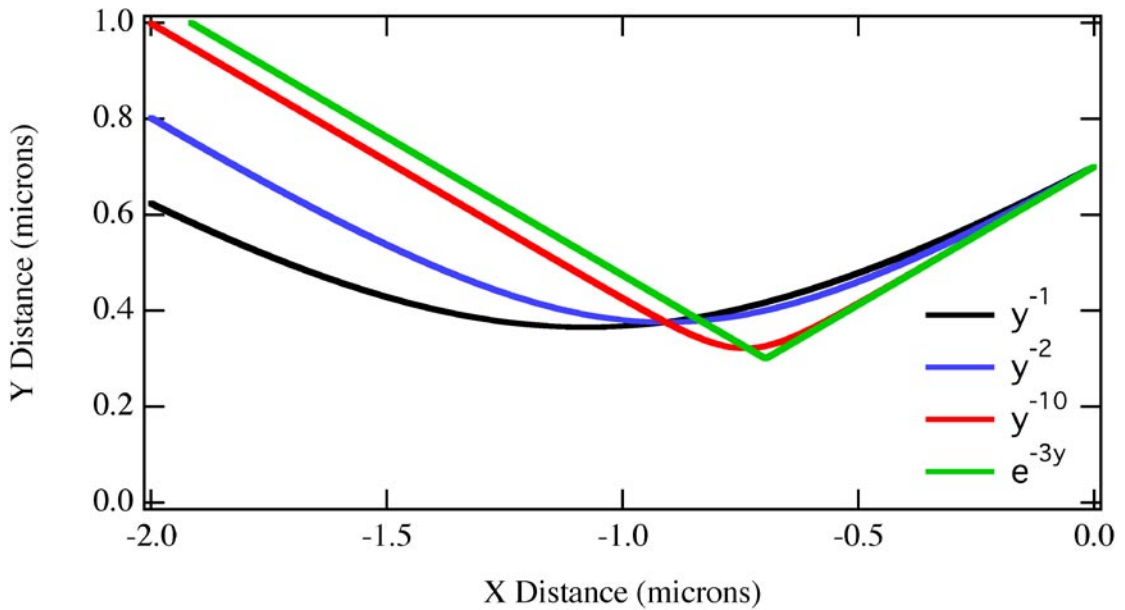
Figure 6.14 Simulated trajectories for electrons hitting a wall created by an electrostatic gate. Electron trajectories for four different potential profiles are plotted showing the effect of the potential on the path of the electrons.

132

of the electron is the same for all of the trajectories and it was chosen to approximate the angle seen in the images. The four trajectories are for the following potential profiles for the wall: (black) $V(y) \propto y^{-1}$, (blue) $V(y) \propto y^{-2}$, (red) $V(y) \propto y^{-10}$ and (green) $V(y) \propto \exp(-3y)$ where y is the distance from the wall in nm. The amplitude of the potential was chosen so that the electrons turned around when they were 300 nm from the edge of the wall. As the potential profile changes more quickly, the electron spends less time near the edge of the wall. In the case of the exponential, the electron is almost immediately reflected back off of the wall at the same angle as incidence. For the modeled potential that goes as the inverse of position, it takes more than one μm for the electron to have its y-momentum fully turned around.

Figure 6.15 shows the image of electron flow with the wall energized. On top of this image, the trajectory of an electron has been superimposed for the case of the potential $V(y) \propto y^{-1}$. The trajectory is shown by the white curved line near the bottom of the image. There is fairly good agreement between the lowest branch of electron flow and this calculated path. This shows that the potential profile is inversely proportional to the distance from the wall as found in previous calculations [Davies, (1995); Larkin, (1995)]. If the potentials that change more rapidly are used, the electron bounces off the wall too quickly and there is not agreement between the measured image and the simulation.

The addition of two walls can create a channel in which electrons must flow. By imaging the paths that electrons take through this confined geometry, we have obtained information on the shape of the potential profile of the walls. We have observed that the electron spends a long time near the edge of the wall indicating that the potential is
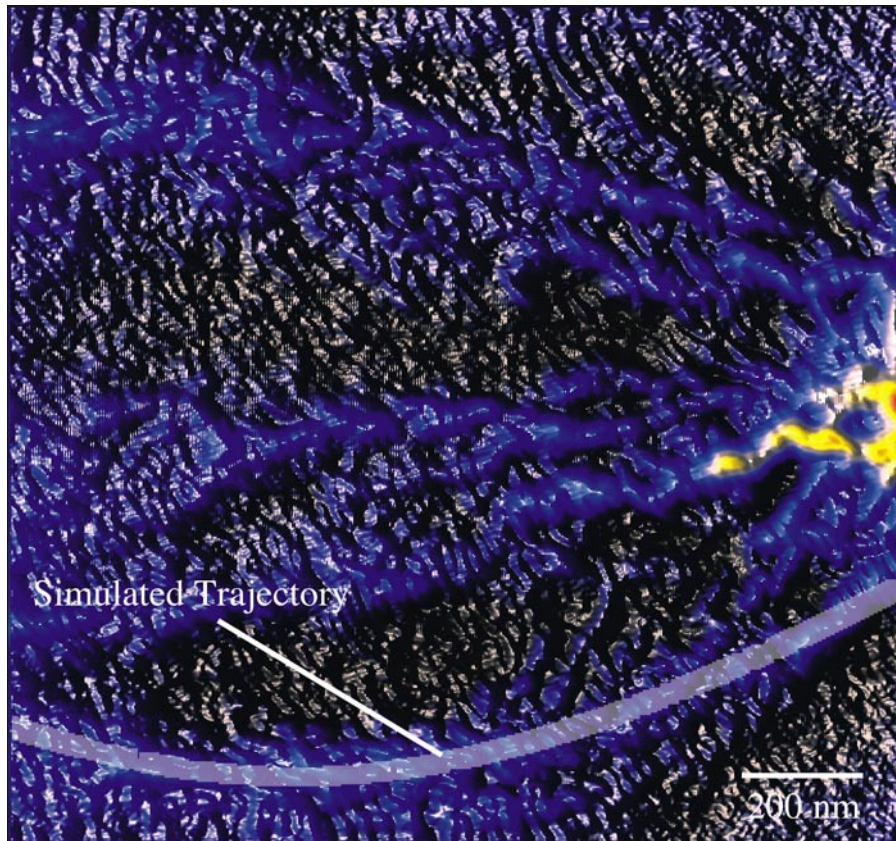
Figure 6.15 Comparison of the image of electron flow with a simulated trajectory. The image of electron flow is from the area given by the gray box in Figure 6.12. The white line is the simulated trajectory for a potential profile that is inversely proportional to the distance from the wall. There is good agreement between the simulation and experiment indicating that we can find the potential profile from images of electron flow.

slowly varying in this region. A comparison of calculated trajectories with the images indicates that the potential from the electrostatic gates is inversely proportional to the distance from the gate. Knowledge of the potential profile from electrostatic gates is important for the design and simulation of future nanoscale devices,

In this chapter, we have imaged electron flow through several electron-optic devices to show how they work. These devices can be used as switches, wires and scatterers for electron waves. The electrostatic prism device changes the direction of electron flow based on the voltage applied to the gate. The circular ball can be used

either as a defocusing lens or as a circular scatterer. The last device that we have studied

is the narrow channel, which can be used to guide electrons through a 2DEG. These

devices will be necessary for the implementation and integration of devices built in

2DEGs.

Chapter 7

Imaging Interference Fringes

This chapter examines the origin of the interference fringes that decorate our images of electron flow. Section 7.1 discusses the possible origins of these fringes. It also shows experimental images of the enhancement of the fringes by a small reflecting gate. In section 7.2, we demonstrate that the location of the interference fringes move with the position of the reflecting gate. Section 7.3 examines the temperature dependence of the interference fringes and shows that they are thermally robust near the reflecting gate.

All of our images of electron flow through a two-dimensional electron gas are decorated by interference fringes spaced by half the Fermi wavelength. The spacing of these fringes formed the basis of our measurement of local electron density. In this chapter, we examine the origin of these fringes and analyze their dependence on distance from the quantum point contact (QPC). Our images show that the fringes do not decay, as a function of distance from the QPC for distances up to at least 3 μm, which is much farther than would be expected with a simple thermal smearing argument. Shaw et al. [Shaw, (2001)] have proposed that the origin of the fringes is interference of the backscattered flux from the tip with backscattering from other objects that are near the same distance from the QPC as the tip. To investigate this mechanism for the robustness of the fringes, we have fabricated samples with small reflecting arcs at various distances from the QPC.

7.1. Origin of Fringes

The images of electron flow are decorated by interference fringes spaced by half the Fermi wavelength. The fringes arise from the interference of two different paths back through the QPC. Theoretical simulations of the electron flow show that the fringes are caused by the presence of the tip measuring the electron flow; they are not present without the tip [Shaw, (2002)]. This can be seen in Figure 7.1, which shows a simulation of the electron flux from a QPC. Figure 7.1 (a) is the calculated electron flux without the tip present. This is in qualitative agreement with the experimental images of electron flow but does not have any interference fringes. Figure 7.1 (b) shows a simulated tip scan for the exact same area, which has interference fringes spaced by half the Fermi wavelength. For each point in this image, the potential from the tip was put at that location and the conductance through the QPC was calculated. Positions where the tip had a large effect on the conductance are plotted in red and yellow whereas areas that the tip had little effect are in white. This simulates the experimental images of electron flow and demonstrates that the interference fringes are produced by the presence of the
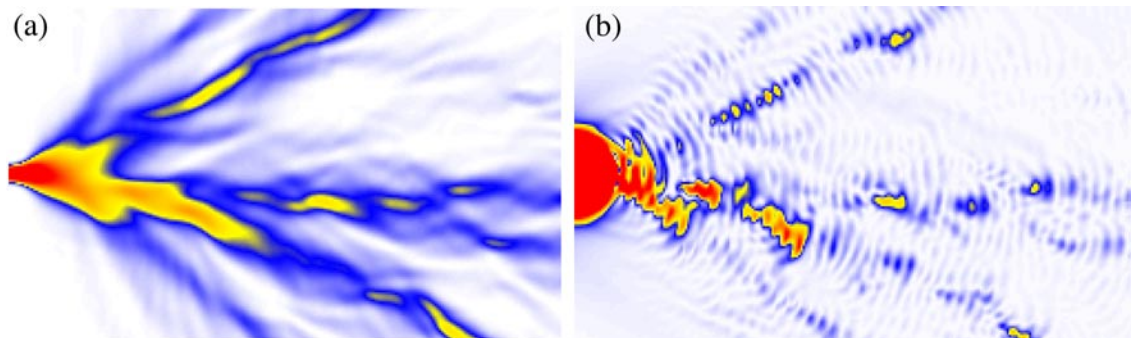
Figure 7.1 (a) Calculation of the electron flux through a 2DEG. (b) Simulation of the image obtained by our imaging technique showing good agreement with the electron flux image and the addition of interference fringes. Taken from [Shaw, (2002)].

137

tip. Because the interference fringes are only present with the tip, at least one of the paths responsible for the interference must involve the tip. The question that we want to address is what is the other path involved in the interference.

There are several mechanisms that may be responsible for the interference fringes in our images. To figure out the possible mechanisms that can lead to fringes it is necessary to identify possible locations where interference can occur. A possible location for the interference to take place is at the QPC. The next thing to consider is which paths can interfere to produce a change in the conductance. Because the tip is backscattering electron flow we must have another path that is going back through the QPC in order to have interference. A path coming through the QPC has a different value of momentum and therefore cannot interfere with the backward traveling flux from the tip as long as the QPC is not tunneling. The simplest mechanism to understand is interference of multiple paths back to the QPC from the tip. Figure 7.2 illustrates the basic idea behind this mechanism for producing interference fringes. In this case, one of the paths is the red one, which goes through the QPC to the tip and straight back through the QPC. The second path is the red and pink ones, which go from the QPC to the tip then back to the QPC gate then to the tip and finally back through the QPC. In this case the fringes arise from interference between a path that makes one roundtrip from the QPC to the tip with one that makes a roundtrip from the QPC to the tip and from the tip to the gate. The path length difference between these paths is twice the distance from the gate to the tip so the fringes would be spaced by half the Fermi wavelength as seen in the images.

Multiple paths backscattering from the tip through QPC seems like a suitable candidate to explain the fringes seen in the images until the effect of temperature is

138
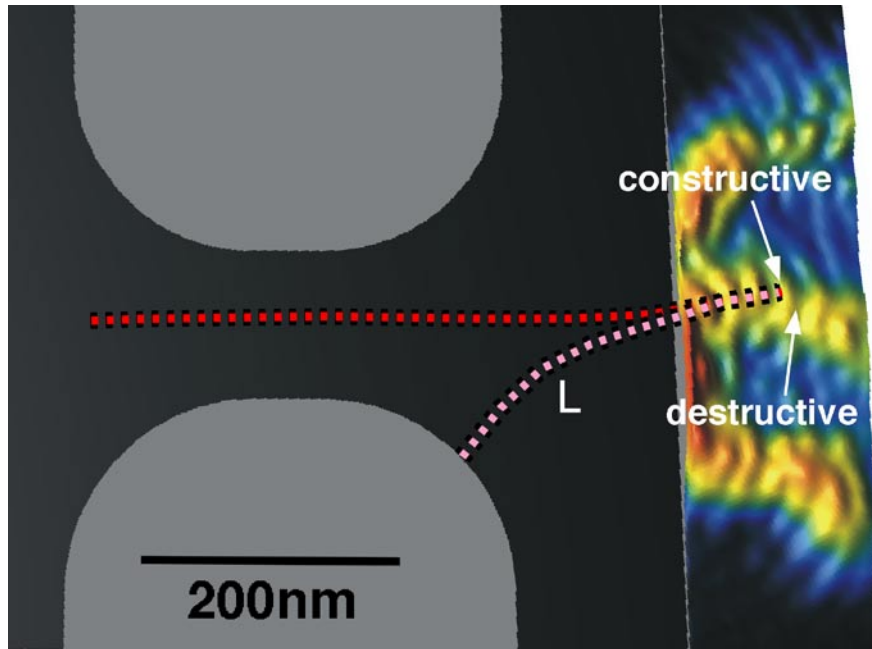
Figure 7.2 Diagram showing how the interference fringes are formed near the QPC. They arise due to interference between two paths through the QPC. The path length difference 2L determines whether the interference is constructive or destructive.

considered. Even though we have done the experiment at low temperatures, there is still

a finite spread in energy for the electrons emitted by the QPC. This spread in energy is

given by the derivative of the Fermi function and has a full width at half maximum of

about 3.5 kT, which corresponds to 0.5 meV at a temperature of 1.7 K. This spread in

energy is a few percent of the Fermi energy. This small difference in energy leads to a

difference in wavelength for the different electrons. As we move away from the QPC, the

interference fringes for electrons with different energy will no longer occur at the same

place but will start to be phase shifted from each other. Since we are measuring many

electrons coming through the QPC to obtain our signal, we will see an average of all of

these interference fringes and they will then blur out due to the range of energies of the

electrons.

To illustrate the effect of the fringes blurring with increasing distance from the QPC, we have performed a simple one-dimensional simulation. In this idealized case, we assume that the potential of both the QPC and tip are delta functions in position and we calculate the transmission probability through the two of them in series as a function of the separation between them. Figure 7.3 plots the transmission probability as a function of distance for three temperatures. At zero temperature, the probability is just a series of sharp peaks spaced by half the Fermi wavelength indicating the presence of the interference fringes. As the temperature is raised, the peaks decay in amplitude with distance with a characteristic decay length given by the temperature. At the temperatures of the experiments, 1.7 K and 4.2 K, the interference fringes are nearly gone by 500 nm. As seen from this simple simulation, this mechanism is not enough to explain the persistence of the fringes with distance from the QPC.

A second mechanism for the fringes has been proposed by Shaw et al. [Shaw, (2001)]. This second explanation was used because it solved the problem of the fringes decaying with distance from the QPC. In their theory for the origin of the fringes, interference takes place between two paths that travel over different areas but have the same path length. As in any explanation of the fringes one of the paths contributing to the interference must be from the QPC to the tip and back. In their theory, the second path is a roundtrip from the QPC to an impurity, which is located roughly the same distance from the QPC as the tip. The impurity is a located near the same plane as the 2DEG and therefore creates a sharp peak in the potential, which can backscatter electrons to the QPC. Clearly, this will produce interference fringes at zero temperature as the tip is moved due to the phase difference accumulated along these two paths. The

140
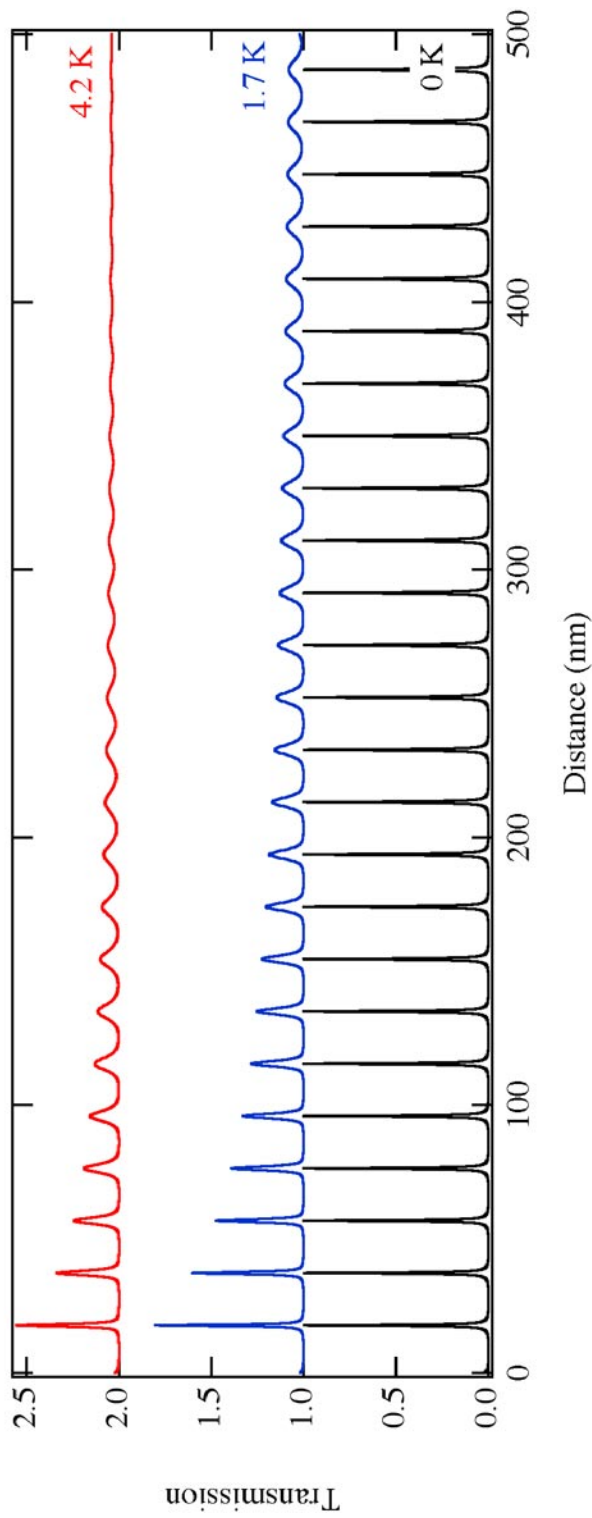
Figure 7.3 Transmission probability through a potential with two delta functions of position as a function of the distance between them. The calculation is done for three different temperatures: (black) 0 K, (blue) 1.7 K and (red) 4.2 K. As the temperature is increased the resonances decay as the distance between the delta functions increases. This shows how the interference fringes would decay with distance.

novel feature of this mechanism is what happens to the interference pattern for different energy electrons. When the tip is at the same distance from the QPC as the impurity, the path lengths are the same and the interference will be constructive for all energies. This gives a maximum in the fringes at this location. As the tip is moved away, the interference fringes for different energies will start to drift out of phase and therefore their average will slowly decay. However, the impurity has brought all of the fringes in phase at a particular distance, which is like moving the QPC to this location. Near this distance from the QPC, the fringes will be strong again. If there are impurities scattered throughout the sample, then the tip will always be near the same radius as one of the impurities and the fringes will appear not to decay with distance.

To test this mechanism for producing interference fringes, we have fabricated a sample that has a reflecting arc located at a fixed distance away from the QPC. Figure 7.4 shows a schematic diagram of the sample used. The reflecting arc acts like a large number of impurities all at the same distance from the QPC. We have then taken images of the electron flow at the same distance from the QPC but in a different area of the sample as shown by the box in Figure 7.4. If the above theory for the origins of the fringes is correct, we should expect a strong enhancement of the fringes due to the presence of the reflecting arc. This is because there will be a large amount of backscattered flux from the arc that the backscattering from the tip can interfere with.

Figure 7.5 shows the electron flow at the same distance from the QPC as the reflecting arc for three values of the reflector gate voltage V_{refl} with respect to the 2DEG: (a) V_{refl} = 0 V, (b) V_{refl} = -0.4 V and (c) V_{refl} = -0.8 V. The images were taken at a temperature of 4.2 K from the area indicated in Figure 7.4, which is located 1500 nm to
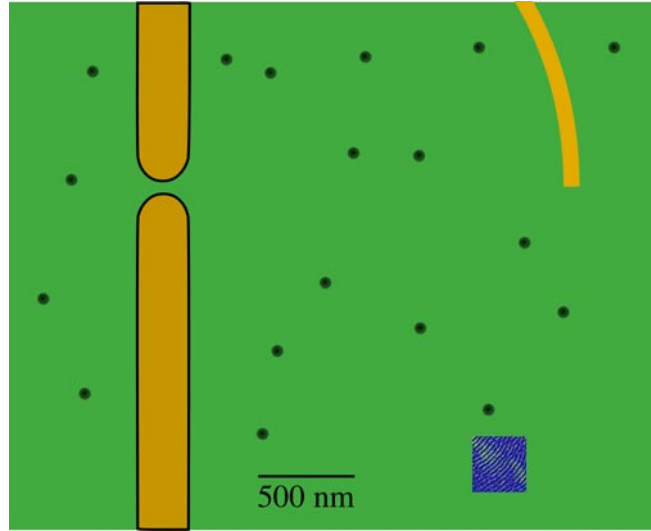
Figure 7.4 Schematic diagram showing the layout of the sample used to investigate the persistence of the interference fringes with distance from the QPC. The reflecting arc is shown in the top right side and the scan area is shown in the bottom right. The black dots are impurities located near the plane of the 2DEG.

the right of the QPC and 1300 nm below it. In Figure 7.5 (a), there is no voltage on the

reflector and therefore there is no backscattering from it. Weak interference fringes are

barely visible in this image of the electron flow. In Figure 7.5 (b), V_{refl} is –0.4 V, which

is just enough to deplete under it and enhance the backscattering. There is a marked
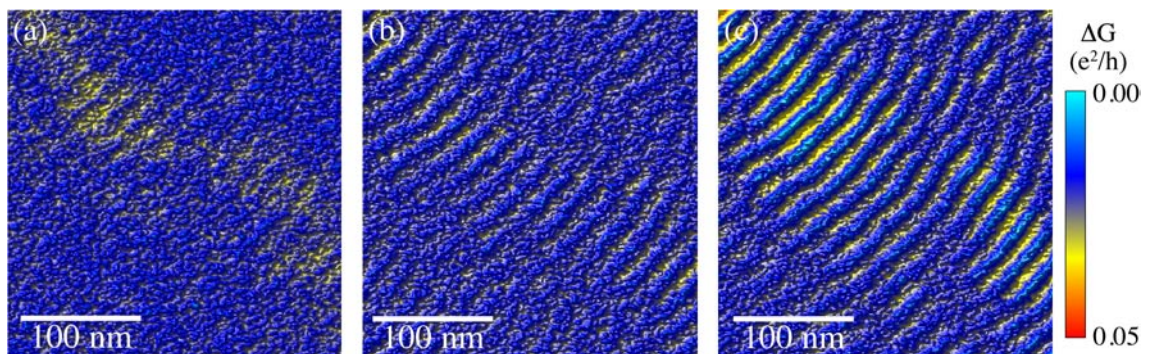
Figure 7.5 Three images of electron flow from the area indicated in Figure 7.4 for different voltages on the reflecting arc, (a) 0.0 V, (b) -0.4 V and (c) -0.8 V. When the arc is energized the interference fringes are enhanced due to the increased backscattering from the arc. These images were taken at a temperature of 4.2 K.

143

increase in the strength of the interference fringes now that the reflector is backscattering

flux to the QPC. In Figure 7.5 (c), V_{refl} is increased to –0.8 V, which continues to

strengthen the backscattering from the reflector. We continue to see an increase in the

strength of the interference fringes in this third image. These images show that the

addition of a backscattering reflecting arc enhances the interference fringes in our images.

This is true if the images are taken at the same radius as the arc but it does not matter if

the image is actually near the arc, as seen here where the scanned area was almost 2 μm

from the reflecting arc.

To further emphasize the role of the reflecting arc in the enhancement of the

fringes we have performed a two-dimensional FFT on the images of electron flow. The

results of these FFTs are shown in Figure 7.6. The top row, (a-c) is the original data as
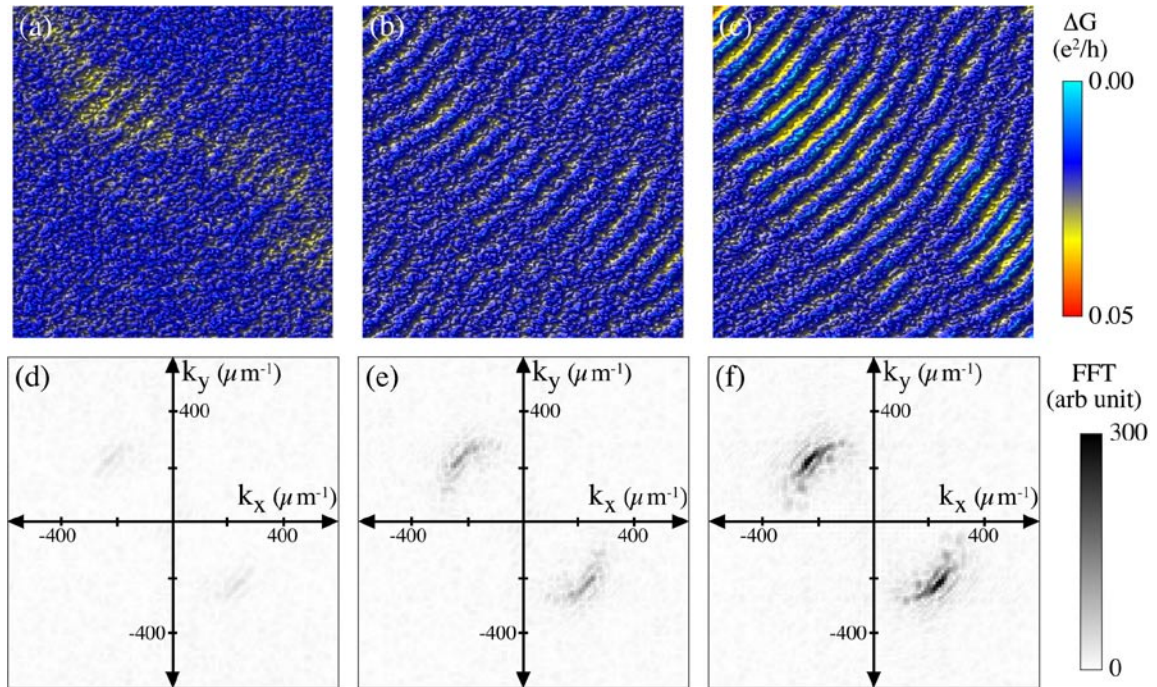
Figure 7.6 Images of electron flow for three voltages on the reflecting arc, (a) 0.0 V, (b) -0.4 V, and (c) -0.8 V. (d-f) Fourier transforms of the previous three images showing the enhancement of the interference fringe as the reflector is energized.

shown previously in Figure 7.5 with the interference fringes present. The bottom row,

(d-f) is the amplitude of the two-dimensional FFT with the two directions indicated.

There is one main radius in the FFT that contributes to the signal seen in the images.

The magnitude of this wavevector, 320 μm^{-1} corresponds to the magnitude of the Fermi

wavevector in the two-dimensional electron gas. The strength of this peak gets stronger

as the voltage on the reflector is increased showing once again that the interference

fringes are being enhanced by the presence of the backscattering gate.

To look more carefully at the effect of the reflecting arc on the strength of the

fringes, we have repeated this FFT procedure for a large number of voltages on the

reflector up to -1.0 V. The results are summarized in Figure 7.7, which plots the peak

value of the FFT amplitude as a function of V_{refl}. When V_{refl} is less than about -0.3 V,

there is a small but constant signal showing that the fringes are not changing strength.

As V_{refl} is increased above -0.3 V the strength of the fringes quickly increases before
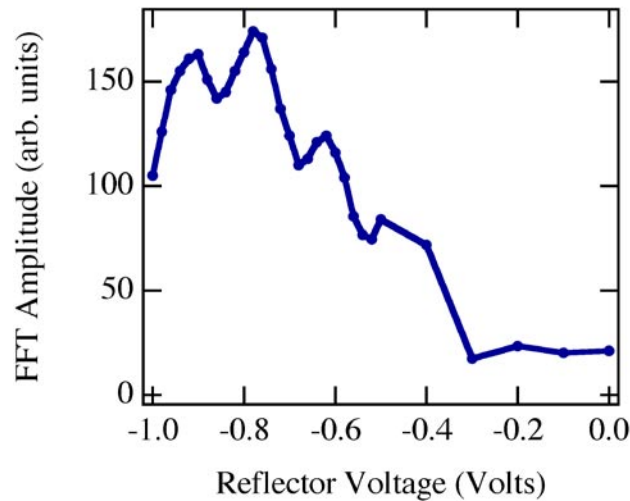
Figure 7.7 Graph of the peak amplitude of the FFT as a function of voltage on the reflector. The signal is constant until the 2DEG is depleted below the reflector at -0.3 Vthen the backscattering and fringes are enhanced.

145

slowly leveling off as the voltage continues to be more negative. This sharp increase in fringe amplitude corresponds to the value of V_{refl} that is necessary to deplete the 2DEG underneath the gate. This is when the gate first starts to backscatter electrons to the QPC. The slow increase in the signal beyond this point is due to the size of the reflecting arc increasing causing an increase in the backscattering and a decrease in the conductance through the device.

7.2. Fringe movement

In this section, we investigate the movement of the interference fringes as a function of the position of the reflecting arc. Because the fringes are due to interference from backscattering from the tip with backscattered paths from the reflecting arc, they should have a definite phase relation with respect to the position of the arc. When the tip is at the same distance from the QPC as the front edge of the arc, the signal should always be constructive since the two backscattered signals will always be in phase. This implies that the fringes should move as a function of the position of the reflecting arc. This position can be controlled by changing the voltage on the gate V_{refl}, which makes the depleted area under the arc grow and therefore the point of backscattering moves closer to the QPC.

We have investigated the behavior of the fringes as a function of the position of the reflector by taking repeated scans over the same area for a series of values of V_{refl}. The scanned area is 1 μm to the left of the QPC and is the same distance from the QPC as the reflecting arc. The resulting images for five different values of V_{refl} are shown in Figure 7.8. The circles on the images are guides to the eye so that the positions of

146
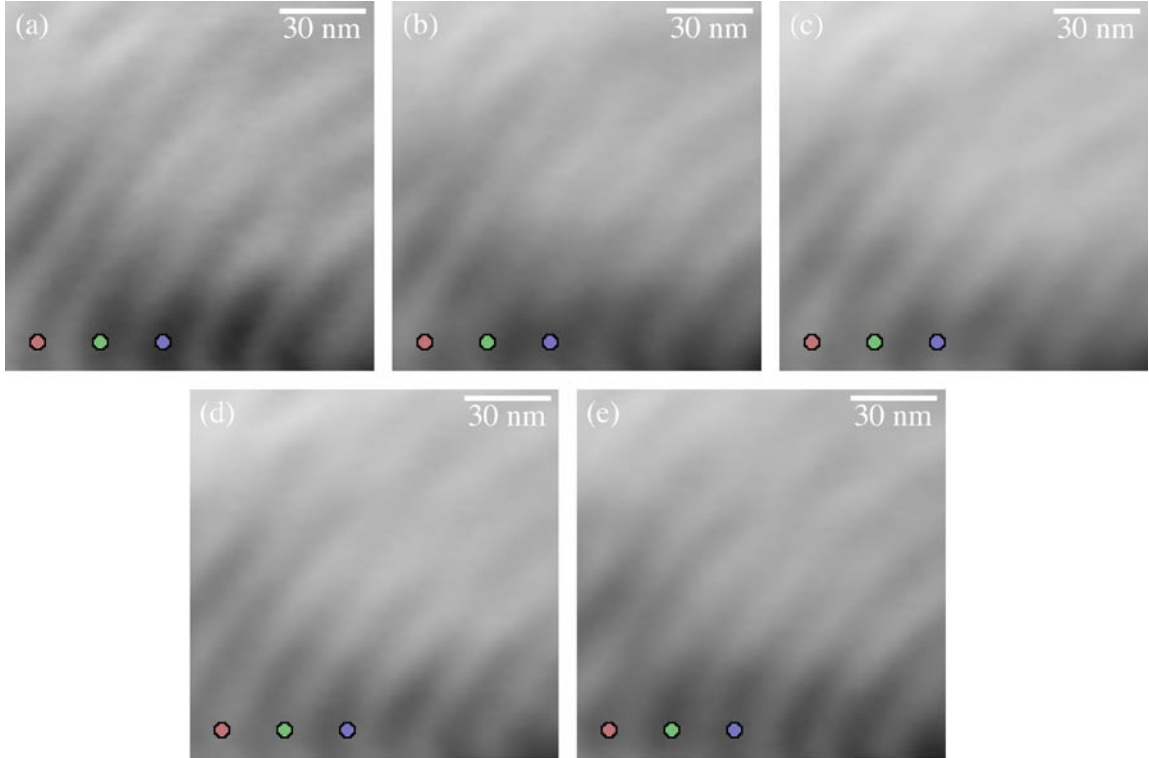
Figure 7.8 Images of electron flow 1 μm to the left of the QPC which is the same radius as the reflecting arc. Each image has a different value of V_{refl}, (a) -0.50 V, (b) -0.52 V, (c) -0.54 V, (d) -0.56 V and (e) -0.58 V. The circles are guides to the eye showing that the fringes move by half the Fermi wavelength in the five images.

the interference fringes can be easily identified. In this series, we have changed V_{refl} by 0.08 V. Moving from (a) to (e) in the images, the guide circles start on the peak of a fringe and then move slowly to a trough before finally ending on a peak in the last image. This corresponds to shifting the position of the interference fringes by half the Fermi wavelength. From a measurement of the conductance through the device as a function of V_{refl}, the movement of the reflector can be determined [Katine, (1997)]. We have performed this measurement and found that the movement of the interference fringes corresponds to the movement of the reflecting arc.

We have repeated this series of images of electron flow at twice the distance of the

147

reflecting arc to see how the fringes move with the position of the arc. Figure 7.9 shows the images of electron flow 2 μm to the left of the QPC. Once again, there are three circles as guides to the eye for judging the movement of the interference fringes. These images are for the same values of V_{refl} as Figure 7.8 but the fringes are clearly moving more quickly in this set of images. Going from (a) to (e) the fringes move in by a full Fermi wavelength. This is twice the movement of the interference fringes at the radius of the reflector and also twice as much as reflector moves.

To look at the difference between these two sets of images more closely, we have tracked the position of all of the interference fringe maxima as a function of reflector
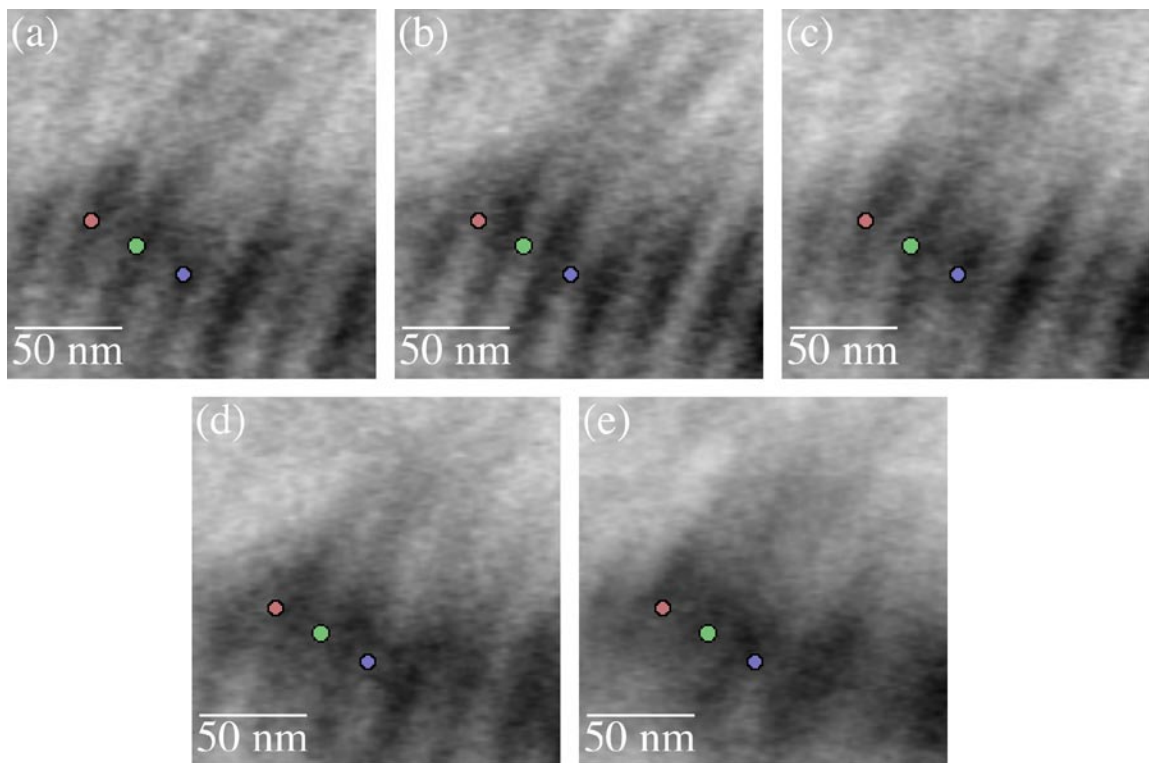
Figure 7.9 Images of electron flow 2 μm to the left of the QPC which is twice the radius of the reflecting arc. Each image has a different value of V_{refl}, (a) -0.50 V, (b) -0.52 V, (c) -0.54 V, (d) -0.56 V and (e) -0.58 V. The circles are guides to the eye showing that the fringes move by the full Fermi wavelength in the five images, which is twice as much as in the images at the radius of the arc in Figure 7.8.

148

voltage. This was done for a series of 26 values of V_{refl} ranging from -0.5 V to -1.0 V.

The results are shown in Figure 7.10 for the two different distances from the QPC. The

circles in the graphs are the measured peak positions found in the images of electron flow.

The solid lines are linear fits to the peak positions as a function of V_{refl}. The peaks move

much more quickly for the images that are taken at twice the radius of the reflecting arc,

Figure 7.10 (b). The average slope of the peaks for the images at the radius of the arc is

0.10 μm/ V_{refl} while for the images at twice the radius the peak movement is

0.23 μm/ V_{refl}.

The reason for the peaks moving twice as fast at twice the radius of the reflector

can be understood by looking at the mechanism that produces the fringes. Figure 7.11

is a schematic diagram of the fringe mechanism at the two distances. Figure 7.11 (a)

shows the two paths that interfere to produce the fringes at the radius of the reflecting

arc. One of the paths goes from the QPC to the tip and back while the other goes from

the QPC to the reflecting arc and back. These have the same path length causing the

fringes to be enhanced as discussed in the previous section. Because one of the paths

goes from the QPC to the arc and back, a change in the arc position will change the path

length and hence the location of the fringes. Figure 7.11 (b) shows the mechanism for

the interference fringes at twice the radius of the reflecting arc. One of the paths has to

go from the QPC to the tip and back. The second path must have the same path length or

else it will be blurred out due to the finite temperature. The only path that has the same

length is one that goes from the QPC to the arc and back two times. If the position of the

reflecting arc is moved by an amount d, this path length will change by 4d, which is twice

as much as the path involved in the interference at the radius of the arc. Therefore, the

149
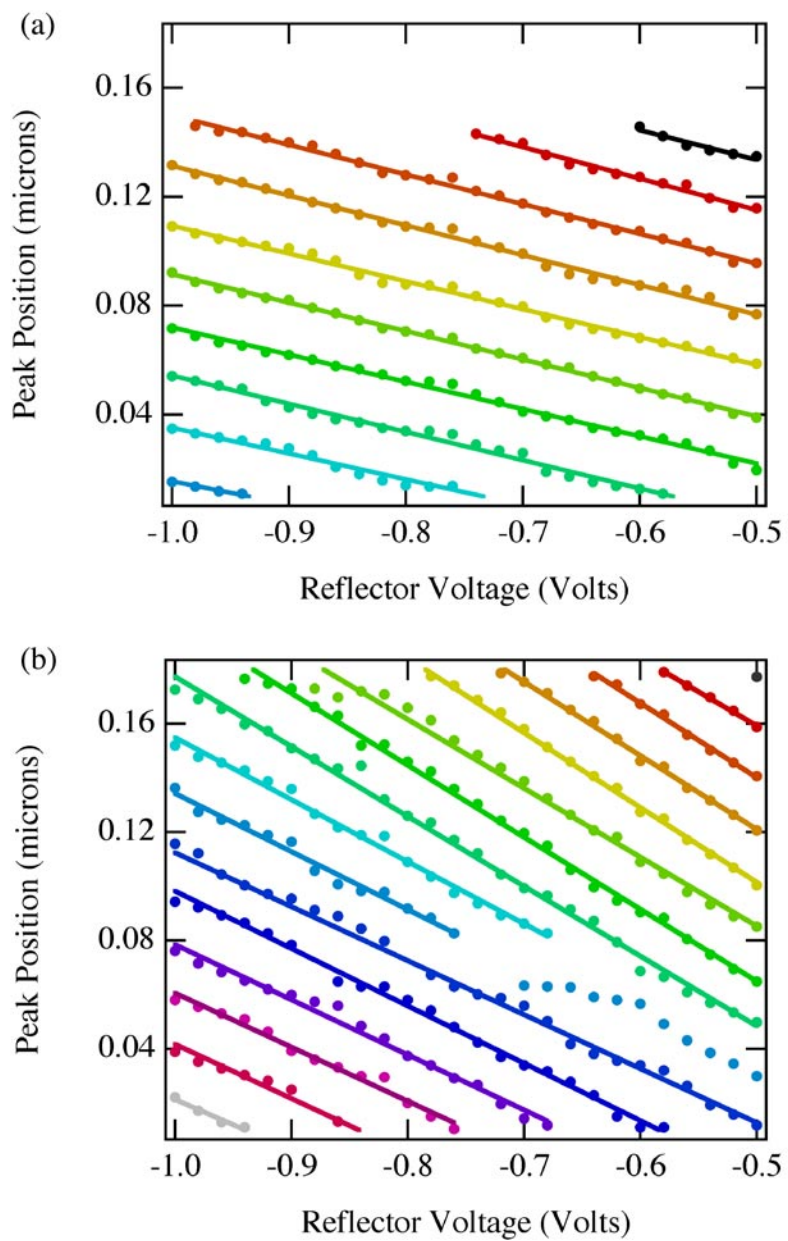
Figure 7.10 (a) Graph of the peak movement as a function of reflector voltage for the images at the radius of the arc. (b) Peak movement as a function of reflector voltage for the images at twice the radius of the arc. These show that the interference fringes move twice as fast at twice the radius of the arc as they do at the radius of the arc.
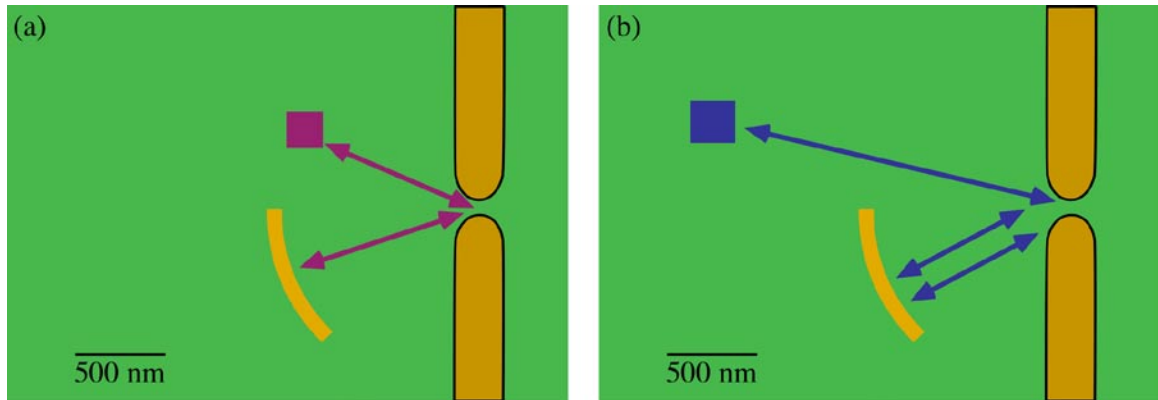
Figure 7.11 Schematic diagram showing the mechanism that leads to the interference fringes (a) at the radius of the arc and (b) at twice the radius of the arc. This mechanism explains why the fringes move twice as fast at twice the radius as seen in the images.

interference fringes should move twice as fast as the reflecting arc. This is observed in the images of electron flow at twice the distance of the reflector.

We can analyze the relationship between the reflector position and interference fringes more closely by looking at the amplitude of the interference fringes. The strength of the interference fringes is a measure of the amount of backscattering from the reflecting arc because they rely on a path returning to the QPC from the reflector. In Figure 7.12, we plot in red the amplitude of the interference fringes as a function of the reflector voltage V_{refl}. The amplitude of the fringes was determined by the peak amplitude of a two-dimensional FFT of the images. In the same graph, plotted in blue is the change in conductance through the device as a function of V_{refl}. This shows a clear oscillatory structure as the voltage is changed. This is due to the reflector going on and off resonance, which enhances and suppresses the backscattering from the reflecting arc [Katine, (1997); Hersch, (1999)]. When the reflector is off resonance, the backscattering from it is enhanced and therefore the conductance decreases. At the same reflector
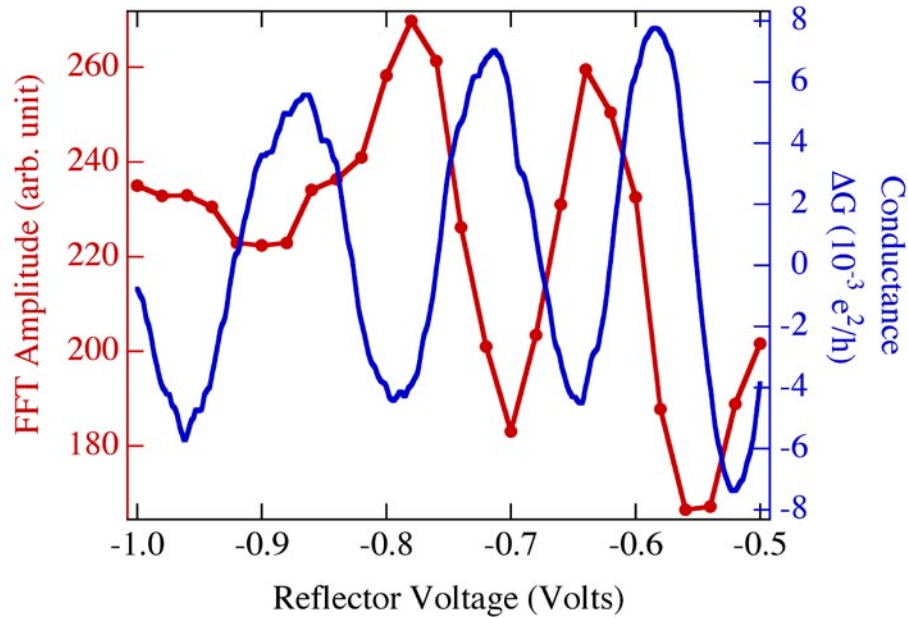
Figure 7.12 (Red) Graph of the fringe strength as measured by the peak amplitude of the FFT versus reflector voltage. (Blue) Change in conductance through the device as a function of the voltage on the reflector. There is an anti-correlation between these two signals showing that an enhancement of backscattering from the reflector also enhances the interference fringes in the images.

voltage, the strength of the interference fringes is enhanced. In contrast, when the conductance is high through the device the strength of the fringes is suppressed. This anti-correlation between the conductance of the device and fringe strength is because when the conductance is high there is less backscattered flux for the signal from the tip to interfere with. The opposite is the case when the reflector is off resonance and the conductance is decreased causing an increase in the observed interference fringes.

7.3. Temperature Dependence

To further emphasize the robustness of the fringes, we have looked at the strength of them near the position of the reflecting arc as a function of temperature. Increasing

the temperature increases the spread in energy of the electrons that contribute to our measured signal. This increased spread in energy means that more wavelengths of electrons contribute to create the interference fringes. At the radius of the arc, there should be no temperature dependence because there is constructive interference for all wavelengths and hence energies. As the tip moves away from the arc, the fringes should only decay weakly with temperature, because the path difference between the two interfering paths will be small. This small difference in length means that a large range of wavelengths can be tolerated while still having constructive interference for all energies. We have simulated a variety of temperatures by applying a voltage across the QPC to match the energy distribution of electrons at the simulated temperature. Using an arbitrary function generator, a time varying signal is applied across the QPC. The voltage from the function generator injects electrons of that energy through the QPC. The amount of time at any given voltage is given by the probability of the electron having that energy for the simulated temperature. Therefore, we spend the most amount of time at 0 V, which corresponds to the Fermi energy and the smallest amount of time at the highest and lowest voltages, which are the tails of the distribution. As the temperature is increased the voltage spends more time away from 0 V because there is a larger spread in energy for the electrons.

Images of electron flow are shown in Figure 7.13 for one real and two simulated temperatures. Figure 7.13 (a) is a schematic diagram showing the location of the reflecting arc and the imaged area. Figure 7.13 (b) is at the base temperature of our experiment, 1.7 K. Figure 7.13 (c) is at a simulated temperature of 4.2 K and Figure 7.13 (d) is at a simulated temperature of 8.4 K. As the temperature is raised, the

153
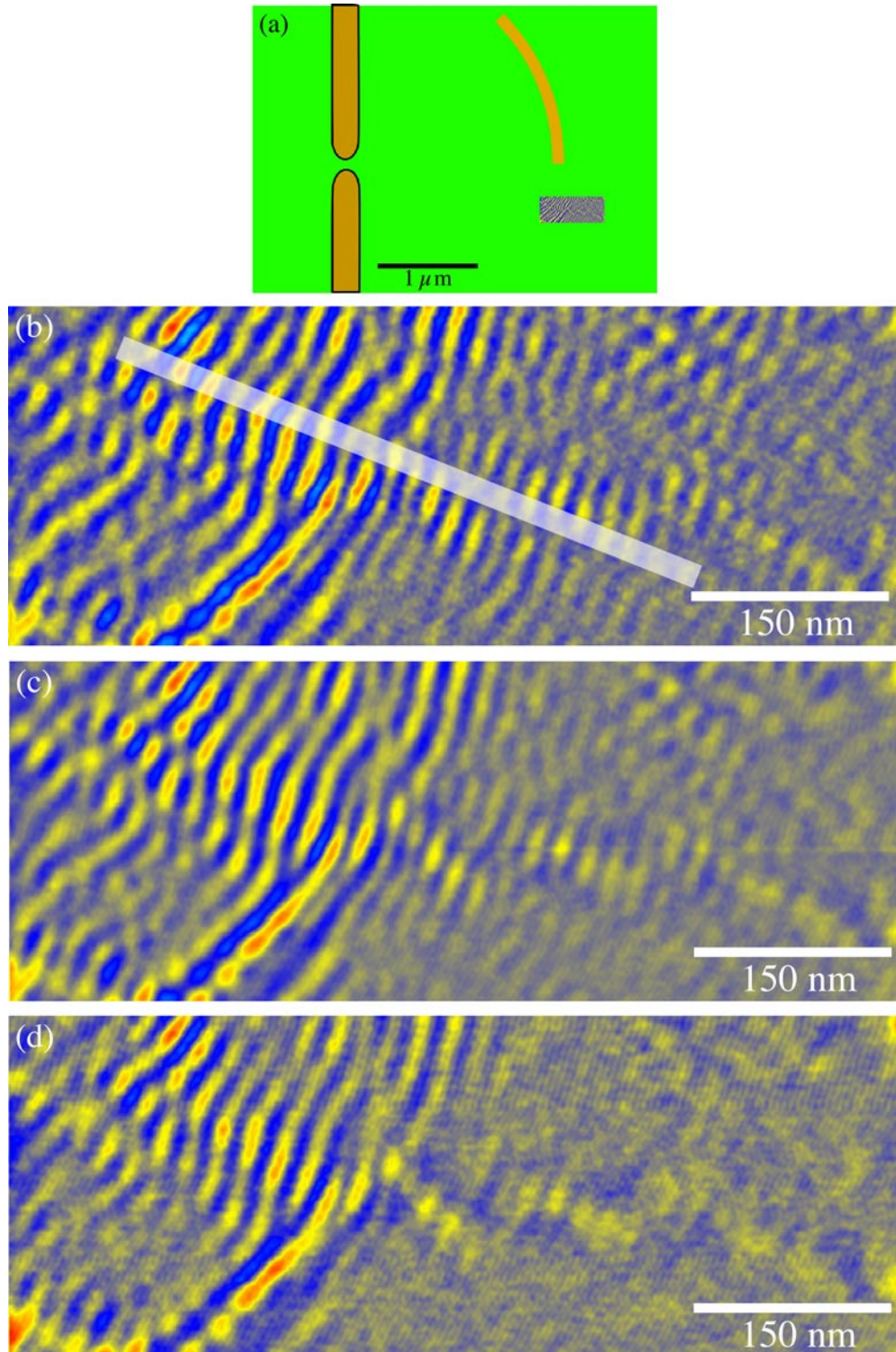
Figure 7.13 (a) Schematic diagram showing the location of the images of electron flow. Images of electron flow at three temperatures, (b) 1.7 K, (c) 4.2 K and (d) 8.4 K showing the robustness of the fringes near the radius of the arc. See the text for an explanation of the procedure used to simulate these temperatues. The white line in (b) shows the location of the one-dimensional line sample used in Figure 7.14.

relative strength of the fringes near the reflecting arc versus those far away is increasing. This shows that the fringes at the same location as the reflector are more robust to increased temperature then those that are away from it. This is what is expected from the theory, which predicts that the fringes at the position of the reflector will not decrease with increasing temperature.

We have repeated these images for two more simulated temperatures and then taken a one-dimensional line sample through all of the images to concentrate on the amplitude of the fringes as a function of distance from the arc. The location of the one-dimensional line sample is shown by the white line in Figure 7.13 (b). Figure 7.14 plots the amplitude of the measured signal as a function of distance for all of the temperatures
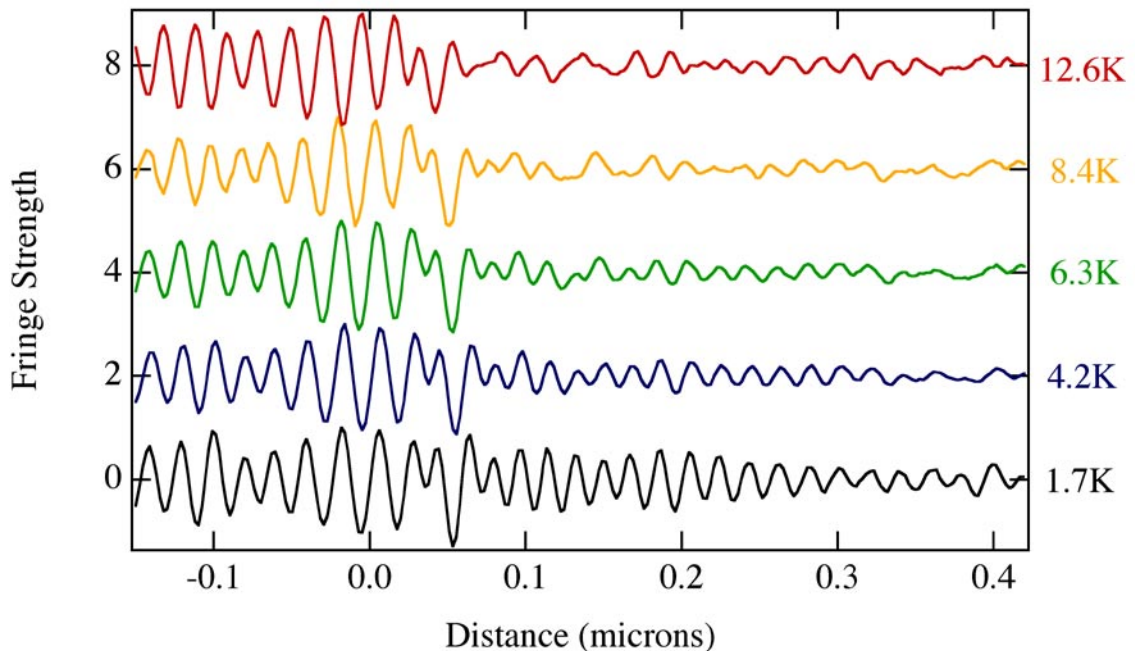
Figure 7.14 Graph of the measured signal as a function of the distance from the arc for a series of simulated temperatures. This shows how the strength of the signal decays more quickly away from the arc for increased temperatures but remains robust at the arc position.

measured. Each curve has been normalized to its maximum value and offset for clarity. Once again, it is clear that the interference fringes are decaying as the tip moves away from the radius of the arc. This decay is more pronounced in the higher temperature images showing that the presence of the arc is causing the fringes to persist at its radius even at increased temperatures.

We have used a reflector arc to investigate the origin of the interference fringes in our images of electron flow. The reflector enhances the fringes in the images at the same radius from the QPC. The position of the fringes moves with the location of the reflector. At twice the distance of the reflector, the interference fringes move twice as fast as the reflector. We have found that the fringes at the same radius as the reflector are robust against thermal smearing. These results show that the fringes are due to interference between the backscattered signal from the tip with the backscattered flux from impurities at nearly the same radius from the QPC as the tip.

Chapter 8

Conclusions and Future Directions

In this thesis, we have developed techniques for imaging coherent electron flow through a two-dimensional electron gas (2DEG). This includes techniques for measuring the local electron density and characterizing the electron-electron scattering rate. We have presented images of electron flow through a variety of semiconductor nanostructures. These images provide more information about the flow of electrons in a two-dimensional electron gas then is available through the use of standard transport measurements. The images of electron flow are decorated by interference fringes spaced by half the Fermi wavelength whose origins are investigated.

We have used these interference fringes to spatially profile the local electron density. We have varied the density of the 2DEG by using a back gate, which changes the spacing of the interference fringes. This imaging technique provides information about the electron density in the 2DEG on a length scale of about 100 nm and can be used to profile changes in density within a sample. We have also seen how the pattern of electron flow changes as a function of density. As the density is reduced, the size of the bumps and dips in the potential due to the donor atoms becomes a larger percentage of the Fermi energy. This causes the electrons to scatter more quickly and the flow becomes more diffusive.

We have measured the electron-electron scattering rate as a function of excess energy added to the electrons. A dc voltage applied across the quantum point contact

157

(QPC) accelerates the electrons as they go through the QPC. The electrons lose

this excess energy through scattering which our imaging technique measures. Our

measurements of the scattering rate in the 2DEG indicate that electron-electron scattering

is the dominant energy loss mechanism in our experiments. This agrees with previous

theoretical and experimental work on scattering in a 2DEG. The previous experiments

required a different sample for each distance measured and were not able to image the

electron flow. Our technique allows the distance and energy dependence of the scattering

to be easily measured in a single sample.

We have also investigated the operation of several electron-optic devices

including a prism, circular scatterer and a narrow channel. The direction of electron flow

can be switched by a voltage applied to the gate of the prism device. We have also shown

how a circular electrostatic gate can scatter electron waves and create new interference

fringes in our images. We have used the narrow channel, defined by two electrostatic

walls, to study the potential profile of a gate on the surface. This shows that the potential

varies slowly as the electron nears the edge of the gate. These experiments show the

operation of electron-optic devices and how a scanning probe microscope can be used to

study them.

In the last part of this thesis we have investigated the origin of the interference

fringes that decorate the images of electron flow. We have found that a small reflecting

arc enhances the fringes in the image at the same radius from the QPC as the arc. The

location of the interference fringes move as the position of the reflector moves. This

shows that the fringes are due to interference from paths backscattering from the tip and

reflecting arc. We have also seen that the strength of the interference fringes is correlated

with the amount of backscattering from the arc. This means that a voltage on the reflecting arc controls the amount of flux traveling through a different part of the sample. This provides another way to coherently control the flow of electrons through the 2DEG.

The work presented in this thesis opens the way for many new experiments. The construction of our new He-3 scanning probe microscope lowers the temperature range that is accessible in our measurements by a factor of 4. This allows new measurements on electron flow through quantum dots and other closed structures to be performed. These structures need the lower temperatures for effects like Coulomb blockade and single electron tunneling. The reduced temperature should also enhance the interference fringes seen throughout the images. The disappearance of these interference fringes may provide a novel way to measure the phase coherence length in the 2DEG.

This new scanning probe microscope also includes a magnetic field, which can be orientated either parallel or perpendicular to the sample. In the perpendicular orientation, the cyclotron orbits of the electrons can be studied. It is also possible to look at the pattern of electron flow in the integer and fractional quantum Hall regimes. If the magnetic field is orientated parallel to the sample, the spin states of the electron are separated by the Zeeman energy. This allows the investigation of the electron flow for the two spin states of the electron.

There are also many other systems that can be studied with the scanning probe microscopes. One of the most promising is InGaAs, which can have a 2DEG formed very near the surface. This will improve the spatial resolution of our imaging techniques because the tip can be brought very close to the 2DEG. It also has a much larger g factor for electrons than GaAs, which enables spin dependant transport to be studied more

easily. This is important for the understanding of new spintronic devices that rely on the

electron spin for their operation.

References

Adachi, Sadao (1985). "GaAs, AlAs, and $Al_xGa_{1-x}As$: Material parameters for use in research and device applications," *J. Appl. Phys.* **58**, R1-R29.

Beenakker, C.W.J., and H. van Houten (1991). "Quantum transport in semiconductor nanostructures," *Solid State Physics* 44, H. Ehrenreich and D. Turnbull, (eds.), Academic Press, San Diego, CA.

Binnig, G., H. Rohrer, Ch. Gerber, E. Weibel (1982). "Surface studies by scanning tunneling microscopy," *Phys. Rev. Lett.* **49**, 57.

Binnig, G., C.F. Quate, and Ch. Gerber (1986). "Atomic force microscope," *Phys. Rev. Lett.* **56**, 930.

Büttiker, M. (1986). "Four-terminal phase-coherent conductance," *Phys. Rev. Lett.* **57**, 1761.

Chen, L,H. (2001). "Charge-imaging field-effect transistors for scanned probe microscopy," Ph.D. Thesis, Harvard University.

Ciorga, M, A.S. Sachrajda, P. Hawrylak, C. Gould, P. Zawadzki, S. Jullian, Y. Feng, Z. Wasilewski (2000) "Addition spectrum of a lateral dot from Coulomb and spin-blockade spectroscopy," *Phys. Rev. B* **61**, R16315.

Crommie, M.F., C.P. Lutz, D.M. Eigler (1993). "Confinement of electrons to quantum corrals on a metal surface," *Science* **262**, 218.

Crook, R., C.G. Smith, M.Y. Simmons, D.A. Ritchie (2000a). "Imaging diffraction-limited electronic collimation from a non-equilibrium one-dimensional ballistic constriction," *J. Phys.: Condens. Matter* **12**, L167.

Crook, R., C.G. Smith, M.Y. Simmons, D.A. Ritchie (2000b). "Imaging cyclotron orbits and scattering sites in a high-mobility two-dimensional electron gas," *Phys. Rev. B* **62**, 5174.

Davies, John H., Ivan A. Larkin, E.V. Sukhorukov (1995). "Modeling the patterned two-dimensional electron gas: Electrostatics," *J. Appl. Phys.* **77**, 4504.

Davies, John H. (1998). "The physics of low-dimensional semiconductors," Cambridge University Press, New York, USA.

Dingle, R., H.L. Störmer, A.C. Gossard, W. Wiegmann (1978) "Electron mobilities in modulation-doped semiconductor heterojunction superlattices," *Appl. Phys. Lett.* **33**, 665.

Elzerman, J.M. R. Hanson, J.S. Greidanus, L.H. Willems van Beveren, S. De Franceschi, L.M.K. Vandersypen, S. Tarucha, L.P. Kouwenhoven (2003). "Few-electron quantum dot curcuit with integrated charge read out," *Phys. Rev. B* **67**, 161308(R).

Eriksson, M.A., R.G. Beck, M. Topinka, J.A. Katine, R.M. Westervelt, K.L. Campman, A.C. Gossard (1996). "Cryogenic scanning probe characterization of semiconductor nanostructures," *Appl. Phys. Lett.* **69**, 671.

Eriksson, M. A. (1997). "Cryogenic scanning probe microscopy for semiconductor nanostructures," Ph. D. Thesis, Harvard University.

Finkelstein, G., P.I. Glicofridis, R.C. Ashoori, M. Shayegan (2000). "Topographic mapping of the quantum Hall liquid using a few-electron bubble," *Science* **289**, 90.

Giuliani, Gabriele F. and John J. Quinn (1982). "Lifetime of a quasiparticle in a two-dimensional electron gas," *Phys. Rev. B* **26**, 4421.

Harris, J.J., J.A. Pals, and R. Woltjer (1989). "Electronic transport in low-dimensional structures," *Rep. Prog. Phys.* **52**, 1217.

Heremans, J.J., S. von Molnar, D.D. Awschalom, A.C. Gossard (1999). "Ballistic electron focusing by elliptic reflecting barriers," *Appl. Phys. Lett.* **74**, 1281.

Herman, M.A. and H. Sitter (1989). "Molecular Beam Epitaxy," Springer-Verlag, New York.

Hersch, J.S., M.R. Haggerty, E.J. Heller (1999). "Diffractive orbits in an open microwave billiard," *Phys. Rev. Lett.* **83**, 5342.

Hopkins, P. (1990). "Magnetotransport in wide parabolic GaAs/AlGaAs quantum wells," Ph. D. Thesis, Harvard University.

Hudson, E. W., S.H. Pan, A.K. Gupta, K.-W. Hg, J.C. Davis (1999). "Atomic-scale quasi-particle scattering resonances in $Bi_2Sr_2CaCu_2O_{8+\delta}$," *Science* **285**, 88.

Katine, J. A., (1996). "Electronic quantum interference in ballistic semiconductor nanostructures," Ph. D. Thesis, Harvard University.

Katine, J.A., M.A. Eriksson, A.S. Adourian, R.M. Westervelt, J.D. Edwards, A. Lupu-Sax, E.J. Heller, K.L. Campman, A.C. Gossard (1997). "Point contact conductance of an open resonator," *Phys. Rev. Lett.* **79**, 4806.

Kouwenhoven, L.P., B.J. van Wees, C.J.P.M. Harmans, J.G. Williamson, H. van Houten, C.W.J. Beenakker, C.T. Foxon, J.J. Harris (1989). "Nonlinear conductance of quantum point contacts," *Phys. Rev. B* **39**, 8040.

Landauer, R. (1957). "Spatial variation of currents and fields due to localized scatterers in metallic conduction," *IBM J. Res. Dev.* **1**, 223.

Landauer, R. (1970). "Electrical resistance of disordered one-dimensional lattices," *Phil. Mag.* **21**, 863.

Larkin, Ivan A., and John H. Davies (1995). "Edge of the two-dimensional electron gas in a gated heterostructure," *Phys. Rev. B* **52**, R5535.

Lemay, Serge G., Jorg W. Janssen, Michiel van den Hout, Maarten Mooij, Michael J. Bronikowski, Peter A. Willis, Richard Smalley, Leo P. Kouwenhoven, Cees Dekker (2001). "Two-dimensional imaging of electronic wavefunctions in carbon nanotubes," *Nature* **412**, 617.

Manoharan, H.C., C.P. Lutz, D.M. Eigler (2000). "Quantum mirages formed by coherent projection of electronic structure," *Nature* **403**, 512.

McCormick, Kent L., Michael T. Woodside, Mike Huang, Mingshaw Wu, Paul L. McEuen, Cem Duruoz, J.S. Harris (1999). "Scanned potential microscopy of edge and bulk currents in the quantum Hall regime," *Phys. Rev. B* **59**, 4654.

Muller, F., B. Lengeler, Th. Schäpers, J. Appenzeller, A. Förster, Th. Klocke, H. Lüth (1995). "Electron-electron interaction in ballistic electron beams," *Phys Rev B* **51**, 5099.

Nabity, J. C., and M.N. Wybourne (1989). "A versatile pattern generator for high-resolution electron-beam lithography," *Rev. Sci. Instrum.* **60**, 27.

Nabity, J. C. (1991). *Nanometer Pattern Generation System Manual*, Bozeman, MT.

Pan, S.H., E.W. Hudson, K.M. Lang, H. Eisaki, S. Uchida, J.C. Davis (2000). "Imaging the effects of individual zinc impurity atoms on superconductivity in $Bi_2Sr_2CaCu_2O_{8+\delta}$," *Nature* **403**, 746.

Pfeiffer, Loren, K.W. West, H.L. Störmer, K.W. Baldwin (1989). "Electron mobilities exceeding 10^7 cm^2/V s in modulation-doped GaAs," *Appl. Phys. Lett.* **55**, 1888.

Predel, H., H. Buhmann, L.W. Molenkamp, R.N. Gurzhi, A.N. Kalinenko, A.I. Kopeliovich, A.V. Yanovsky (2000). "Effects of electron-electron scattering on electron-beam propagation in a two-dimensional electron gas," *Phys. Rev. B* **62**, 2057.

Rimberg, A.J. (1992). "Magnetotransport in uniform and modulated electron gases in wide parabolic quantum wells," Ph.D. Thesis, Harvard University.

Schäpers, Th., M. Krüger, J. Appenzeller, A. Förster, B. Lengeler, H. Lüth (1995). "Effect of electron-electron interaction on hot ballistic electron beams," *Appl. Phys. Lett.* **66**, 3603.

Shaw, S.E.J., R. Fleischmann, and E.J. Heller (2001). "Quantum coherence beyond the thermal length," cond-mat/0105354.

Shaw, S.E.J. (2002). "Propagation in smooth random potentials," Ph.D. Thesis, Harvard University.

Sivan, U., M. Heiblum, C.P. Umbach (1989). "Hot ballistic transport and phonon emission in a two-dimensional electron gas," *Phys. Rev. Lett.* **63**, 992.

Sivan, U., M. Heiblum, C.P. Umbach, H. Shtrikman (1990). "Electrostatic electron lens in the ballistic regime," *Phys. Rev. B* **41**, 7937.

Sohn, L.L., L.P. Kouwenhoven and G. Schön (eds) (1997). "Mesoscopic electron transport," Kluwer Academic, Boston MA.

Spector, J., H.L. Störmer, K.W. Baldwin, L.N. Pfeiffer, K.W. West (1990a). "Control of ballistic electrons in macroscopic two-dimensional electron systems," *Appl. Phys. Lett.* **56**, 967.

Spector, J., H.L. Störmer, K.W. Baldwin, L.N. Pfeiffer, K.W. West (1990b). "Refractive switch for two-dimensional electrons," *Appl. Phys. Lett.* **56**, 2433.

Spector, J., H.L. Störmer, K.W. Baldwin, L.N. Pfeiffer, K.W. West (1991). "Noninteracting beams of ballistic two-dimensional electrons," *Appl. Phys. Lett.* **58**, 263.

Spector, J., J.S. Weiner, H.L. Störmer, K.W. Baldwin, L.N. Pfeiffer, K.W. West (1992). "Ballistic electron optics," *Surface Science* **263**, 240.

Tarucha, S., D.G. Austing, T. Honda, R.J. van der Hage, L.P. Kouwenhoven (1996). "Shell filling and spin effects in a few electron quantum dot," *Phys. Rev. Lett.* **77**, 3613.

Tessmer, S.H., P.I. Glicofridis, R.C. Ashoori, L.S. Levitov, M.R. Melloch (1998). "Subsurface charge accumulation imaging of a quantum Hall liquid," *Nature* **392**, 51.

Topinka, M.A., B.J. LeRoy, S.E.J. Shaw, E.J. Heller, R.M. Westervelt, K.D. Maranowski, A.C. Gossard (2000). "Imaging coherent electron flow from a quantum point contact" *Science* **289**, 2323.

Topinka, M.A., B.J. LeRoy, R.M. Westervelt, S.E.J. Shaw, R. Fleischmann, E.J. Heller, K.D. Maranowski, A.C. Gossard (2001). "Coherent branched flow in a two-dimensional electron gas" *Nature* **410**, 183.

Topinka, M. A. (2002). "Imaging coherent electron wave flow through 2-D electron gas nanostructures," Ph.D. Thesis, Harvard University.

van Wees, B.J., H. van Houten, C.W.J. Beenakker, J.G. Williamson, L.P. Kouwenhoven, D. van der Marel, and C.T. Foxon (1988). "Quantized conductance of point contacts in a two-dimensional electron gas," *Phys. Rev. Lett.* **60**, 848.

Wharam, D.A., T.J. Thornton, R. Newbury, M. Pepper, H. Ahmed, J.E.F. Frost, D.G. Hasko, D.C. Peacock, D.A. Ritchie, and G.A.C. Jones (1988). "One-dimensional transport and the quantization of the ballistic resistance," *J. Phys. C: Solid State Phys.* **21**, L209-L214.

Woodside, Michael T. and Paul L. McEuen (2002). "Scanned probe imaging of single-electron charge states in nanotube quantum dots," *Science* **296**, 1098.

Yacoby, A., U. Sivan, C.P. Umbach, J.M. Hong (1991). "Interference and dephasing by electron-electron interaction on length scales shorter than the elastic mean free path," *Phys. Rev. Lett.* **66**, 1938.

Yacoby, A., H.F. Hess, T.A. Fulton, L.N. Pfeiffer, K.W. West (1999). "Electrical imaging of the quantum Hall state," *Solid State Comm.* **111**, 1.

Appendix

A. SEM Procedure

This section details the procedure that is used for writing ohmics and devices on the JEOL SEM. It is divided into six sections, loading a sample, imaging, focusing, writing, changing samples and shutting down.

A.1. Loading Sample

a. Put the sample into the sample holder and screw it onto the end of the manipulator.

b. Pump out the airlock by pushing the red button.

c. Make sure that the Nitrogen cold trap is full.

c. Check that the detector is off in the EOS menu.

d. Load the correct setup from Memory. We use a working distance of 15 mm and an accelerating voltage of 35 kV.

e. Put the sample all the way in and check that it is securely in place. Unscrew the rod and pull it out. Close the airlock and vent it by pushing the red button again.

A.2. Initial Images

a. Move the sample away at least 7 mm in some direction. This ensures that you will not expose the sample by accident.

b. Change the working distance with the big knob to 15 mm.

c. Check that the magnification is 500.

d. Turn on the accelerating voltage.

e. Switch to fast, line mode with the maximum contrast.

f. Slowly turn up the current. It should take about 1 minute to turn up the current. The signal on the screen should go up then down and back up again before hitting a plateau. Turn down the current so that it is just below this plateau.

g. Switch to the picture mode and find your chips.

A.3. Aligning and Focusing

a. Get a rough focus on one of the corners of the chip.

b. Change the mode to the one with the crosshairs and make sure that the image zooms in on them. If it does not you have to adjust their position in the EOS menu.

c. Adjust the mechanical rotation so that when you move in the x direction you go from the top right to the top left of the chip.

d. Adjust the scan rotation so that image moves straight across the screen.

e. If only writing large features find the focus on two opposite corners of the chip and set the value to the average of these.

f. If writing fine features focus on the silver paint on the four sides of the sample. Adjust the astigmatism at the first silver paint location. Fit a plane to these four values of the focus to determine the appropriate focus for the device location.

A.4. Writing

a. Turn the contrast and brightness all the way down.

b. Switch the beam blanking to external.

c. Switch to slow mode.

d. Switch to computer control using the Pomona box.

e. Turn up the brightness until the dot appears at the center of the screen. This should be about 220.

f. Adjust the tilt and shift to maximize the current. The tilt should be adjusted on condenser lens 16 and the shift on condenser lens 1. I usually do this into the PCD cup but it can also be done into the hole on the sample holder. I find the only thing that really matters is that you consistently use one or the other because they give different readings

of the current, which can affect the writing of the pattern.

g. Move to the position for the device.

h. Set up the run file for the pattern. This is done with the command "mrf filename" were filename is the name of the file to write.

i. Set the magnification and condenser lens for the first layer.

j. Run the command "pg filename" where filename is the name of the file that you are writing.

k. Continue setting the magnification and current until all the layers are written.

A.5. JEOL Control

a. Move away from the chip and turn the current down to condenser lens 16.

b. Make sure the magnification is above 100 and the PCD cup is in.

c. Turn the brightness down to zero to avoid a bright spot showing up on the screen.

d. Switch the Pomona box back to JEOL control and switch back to fast mode.

e. Turn up the contrast and brightness. Remove the PCD cup to go back to the imaging mode.

A.6. Shut Down

a. Slowly turn down the current.

b. Turn off the accelerating voltage.

c. Check that the detector is off in the EOS-3 menu.

d. Move the sample back to the exchange position. Set the working distance to 39 mm and the rotation back to zero. Then remove the sample using the same procedure as putting it in.

e. Set the magnification to the maximum value, 300,000, go to slow picture mode. Make sure that the beam blanking is off, the PCD cup is out and the scan rotation is off.

f. Get rid of the writing on the screen using the PF1 key.

B. Script Commands

This section lists all of the commands that can be used in the script window of the AFM program. They are broken down into subsections relating to scans, sweeps, graphics, utilities, movies, simulations and several others.

B.1. Utility Commands

These are basic utility commands used in the program. Most of the variables that can be set in the dashboard are also available in these commands. They set internal variables like how long to wait when finding the surface, the working directory, and the conversion factor from voltage to conductance.

af.drift [drift (Volts)]
The amount of drift in the cantilever signal when doing the autoflatten routine.

af.pause [wait (secs)]
The amount of time to wait between points when doing the autoflatten routine.

atan [x] [y]
Calculates the arctan(y/x).

constantstep [# of bits]
Sets distance between pixels in scan to be the given number of bits.

debugout.start [outCh]
Prints the values being sent to the given channel in the sweep window.

debugout.end
Turns off the output printing in the sweep window.

decfnum
Decreases the current file number by one.

decimal [number]
Prints the decimal portion of the number.

delay [time (secs)]
Waits the specified time before doing the next command.

dialog [str0] [str1] [str2] [str3]
Creates a dialog box with the strings in it.

feedbackreturn [straight/cw/ccw] [margin (Volts)]
Determines which way the tip moves back to the origin after finishing a scan. Straight is the default type. It can also move either clockwise or counterclockwise. Margin determines the distance in volts outside of the current scan area that the tip moves. This is only used for cw and ccw. The default value is 1.

filecomment= [comment0] [comment1]
Sets the file comment that is saved with the scan, can be seen using the get info command in the Finder. This does not work in OS X because comments are no longer supported by the operating system.

floor [number]
Prints the integer portion of the number.

fs.downtime [time (secs)]
How long to sit on the surface when running FindSurface, default is 0.2s.

fs.offheight [height (Volts)]
How far off the surface to move when running FindSurface, default is 0.5V.

fs.tau [tau (secs)]
How long to take moving to the surface when running FindSurface, default is 0.01s.

fs.uptime [time (secs)]
How long to sit off the surface when running FindSurface, default is 0.02s.

graphinchan [graph: a-d] [ch]
Sets the channels to read into the given graph.

graphonoff [graph: a-d] [on/off]
Turn on or off the reading into the given graph.

help [command]
Find help on the given command.

incfnum
Increases the current file number by one.

makesafe
Sets the gate, reflector and tip voltage to zero.

movecursors [cursor: r,g,b] [x] [y] [cursor: r,g,b] [x] [y] [cursor: r,g,b] [x] [y]
Moves the indicated cursors to the specified location.

print [string0] [string1] [string2] etc.
Prints the given string(s) to the console window.

printfilecomment
Prints the current file comment in the console window.

printscanstats [graph: a-d]
Prints the stats associated with the given graph to the console window. These stats currently include the size of the image, the speed, the direction of the scan and the settings of the output voltages.

printscanval [graph: a-d] [x] [y]
Prints in the console window the value at point (x,y) in the specified graph. The value of x and y are the voltage values.

setanalysisradius [radius (pixels)]
Sets the radius to use in calculating a sweep from a collection of slides, default is 1.

setdigital [a0/a1/a2/a3/b0/b1/b2/b3] [0/1]
Sets one of the eight digital output to either 0 or 1.

setdioout [upper] [lower]
Toggles the dio output between the upper+lower and 0.

setdir [directory]
Sets the directory for saving files.

setfastdir [l2r/r2l/b2t/t2b]
Sets the fast scan direction. There are four choices: Right to Left, Left to Right, Bottom to Top, or Top to Bottom.

setfeedback [setpoint]
Sets the feedback to the desired setpoint.

setflyback [speed (V/s)]
Sets the speed for the flyback.

setfnum [#]
    Sets the current file number.

setgateExtra [Extra (Volts)]
    The amount to pull off the surface when over a gate as defined by setgatethreshold.

setgatethreshold [Thresh (Volts)]
    Used to define the area in a scan that is over the gate, when using the z-guide.

setgatev [voltage]
    Sets the gate voltage.

setheight [Height (Volts)] [Drift (Volts)]
    Finds the surface and then pulls away by the amount in height. Drift sets the average drift on the cantilever in order to make sure that we find the real surface.

sethover
    Moves the tip 0.5V off of the surface. There must be a zguide to run this.

setnpts [# of pts]
    Sets the number of points in the scan.

setpixelbuffer [# of pixels]
    Sets the buffer around the edge of gates. This is used when making a z-guide to give an extra margin of safety.

setreflv [Volts]
    Sets the reflector voltage.

setscanrot [angle] [opt: ok]
    Rotates the scan to the given angle. Option ok moves the tip without a warning.

setslowdir [l2r/r2l/b2t/t2b]
    Sets the slow scan direction. There are four choices: Right to Left, Left to Right, Bottom to Top, or Top to Bottom.

setsweepio [inCh] [mio16x/ao6] [outCh]
    Sets the I/O parameters for a sweep. Lets you specifiy the input channel on the MIO and also the output channel on either the MIO or AO.

setsweeprange [start] [end] [step] [reads per point]
    Sets the starting and ending voltage values for a sweep. Also sets the step size and the number of reads to do per point.

settau [tau (secs)]
Sets the slow down time used in smooth scans.

settempparams [alarm delta] [vShift_He] [vShift_N]
Changes the calibration settings for the thermometers.

settipspeed [V/s]
Sets the scanning speed.

settipv [Volts]
Sets the tip voltage.

setvbuffer [buffer (Volts)]
Extra amount to be off the surface for all points on a z-guide.

setvoltconv [ao6/mio16x/tip/gate/refl] [ch#] [Voffset] [Vmult]
Changes the multiplier. If tip/gate/refl is specified then ch# can be left blank. The actual voltage put onto the sample is Vreal = Voffset +(Vcomp * Vmult)

setvout [mio16x/ao6/dio] [Ch] [volts]
A more general output setting call. Lets you specify the board and also the channel that you want the voltage to be set on.

setxchannel [ch]
Changes the channel that is the x axis of the scans.

setxmultiplier [mult]
Changes the multiplier for the output to the x axis.

setxyrot [xCh] [yCh] [angle]
Changes the x and y channel along with the scan rotation.

setychannel [ch]
Changes the channel that is the y axis of the scans.

setymultiplier [mult]
Changes the multiplier for the output to the y axis.

setzv [Volts]
Sets the voltage to the z piezo. This controls the height of the tip off the surface.

smoothscan [on/off]
Whether or not to do smooth scans.

squarepixels [on/off]
Whether or not the pixels in a scan have to be square.

temps2sweep
Takes the data from the temperature plot and moves it into the sweep window.

unstickv= [Volts]
Sets the amount of volts the tip pulls off the surface with the unstick tip command.

userpause.off
Turns off the pausing.

userpause.on
Turns on a pause that requires the user to hit a key to continue.

v124tog.on
Turns on the conversion from the PAR124 to G values for sweeps.

v124tog.off
Turns off the conversion from the PAR124 to G values for sweeps.

v124togparams [V10k] [Rseries] [Gmax] [Vzero]
Sets the parameters necessary to convert the output of the PAR124 into G values.

v124togvalue [value]
Converts value into a G value using the parameters stored in v124togparams.

vguide [on/off]
Turns the vguide on or off.

zguide [on/off]
Turns the zguide on or off.

B.2.   Graphics Commands

These commands are all related to the graphics display in the program. There is a set of commands for displaying the data in 3D including the placement of lights for highlighting it. There are also a set of commands for setting the color scale, location and other parameters of the image.

174

3d.backcolor [r] [g] [b]
Sets the color of the background.

3d.eye [x] [y] [z]
Sets the eye position.

3d.fieldofview [angle (deg)]
Sets the angle for the field of view.

3d.focus [auto, x] [y] [z]
Sets the focus point. If the first parameter is auto, then the focus is the center of the data. Otherwise, the focus is set to the position given.

3d.geteye
Prints the position of the eye in the script window.

3d.glarefactor [factor]
Sets the glare factor.

3d.glarewidth [width (deg)]
Sets the width of the glare in degrees.

3d.grid [dx (pixels)] [dy (pixels)]
Places a grid on the data with the given spacing in x and y.

3d.light [number] [x] [y] [z] [r] [g] [b] [ambient/non] [width]
Adds a light. Number is the light number to add. (Use 0 for ambient). The position of the light is given by x,y,z and its color is given by r,g,b. The width of the light is given by width.

3d.off [graph: a-d]
Turns off 3D for the given graph.

3d.on [graph: a-d]
Turns on 3D for the given graph.

3d.polyarc [x] [y] [z] [radius] [StartAngle] [EndAngle] [NumPts]
Creates an arc. x,y,z gives the center coordinates of the arc. The radius is given by radius and the starting and ending points are given by StartAngle and EndAngle. Creates the arc by dividing it into NumPts straight lines.

3d.polyclear [graph: a-d]
Clears all the polygons in a given graph.

3d.polyend
Ends the polygon by drawing a line from the last point defined to the starting point.

3d.polyline [x] [y] [z]
Draws a line from the previous point defined to the point given by x,y,z.

3d.polystart [graph: a-d] [r] [g] [b] [x] [y] [z]
Starts a polygon in the given graph. The color of the ploygon is determined by r,g,b and the first point is given by x,y,z.

3d.removelight [number]
Removes the light given by number. Also shifts the numbers of all the other lights.

3d.scale [xScale] [yScale] [zScale]
Changes the scale.

3d.scalefactor [factor]
Changes the scale by a factor.

3d.sidecolor [r] [g] [b]
Sets the color of objects that have cMarker0_f64 as one of their points.

3d.viewangle [angle (deg)]
Sets the viewing angle in degrees.

autoxy [graph: a-d]
Automatically changes the range on the specified graph to include all of the data.

autoz [graph: a-d]
Sets the color scale so that all of the data is within the scale.

backcolor [r] [g] [b]
Sets the background color of all the graphs.

bandsoff [graph: a-d]
Turns off the display of the bands.

bandson [graph: a-d] [base] [width] [spacing] [exclude] [r] [g] [b] [weight] [ave/add]
Puts color bands on the data in the graph. The width, spacing and color are controlled by the parameters.

colorscheme [graph: a-d] [scheme]

Sets the color scheme for the selected graph. The scheme must include special0 and then one of the following schemes blackbottom, halloween, sand&water, water&sand, ice&fire, fire&ice, emerald&sapphire or sapphire&emerald. You can also specify where to take the average value. The choices are bottom, top, right or left. There are also two other options maxmid() and minmid().

copycolors [graph1: a-d] [graph2: a-d]

Copies the colors from graph1 into graph2. This does not change the colors stored in the data for graph2. To do this, use the command storecolors.

copygraph [graph: a-d] [Width (pixels)] [Height (pix)] or [Magnification (x1,x2)]

Copys the specified graph into a new window so that it is available to other programs.

copygraph.raytrace [graph: a-d] [density]

Same as copygraph except lines are drawn for the prism data.

depixel [graph: a-d]

Sets the graph limits so that one screen pixel is one data pixel.

drawellipse [graph: a-d]

Draws an ellipse in the given graph. The red and green cursor are at the foci, the blue is at a point on the ellipse.

drawellipse [graph: a-d] [focus1x] [focus1y] [focus2x] [focus2y] [xPt] [yPt]

Draws an ellipse on the graph with the given foci and a point on the ellipse.

getcolors [graph: a-d]

Prints the colors of the specified graph into the script window.

line.clear [num]

Clears the specified line.

line.clearall

Clears all of the lines.

line.get [num]

Prints the coordinates of the line in the script window.

line.make [num] [pt1x (Volts)] [pt1y (Volts)] [pt2x] [pt2y] etc.

Draw a line on the graphs through the given points.

line.move [num]

Moves the start of the line to the blue cursor.

line.slice [graph: a-d] [num Cuts]
　　Take cuts perpendicular to the lines in the given graph, display in the sweep window.

line.start [num]
　　Clears the line information so that it can be started.

outlinegate [graph: a-d] [sign] [thresh] [r] [g] [b] [rWeight] [gWeight] [bWeight]
　　Draws a line of color rgb around the area that is a gate defined by thresh and sign.

plots.on
　　Turns plotting of scans on.

plots.off
　　Turns plotting of scans off.

restorecolors [graph: a-d]
　　Restores the colors that are saved with the data for the specified graph.

resizewindow [window] [top (pixels)] [left] [width] [height]
　　Resizes the given window.

setcolors [graph: a-d] [value1] [r1] [g1] [b1] [rgb/hsv/hsl] [value2] [r2] [g2] [b2] etc
　　Sets the colors on the color bar. Value gives the value on the color bar and r,g,b gives the color at that point. Then rgb/hsv/hsl gives the method to go to the next value.

setgraphsigfigs [graph: a-d] [# sigFigs]
　　Changes the number of significant figures displayed on the colorbar and scan range for the given graph.

setgraphxy [graph: a-d] [xStart] [yStart] [xEnd] [yEnd]
　　Changes the range on the specified graph to be from xStart to xEnd and yStart to yEnd.

setgraphz [graph: a-d] [min (Volts)] [max] or [graph: a-d] [type] [range]
　　Sets the range of the color scale on the graph

shiftcolorstop [graph: a-d] [cStop] [newV (Volts)]
　　Shifts the color stop to the new voltage.

storecolors [graph: a-d]
　　Stores the colors of the specified graph in the data.

supimpgate [graph: a-d] [sign] [thresh] [r] [g] [b] [rWeight] [gWeight] [bWeight]
　　Superimposes the gate on the other graphs. Puts everything above thresh in graph onto the other graphs with the given color. Call with no parameters, to turn off.

waveplot.off
   Turns off plotting of phase information.

waveplot.on
   Plots phase information from graph d onto data in graph a.

zoomin [graph: a-d]
   Zooms in on the cursors in the given graph.

B.3.　　Scan Commands

These commands all manipulate scan data. There are also commands, which are

used for data analysis on the scans. These commands are mostly used when looking at a

scan after acquiring it.

scan.addsweep [graph: a-d] [sweepNum] [x]
   Adds a sweep as a column at the given x position in the graph.

scan.approxmedians [graphFrom: a-d] [graphTo: a-d] [percentile] [bins] [radius]
   Approximates the given percentile in a radius around each point in the scan.

scan.autoshiftdata [graph1: a-d] [graph2: a-d] [dx] [dy] [opt: c]
   The program shifts graph1 to try to match graph2. If parameter 5 is c, then the area of
   interest is just between the cursors, otherwise the entire scan is used.

scan.arcsample [graph: a-d] [nBins] [start angle] [end angle] [center angle] [datainc]
   Takes a sample of the given graph in an arc shape. The blue cursor defines the center
   of the arc. The red and green cursors give the inner and outer radii.

scan.average [graph1: a-d] [graph2: a-d] [weight]
   Takes the average of graph1 and graph2 with weight given to graph1.
   Graph1 = (weight*graph1 + graph2)/(weight+1).

scan.chop [graph: a-d] [min (Volts)] [max (Volts)]
   Chops off the values of the scan that lie outside of min and max.

scan.circpeakfind [graph: a-d] [radius step] [sign] [excl: startang] [excl: endang]
   Finds the peak in the circular slice. The area from startang to endang is excluded
   in the search. If sign is 1 finds the maximum, -1 finds the minimum and 0 finds the
   average. The red cursor defines the center of the circle.

scan.circpeakfind2 [graph: a-d] [radius step] [sign] [fraction]
Finds the peak in the circular slice. The analysis only looks at fraction of the scan. If sign is 1 finds the maximum, -1 finds the minimum and 0 finds the average. The red cursor defines the center of the circle.

scan.clear [graph: a-d]
Clears the specified graph.

scan.combinescan [graph1: a-d] [graph2: a-d] [spacer]
Puts two scans together with spacer pixels between them in the x direction.

scan.constant [graph: a-d] [value]
Puts a scan of constant value into the specified graph.

scan.contourfillin [graph: a-d] [smooth1] [skew1] [smooth2] [skew2] [smooth3] [skew3] opt: storeguide()
Smooths the data to eliminate the high frequency components. The skew parameters are used to set the weight for the x direction as compared to the y direction.

scan.copyintofrom [graphIn: a-d] [graphFrom: a-d]
Copies the scan from graphFrom into graphIn.

scan.crop [graph: a-d] [left (pixels)] [top] [right] [bottom], opt: cursors
Crops some of the scan in graph based on the values in left, top, right, and bottom. If the option cursors is selected the scan is cropped using the boundary of the cursors.

scan.crop.multipleof [graph: a-d] [number]
Crops the scan so that the number of pixels in each direction is a multiple of number.

scan.cutoffpeaks [graph: a-d]
Calculates the average between the cursors and also the minimum value. Then sets all peaks greater than (average+minimum)/2 to the average.

scan.destreak [graph: a-d] [threshold]
Attempts to remove jumps in the graph greater than threshold by adjusting the values.

scan.disttopeak [graph: a-d]
Uses the red and green cursors to define an area of the scan and then calculates the distance from the origin to the peak in this area.

scan.difference [graph1: a-d] [graph2: a-d]
Takes graph1 and subtracts graph2, puts the result in graph1.

scan.divide [graph1: a-d] [graph2: a-d]
Divides graph1 by graph2 and puts the result in graph1.

scan.dy [graph: a-d]
Calculates the differential in the y direction by multiplying the difference between two adjacent sets of data.

scan.enforcemirror [graph: a-d] [yMirror (pixels)]
Mirrors the data across the horizontal line given by yMirror.

scan.fft [graphIn: a-d] [graphOut: a-d]
Takes the fft of graphIn and puts it into graphOut. Must have 2^Nx2^M pixels.

scan.fillin [graph: a-d] [# of fills]
Fills in the graph by raising any point that is lower than its neighbors.

scan.fillintofrom [graph1: a-d] [graph2: a-d]
Fills in the graph1 by raising any point that is lower than the corresponding region in graph2.

scan.filter [graph: a-d] [FilterType (number)] [freq1] [freq2]
Filters the scan using a FFT. The possible filter types are a high pass filter (1), a low pass filter (2), a notch filter (3), filter near x=0 (4) and filter near y=0 (5). The last two parameters set the relevant frequencies in the filter.

scan.findmedians [graphFrom: a-d] [graphInto: a-d] [radius (pixels)]
Finds the local median in graphFrom using the radius and puts the result in graphInto.

scan.findplateau [graph: a-d] [start] [end] [range] [wght] [grphX: a-d] [grphY: a-d]
Looks for plateaus starting with graph+start and going to graph+end. Once a plateau is found calculates the value of it by averaging points within range of it using weight. Then stores the value in graphX or graphY.

scan.flipl2r [graph: a-d]
Flips the graph from left to right.

scan.getvalue [graph: a-d] [x (pixels)] [y (pixels)]
Prints in the console window the value at point (x,y) in the specified graph.

scan.gradient [graph: a-d]
Takes the gradient squared of the given scan.

scan.levelize [graph: a-d]
Takes the average in the x direction between the red and green cursors. Then computes the average over each line between the cursors. The difference between these two averages is added to all of the data in the line.

scan.linesample [graph: a-d] [nBins] [radius (pixels)] [microns per volt]
Takes a sample of the data between the red and green cursors, displays in sweep.

scan.linestack [graph: a-d]
Turns each line in the graph into a sweep.

scan.ln [graph: a-d]
Takes the natural log of the scan.

scan.load [graph: a-d] [fname] [fname add-on] etc
Loads the scan into the graph.

scan.localmedian [graph: a-d] [x (pixel)] [y (pixel)] [radius (pixels)]
Finds the local median at the point (x,y) using radius to define the region.

scan.makesinewave [graph: a-d] [amplitude (volts)] [period (volts)] [angle] [opt: Nx] [opt: Ny] [xWidth (volts)] [yWidth (volts)]
Creates a scan with a sine wave of the given parameters in it. The optional parameters set the total number of points in the scan and the area of it.

scan.match [graph1: a-d] [graph2: a-d]
Takes graph1 - # graph2 and puts it into graph1. The routine attempts to minimize the least squares difference in the two scans.

scan.minusconstant [graph: a-d] [constant]
Subtracts a constant value from the scan.

scan.normalize [graph: a-d]
Normalizes the scan so all of the values lie between 0 and 1.

scan.padwithzeros [graph: a-d] [numX (pixels)] [numY (pixels)]
Pads the scan with zeros so that it has the given total number of pixels in X and Y.

scan.percentilelevelize [graph: a-d] [perc Base] [perc Line] opt: mult
Removes jumps in the data between the red and green cursors that are caused by charging events. Makes the value of the percentile of each line equal to the value of the percentile of the base scan.

scan.plusconstant [graph: a-d] [constant]
Adds the constant to the scan.

scan.polishsurface [graph: a-d] [surfaceWiggle]
Anything that is smaller in magnitude than surface wiggle is made constant.

scan.psd [graph: a-d] [max freq]
    Calculates the power spectrum of a scan.

scan.radialintegrate [graph: a-d] [nBins] [startAng] [endAng] opt: !total, !oversample(), !weight(x^2), !weight(x^4)
    Performs a radial integration of the data in the graph. The integration goes from the red to the green cursors and is divided into bins. The data from the strating to the ending angle is averaged. The options allow the total signal to be given, different weights for the distances and also oversampling of the graph.

scan.radialmarkpercentile [graph: a-d] [bins] [ang0] [ang1] [percentile] opt: keep+, total
    Basically the same as scan.radialpercentile but uses a different algorithm to find the percentile, which may speed up the execution of the command.

scan.radialmode [graph: a-d] [nBins] [ang0] [ang1] [nSubBins]
    Calculates the mode in the region bounded by the two angles and the red and green cursors.

scan.radialpercentile [graph: a-d] [bins] [ang0] [ang1] [percentile]
    Calculates the value of the given percentile in the area defined by the two angles. The red and green cursors determine the beginning and end of the region. The blue cursor sets the center for plotting in the sweep window.

scan.random [graph: a-d]
    Creates a random scan.

scan.rectify [graph: a-d]
    Rectifies the given scan.

scan.resample [graph: a-d] [# times]
    Resamples the scan by averaging the nearest points to get the value at the new point.

scan.save [graph: a-d] [fname] [fname add-on] etc
    Saves the scan in graph. Does not put the usual prefixes on the filename. The complete file name must be specified in the parameters after the graph.

scan.savegraph.raytrace[graph: a-d] [density] [fname] [fname add-on] etc
    Saves the scan as a PICT file. The rays for the given density are also plotted.

scan.savenext [graph: a-d] [+/0] [fname add-on] [fname add-on] etc
    Saves the scan. Chooses the proper prefix based on fnum and the graph that is being saved. Then fname addon is appended to the filename. The second parameter controls whether fnum is incremented or not.

scan.savenext.both [graph: a-d] [+/0] [fname add-on] [fname add-on] etc
Same as scan.savenext except it also saves the scan converted to G values. When doing this it adds a + before the first fname addon.

scan.savepict [graph: a-d] [fname] [fname add-on] etc
Saves the scan as a PICT file.

scan.setwrap [graph: a-d] [on/off]
Determines whether to use periodic boundary conditions when finding values of the data in the given graph. If a location outside the graph boundaries are specified with this on the value will just wrap around to find the value.

scan.setxyscale [graph: a-d] [xScale] [yScale]
Sets the number of microns per volt for the scan.

scan.shiftdata [graph: a-d] [dx (pixels)] [dy (pixels)]
Shifts all the data in the graph. A negative dx causes the image to move to the left and puts cMarker_f64 into the data on the right. A negative dy causes the image to move down and puts cMarker_f64 into the data on the top.

scan.shiftdatag2r [graph: a-d]
Shifts data from the green cursor to the red cursor.

scan.smooth [graph: a-d] [# of smooths]
Smooths the graph by taking the average of the five nearest points. The center point gets a weight of one while the four nearest neighbors each get a weight of 0.5.

scan.smoothgaussian [graph: a-d] [radius] [mesh]
Smooths the given scan using a gaussian weighting scheme. Radius determines the half width, mesh determines the number of points to include in the smooth.

scan.smoothnotch [graph: a-d] [radius (pixels)] [freq]
Performs a notch smoothing filter on the given scan. The smoothing uses a guassian weighting scheme with the radius and frequency given.

scan.smoothradial [graph: a-d] [# smooths] [xCent (Volts) or b] [yCent]
Performs a radial smoothing of the data using the specified point as the center or if the third parameter is b then the blue cursor is used as the center.

scan.squared [graph: a-d]
Squares the given scan.

scan.supersmooth [graph: a-d] [xComp (pixels)] [yComp (pixels)]
Smooths along the vector given by xComp and yComp.

scan.tile [graph: a-d] [xTile] [yTile]
 Tiles the scan in x and y the number of times indicated.

scan.timesconstant [graph: a-d] [constant]
 Multiplies the given graph by constant.

scan.topercent [graph: a-d] [baseline]
 Converts the scan into percentages using the baseline.

scan.unnotch [graph: a-d]
 Finds the row between the cursor, which has the biggest change in its average. This change is then added to the rest of the rows above this one in the scan.

scan.v124tog
 Converts a scan from voltage values to one in G values.

scan.widelinesample [graph: a-d] [nBins] [radius (pixels)] [scale] [width] [nWidths]
 Takes a number of samples of the data between the red and green cursors.

scan.window [graph: a-d] [windowType: Bartlett, Hanning]
 Applies the window function to the graph.

scan.xderivative [graph: a-d]
 Takes the x derivative of the scan.

scan.yderivative [graph: a-d]
 Takes the y derivative of the scan.

scan.zoom [graph: a-d] [scale factor]
 Zooms the scan by the factor indicated.

B.4.   Sweep Manipulation Commands

These commands are used to manipulate sweep data. The also are used for data analysis of the sweeps. The commands in this section are also used to adjust the display properties of the data in the sweep window.

sweep.append [sNum] [xVal0] [yVal0] [xVal1] [yVal1] etc
 Appends the values to the given sweep.

sweep.autoy0 [on/off]
Whether or not to force y=0 to be in the sweep window.

sweep.ave [on/off]
Whether or not the next sweep will be averaged.

sweep.average [sNum1] [sNum2] opt: alreadyaveraged=
Averages the two sweeps with an optional weight on the first one.

sweep.averagevalue [sNum]
Prints the average value of the sweep.

sweep.centerofmass [sNum] [y offset]
Calculates and prints the center of mass of the sweep.

sweep.charge.z>0 [dielectric1] [dielectric2] [d (nm)] [h (nm)] [numReps] opt: xmin=, xmax=, npts=
Finds the induced charge in the 2DEG from a charge above the surface.

sweep.charge.z<0 [dielectric1] [dielectric2] [d (nm)] [h (nm)] [numReps] opt: xmin=, xmax=, npts=
Finds the induced charge in the 2DEG from a charge below the surface.

sweep.chop
Chops sweep so that x-axis goes from −1 to 1.

sweep.color [sNum] [r] [g] [b]
Sets the color of the sweep.

sweep.crop [sNum] [beginning] [end]
Crops the indicated number of points from the sweep.

sweep.clear
Clears the currently displayed sweep.

sweep.combine [sNum0] [sNum1]
Combines the two sweeps.

sweep.copyintofrom [sNum0] [sNum1]
Copies sNum1 into sNum0.

sweep.derivative [sNum]
Takes the derivative of the sweep.

sweep.difference [sNum0] [sNum1]
Subtracts the two sweeps.

sweep.divide [sNum0] [sNum1]
Divides sNum0 by sNum1 and puts the results in sNum0.

sweep.divideR [sNum]
Divides each point by its x value.

sweep.exp [sNum]
Takes the exponential of the sweep.

sweep.fft [sNum]
Takes the FFT of the sweep.

sweep.fft.inverserange [sNum] [nmPerPixel]
Takes the FFT of the sweep, converts the x axis to nanometers.

sweep.filter [sNum] [freq to remove]
Applies a high pass filter to the data.

sweep.filterIIR [sNum] [freq]
Applies an IIR filter to the sweep.

sweep.findaverage [inSweep] [outSweep]
Finds a sweep that is the average of the inSweep and outputs it in outSweep.

sweep.findmaximas [inSweep] [outSweep]
OutSweep contains the points in inSweep that were maxima.

sweep.findminimas [inSweep] [outSweep]
OutSweep contains the points in inSweep that were minima.

sweep.fitcurve [sNum] [fit sNum] [equation] [param1 min] [param1 max] etc.
Fits the curve given by equation to the sweep in fit sNum. The result is plotted in sNum.

sweep.flip [sNum] [x/y]
Flips the sweep over either the x and y axis.

sweep.gtov124
Converts a sweep that is in G values back into a sweep in voltage.

sweep.line [ch] [nPts] [readsPerPt]
Sweeps from the red to the green cursors.

sweep.ln [sNum]
Takes the natural log of the sweep.

sweep.load [fname] [fname add-on]
Loads the given sweep and removes all other sweeps from the window.

sweep.load.noclear [fname] [fname add-on]
Same as loadsweep but does not clear other sweeps that are already in the sweep window.

sweep.make [sNum] [xVal0] [yVal0] [xVal1] [yVal1] etc
Creates a sweep with the indicated values.

sweep.makesinewave [sNum] [numPts] [freq1] [freq2]
Creates a sweep with the two frequencies.

sweep.matchXPoints [inSweep] [matchSweep] or [inSweep] [Start] [End] [numPts]
Matches the x points in the matchSweep with the ones in inSweep.

sweep.minusconstant [sNum] [constant]
Subtracts a constant from the sweep.

sweep.normalize [sNum]
Normalizes the sweep so that the highest value is 1 and the lowest value is 0.

sweep.off [sNum]
Turns off the display of the given sweep.

sweep.on [sNum]
Turns on the display of the given sweep.

sweep.orderX [sNum]
Puts the points in order based on x value.

sweep.padwithzero [sNum] [num zeros]
Pads the sweep with the indicated number of zeros.

sweep.printxmax [sNum]
Prints the x value of the point with the maximum y value.

sweep.printxmin [sNum]
Prints the x value of the point with the minimum y value.

sweep.printymax [sNum]
Prints the value of the point with the maximum y value.

sweep.printymin [sNum]

Prints the value of the point with the minimum y value.

sweep.resample [sNum]

Resamples the sweep to double the number of points in it.

sweep.save [fname]

Saves the current sweep in sweep number 0.

sweep.saveall [on/off]

On means save the normalized, averaged etc sweeps

sweep.savenext [+/0] [fname add-on] [fname add-on] etc.

Saves the sweep. The filename has the format #sw fname addon. The first parameter controls whether to increment the fnum.

sweep.savenext.both [+/0] [fname add-on] [fname add-on] etc.

Same as sweep.savenext except the sweep is also saved converted to G values.

sweep.smooth [sNum] [nSmooths]

Smooths the given sweep.

sweep.sqrt [sNum]

Takes the square root of the sweep.

sweep.swap [sNum 1] [sNum 2]

Swaps the two sweeps.

sweep.timesR [sNum]

Multiplies each point in the sweep by its x value.

sweep.timesconstant [sNum] [constant]

Multiplies the given sweep by a constant.

sweep.v124tog

Converts a sweep that is in voltage to a sweep in G.

sweep.window [sNum] [windowType]

Applies a window function to the sweep. The supported windows are Hanning, Parzen and Welch.

sweep.xlims [xMin] [xMax]

Sets the limits of the sweep window to be from xMin to xMax. Can also enter auto instead of xMin. This should put all of the data in the sweep.

sweep.ylims [yMin] [yMax]
Sets the limits of the sweep window to be from yMin to yMax. Can also enter auto instead of yMin. This should put all of the data in the sweep.

B.5.   Printing Commands

These commands are all related to printing scans and sweeps. When you want to print a scan the general procedure is to start the layout with the command print.start and then make all the necessary calls of print.scan and print.sweep for the scans and sweeps that you want on the page. Once everything has been laid out including the text, you should call print.layout to send the page to the printer. Currently only one page at a time can be printed.

print.bottomnote [note]
Setup the note that goes on the bottom of the page.

print.layout
Finishes the layout and sends it to the printer.

print.scan [graph: a-d] [xPage0] [yPage0] [width] [opt: title] [opt: subtext]
Prints the scan in the given area on the page. There are several other options including nocolorbar, percent and scalebar().

print.scan.full [graph: a-d] [mag factor] [] [x0] [y0] [x1] [y1] [opt:title] [opt:subtext]
Prints the full scan in the square given. There are the same options as print.scan.

print.start [landscape or portrait]
Starts the layout of a page in either landscape or portrait mode.

print.sweep [xPage0] [yPage0] [xW] [yW] [opt: title] [opt: subtext]
Prints the first sweep, with the given position and size.

print.title [title]
Setup the title for the top of the layout.

print.topnote [note]
Setup the note that goes at the top of the page.

printslide [# cols] [col border ratio] [row border ratio]
    Prints out the slides in a movie. Prints with the specified number of columns and the specified ratio of the border to the slides.

B.6.   Movie Commands

These commands all manipulate the slide data. The slides are used to generate

movies and also to store data. A movie is a series of slides whose images are captured by

the program, so that they may be played back quickly without having to redraw the data

for each image.

addslide [x] [opt: y] option: nodata
    Adds the slide. X is the value of the variable that is changing from slide to slide. Y can also be used if the movie has two variables that change.

addslide.nosweep [x] [opt: y] option: nodata
    Same as addslide, but does not load anything from the sweep.

emptyslides
    Clears all the slides.

getdata [graph: a-d] [slide]
    Gets the data stored in slide and puts it into the graph.

loadslides
    Loads the slides that are specified using slidenames.

nextslide [inc]
    Moves forward the given number of slides.

putdata [graph: a-d] [slide]
    Puts the data from the graph into the slide.

redoslides
    Re-plots all the slides. This must be called after any change to the slides.

saveslidedata.off
    Does not save the slide data into a data block. Not necessary with addslide.

saveslidedata.on
Saves the slide data into a data block. Not necessary with addslide.

setslideOps.midColorNum [midcolor #]
Sets which color should be the middle color for the slides.

slideautocopy [on/off]
Whether or not to automatically copy the slide when it is plotting.

slideautomovie [on/off]
Whether or not to automatically make a movie when plotting the slides.

slideautoprocess [#smooths] [#resamples] [#smooths] [#resamples] [#smooths]
Does the specified data processing on the slides.

slideautov124tog [on/off]
Whether to automatically convert the slide into G values.

slideautoz [on/off]
Whether or not to autoz each slide.

slidebigstep [step]
Used in 2-D movies to set the length of each 1-D movie

slidecirc [x] [y] [xy to volts] [base]
Sets up parameters used to draw a circle on each of the slides.

slidecolorscheme [off/instruction]
The color scheme to use for the slides. The usage is the same as for colorscheme.

slidecrop [left (pixels)] [top] [right] [bottom]
Crops off some of the slide. The values are the number of pixels to crop off the side.

slidecursor [on/off]
Puts cursor on the printed page.

slidegrid [on/off]
Puts a grid on each scan when it is printed. The default size is 0.1 Volts.

slidemidcolors [midcolor] [midcolor] etc
Sets the value of the middle of the color range for each of the slides.

slideminmax [min] [max]
Sets the minimum and maximum values on the color bars for the slides.

slidenames [name of slide] [name of slide] etc.

Takes the full name of the slide. This command takes the entire list of files to be included in the movie.

slidenotes [note about slide] [note about slide] etc

Takes notes to include about each slide.

slidenums [# of slide: 001,002] [# of slide] etc

Assumes file names are 001sc.e, 002sc.e etc. This command takes the entire list of file numbers to be included in the movie.

slidenums.old [# of slide: 001,002] [# of slide] etc

Assumes file names are #001 scan.e, #002 scan.e etc. This command takes the entire list of file numbers to be included in the movie.

slideOps.gridSize [grid size (Volts)]

Changes the grid size from the default value of 0.1 Volts.

slidepresetminmax [on/percent/off]

On means that the range of the colorbar does not change. Off means that it does. Percent means that percent change is given.

slideseries [firstslidenum] [lastslidenum]

slideseries [firstslidenum] [# of slides] [inc]

Generates a series of slides given the number of the first slide and either the number of the last slide or the number of slides to include. Assumes the filenames are of the form XXXsc.e.

slidesweepnames [name of sweep] [name of sweep] etc

Takes the full name of the sweep that goes along with the scan.

slidesweepnums [# of sweep: 001,002] [# of sweep] etc

Takes the number of the sweep to go with the scan. Assumes names are 001sw.

slidesweepnums.old [# of sweep: 001,002] [# of sweep] etc

Takes the number of the sweep to go with the scan. Assumes names are #001 sweep.

slidetitle [title]

Puts a title on the page when the slides are printed.

slidevolts [volts] [volts] etc.

Takes the value in volts of each slide given in slidenames.

B.7.   Loop and Variable Commands

These commands are used for creating and manipulating variables. Variables are used in the program for running loops, performing logic operations like if then statements. There are also commands for putting breaks in the script or stopping it.

addto.var [var name] [inc]
    Adds inc to the variable given in var name.

else [name]
    Can be used with ifthen statements. Name must match the ifthen statement.

endif [name]
    This is the end of the ifthen statement.

endloop.var [loopvar $c, etc]
    Put at the end of a loop so the program knows how long the loop is.

endmacro
    Used to stop the definition of a macro.

ifthen [name] [A] [type of ifthen; str,str.contains, mult.of] [B]
    Checks if A statement B is true where statement is one of the types of ifthen
    statements. The ifthen must have a name so that the program can find the end of it.

macro ["name"]
    Used to start the definition of a macro. Must be followed by the name of the macro.

onelinestop
    A one line stop, used when not running a script.

pausescript
    Used to pause the script. Keeps the value of all the current variables.

readin.var [var name] [channel] [#reads]
    Reads in the value of the variable from the given channel.

set.var [var name] [value]
    Sets the value of a variable to value. Variable names start with $.

startloop.var [loopvar $c,etc] [start] [end] [inc]
    Starts a loop. The first parameter is the variable that is looped over. The next
    parameters are the starting, ending and increment value.

stopscript
    Stops the script. Clears the value of all the current variables.

B.8.   Setup Commands

These commands are used for setting up the AFM. They include routines for

finding the surface, fitting a plane to the surface, calibrating the output voltages, cleaning

the surface.

adjustg [G] [inCh] [time]
    Adjusts the output to the gate so that the value coming into the computer on inCh is G
    (after conversion). Time is used to set a settling time for the readings.

adjustv [volts] [inCh] [time]
    Adjusts the output to the gate so that the value coming into the computer on inCh is
    volts. Time is used to set a settling time for the readings.

autoflatten [x0] [y0] [x1] [y1] etc. opt: rejectneg=, rejectpos=
    Finds the surface and fits a plane at the given points rejecting the given number.

boxroute [dist] [# steps]
    Moves the tip around in a box defined by the red and green cursors for each step.
    Each time the box shrinks by dist/4 * #steps. This is used to clear stuff out of the scan
    area.

checkautoheight2
    Checks the height of the surface at the coordinates given in the most recent call to
    setautoheight2. This will also change the values for the height at those points.

findsurface
    Finds the surface at the current location.

offsetaxii [dx] [dy]
    Changes the axii on the scans. Used to shift a guide due to drifting. Note: hitting on
    left of gate: to correct, dx should be negative

outputcalibration [channel 1-4] [computerV0] [finalV0] [computerV1] [finalV1]

outputcalibration [channel 1-4] [finalV @ 0V] [Delta 1V]
Calibrates the output of the voltage used in the guides. The two options are two values that the computer outputs along with the associated values that reach the sample or the value at the sample when the computer outputs 0 Volts and the change for a 1 Volt change from the computer

read3561a [start freq] [freq. span] [linear/log] [# of aves] [run/norun]
Reads the spectrum analyzer and displays the result in the sweep window

remove60hz [graph: a-d] [freq1] [freq2] etc
Removes the frequency in freq1, freq2 etc. These must be multiples of 60hz.

route-ne [dist] [# steps]
Moves the tip from the green to red cursor for each step. Each step moves dist/# steps towards the NE. This is used to try to clear stuff out of the scan area.

route-nw [dist] [# steps]
Moves the tip from the green to red cursor for each step. Each step moves dist/# steps towards the NW. This is used to try to clear stuff out of the scan area.

route-se [dist] [# steps]
Moves the tip from the green to red cursor for each step. Each step moves dist/# steps towards the SE. This is used to try to clear stuff out of the scan area.

route-sw [dist] [# steps]
Moves the tip from the green to red cursor for each step. Each step moves dist/# steps towards the SW. This is used to try to clear stuff out of the scan area.

setautoheight1 [x0] [y0] [x1] [y1] etc
Finds the height of the surface at the given coordinates.

setautoheight2 [x0] [y0] [x1] [y1] etc
Finds the height of the surface at the given coordinates.

setcirc.datacoord [graph: a-d] [x0 (pixels)] [y0] [radius] [value]

setcirc.realcoord [graph: a-d] [x0 (Volts)] [y0] [radius] [value]
Sets the area inside of the circle to value for the given graph. If value is marker0 then the value becomes cMarker0_f64.

setrect.datacoord [graph: a-d] [x0 (pixels)] [y0] [x1] [y1] [value]

setrect.realcoord [graph: a-d] [x0 (Volts)] [y0] [x1] [y1] [value]
Sets the area inside of the rectangle to value for the given graph. If value is marker0 then the value becomes cMarker0_f64.

sinerect.datacoord [graph: a-d] [x0 (pixels)] [y0] [x1] [y1] [freq] [ang] [mag]

sinerect.realcoord [graph: a-d] [x0 (Volts)] [y0] [x1] [y1] [freq] [ang] [mag]
Sets the area inside of the rectangle for the given graph to be a sine wave with the given parameters. If value is marker0 then the value becomes cMarker0_f64.

special [subtractfrom] [amount]
Takes the value of ch1 and makes it amount-ch1.

storegreading [input channel] [# of aves] [graph: a-d] [noteval]
Stores the G reading in the notes of the given graph.

B.9.   Data Taking Commands

These commands are all related to the taking of data. They are used to start scans or sweeps and also to process the incoming data.

preparefastscan [tau] [oneway/twoways]
Prepares a fast scan with a turnaround time of tau. The oneway/twoway flag determines whether to take data both directions or only one.

processstoredfastscan
Processes the last fast scan that was taken.

startfastscan
Starts a fast scan.

startscan
Start a scan.

startsweep [-] [-] [-] [-] [opt: noclear/ave]
Repeats the last sweep that was called. There is no setting of the starting and stopping voltage nor the channel to read.

197

sweepgatev [Vstart] [Vend] [inCh] [reads per point] [opt: noclear/ave] [opt: Vstep]
  Sweeps the gate voltage from Vstart to Vend reading inCh. If noclear is specified, the sweep window is not cleared from the previous sweep and the new sweep is just plotted in the same window. If ave is specified, the new sweep will plot along with the average of the new and old sweep. If Vstep is not specified, the step size will be one DAC step.

sweepheight [start] [end] [inCh] [reads per point] [opt: noclear/ave] [opt: Vstep]
  Does a sweep as a function of the height of the tip. Start and end give the difference in height from the current position. The rest of the parameters are the same as sweepgatev.

sweepreflv [Vstart] [Vend] [inCh] [reads per point] [opt: noclear/ave] [opt: Vstep]
  Sweeps the reflector voltage from Vstart to Vend reading inCh. The rest of the parameters are the same as sweepgatev.

sweeptipv [Vstart] [Vend] [inCh] [reads per point] [opt: noclear/ave] [opt: Vstep]
  Sweeps the tip voltage from Vstart to Vend reading inCh. The rest of the parameters are the same as sweepgatev.

waitforfastscan
  Used after starting a fast scan to wait for the data to come in.

B.10.   Simulation Commands

These commands are used when you want to run a simulation using the program. Currently there are two types of simulations: a model of the 2DEG potential with the classical trajectories through it and a calculation of the phase coherence time as a function of various parameters.

addlorentzian [graph: a-d] [xCent] [yCent] [width] [height]
  Adds a lorentzian to the graph with the given center position, height and width.

anneal2deg [graph: a-d] [density (#/cm^2)] [ionization] [impurities (#/cm^3)] [setback (nm)] [depth (nm)] [anneals] opt: seed(), blend(), dots, quickfind, onlypercent, onlydistance, mult
  Creates a potential and anneals it to relax the position of the donor atoms.

classicalsim [graphPot: a-d] [graphTraj: a-d] [x0] [y0] [x1] [y1] [ang0] [ang1] [linesteps] [angsteps] [energy] opt: noclear, stepsperpixel(), energy, halfway, cosangle, cospos, mfp()
Performs a classical simulation of trajectories moving through the given potential.

model2deg [graph: a-d] [density (#/cm²)] [ionization] [impurities (#/cm³)] [setback (nm)] [depth (nm)] [anneals] [dimplecutoff (nm)] opt: seed(), blend(), dots, quickfind, onlypercent, onlydistance, mult
Models the potential in the 2DEG given the parameters. Used for simulations of the expected electron flow.

model2deg.old [graph: a-d] [density (#/cm²)] [impurities (#/cm³)] [closest (nm)] [setback (nm)] [depth (nm)] opt: seed(), blend()
Models the potential in the 2DEG given the parameters. This is the old version, which does not anneal. Used for simulations of the expected electron flow.

phasecoherence.time [graph: a-d] [nX] [nY] [temp 0] [temp 1] [density 0] [density 1]
Calculates the phase coherence time as a function of temperature and density.

phasecoherence.distance [graph: a-d] [nX] [nY] [temp 0] [temp 1] [Dens 0] [Dens 1]
Calculates the phase coherence distance as a function of temperature and density.

phasecoherence.mfp [graph: a-d] [nX] [nY] [temp 0] [temp 1] [density 0] [density 1]
Calculates the phase coherence mfp as a function of temperature and density.

phasecoherence.mobility [graph: a-d] [nX] [nY] [temp 0] [temp 1] [Dens 0] [Dens 1]
Calculates the phase coherence mobility as a function of temperature and density.

B.11.   MetaScan Commands

These commands all perform functions on metascans. A metascan is a collection of several different scans that have been grouped together. This is done when a series of images is taken as a function of some parameter like back gate voltage.

metascan.fill [radius] [opt: mesh]
Fills the meta scan using all the slides loaded. If radius is 0 then metascan is just an exact copy of all the data in the slides. Otherwise a gaussian weighting system is used where radius is the half width and mesh is the number of points to consider.

metascan.slice [graphIn: a-d] [graphOut: a-d]
  Looks at a meta scan to find the value at each point in graphIn and puts into graphOut.

metascan.smooth [radius (# of scans)]
  Smooths the data in a meta scan. Smooths a point compared to the nearby scans. The smoothing is a gaussian weight with the half width determined by the specified radius.

B.12.   Autoalign Commands

These commands are used to do the autoalign procedure. This is used to align the position of a scan to a particular base scan. This is not really used anymore now that we have a better routine for finding the surface and we are able to adjust the positions of the scans after acquiring them if necessary.

autoalign.60hz [on/off]
  Should 60hz automatically be removed from scans.

autoalign.clear
  Clears all the variables in the autoalign structure. This must be called first.

autoalign.init
  Does the full XY & Z intialization steps.

autoalign.init.xy
  Does just the XY initialization steps.

autoalign.init.z
  Does just the Z initialization steps.

autoalign.npts [nPts]
  Number of points in the most recently defined autoalign.scan.

autoalign.pause.0 [# secs]
  Time to pause before Scan0.

autoalign.pause.n [# secs]
  Time to pause before each non-Scan0 scan.

autoalign.run
　　　Runs the full XY & Z autoalign.

autoalign.run.xy
　　　Runs just the XY autoalign.

autoalign.run.z
　　　Runs just the Z autoalign.

autoalign.scan [xStart] [yStart] [xEnd] [yEnd]
　　　This defines the alignment area.

autoalign.vpers [V/s]
　　　Tip speed in scan defined by autoalign.scan.

autoalign.zpause [# secs]
　　　Number of seconds to pause between checking z points.

autoalign.zpt [x] [y]
　　　Define a point to check the z-level.

B.13.　　　Powerscan Commands

　　　　　Powerscan moves to a specified number of points in a grid and performs a sweep

of the reflector gate voltage at each of these points. This generates a movie of reflector

gate voltage versus tip position. The powerscan functionality is currently commented out

of the program.

powerscan.checker [graph: a-d]
　　　Fills the powerscan with an alternating set of plus and minus one. If this is called
　　　without a parameter, assumes that the graph is a.

powerscan.clear
　　　Clears all the parameters associated with a powerscan.

powerscan.coords [xStart] [yStart] [xEnd] [yEnd]
　　　Sets up the coordinates for a powerscan. The powerscan will use these values as the
　　　outside of the box to scan in.

powerscan.gatev-slice [graph: a-d] [vSlice]

Takes a pre-run powerscan and generates a "scan" of the voltage on the point contact for each point. Does this by looking through all of the sweeps to get the value at each position.

powerscan.getsweep [x] [y]

Takes a sweep with the tip at the given position. If no x,y is specified then takes the sweep with the tip at the red cursor.

powerscan.go

Starts a powerscan. All of the parameters must have been specified before running this command.

powerscan.goalg [G value]

Sets the conductance value that the computer attempts to keep the point contact at during a powerscan.

powerscan.ns [x pts] [y pts]

Sets the number of points to sample in both the x and y direction. If there is not a second parameter, assumes that it is the same as the first parameter.

powerscan.prescan [graph: a-d]

Moves the cursors on the specified graph to the corners of the range for the powerscan. If no graph is specified then graph a is assumed. Then takes a scan between the cursors.

powerscan.reflv-slice [graph: a-d] [Vrefl]

Takes a pre-run powerscan and generates a "scan" for a given voltage on the reflector gate. Does this by looking through all of the sweeps to get the value at each position for the given Vrefl.

powerscan.silent [on/off]

Determines whether or not the dashboard and sweep window should be updated with ever point that is output.

powerscan.sweepreflv [start] [end] [inCh] [reads per pt] [# sweeps] [delay]

Sets up the parameters to use in generating a powerscan. This sets the end points of the reflector voltage sweep and also the number of times to sweep and the input channel.